

UNIVERSITÀ DEGLI STUDI DI BERGAMO

Facoltà di Ingegneria  
Dipartimento di Ingegneria Industriale

DOTTORATO DI RICERCA  
IN  
TECNOLOGIE PER L'ENERGIA E L'AMBIENTE

XXVI ciclo  
Anno 2013



In cooperation with



# Design and assessment of optimized control strategies for solar heating and cooling systems

Supervisor:

Prof. Giuseppe Franchini

Co-Examiner:

Roberto Fedrizzi

Doctoral thesis:

Davide Bettoni

© 2013

Dipartimento di Ingegneria Industriale. Università degli studi di Bergamo

ISBN XXX-XX-XXXXX-XX-X

Open access copy available at: <http://hdl.handle.net/XXXXX/XXXXX>

Terms of use: <http://aisberg.unibg.it/doc/disclaimer.html>

# Table of Contents

Table of Contents .....	3
Executive summary .....	5
1. Solar thermal systems.....	14
1.1 Introduction.....	14
1.2 Components .....	18
1.2.1 Solar collectors energy balance .....	22
1.3 System for heating domestic water (SDHW) .....	25
1.3.1 Hygienic requirement for domestic hot water .....	27
1.4 Solar Combisystems (DHW and space heating).....	29
1.4.1 Small solar combisystems .....	29
1.4.2 Two stores systems.....	31
1.4.3 Tank in tank system .....	32
1.4.4 Space heating store with load side heat exchanger for DHW and external auxiliary boiler.....	33
1.4.5 Two stratifiers in space heating storage with external heat exchanger for DHW .....	33
1.5 Solar Combi+ systems (DHW, space heating and space cooling) .....	34
1.5.1 SHDC - Solar Heat Driven Chiller Systems.....	39
1.6 Literature review on control of solar thermal systems .....	42
2. Numerical models for solar thermal systems .....	45
2.1 Introduction.....	45
2.2 Climatic data considered .....	45
2.3 Buildings description .....	49
2.3.1 Stratigraphy for Bolzano base model.....	50
2.3.2 Stratigraphy for Rome base model.....	52
2.3.3 Shading systems.....	54
2.3.4 Internal gains .....	54
2.3.5 Infiltrations.....	55
2.3.6 Natural night ventilation.....	55
2.3.7 Domestic hot water demand .....	56
2.3.8 Distribution control for active layer in the two floors building .....	57
2.3.9 Sensitivity analysis with Morris method .....	57
2.3.10 Building simulation results.....	62
2.4 Other components used .....	63
2.4.1 Dry cooler.....	63
2.4.2 Adsorption machine.....	64
2.4.3 Flat plate heat exchanger .....	64
2.4.4 Compression heat pump.....	64
2.4.5 Collectors .....	65
2.4.6 Thermal storages .....	65

2.4.7	Circulation pumps .....	65
2.4.8	Valves .....	66
3.	Numerical model validation.....	67
3.1	Introduction.....	67
3.2	Validation of the Dry Cooler numerical model.....	70
3.3	Validation of the adsorption machine numerical model.....	80
3.4	Validation of the heat exchanger numerical model .....	84
3.5	Validation of the variable circulation pump model.....	89
3.6	Other components numerical model validation .....	91
4.	Traditional control strategies.....	92
4.1	Introduction .....	92
4.2	Working schemes .....	92
4.3	Components activation logic and signals .....	100
4.4	Sensitivity analysis and optimization of the control.....	104
4.5	Results of Solar Combi+ system considered.....	106
5.	Innovative control system.....	115
5.1	Introduction.....	115
5.2	Fuzzy Logic .....	115
5.2.1	Fuzzy Logic Controllers.....	119
5.2.2	Fuzzification process .....	120
5.2.3	Inference mechanism/engine .....	120
5.2.4	Defuzzification process .....	121
5.3	Reinforcement learning.....	123
5.3.1	Q-learning .....	124
5.3.2	Application of RL and Q-learning .....	128
5.4	Application of RL and Fuzzy logic.....	129
5.5	Application of FLC and RL to thermal system .....	130
5.6	Example of FLC and RL application to a SDHW.....	136
5.7	Future development.....	148
Annex 1	.....	150
Annex 2	.....	153
Annex 3	.....	159

# Executive summary

The solar thermal systems adopted to cover heating, cooling and domestic hot water demands are normally identified with the name “Solar Combi+ systems”, in order to differentiate them from the Solar Combi systems (where the solar thermal energy is employed to meet the heating and DHW demands), and from the most diffuse simple solar thermal systems covering only the DHW energy loads.

In these complex plants thermally driven chillers are employed, further than the traditional components used in the normal solar thermal applications (usually collectors, storages and auxiliary heating backup). These kind of devices are driven by thermal energy and are adopted in these applications mainly for two reasons: the first is related to the simultaneity between solar radiation and cooling demand; on the other hand, installing wide collectors’ areas allows also to cover large portions of the heating and DHW demands.

The case study presented in the first part of the thesis is a Solar Combi+ system for residential applications (Fig.1).

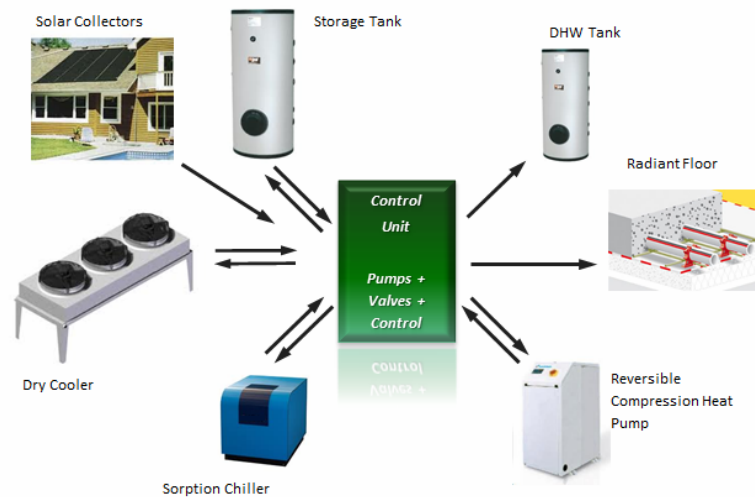


Fig.1 - Components of the residential Solar Combi+ system considered

In order to design an optimized control and predict the performance of such complex plants, dynamic simulations are performed through numerical software (such as Trnsys, Matlab, Energy+). Furthermore, these systems usually work always under different boundary conditions related on the one hand to the different environment and on the other to the diverse thermal loads that a variety of buildings present -though within the same construction category-. These requirements make the control optimization problem a hard issue to solve, if high performance is pursued. For this reason, traditionally a numerical model validated through an experimental campaign is used to optimize the control.

In this thesis, two approaches are compared, the traditional and an innovative one based on self-learning algorithms.

The traditional method, started from the numerical models adopted in the studied Solar Combi+ application: a deep analysis was tackled on the boundary conditions given by the employed climatic conditions. Two climatic locations have been considered (Rome and Bolzano). Furthermore two classes of residential buildings (Fig.2) have been implemented: the first one called Building with High energy Demand "BHD" that respect the actual Italian norm in terms of opaque and transparent surfaces transmittance, while a second one called Building with Low energy Demand "BLD" where the transmittances and infiltration rate are reduced. In this way, the effects due to different building loads were assessed.

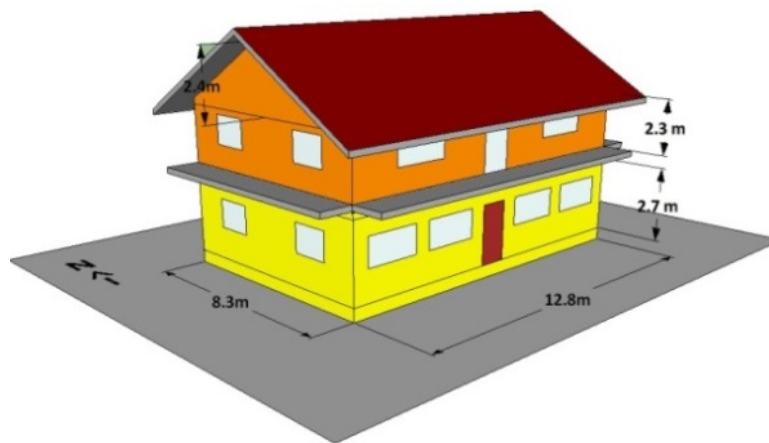


Fig.2 - Residential buildings analysed

As already mentioned, the numerical models used to simulate the system components with Trnsys have been validated. The validation procedure developed within the PhD is structured mainly in three phases, as reported in Fig.3.

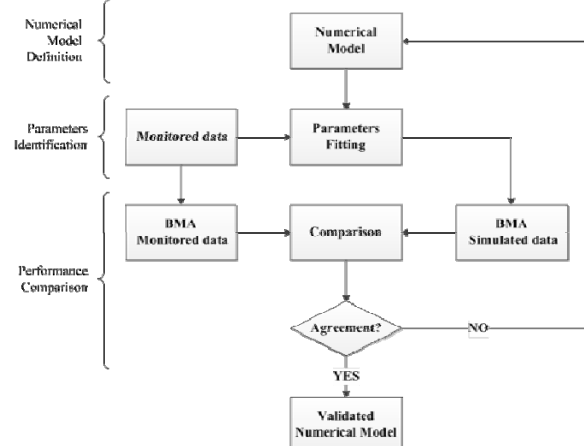


Fig.3 - Iterative validation procedure.

After a first **Numerical Model Definition** phase, a second phase, needed for the **Parameter Identification** (PI), is implemented; here monitored inlet quantities (temperatures and mass flow rates) are used as boundary conditions to the simulation models, while simulated and monitored outlets quantities are compared. During the PI, minor component parameters have been varied within realistic bounds, in order to minimize an opportune objective function. The historical data period on which carrying out the PI should represent typical working conditions of the system component.

When the objective function converges towards the minimum, the maximum agreement has been found. This however, does not say anything on the accuracy of the model. A comparison of the numerical results with the monitoring data has to be performed on the basis of quantitative performance figures. To this purpose, a Bin Method Analysis (BMA) is made on the simulation outputs as the main technique for data reduction. A quantitative comparison among the monitoring and simulated BMA curves is then performed (**Performance Comparison**). If the Root Mean Square Error (RMSE) value of the curves is within the acceptance criterion defined by the user, then the validation is accomplished, otherwise the numerical model has to be revised or upgraded. This process is iterative and repeated until an adequate level of agreement is found.

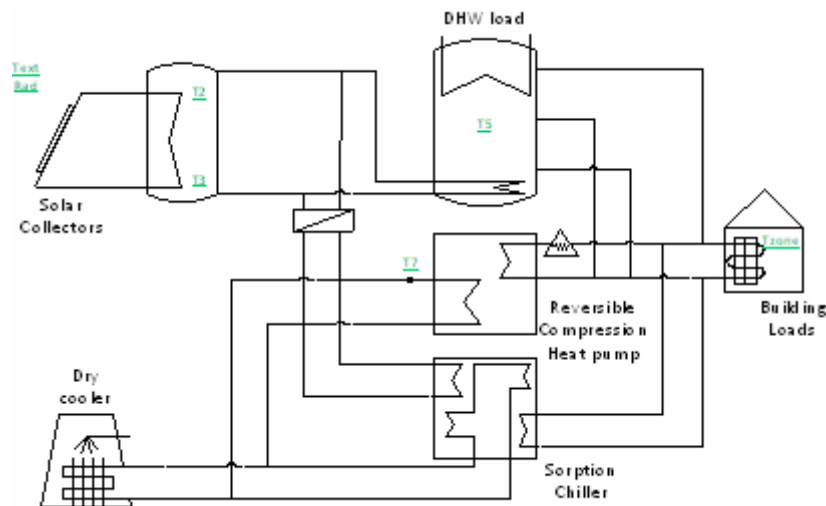


Fig.4 - Scheme of connection for a Solar Combi+ application

Once validated the Solar Combi+ system numerical model studied (Fig.4), a traditional control structure has been developed and implemented. In the system analyzed the solar energy is employed, in summer time, to cover the cooling load through the adsorption machine. When solar thermal energy collected is not enough to drive the sorption chiller, the cooling load is covered by the backup reversible compression heat pump. In winter, solar energy is used to directly cover the heating load or indirectly by driving the reversible compression heat pump at the evaporator. When solar thermal energy is not available the heat pumps exploit thermal energy from air, thanks to an air-to-water heat

exchanger. When energy neither from the solar or the air sources is harvested, an electrical backup is activated to meet the thermal heating or the DHW loads. The solar energy is also used, during the whole year, to cover as much as possible of the DHW demand.

Once defined the operating modes of the system studied, the control has been designed following the structure reported in Fig.5. Starting point has been the analysis on the “**Control Variables**” needed for the activation or the deactivation of the single operating mode. Furthermore, the range of values of these control variables has to be defined in order to implement the “**Control Signals**” in the form of hysteresis. The Boolean combination of the control signals activates or deactivates the single operating mode (“**Schemes**”). Finally, the schemes are weighted with the “**Modulation**” and this combination constitute the “**Component control signal**”.

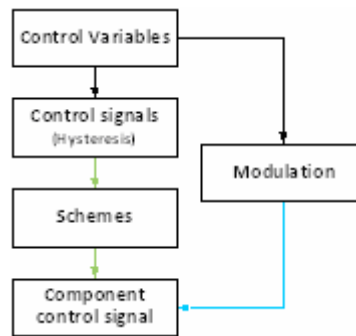


Fig.5 - Traditional control structure

Once the structure of the control and the hysteresis parameters have been defined, a sensitivity analysis has been performed with the aim to detect which are the variables with the larger effect on the system performance. An optimization study has been carried out afterwards, by varying only the most influencing parameters.

Looking at the results before and after the optimization of the control the difference is sizeable. In Tab.1 the results for a system located in Bolzano with 32m<sup>2</sup> of flat plate collectors are reported. The table reports on the performance of the system in terms of the solar fraction for heating (**SF<sub>heat</sub>**) and air fraction for heating (**AF<sub>heat</sub>**). These two indexes are related to the percentage of the heating load covered using energy from the air or and solar sources. In addition, the seasonal performance factors for cooling (**SPF<sub>cool</sub>**), heating (**SPF<sub>heat</sub>**), DHW (**SPF<sub>DHW</sub>**) and the total seasonal performance factor (**SPF<sub>el\_tot</sub>**) are presented, computed as the ratio between the yearly thermal demand and the yearly electrical consumption. On the right side, the different yearly thermal demands for heating (**Heat<sub>demand</sub>**), cooling (**Cool<sub>demand</sub>**), and DHW (**DHW<sub>demand</sub>**) are reported.

The solar fraction decreases after the optimization process and air fraction used for heating increases. The seasonal performance factors, increases heavily, in particular for heating and DHW where respectively an increase of 67% and 45% is visible. This is reflected on the total performance factor, which increases from 3.56 to 5.49. In this way, the optimized control allows to save 35% of the electric energy originally used.



Tab.1 - Performance comparison before and after control optimization. Standard (STD) weather data and building with low heating demand (BLD).

Bolzano 32m <sup>2</sup>	SF <sub>heat</sub>	AF <sub>heat</sub>	SPF <sub>cool</sub>	SPF <sub>heat</sub>	SPF <sub>DHW</sub>	SPF <sub>el_tot</sub>	Heat <sub>demand</sub>	Cool <sub>demand</sub>	DHW <sub>demand</sub>
	[-]		[-]				$\left[\frac{\text{kWh}}{\text{m}^2}\right]$		
Validated	49%	32%	6.01	2.37	14.86	3.56			
Optimized	27%	72%	5.76	3.95	21.56	5.49	40	13	14

This optimization process has increased the performance of the solar thermal system, but to reach this goal a huge effort has been invested during the process of numerical model design, validation and optimization. In order to explore the possibility to reduce this simulation effort, an alternative idea has been explored: a rough numerical model is created and used for the design of the controller without undergoing the model validation steps. The fine-tuning of the controller is done in part on the simulation model and in part directly on field where the control parameters are optimized using a reinforcement learning methodology.

This idea has been implemented using two Machine Learning paradigms: **Fuzzy Logic Control** and **Reinforced Learning**. The adoption of fuzzy logic allows to easily design complex non-linear controllers even without a particular knowledge of the control system theory; the application of the Reinforcement Learning method allows to implement self-optimizing mechanism using data collected from the simulation environment or directly from the real plant. These two methodologies can be efficiently combined allowing for a robust model-free learning approach able to find the best operative point of an underlying fuzzy controller.

The adoption of this method is supported by the fact that an easy implementation of a static nonlinear mapping between inputs and outputs is possible settings only a few parameters compared with normal PID controllers where the three parameters (proportional, derivative and integrative) have to be correctly set. Moreover, for the integrated hierarchical control of such a complex systems, FLC seems to be more adequate for design nonlinear controllers based on two or more variables (as reported in Fig.6).

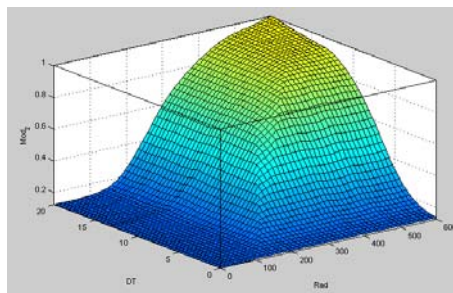


Fig.6 - Fuzzy static map between two inputs and one output

**Reinforcement Learning** is a methodology belonging to machine learning area. When we think about the learning process, we could easily refer to the interaction that humans have with the nature. If we speak, for example, about an infant that approach the real space around him, he trying to explore it without having a a-priori knowledge or a teacher that give him information about the universe that he is discovering. He has only a direct sensorial contact with this environment. During this phase of exploration, the child trying to learn information using a simple cause-effect process, where the consequence of his actions bring him to reach a determinate goal in the most simple and pleasant way.

Following the same approach, the theory of Reinforcement Learning RL is based on the interactions between an active system usually called “**Agent**” with the connected “**Environment**”. As reported in the Fig.7, the agent makes an action on the environment, receives from it an information related to the characteristics modification of the environment (State) and some evaluative feedback signal usually called reinforcement that could be a reward or a punishment.

This leads to clarify better the meaning of learning process that is based on trial and error interaction between agent and environment with the result of discovering which actions yields the most reward by trying them. All the actions have an impact on the environment, and the environment “guides” the learning process of the Agent giving him a feedback in form of rewards. The objective of the whole learning process is to map situations (States) to actions in order to find the best policy to use for maximize the positive effect giving by the environment in form of rewards. In other words, in RL the agent learns how to act when it is in a certain state, given an observation of the environment.

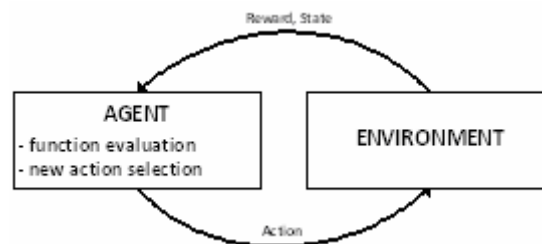


Fig.7 - Reinforcement Learning scheme

A particular class of RL is required to design a self-learning controller without the need of developing a mathematical model of the environment, which goes under the name of model-free RL. Here the agent does not have a prior knowledge of all the system characteristics and cannot make an estimation of the next state resulting from the application of a particular action before having somehow observed its effect. Among the class of model-free RL methods, the **Q-learning** method is adopted because it is widely used and easy to implement. This basic RL algorithm is designed around an evaluation “Q-value” function  $Q(s_t, a_t)$  essentially recording the effect of an action  $a_t$  carried out while the environment (system analyzed) was in state  $s_t$ . Roughly speaking, the value of this function indicate how good is to perform action  $a_t$  in a certain state  $s_t$ . The target of the

Q-learning process is to find a policy that the agent has to follow to maximize the cumulative reward strictly connected with the objective function.

Some modifications have been developed on the traditional Q-learning in order to successfully apply this method to the solar system used to investigate the potential of the above concept. Mainly these changes have been performed because the thermal systems analyzed allow a limited number of useful trials during learning process, if a very long learning process is not acceptable. Moreover, a local convergence criterium has been established, allowing a simple representation of the learning process speed and the percentage of the matrix explored.

As an application example of the developed methodology (FLC + Q-learning), a simple traditional solar thermal system for domestic hot water (Fig.8) has been considered. Different control strategies have been studied on the solar system using a Trnsys model.

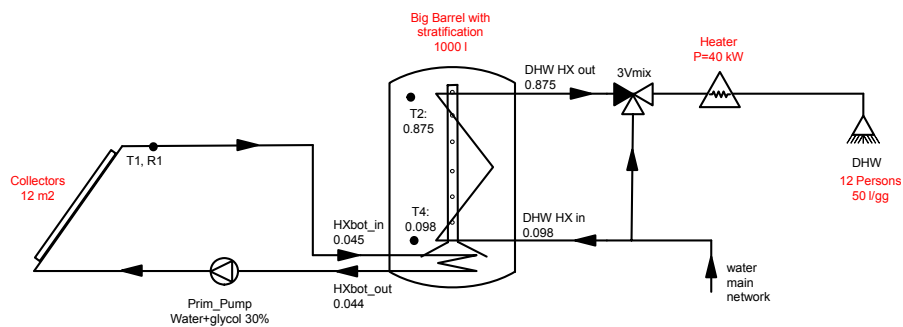


Fig.8 - Layout of SDHW

Three different steps are here shortly reported (Tab.2, Tab.3, Tab.4) in order to show the performance of the Q-learning method applied to the FLC for control the circulation pump of the solar system in Fig.8.

The objective function adopted in the Q-leaning is the seasonal performance factor of the primary solar circuit  $SPF_{coll}$ , evaluated as the ratio between the thermal energy harvested and the electric energy used to drive the circulation pump. In the first table (Tab.2) the yearly result of the simple circulation pump control is reported, based on an on/off hysteresis with fixed radiation values equal to 100 and 150 W/m<sup>2</sup>; a value of  $SPF_{coll}$  of 159 is obtained.

Tab.2 - Result of simple control on minimum radiation - yearly data

Case	$\eta_{coll}$	$SPF_{coll}$	on/off pump	$SPF_{DHW}$
	[-]	[-]	[-]	[-]
B	0.398	159	371	4.962

As a second result, the Fuzzy Logic Controller is applied alone without Q-learning, in order to obtain a rule-of-thumb number describing the performance expectable from the Q-

learning algorithm. Seven different fixed fuzzy control curve are applied. The yearly results with fixed curves are reported in Tab.3, where the action 7 ("a7") shows the best performance in terms of  $SPF_{coll}$ , with a value of 415.

Tab.3 - Comparison of performance with Fuzzy Logic Controller - yearly data

FLC	$\eta_{coll}$	$SPF_{coll}$	on/off pump	$SPF_{DHW}$
	[-]	[-]	[-]	[-]
a1	0.391	<b>114</b>	367	<b>4.90</b>
a2	0.396	<b>150</b>	399	<b>5.05</b>
a3	0.398	<b>188</b>	414	<b>5.14</b>
a4	0.399	<b>231</b>	406	<b>5.14</b>
a5	0.398	<b>287</b>	420	<b>5.11</b>
a6	0.397	<b>352</b>	428	<b>5.01</b>
a7	0.396	<b>415</b>	413	<b>4.92</b>

As a last step, the results of the Q-learning application to the FLC are presented: the 7 above actions are explored by the Q-learning agent. A simulation on consecutive 5 years has been performed and the yearly results are reported in Tab.4: after the second year, a value of the  $SPF_{coll}$  close to the maximum reachable with the simpler FLC (Tab.3) is obtained.

Tab.4 - Q-learning applied to the FLC - Five consecutive years data

FLC + Q-learning	$\eta_{coll}$	$SPF_{coll}$	on/off pump	$SPF_{DHW}$
	[-]	[-]	[-]	[-]
1 <sup>st</sup> year	0.397	<b>370</b>	446	<b>4.97</b>
2 <sup>nd</sup> year	0.396	<b>409</b>	425	<b>4.94</b>
3 <sup>rd</sup> year	0.396	<b>408</b>	422	<b>4.93</b>
4 <sup>th</sup> year	0.396	<b>410</b>	420	<b>4.93</b>
5 <sup>th</sup> year	0.396	<b>411</b>	422	<b>4.92</b>

Looking to the convergence of the problem in the Fig.9, the percentage of the matrix [Q] that has been reached convergence is plotted versus simulation time. In particular, 70% of the matrix exploration is reached after five months. Minor increase is observed in the following 7 months, due to the states that are not often visited during the normal operation of the system. This is reflected in the yearly  $SPF_{coll}$  (Tab.4) that is greater than the simple control (Tab.2) also at the end of the 1<sup>st</sup> year.

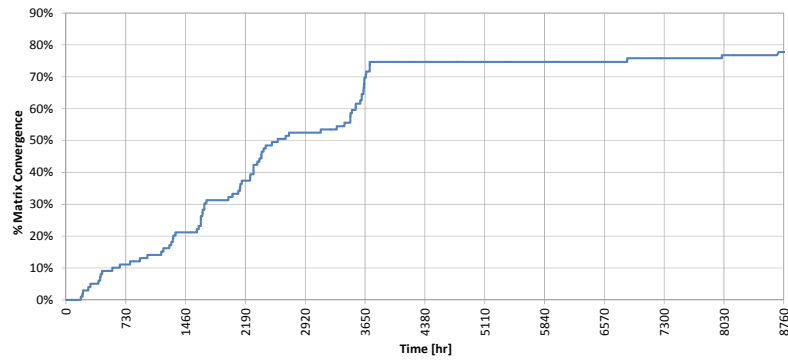


Fig.9 - Matrix convergence

The application of the new control paradigms to a simple SDHW system has shown clearly that the self-learning can be successfully applied to solar systems.

The use of this methodology with respect to different parts of the solar Combi+ system could be a powerful tool for the optimization of a complex systems. Moreover, this new approach allows significant time savings because the validation of the model components is skipped and the optimization of the control is obtained on the field.

Finally the analysis performed highlighted that there are major opportunities to improve the concept in many aspects, with respect to the Q-learning algorithm (other exploration methodologies, objective function and reward definition and state definition), the FLC (controller based on two variables), and the combination of Q-learning and FLC (action on the rule-base definition).

# Chapter 1. Solar thermal systems

## 1.1 Introduction

Solar thermal systems are installations where the solar radiation is captured and converted to heat using a heat transfer medium. This is normally called heat carrier, commonly fluid or air, and it is used directly to transfer the heating to other part of the system (such as thermal storages) or directly to the final users (such as direct heating of buildings or water in swimming pool).

The traditional use of such system is the application to the heating of domestic hot water, and in the last decade applications of solar thermal system providing building space heating as well as domestic hot water (also known as Combisystems) arrived on the market. The International Energy Agency IEA started the “Solar Heating and Cooling (SHC) platform” a program to support the development of the solar technology, promoting the standardization of the system and assisting the national R&D programs. Two projects, called tasks, were developed in the past years. The first one was Task 14 [1] on “Advance active solar energy system” between 1989 and 1995 focused on solar DHW systems while the second was Task 26 [2] on “Solar Combisystems” between 1998 and 2002 focused on the standardization. In recent years, a new application area of solar energy for cooling purposes arrived on the market. Also in this field the IEA started two tasks, the first one was the Task 25 [3] on “Solar assisted air conditioning in buildings” between 1999 and 2004 and another one Task 38 [4] on “Solar air conditioning and refrigeration” between 2006 and 2010. These two tasks were focused on the usage of solar thermal energy with thermally driven cooling devices for providing cold in buildings using air conditioning systems and on the implementation of measures for an accelerates market introduction of these technologies. At the present, another two tasks are in progress, Task 48 [5] “Quality Assurance & Support Measures for Solar Cooling Systems” in which the main objective is to assist the market development of solar cooling systems and Task 45 [6] “Large scale Solar heating and cooling systems” focused on the cost effectiveness, high performance and reliability of large solar heating and cooling systems.

At European level different research programs have been developed in the last 10 years: SACE [7] (2002-2003) where the analysis of the current solar cooling market and its future development; SOLAIR [8] (2007-2009) focused on residential and commercial applications

with the aim to create tools to support the market diffusion of such a systems; SOLAR COMBI + [9] (2007-2010) with aim to identify and promote standardized small scale systems (residential and office with cooling power <20kW); HIGH-COMBI [10] (2007-2011) focused on high solar fraction heating and cooling system with combination of innovative components.

Looking the market state of solar thermal systems for the European Union (Fig.1.1), it is clear that this economical area suffers from the constraints imposed by the financial and economic crises. The result is a contraction of the annual market since the peak of the year 2008 (3.36 GW<sub>th</sub> - 4.8 mio m<sup>2</sup>). Over the past ten years there was a continuous steep uptrend in the growth rate up to 2008, after that a decline in the following two years (2009, 2010) and then a flattering out (2011, 2012). The blue line in the Fig.1.1 shows the trend of new plant capacities in m<sup>2</sup> while the total installed capacity in MW<sub>th</sub> due to new installations is reported as a bar diagram. The traditional market segments are the most affected by the crisis; the domestic hot water systems for the single family dwelling are still affected of the drop in constructions and retrofitting caused by the 2008 crisis.

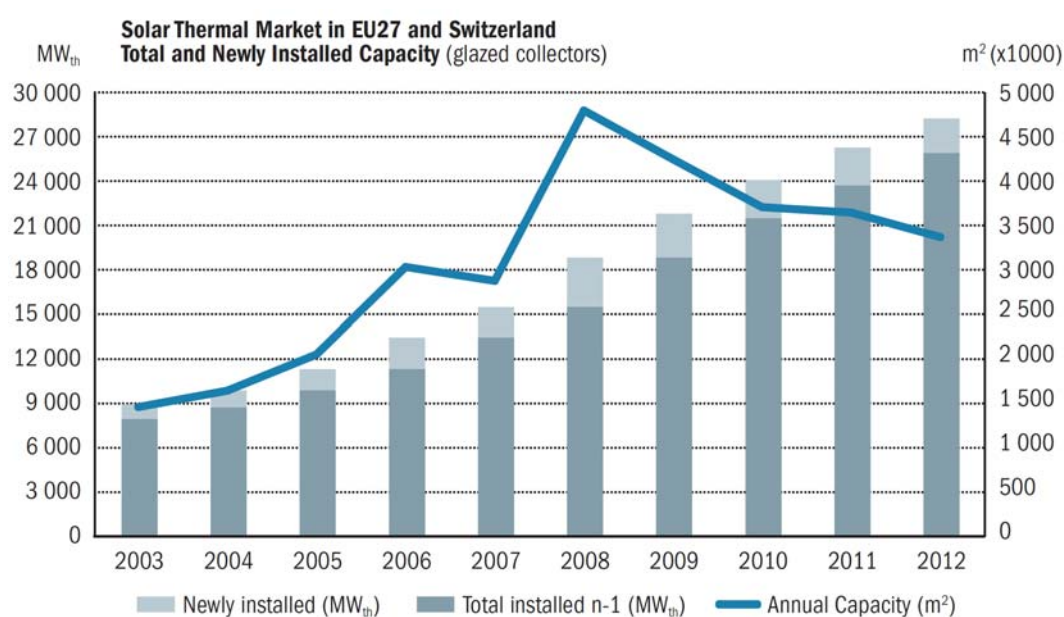


Fig.1.1 - Solar thermal market in EU 27 and Switzerland - Total and Newly installed capacity (glazed collectors) [11]

The Italian market (Fig.1.2) is the second larger EU marker in terms of newly installed capacity after Germany. Also here could be seen the behavior showed in Fig.1.1, related to the whole Europe, with a market decrease of 15% over the last two years. At the end of 2012 the total installed capacity amounted to 2.4 GW<sub>th</sub>.

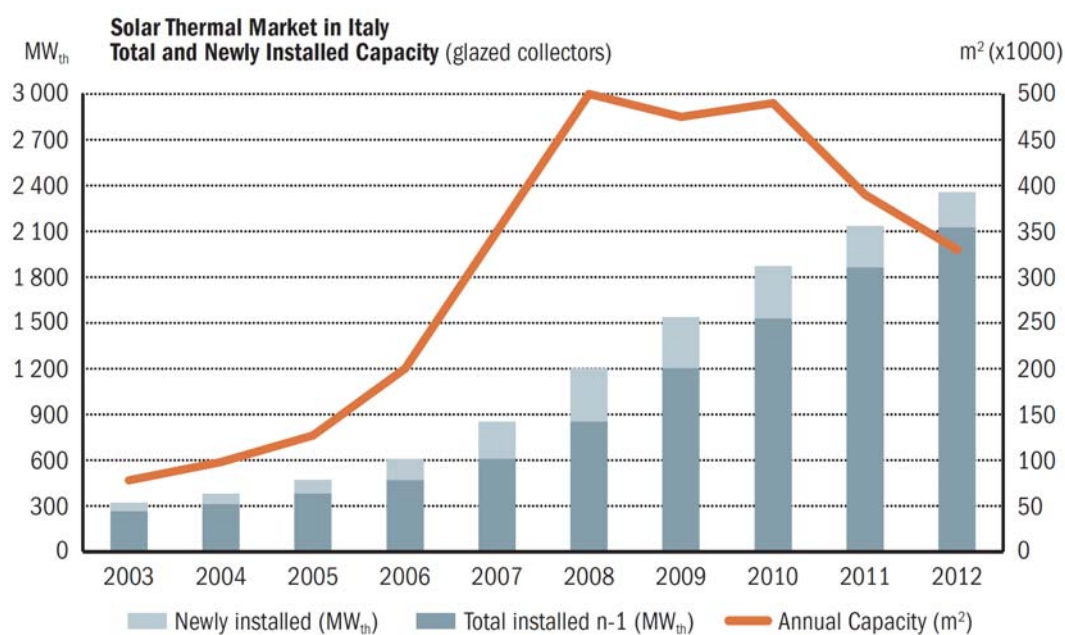


Fig.1.2 - Solar thermal market in Italy -  
Total and Newly installed capacity (glazed collectors) [11]

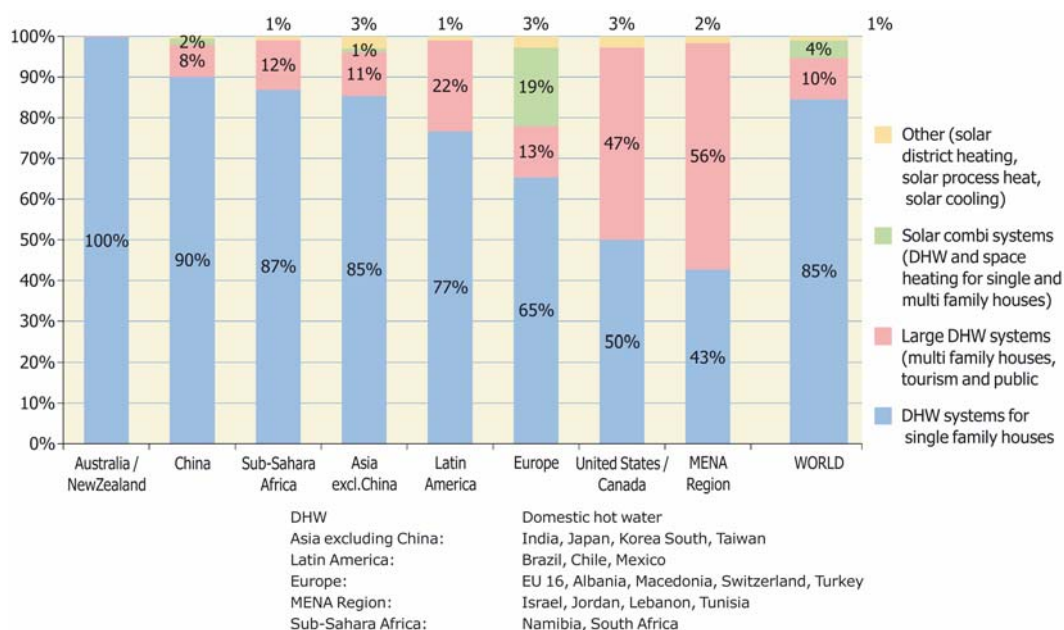


Fig.1.3 - Distribution of solar thermal systems by application of total installed glazed water collector installed capacity (by the end of 2011) [12]



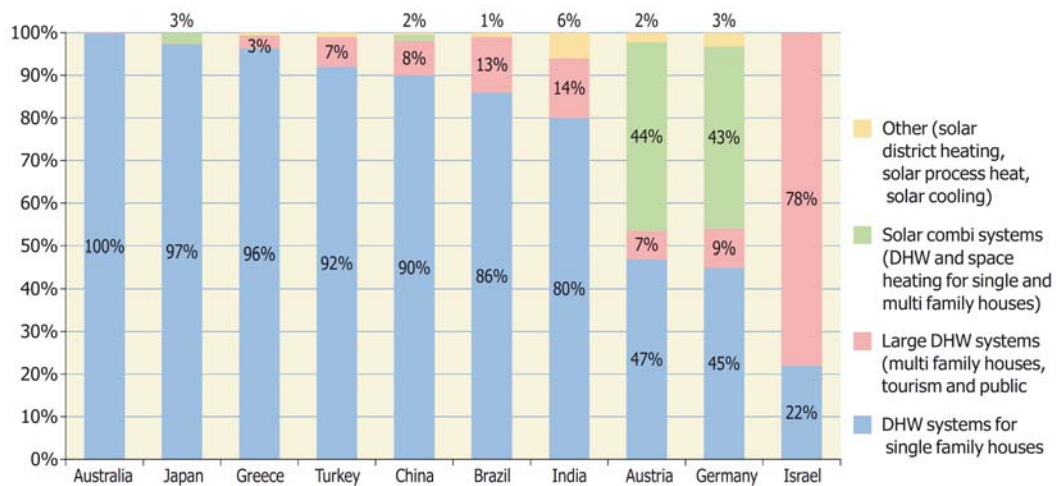


Fig.1.4 - Distribution of solar thermal systems by application for the 10 leading markets of the total installed glazed water collector capacity (by the end of 2011) [12]

An interesting analysis is made on the distribution by application of the total installed capacity [12]. In the Fig.1.3, a global analysis on the solar thermal division is showed including the European data. Here, the level of installation for solar Combi system is close to 20% of the total installations while the cooling installations are assessed around 3%. This is due to the fact that in some European nations, such as Germany or Austria, the market for solar system for DHW and heating purposes is well established and furthermore the percentage of solar thermal system for cooling installed are 3% and 2% respectively (Fig.1.4).

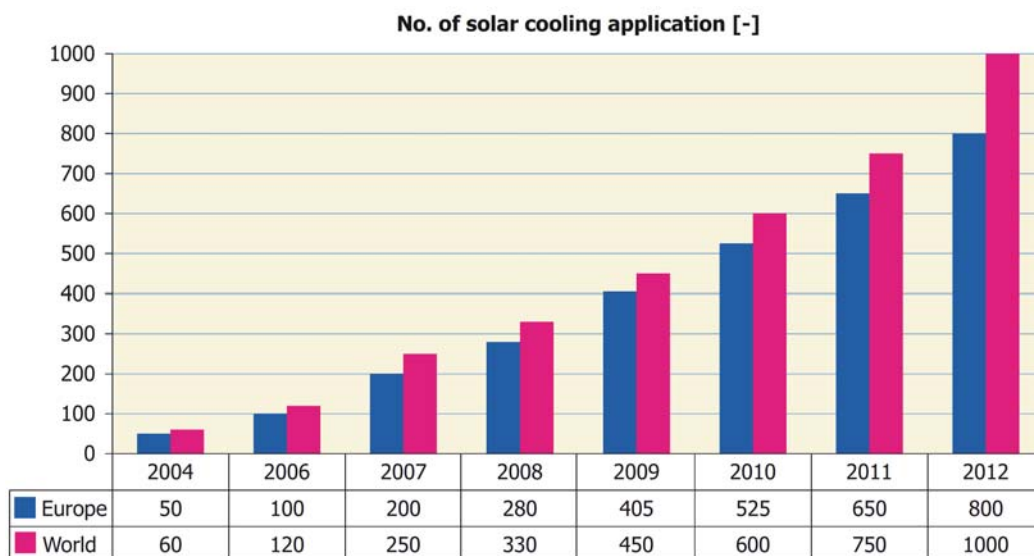


Fig.1.5 - Market development of small to large-scale solar air conditioning and cooling systems [12]

According to the statistic made in 2013 by the IEA, the Fig.1.5 shows the number of solar cooling systems for air conditioning installed. The 80% of the system are installed in Europe (most notably in Spain, Germany and Italy) with an increasing in the number of installations about 23% between 2011 and 2012. These numbers indicate that solar cooling is still a niche market, but one which is developing. The increasing from 2007 is due to the reduction of the cost related to the standardization process on the solar cooling kits [12].

In this chapter the analysis of the three kind of solar thermal systems is made starting from an introduction on the components normally installed in these systems following with a description of the solar thermal system for domestic hot water, solar Combisystems and finally solar Combi+ systems. The chapter ending with a review analysis on the control strategy normally adopted for control these three classes of systems.

## 1.2 Components

The analysis of thermal system for convert solar energy to thermal energy starting with the main component adopted for this conversion. Usually, the most common collector use to transfer solar energy to a heat transfer medium are the solar flat plate collectors. A normal flat plate collector is constitute by a metallic absorber, a cover, the collector box with internal thermal insulation and other components for on-roof installation (Fig.1.6).

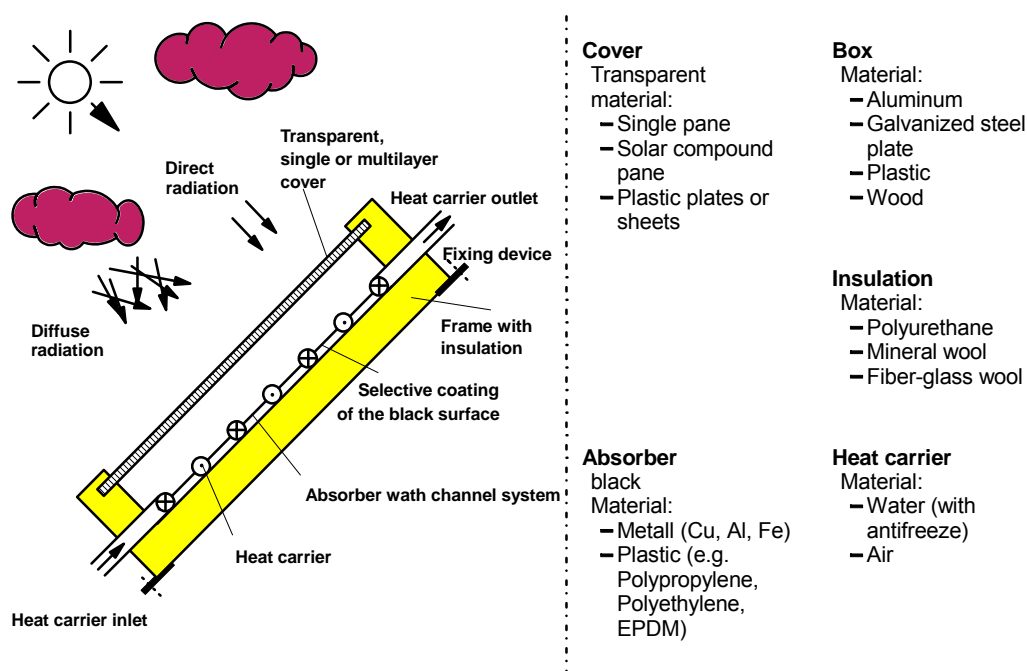


Fig.1.6 - Flat plate liquid collector, components and material [13][14].

Starting with absorber, it is made by metallic material (copper or aluminum), allowing to collect as much solar energy as possible and normally a pipe system is welded on it. In this pipe an heat carrier flows for moving the heating from collector to thermal storage or directly to the loads. The surface of this absorber is normally coated with the aim to obtain the highest value of absorption in the visible and the lowest possible emissivity in the long wave infrared range, reducing in this way heat losses for radiation [15]. Looking at the cover, this is normally used to reduce the convective thermal losses between the absorber element and the environment. An ideal cover has to present transmission coefficient equal to one in the range of the solar radiation instead of reflection and absorption coefficients equal to zero. Furthermore it has to be not transparent in the long radiation spectrum in order to keep back the thermal emission of the absorber. This because the absorber has a surface temperature lower than the sun surface temperature and it reflects a part of the solar radiation in the infrared wavelength. An ideal behavior of the cover is reached with  $\alpha=0$  and  $\rho=1$  in the infrared wavelength but only value close to these ones are reachable with coated glasses [13][15][16]. The collector, in other words, operates following a mechanism similar to the greenhouse effect, allowing the solar energy to reach the absorber, inside the collector, avoiding that the part of this energy reflected by the absorber leave the collector. The consequent effect is a sort of confinement of the energy between the absorber and glass cover.

The collector box, where all the components are installed, has the function from one side to protect them from the external agent, from the other to reduce the heat losses of the component due to conductive and convective phenomena. This box is normally made in aluminum and equipped with an opportune insulation in the back part of the collector and on the four lateral surfaces while in the top part, a glass is mounted with the function of cover explained before.

Different kind of collectors are present on the market. A categorization could be made between collectors that concentrate or not the radiation. Another classification could be made using the heat carrier and the mechanism employed for absorb the radiation. In the following Fig.1.7, an overview of the different technologies are reported divided by concentrating or not technologies or liquid-air collectors [13][15][16].

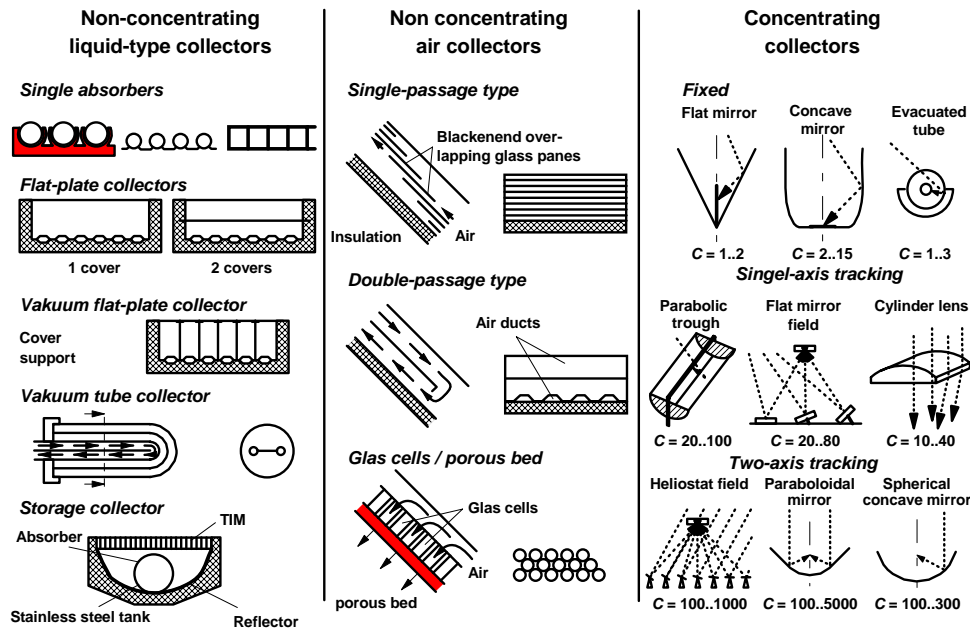


Fig.1.7 - Different typology of solar collectors divided by heat carrier and concentration effect (parameter C is the concentration ratio defined as the ratio of the optically active collector area to the absorber area exposed to radiation) [13]

The other main components normally adopted in solar thermal installation are the storage systems normally installed with the aim to cover the mismatch between solar gain and loads (heating, DHW or cooling) [17][18]. Different kind of systems are present on the market, and could be divided in passive and active storages. When the passive system is mentioned, normally it is referred to the thermal energy storage made by wall, floor or ceiling in buildings and is passive because the loading and unloading processes are incontrollable compared with the active system. The heat transfer between the storages and the environment is only driven by the storage-ambient difference of temperature. The active storage could be the building active layer, such as a system to activate the thermal mass of the building or a devices such as thermal storage where an insulated system is used for storing a fluid or a medium and actively controlled during the energy charging and discharging phases. The medium used in the storage is chosen in function of the heat capacity and thermal level at which the thermal energy has to be stored and could be liquid heat storage, solid matter storages and latent stores. In solar thermal systems particular care has to be taken during the design of such a system, in order to maximize the solar thermal energy gained For complex system (solar thermal system for DHW, heating and cooling) guidelines are given on the dimension of the components (mainly solar collector area and thermal storages volume function of nominal cooling power) but dynamic simulations are suggested in order to find the best characteristics between these parameters [18].

The absorption part of the system (thermal collectors) and the thermal storages are connected by pipes. The pipes material is normally chosen in function of the absorber

material. This is due to the fact that different materials can be coupled in the building of such a system creating some problem related to the corrosion (e.g. absorber in aluminum and pipes made in copper without galvanic insulation). The diameter of such a pipe is designed in function of the mass flow selected for the heat carrier and its composition. This is a balance between the pressure losses and the heat exchange coefficient. Some indications about pipes dimensions and insulation are reported in the EN12977-1 [19].

As we saw in the classification made in the Fig.1.7, the heat carrier can be usually liquid or air. The heat carrier employed in such systems has to be characterized by an high specific heat capacity in order to store as max heat as possible before to “discharge” it to the storage system. Related to the pressure drop, the carrier has to possess low viscosity in order to reduce the resistance to flow between the absorber system and the storage. Other physical properties that, in the choice of the carrier, are important are the freezing and boiling temperatures that has to be out of the operating temperature range and the lowest values possible of characteristics that can make them dangerous for humans (toxicity, flammability, etc.).

Normally the fluid employed into the solar thermal systems is a mixture of water and antifreeze with an anticorrosive agent for protect the system from freezing problem during the winter seasons. These additives, the most used are ethylene and propylene glycol, normally have the disadvantages to possess less specific heat capacity and higher viscosity compared with pure water with the results of an increasing of the pressure losses for moving the fluid and a worse heat exchange coefficient [20]. Another problem could be the thermal decomposition of this mixture that may lead to highly corrosive product that can damage the plugging of the pipes. This problem appears when high temperature is reached (stagnation problem). For the fluid normally used (water + glycol) this thermal level is around 170 °C ([14]).

Two different kind of solar thermal systems are present on the market. Their definition and operation will be explained in the following subchapters but here a division between natural circulation system and forced driving system is made [13][14]. The first is a system where the heat carrier flows between the collector and the thermal storage using natural circulation. In this system the force used for move the fluid is only related to the difference of density between cold and hot fluid. The second is a forced solar thermal system, where a pump is required to operate on the collector circuit. This pump is normally a centrifugal pump usually equipped with a manual adjustable speed control or an electronic equipment that continuously control the mass flow or the pressure elaborated by the pump.

Another component normally installed in solar thermal system is the heat exchanger. This is adopted with the function to transmit the thermal energy between fluids or substances without a direct contact between them. Normally heat exchangers are used when the thermal storage system is charged and discharged indirectly, and in solar thermal application is normal to use both internal or external heat exchangers. The heat transferred depends on the difference of temperature of the two media, the exchange area and the characteristic of the flow on both sides of the heat exchanger (flow speed and heat transfer medium).The internal heat exchangers from one side do not require

much space but at the same time their size are limited to the dimension of the thermal storage from the other they are characterized by a low heat output and require an high difference of temperature between two media. The external heat exchange has the problem related to the space occupied but in the other hand the heat transfer output is higher with lower difference of temperature.

Other components are installed in the real plant in order to promote the correct system operation: deventing device that is installed in the higher part of the circuit allowing the removing process of the air during the first filling process; expansion vessel used for absorb the volume expansion of the entire medium present in the circuit between the range of operative temperature.

### 1.2.1 Solar collectors energy balance

In order to describe mathematically the collector behavior, a general energy balance equation could be write as follow:

$$\dot{Q}_{coll} = I_g \cdot A_{coll} - \dot{Q}_{re,abs} - \dot{Q}_{rad} - \dot{Q}_{conv} - \dot{Q}_{cond} \quad [kW] \quad (eq.1.1)$$

Where the definition of power gained by the collector ( $\dot{Q}_{coll}$ ) is equal to the radiation that arrive on the collector subtracted by the thermal losses for reflection, radiation, convection and conduction.

The definition of these four values subtracted are:

$$\dot{Q}_{re,abs} = I_g \cdot A_{coll} \cdot (1 - \tau_{cov} \cdot \alpha_{abs}) \quad [kW] \quad (eq.1.2)$$

$$\dot{Q}_{rad} = A_{coll} \cdot \epsilon_{abs} \cdot \sigma (\bar{T}_{abs}^4 - T_a'^4) \quad [kW] \quad (eq.1.3)$$

$$\dot{Q}_{conv} + \dot{Q}_{cond} = A_{coll} \cdot U^*_{coll} \cdot (T_{abs} - T_{amb}) \quad [kW] \quad (eq.1.4)$$

Where:

$\alpha_{abs}[-]$ : absorption coefficient of the absorber surface;

$\tau_{cov}[-]$ : transmittance coefficient of the glazing cover;

$\epsilon_{abs}[-]$ : emission coefficient of the absorber;

$\sigma = 5.67 \cdot 10^{-8} \left[ \frac{W}{m^2 \cdot K^4} \right]$ : Stefan-Boltzmann constant;

$\bar{T}_{abs}[^\circ C]$ : mean absorber temperature;

$T_a'[^\circ C]$ : sky temperature;

$T_{amb}[^\circ C]$ : ambient temperature around collector;

$U^*_{coll} \left[ \frac{W}{m^2 \cdot K} \right]$ : mean heat transfer coefficient for convective and conductive heat losses.

A parameter called efficiency ( $\eta_{coll}$ ) is evaluated for compute the performance of the collector and is given by the ratio between power gained by the collector and the solar radiation that arrive on the collectors plane. Using the terms given before, the efficiency of the collector could be write as:

$$\eta_{coll} = \frac{\dot{Q}_{coll}}{I_g \cdot A_{coll}} = \tau_{cov} \cdot \alpha_{abs} - \frac{U^*_{coll}}{I_g} \cdot (\bar{T}_{abs} - T_{amb}) - \frac{\epsilon_{abs} \cdot \sigma}{I_g} \cdot (\bar{T}_{abs}^4 - T_a^4) \quad [-] \quad (eq.1.5)$$

Commonly this index is expressed in an approximated form:

$$\eta_{coll} = c_0 - c_1 \cdot \frac{(\bar{T}_{abs} - T_{amb})}{I_g} - c_2 \cdot \frac{(\bar{T}_{abs} - T_{amb})^2}{I_g} \quad [-] \quad (eq.1.6)$$

Where  $c_0$ , normally called optical efficiency, is related to the optical losses of the collectors (product of the cover transmission coefficient and the collector absorption coefficient);  $c_1$  is related to the heat losses due to convective and conduction losses and related to the difference between the average temperature of the absorber and the ambient temperature. The parameter  $c_2$  is the quadratic term and represent a simplified approach to the radiation losses. An example of the efficiency curves and the application fields of four different kind of liquid collectors is reported in Fig.1.8. The different non-concentrating, liquid-type collectors are reported in the Tab.1.1 where some technological parameters (range of operative temperature, efficiency) are indicated with the field of application.

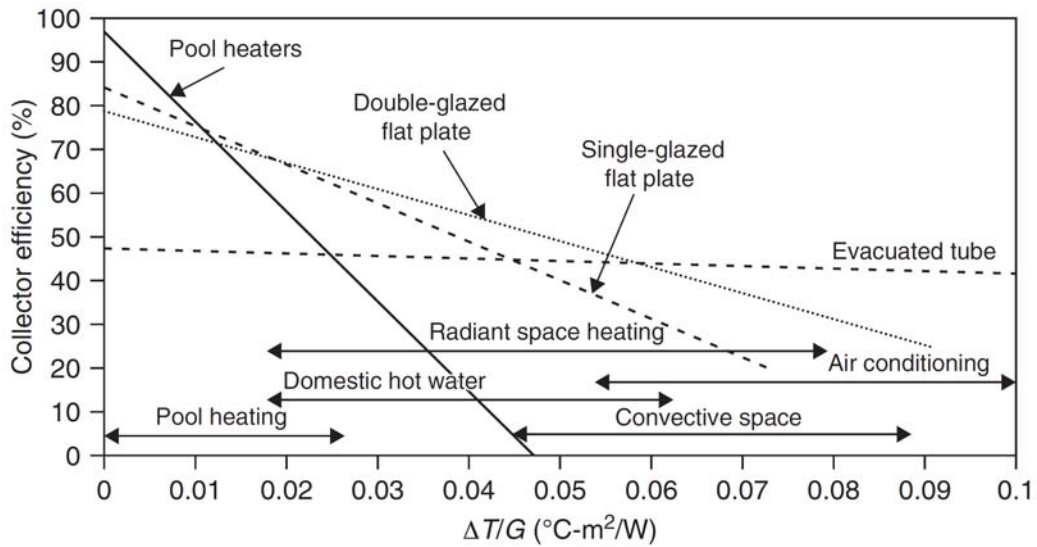


Fig.1.8 - Collectors efficiencies of various liquid collectors [16]

Tab.1.1 - Parameters of various non-concentrating liquid-type collector designs [13]

	Optical Efficiency	Thermal loss factor [W/(m <sup>2</sup> K)]	Typical Temperature range <sup>a</sup> [°C]	Required production input <sup>f</sup>	Typical application
Single absorber <sup>b</sup>	0.92	12 – 17	0 – 30	small	OASW
Flat-plate collector 1 <sup>c</sup>	0.80 – 0.85	5 – 7	20 – 80	medium	DHW
Flat-plate collector 2 <sup>d</sup>	0.65 – 0.70	4 – 6	20 – 80	medium	DHW
Flat-plate collector 3 <sup>e</sup>	0.75 – 0.81	3.0 – 4.0	20 – 80	medium	DHW, SH
Vacuum flat-plate collector	0.72 – 0.80	2.4 – 2.8	50 – 120	large	DHW, SH, PH
Vacuum-pipe collector	0.64 – 0.80	1.5 – 2.0	50 – 120	very large	DHW, SH, PH

**OASW**: Open-air swimming pool; **DHW**: Domestic hot water; **SH**: Space heating; **PH**: Process heat;  
<sup>a</sup>: medium work temperatures; <sup>b</sup>: black, non-selective, not covered; <sup>c</sup>: non-selective absorber, single cover; <sup>d</sup>: non-selective absorber, double glass and supporting foil; <sup>e</sup>: selective absorber, single cover; <sup>f</sup>: necessary effort for the production of the absorber.

Another interesting figure (Fig.1.9) is reported with the aim to show graphically the difference between optical and heat losses and the behavior of a flat plate collector efficiency curve when the global radiation is modified. Furthermore, the difference of the behavior between the real and the approximate model is pointed out. This difference is main due to the approximation of the efficiency curve with the quadratic difference of temperature for the radiation losses of the collectors [13].

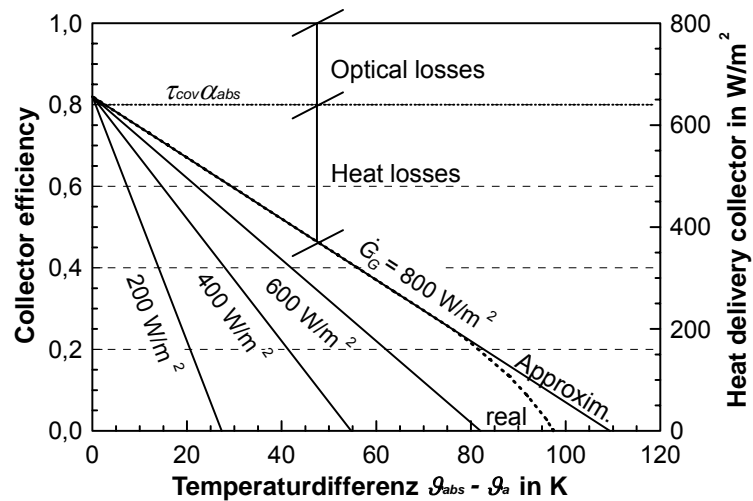


Fig.1.9 - Characteristic curves of single flat-plate collectors ( $\tau_{cov} \cdot \alpha_{abs} = 0.82$ ;  $\dot{G}_G$  = global radiation on horizontal receiving) [13]



Normally, for the energy balance calculation and in simulations, another parameter is considered: the Incident Angle Modifier (IAM). It describes the dependency of the transmission through the cover system of the collector (glazing) with the variation of the incidence angle between the normal direction of the collector and the normal direction of the solar beam radiation. The IAM for irradiation normal to the collector plane (0°) is 1 by definition and its effect is to reduce the optical efficiency of the solar collector. For a single cover collector the equation that describe this effect is:

$$IAM(\theta) = 1 + b_0 \cdot \left( \frac{1}{\cos\theta} - 1 \right) \quad (\text{eq.1.7})$$

### 1.3 System for heating domestic water (SDHW)

The components introduced in the previous subchapters are normally installed in the solar thermal system. The most common and simple configuration of this kind of application is the solar thermal system for heating the domestic water. The diffusion of such systems is due to the fact that they are composed by a few component connected in a relatively simple manner. The importance of such a system is increased recently because the load for heating is drastically decreased by the improvement of the buildings insulation or passive solar energy techniques. The fraction of the heating energy request for domestic hot water in this scenario became a significant part of the annual heat load. The diffusion of such a system is due also to the standardization made by the factories that built and sold optimized solution (usually called “kits”) either from the economical point of view than from the performance ensured.

This kind of systems are still by far the major solar thermal application in Europe, as reported in Fig.1.3, where this kind of applications are designed for deliver 100% of the domestic hot water requirements in summer and 40-80% of the total annual hot water demand [14]. These systems are composed by solar collectors array, energy transfer system, storage tank and usually include also a supplementary heater for cover the heating requests when no solar energy is available.

The solar collectors convert the solar energy into heat absorbing the radiation. This energy is absorbed by an heat carrier (usually an heat transfer fluid) that circulates in the collectors. This energy could be stored in an opportune thermal storage or directly used. Two types of solar water heating systems are available, the first is a direct or open loop system where the water is directly heated by the collectors or an indirect (closed system) where the water is heated up indirectly using an heat transfer fluid that is heated in the collectors and passes through an heat exchanger. As mentioned in the previous chapter, a classification can be made function of the mechanism used for heat carrier movement. The first ones are natural systems where the movement of the fluid is caused by the difference of fluid density differently from the second ones where the circulation of the fluid in the collectors is due to an active system such a circulation pump. A wide range of collectors are employed in such a system like flat plate, evacuated tube and compound parabolic in according with what reported in Fig.1.8 and Tab.1.1.

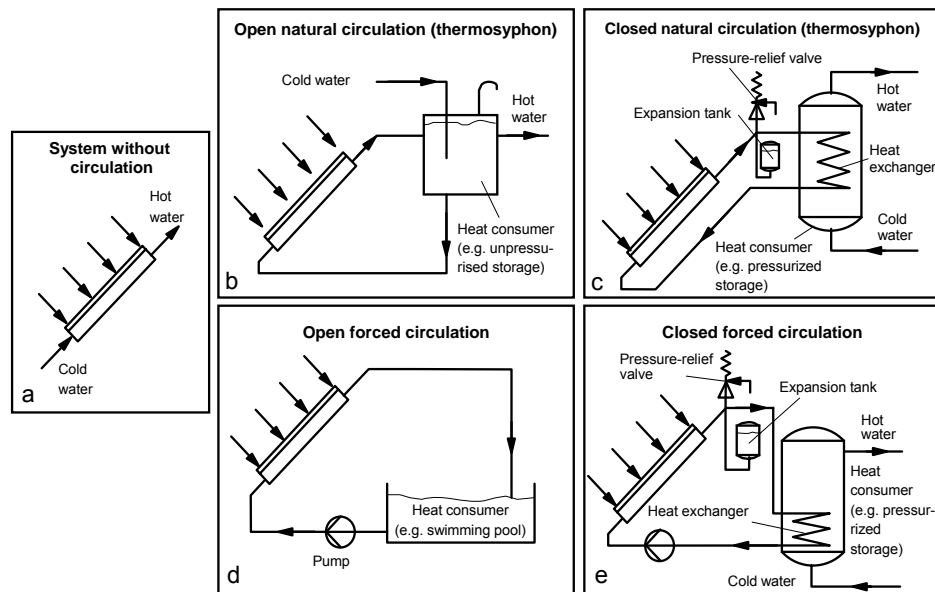


Fig.1.10 - Solar active and passive system [13],[14].

The natural circulation system is based on the fluid mechanism of natural circulation and sometimes it is called “thermosiphon system”. It is also usual to refer to such a system with the name “passive” because no active system is installed for the movement of fluid (pump) between the collectors and the storage. For this movement the thermosiphoning effect occurs because the density of water decreases at the increasing of the temperature level. The solar energy collected from this system is transmitted to the fluid increasing its temperature, this through an expansion becomes less dense and try to reach the highest part of the circuit where a thermal storage is normally installed. As a consequence, the colder water is pushed to the bottom of the collector and this circulation is continuous when the sun is shining. Particular attention is made in the design phase in order to reduce the pressure losses allowing the correct operation.

The advantages of such a system are the absence of the pump, the controller and the related electrical consumption due to their functioning in phase with the sun presence. In their basic form these systems can work without sensors and control instruments that make these solutions simple, robust and very cost effective. This is an advantage from the costs point of view but from the control point of view in the closed natural circulation systems some problems can appear when the maximum temperature of the storage is reached, and the sun keeps on shining. In this situation the water in the storage starts boiling and a steam release valve has to be installed in the water circuit [13][14].

Furthermore, other disadvantages are in terms of volume occupied that makes natural circulation systems not very aesthetically attractive. Moreover the quality of the water, when an opening system is installed, could become extremely acid or hard, compromising the correct operation of the system. To prevent the freezing and corrosion problems, when this system is not installed in the Southern Europe, the collector circuit can be closed. In this way in the primary circuit flows the mixture of water/glycol and in a second

circuit or directly in the thermal storage drink water. Schematic figures of open and closed natural circulation systems are reported in Fig.1.10, case b and case c. Typical DHW thermosyphon system for one dwelling has 2-5 m<sup>2</sup> of collectors area and 100-200 liters storage [13][14].

The forced circulation system is based on an active system that move the heat carrier through the collectors. Also in this case the open or closed systems could be defined and this two different typologies are reported in Fig.1.10, case d and case e respectively. Typical DHW forced circulation systems for one dwelling has 3-6 m<sup>2</sup> of collector area and 150-400 liters storage.

Going more in detail with the optimum flow rate of a system, high flow rate have employed in pumped circulation solar water heaters to improve efficiency of the collectors increasing the heat removal factor (related to the capacity of the absorber to collect energy and strictly connected with parameter  $c_0$  of the efficiency equation eq.1.6). When the entire system is considered and not only the performance of the collectors, it is found that the solar fraction can be increased if a low flow rate and thermally stratified tank is adopted ([16]). According to [14] and [16], the flow in the loop of collectors is in the range of 12-24 l/h for each square meter of the collector area, instead of 30-80 l/h for square meter for high flow system. A deep analysis on the control is reported in Chapter 1.8.

### **1.3.1 Hygienic requirement for domestic hot water**

During the store of drinking water, particular care has to be taken with the material of the components such as storages, pipes or heat exchangers where this water flowing. In addition to these hygienic requirements attention should be given in order to prevent the growing of microorganisms such as legionella, that create a problem when inhaled and reach the lungs. Legionella in this case could cause an infection creating illness (pneumonia) or in the worst cases the death.

These microorganisms are a problem for the solar thermal storages because they may occur when the water temperatures are between 30 and 40 °C (favorable growing temperature level) standing still over a long time period. The installations with high risk of legionella presence are:

- Distribution systems of domestic hot and cold water (network, tanks, boilers, heaters, and wells) from hospitals, and other installations of collective use with showers (hotels, sports installations, saunas, etc.);
- Refrigeration towers and evaporative condensers and their water circuit;
- Humidifiers that generate aerosols, and similar equipment;
- Hydro massage baths;
- Thermal installations and their distribution systems;
- Other installations using water between 20 and 60°C and that could produce aerosols during any operation, or maintenance.

The normal method used for controlling legionella in the potable water circuit is the thermal prevention and disinfection. In order to reduce the growing effect, the

temperature of the storage should stay below 20-25°C or above 50°C. What usually in practice is implemented, is a thermal cycle where the temperature is increased in the storage for a different time function of the temperature level adopted for the thermal treatment, as reported in Tab.1.2. Alternatively, a chemical or physical disinfection and prevention is implemented [22].

Tab.1.2 - Re-heating time for prevent legionella growing as function of temperature [14]

Temperature [°C]	Re-heating time
60	10 min
65	1 min
70	10 sec

Another approach used to prevent legionella growth is an appropriate hydraulic design of the solar thermal system. These microorganisms grow mainly in the thermal storages, so a simple way to avoid this phenomena is to use a system where the water used for satisfy the domestic hot water demand is not stored in a water tanks but by means the usage of heat exchangers, creating a sort of instantaneous heating system for the drinkable water. In this way the water is only heated up when it is used (Fig.1.11 case “a”). Another solution, instead of an instantaneous heat exchanger, is the usage of a small store for domestic hot water, connected to a big storage dimensioned for the correct function of the solar thermal system. This solution with small storage for DHW allow a fast turnover of the water avoiding legionella growth.

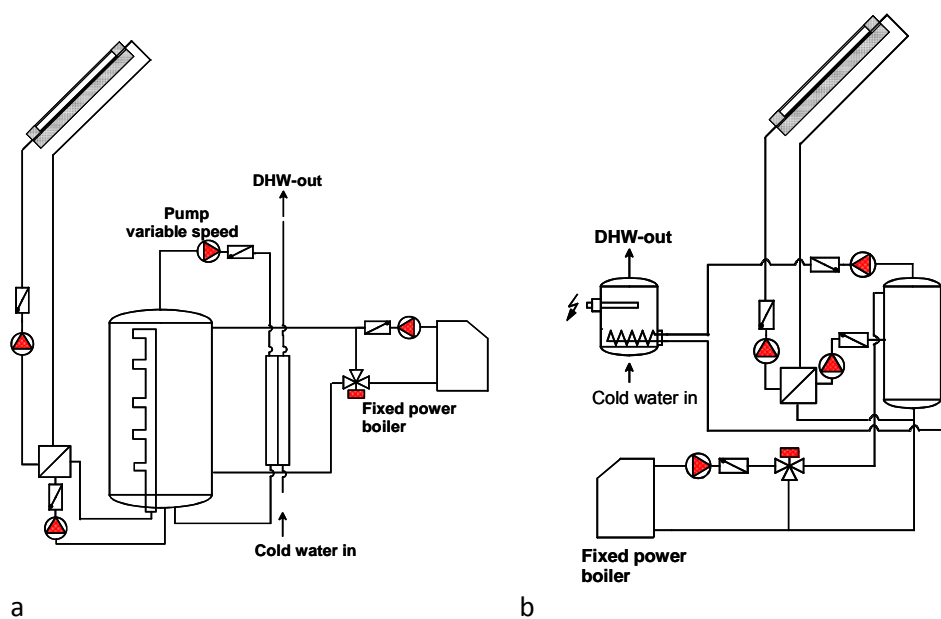


Fig.1.11 - Hydraulics solution adopted to avoid legionella [14]

#### **1.4 Solar Combisystems (DHW and space heating)**

Nowadays the combination of thermally well insulated buildings and low-temperature heat supply systems offered a wealth of new possibilities for solar space heating systems with short-term storage. Before 1990 the industry offered this kind of systems but there were lacking of methodologies for design in different climatic conditions and for compare different layouts. For these reasons the International Energy Agency (IEA) developed the Task 26 of the Solar Heating and Cooling Program between 1998 and 2002 [2]. In this program, the development and optimization of Solarcombi systems for detached one-family house, groups of one-house family and multi-family houses were investigated with the aim to develop standardized classification of systems, evaluation process and design tools [23].

The main rule of such a system is to deliver as much solar gain as possible into the storage reducing the thermal losses and distribute all heat required by the heat sinks (heating load and DHW). Normally this kind of system is equipped with an auxiliary heating system that is used for cover the energy requests when no solar energy is available or stored. The calculation of the volume of the storage is essential for an efficient operation of the integrated system (solar thermal system + auxiliary heater) for this reason, the heat storages are one of the key element of the combisystem installations. The collector size for this application is typically in the range of 7-20 m<sup>2</sup> and tank in the range of 300-2000 liters. Different solutions were analyzed during the Task 26 [2]. Some of these configuration are here reported with a short description of the characteristics.

##### **1.4.1 Small solar combisystems**

Starting from this simple configuration, three different kind of systems can be detected, as reported in the Fig.1.12. In the system “a”, the thermal energy from heating space is extracted from the DHW tank using an internal heat exchanger. The energy available for space heating purposes is normally limited, due to the fact that the auxiliary heat exchanger in the barrel is positioned above the heat exchanger for heating space purposes, suggesting that only the surplus of solar energy can be used for heating purposes. Normally in this heat exchanger additional sink is connected, such as radiator system of the bathrooms due to their high operative temperature level (compared to low temperature radiative heating systems). Other heating space loads are fulfill by an auxiliary boiler. A problem of this system could be the cooling down effect of the DHW store when the energy stored is used for heating. To address this issue, the “b” configuration (Fig.1.12) is implemented, where a direct heating from the collectors is realized only when the set temperature in the store is reached.

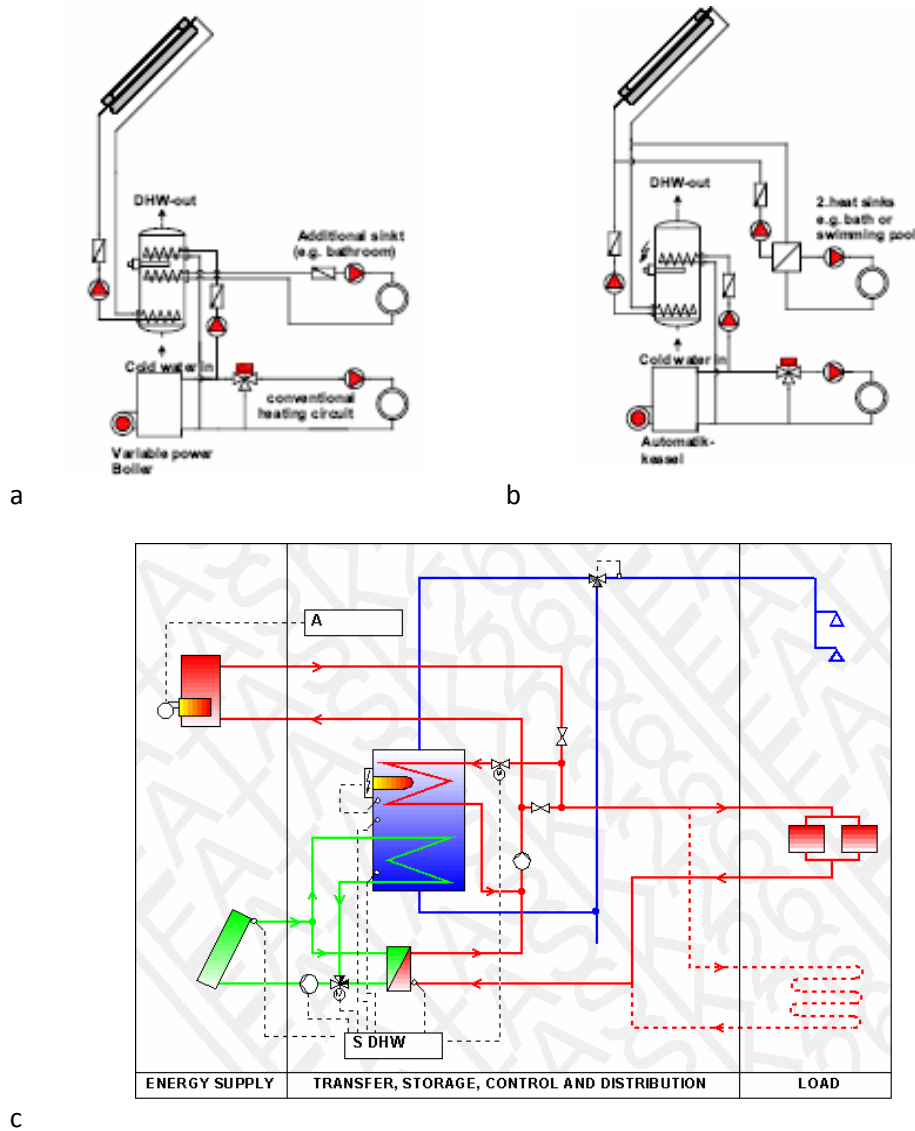


Fig.1.12 - Three examples of small solar combisystems  
(a,b [14]; c, system #2 of IEA TASK26 [2])

Both of these two configurations have the problem to fulfill the energy loads for additional sink only when solar thermal energy is stored (case "a") or there is presence of sun (case "b"). For cover the heating space request also in these cases, a scheme of the system used is reported as case "c" (Fig.1.12). Here, two heat exchangers are installed in the DHW store one connected to the collector circuit and one with the auxiliary heater. A direct connection between collectors circuit and heating system, through an appropriate three-way valve, allow to use directly the solar energy when a surplus of energy is present (e.g set point temperature reached in the upper part of the thermal storage). If no solar energy is available, a system of valves is installed to create a direct connection between

auxiliary heater and heating loads. This kind of configuration is derived from the standard solar system for domestic hot water (Fig.1.10) with an oversizing of the solar collectors area (to have more solar energy to deliver to the heating system) and with a secondary heat exchanger for the auxiliary heater.

The disadvantages of such a system is the absence of a thermal storage for space heating, this means a direct transfer of energy to the building with a decrease of internal comfort. For reduce this effect, normally is installed an emission system with high capacitance, like the low temperature radiative heating floors, that allow to increase the solar energy used by means of the structure of the building employed as a space heating storage. The combination of high solar energy utilization maintaining internal comfort is the challenge of the control system for these kind of applications.

#### 1.4.2 Two stores systems

In the two stores configuration, the heating storage is divided from the storage for DHW. Traditionally belongs to such configuration the heating system with an added solar thermal system for DHW. In the Fig.1.13 and Fig.1.14, two examples of this kind of system are reported. The difference between these two systems is the hydraulic connection between the auxiliary heater and the system of distribution. In the first one, case “a”, between the auxiliary heater and the distribution system there is a thermal storage, while in the second one, case “b”, the energy supply system is connected directly with the loads. In this case a backup system with fixed power can be installed or heating system that need a big volume of water to function correctly (e.g. wood heating system) while in the second a variable power boiler is installed allowing an improvement of the system performance (in terms of energy saved and better control of internal comfort).

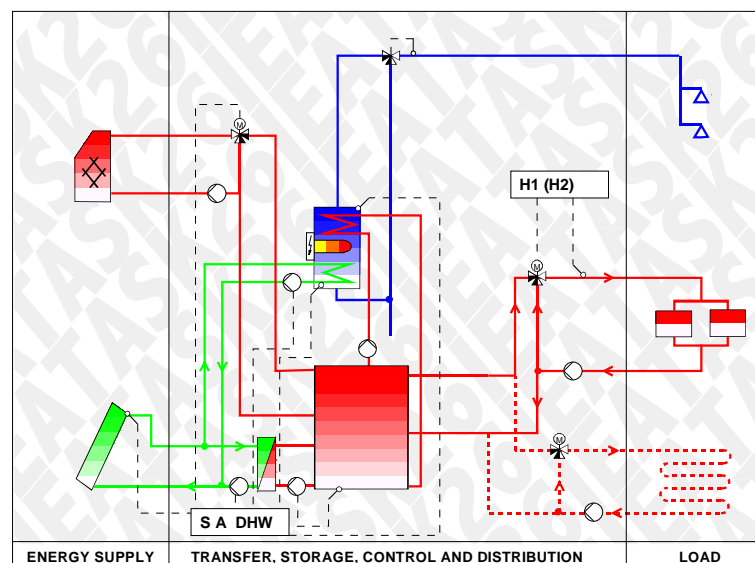


Fig.1.13 - Two-stores combisystems (system #13 of IEA TASK26 [2])

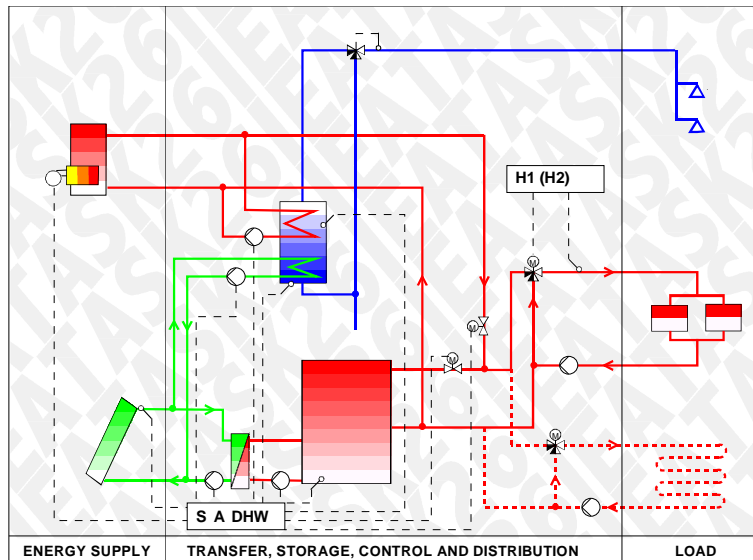


Fig.1.14 - Two-stores combisystems (system #14 of IEA TASK26 [2])

### 1.4.3 Tank in tank system

The system reported in Fig.1.15 is a compact solar combisystem. A particular kind of storage is installed in this configuration with a store for heating that includes a particular shape DHW tank. This tank in tank allows to preheat the water for DHW starting from the bottom of the storage and after heating a specific volume of at the top of the tank. The main advantage of such a system is the limited number of components (pumps, valves) that lead a simple design and control reducing the risk of failure.

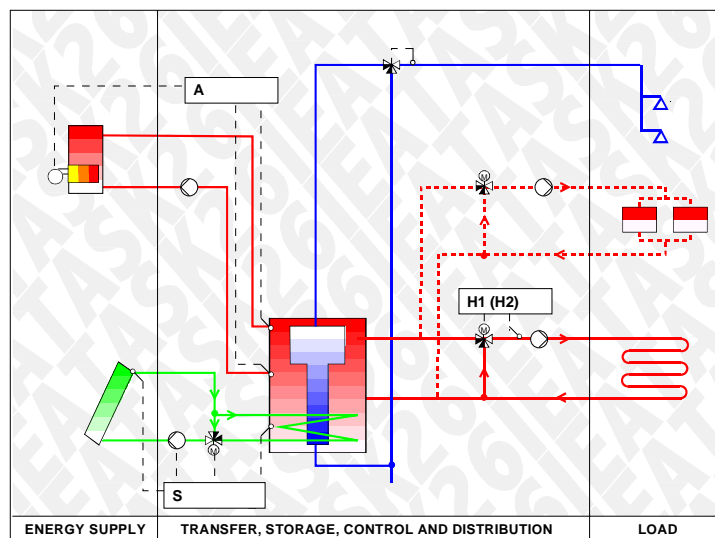


Fig.1.15 - Tank in tank combisystem (system #9 of IEA TASK26 [2]).



#### 1.4.4 Space heating store with load side heat exchanger for DHW and external auxiliary boiler

Differently from the configurations presented previously, in this system (Fig.1.16) internal heat exchangers are installed for DHW preparation. Moreover, two heat exchangers are connected to the primary solar circuit with the aim to increase the internal temperature stratification. In this configuration the auxiliary heater installed could be a wood boiler or pellet boiler that normally need long running time and high thermal storage volume instead of a variable power boiler or fixed power gas boiler that need less water volume for the correct operation. According with the class of boiler used, the outlet connection is located in the bottom part of the storage or in the middle. In the load side a 4-way valve is installed allowing the use of the two thermal level of the energy stored in the tank. The instantaneous DHW preparation system has the advantage to avoid legionella risk.

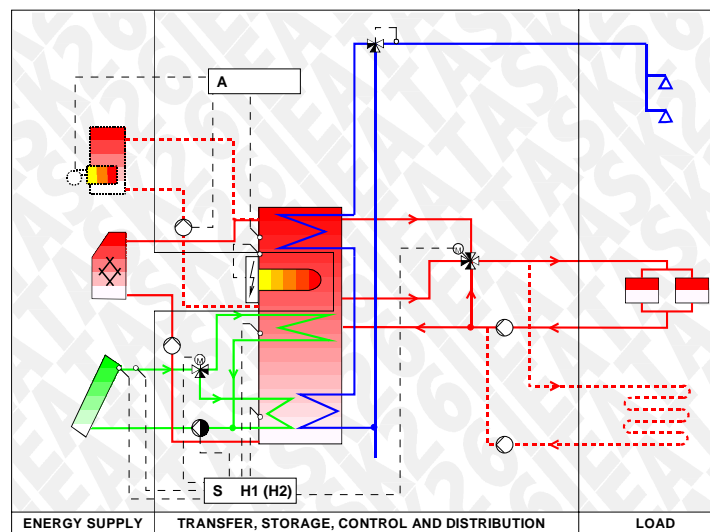


Fig.1.16 - Space heating store with load side heat exchanger for DHW and external auxiliary boiler (system #12 of IEA TASK26 [2]).

#### 1.4.5 Two stratifiers in space heating storage with external heat exchanger for DHW

The last system presented (Fig.1.17) is a compact system, where all the components used (flat plate heat exchanger, auxiliary gas condensing burner) are integrated in a compact unit. Also in this case the DHW is directly heated using an external flat plate heat exchanger that guarantees the hygienic quality of the water used avoiding legionella problems. Inside the thermal storage a device is installed in order to improve the thermal stratification effect.

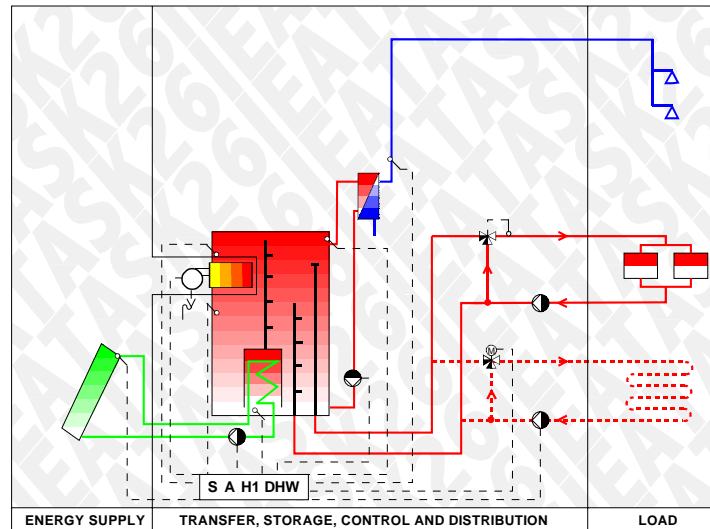


Fig.1.17 - Combi-system with solar stratification unit, integrated burner and external heat exchanger for DHW production (system #15 of IEA TASK26 [2]).

### 1.5 Solar Combi+ systems (DHW, space heating and space cooling)

Increasing the complexity of the systems, the analysis arrive to solar thermal system that use the solar energy for cover the thermal loads related to DHW, space heating and cooling. For DHW and space heating an introduction and explanation of the systems are made in the previous part of this chapter. For the cooling loads, heat generated with solar collectors can be converted into cooling using thermally driven refrigeration or air-conditioning sorption technologies.

There are different ways to use the solar energy for cooling process or air conditioning purposes. In the Fig.1.18 an overview on these different ways is given. A first classification is made between thermal or electrical driven system using from one side solar thermal collectors, from the other photo-voltaic modules. Going more in detail with thermal systems, the heat collected can be used in open or closed cycles and here all the systems used in solar Combi+ systems are included. In the open cycle, the system is connected directly with atmosphere and the water is used as refrigerant while in the closed cycle, the cycle is isolated and the refrigerant could be different, such as ammonia. Normally the opening cycle systems most diffused are Desiccant Evaporative Cooling systems (DEC) with a desiccant as the sorbent for direct treatment of air in the ventilation systems.

All the systems analysed in this work are based on the sorption technology. This technology that employ the sorption principle, is the base of thermal refrigeration techniques. The cooling effect in these systems is obtained from the chemical or physical changes between the sorbent and the refrigerant. The closed cycle, mentioned before, is mainly based on two different mechanisms: the liquid sorbent, based on absorption process or the solid sorbent based mainly on adsorption process.

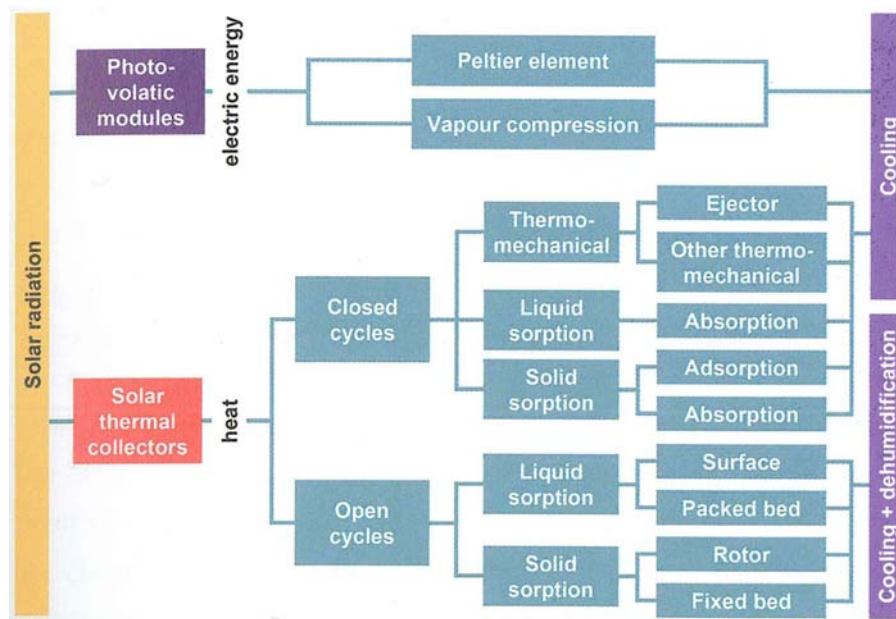


Fig.1.18 - Methods to use solar radiation for cooling and air conditioning [18]

The most diffuse type of thermally drive cooling technology is based on the absorption mechanism. This because it was traditionally employed in combination with cogeneration plant or using waste or district heating [18]. In this kind of machine, the working principle is similar to the mechanical compression cycle for the evaporator, condenser and throttle valve components. A vaporising liquid extracts heat at a low temperature in the evaporator side of the chiller while the vapour is compressed to a higher pressure and condenses at high temperature in the condenser side of the chiller. The compression between two pressure levels is performed by means of a thermally driven compressor that is constitute by two components: generator and absorber. The absorption chiller (Fig.1.19) operation can be summarized in the following five steps:

- The refrigerant evaporates in the evaporator creating the useful cooling effect;
- The vapour of this refrigerant flows from the evaporator to the absorber where it is absorbed in a concentrated solution. In this step the latent heat of condensation as to be removed with an appropriate cooling medium (normally a water cooling system with a cooling tower);
- The diluted solution is pumped in the generator connected with the driving heat circuit. Here the solution is heated above its boiling temperature and the refrigerant vapour is released at high pressure while the concentrated solution flows back in the absorber;
- The desorbed refrigerant condenses in the condenser, whereby heat is rejected at an intermediate temperature level. The condenser is usually water cooled using a cooling tower;
- The refrigerant condensate pressure is reduced and the refrigerant flows to the evaporator through an expansion valve.

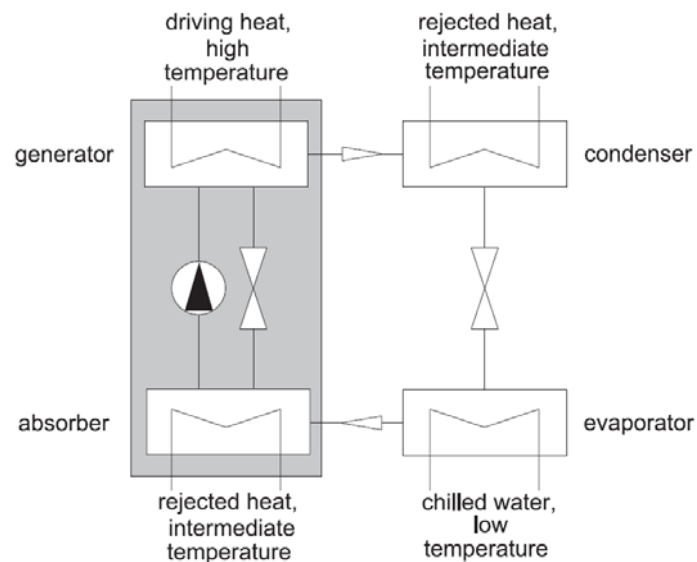


Fig.1.19 - Schematic drawings of an absorption chiller [17]

The mixture used in these kind of systems play an important rule on the absorption cooling systems performance. The most widely used pair, for cooling and heating purposes is the water ammonia ( $\text{H}_2\text{O}/\text{NH}_3$ ) where the ammonia works as refrigerant and water is the absorbent. This mixture shows high stability under a wide range of pressures and temperatures and it could be used for very low temperature because the ammonia freezing point is  $-77^\circ\text{C}$  moreover the high latent heat of vaporization of the ammonia makes this pair a good combination. From the other side the high corrosive characteristics of the ammonia and its toxicity makes this mixture not attractive. Another important pair well diffused is the lithium-bromide and water ( $\text{LiBr}/\text{H}_2\text{O}$ ). Here the water is used as a refrigerant with problems when temperature is below  $0^\circ\text{C}$ .

Analysing the thermal absorption cycle, three different kind of technologies can be found on the market: the single effect system, the double effect and the half effect [23]. The difference between these three technologies are related to the connection between generator and absorber and the number of heat exchangers between them. The different operative cycles with more than one effect allow to increase the machine performance but with higher driving temperatures and complicated cycle, as reported in the following Tab.1.3. Here the performance of the different sorption technologies based on solid or liquid sorbent are reported. The table indicates the driving temperature range adopted for each machine and, connected to this aspect, the possible solar collectors technology applicable.

The other technology used in solar thermal cooling system is the adsorption. Adsorption cycles were first used in refrigeration and heat pumps in the early 1990s. The adsorption process differ from absorption in that absorption is a volumetric phenomenon instead of adsorption that is a surface phenomenon. For this reason the main component of an adsorption machine is the solid porous surface with a large area and large value of adsorptive capacity. The machine is called adsorption machine because the main

mechanism used from this kind of machine is the chemical-physical water adsorption by a porous surface. Also here the working pair selected in the machine is important for the correct machine operation. There are some working pairs that usually employed in the thermal driven machines such as: silica gel/water, activated-carbon/methanol, activated-carbon/ammonia, zeolite/water, activated-carbon granular and fiber adsorbent, metal chloride/ammonia, metal hydrides and hydrogen, metal oxides and oxygen [25][26]. The most diffuse technology on the market is the silica-gel/water machines. In these machines the solid sorbent properly deposited on a surface has to be alternately cooled and heated to be able to adsorb and desorb the refrigerant, in this case water. These kind of machines are composed usually with two chambers that are alternatively connected with generator or evaporator. This process is fully reversible and the cycle followed by the machine could be resumed in four phases:

- The refrigerant previously adsorbed in the first chamber (left chamber in Fig.1.20) is driven off by the use of driving heat;
- The refrigerant condenses in the top of the machine (condenser) and the heat of condensation is removed using an appropriate heat rejection system;
- The condensate is sprayed in the bottom part of the machine (evaporator), and evaporates under low pressure creating the useful cooling effect of the adsorption machine;
- The refrigerant vapour is adsorbed in the second chamber (right chamber) and also here the heating is removed by means an appropriate heat rejection system.

Once that the left compartment has been fully charged and the right compartment fully regenerated their connection is interchanged creating a periodic function between the two chambers that is characteristic of these machines.

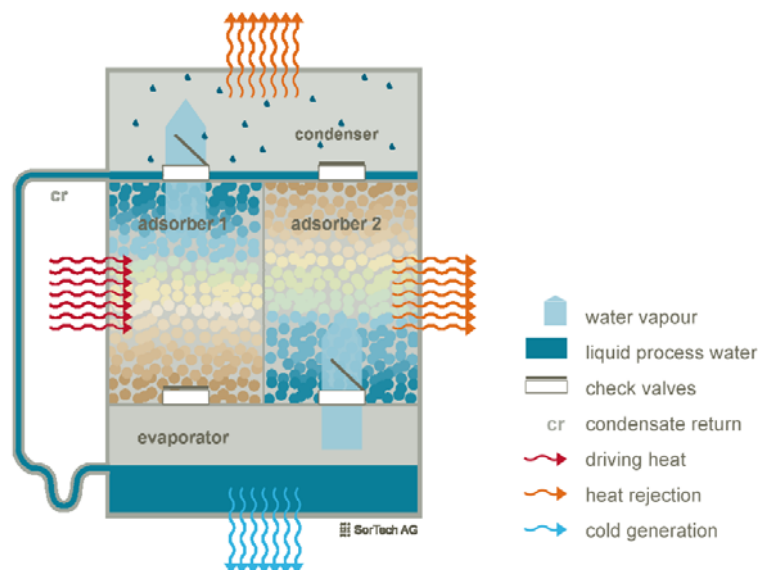


Fig.1.20 - Working principle of adsorption machine [62]

In the Fig.1.21 a schematic drawing of the heat fluxes and the temperature levels of a thermally driven cooling system is reported. Following that is possible to define the thermal energy efficiency ratio  $EER_{th}$  (also commonly denoted as thermal coefficient of performance) of the thermally driven cooling system as the ratio between the heat flux extracted from the low temperature heat source (useful cooling effect) and the driving thermal power given to the machine at high temperature. The  $EER_{th}$  varies with the equipment operation conditions, such as temperatures level, or percentage of load. In the following Tab.1.3 an overview on systems using sorption technology and their main characteristics are reported.

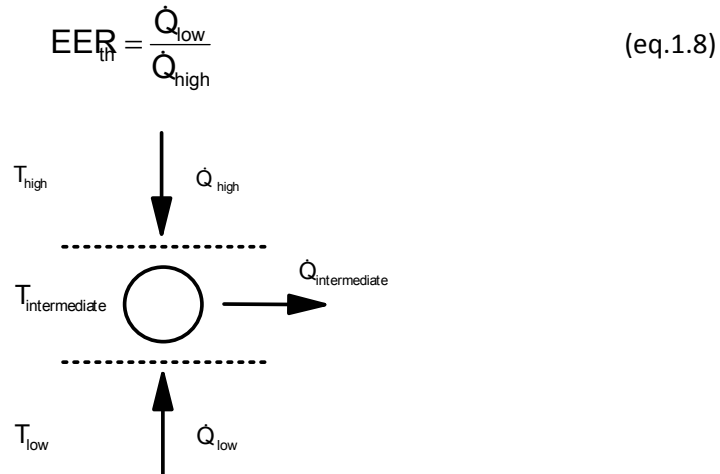


Fig.1.21 - Heat fluxes of a thermally driven cooling system [17] [27]

In the Tab.1.3, the different sorption technologies performance based on solid or liquid sorbent are reported. The table indicates the performance, the driving temperature range adopted for each machine and, connected to this aspect, the possible solar collectors technology applicable.

Another component that is characteristic of such a installations is the heat rejection system. As reported in the Fig.1.21, the sorption machines described, work mainly on three levels of temperature. The higher and the lower thermal level that correspond respectively to the heat exchanged for driving the sorption machine and the energy exchanged with the cooling loads. The intermediate temperature is normally the level at which the sorption machine has to reject the heating and usually this task is carried out by an heat rejection system that work at the ambient temperature.

Mainly two classes of air heat rejection systems can be defined: open or closed circuit systems. The difference is mainly due to the direct contact in open-circuit between the primary cooling water and the air while in the closed-circuit only an indirect contact is done across the walls of an air/liquid heat exchanger. The open-circuit systems, besides, show an highly efficiency in cooling operation but a significant water consumption has to be computed with the risk of legionella bacteria that could arise when the water is employed at these temperatures [18]. The closed-circuit systems, on the contrary, show

an increasing of the fan electrical consumption due to the decrease of the heat exchanger coefficient due only to the sensible thermal power exchanged but is free of the problem underlined previously. In some application an hybrid dry cooler is installed, where an auxiliary water circuit is incorporated to a closed-circuit systems, for water spraying on the fin and tube heat exchanger surface. This solution increases the heat exchanged between air and liquid thanks to the evaporative effect of the water sprayed in the air stream.

Tab.1.3 - Overview on market available thermally driven cooling systems [27]

Type of system	Water chillers (closed thermodynamic cycles)						Direct air treatment (open thermodynamic cycles)	
Physical phase of sorption material	Liquid			Solid			Liquid	Solid
Sorption material	Water	Lithium-bromide		Zeolite	Silica gel	Lithium-chloride	Lithium-chloride	Silica gel (or zeolite), cellulose matrix with lithium-chloride
Refrigerant	Ammonia	Water		Water	Water	Water	Water	Water
Type of cycle <sup>(1)</sup>	1-effect	1-effect	2-effect	1-effect	1-effect	1-effect	Cooled sorption process	Desiccant rotor
EER <sub>thermal</sub> range	0.5-0.75	0.65-0.8	1.1-1.4	0.5-0.75	0.5-0.75	0.5-0.75	0.7-1.1	0.6-0.8
Driving temperature range, °C	70 ... 100 120 ... 180 <sup>(2)</sup>	70 ... 100	140 ... 180	65 ... 90	65 ... 90	65 ... 90	60 ... 85	60 ... 80
Solar collector technology <sup>(3)</sup>	FPC, ETC SAT <sup>(2)</sup>	FPC, ETC	SAT	FPC, ETC	FPC, ETC	FPC, ETC	FPC, ETC, SAHC	FPC, ETC, SAHC

Comments:

- 1 1-effect: single-effect thermodynamic cycle (no internal heat cascade); 2-effect: double-effect thermodynamic cycle (with internal heat cascade)
- 2 Valid for production of cold at temperatures significantly below the freezing point of water, i.e. < 0°C
- 3 Abbreviations for solar thermal collector types: FPC = flat plate collector; ETC = evacuated tube collector; SAT = single-axis tracking solar collector (e.g. parabolic trough collectors or Fresnel type collectors); SAHC = solar air heating collector

After the definition of the main components that characterize the solar Combi+ systems, an overview on the different system configuration is reported.

### 1.5.1 SHDC - Solar Heat Driven Chiller Systems

In this section the Solar Heat Driven Chiller (SHDC) systems are presented. In such systems, the thermally driven cooling devices (absorption or adsorption machines introduced previously) are employed. These kind of systems are normally driven with liquid and then installed in combination with solar liquid collectors. The selection of which solar collectors adopt is based on the thermal level required for driving the sorption machine selected (as underlined in Tab.1.3). Three typical configurations are possible:

- Solar-thermally autonomous systems;
- Solar-assisted system with backup heat source;
- Solar-assisted system with electrically driven compression chiller as backup.

The first configuration analyzed (Fig.1.22) represents the simpler configuration possible for SHDC systems. It has a basic composition with solar liquid collectors, heat storage, sorption machine and heat rejection system. Normally the collectors are connected with the storage and from this one begin the driving circuit of the sorption machine. This allow to a continuous and effective cold generation, overcoming the problems connected from one side to the inertia of the chiller form the other to the variable solar irradiation. The last connection is between the machine and the cooling load (in this configuration the water distribution network but also with an air-handling unit in an air-water system can be enslaved).

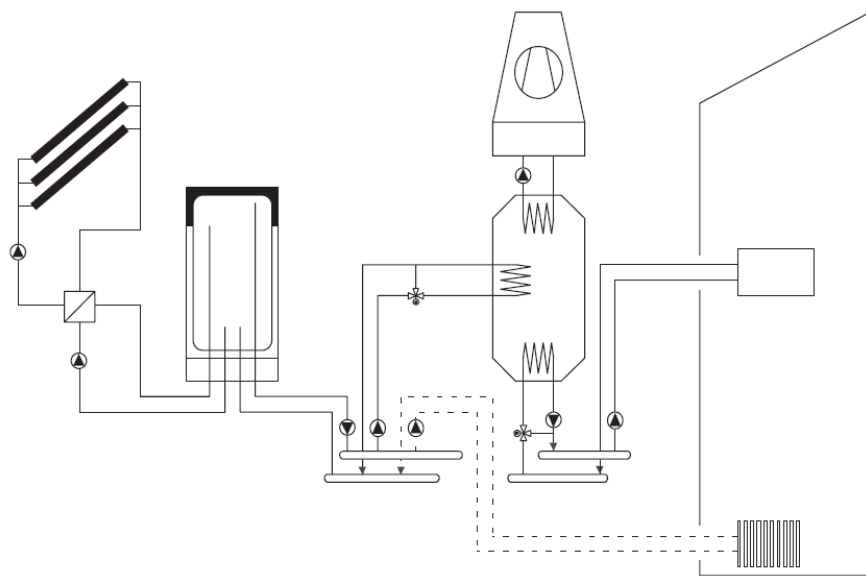


Fig.1.22 - Solar-thermally autonomous systems with thermally driven chiller for chilled-water production - water distribution network [17]

Looking the Fig.1.22, two 3-way mixing valves are installed for control the correct sorption machine operation as on the generator side as on the evaporator side while the third source connected with the sorption machine, the heat rejection system (intermediate thermal level of the Fig.1.21), is connected directly.

The problem that such a configuration could met is related to the complete satisfaction of all the cooling loads. The solar-thermally autonomous systems normally follow the strategy to give as much cooling energy than they can and this happen when enough solar thermal energy is present or stored. From this point of view, the system could not be able to cover all the cooling loads under all conditions. Different strategies are in this case adopted in order to maximize the cooling capacity or the chilled-water temperature.

In order to overcome this limitation, a second configuration has implemented (Fig.1.23). In this layout a backup heater (generally a gas burner) is connected directly with the generator side of the sorption machine and when no solar energy is present the gas burner is switched on for driving the sorption machine and efficiently satisfy all the



cooling loads. The heating backup could be also connected with the thermal storage in order to exploit the storage volume, e.g. case of the wood burner.

In the configuration reported, also the dehumidification problems are satisfied by means the air-handling unit system. Two thermal levels of chilling water are needed to meet the sensible loads through the water terminal and the latent loads through the air-handling unit.

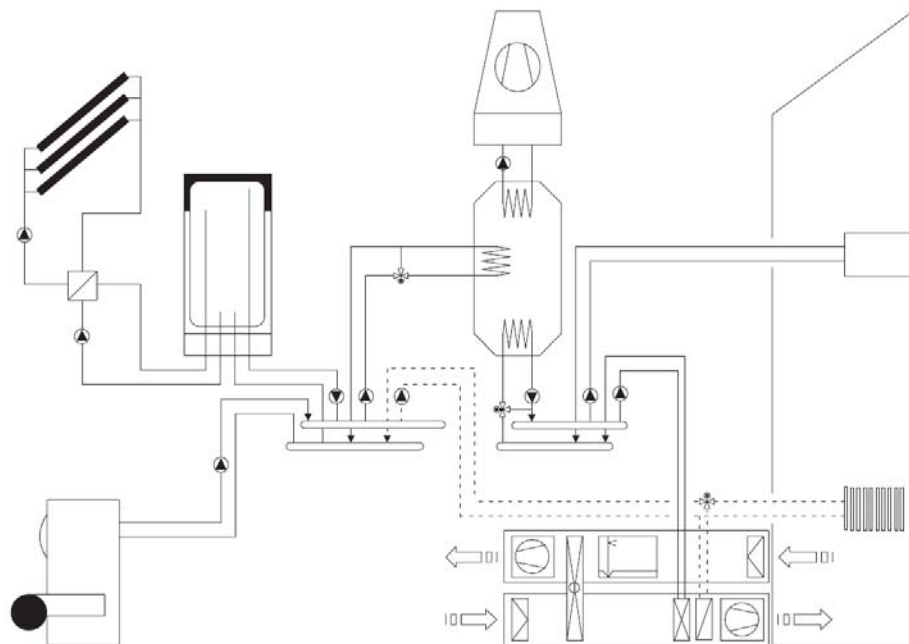


Fig.1.23 - Solar-assisted cooling systems with thermally driven chiller for chilled-water production and backup gas heater - water and air distribution network [17]

The last configuration presented has an electrically driven backup chiller installed in parallel with the thermally driven chiller (Fig.1.24). Here also a chilled water storage is installed and this one is connected with a water distribution system based on fan coils in order to satisfy sensible and latent loads. In the case of installation with radiative low temperature distribution system or chilled ceiling systems for some climatic locations the installation of an air-handling unit is needed for solve dehumidification problems.

Looking the installation in Fig.1.24, the sorption machine is adopted for satisfy the cooling load when there is enough solar energy otherwise this task is performed by the electrically driven backup chiller. This reversible compression machine could be used also as heating backup system when in winter the solar thermal energy is not enough for satisfy the heating demand of the building or the DHW requests. Furthermore, the compression machine and the thermally driven sorption machine needs a source to reject the heating at medium temperature (usually a dry cooler or a cooling tower). This device can be shared in order to save space e reduce the number of components. The configuration just explained are similar to the case presented deeply in the Chapter 4.

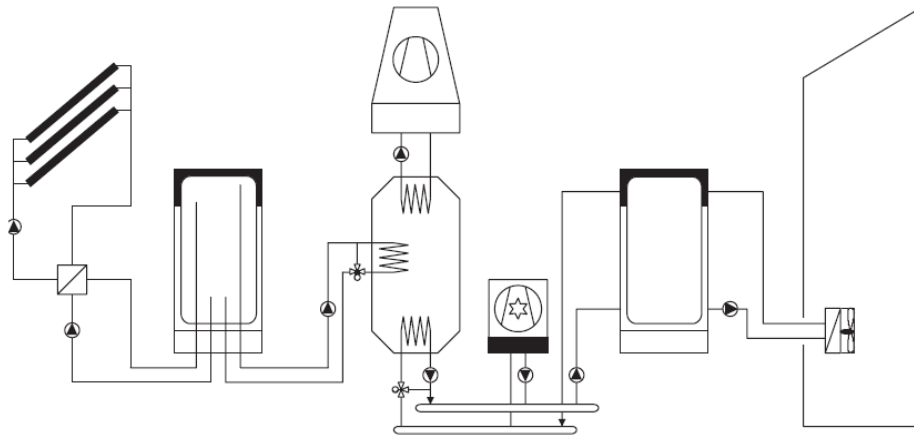


Fig.1.24 - Solar-assisted cooling systems with thermally driven chiller for chilled-water production and electrically driven backup chiller - water distribution network [17]

### 1.6 Literature review on control of solar thermal systems

Starting from the control of the simple solar systems, we start from papers made by Kaltschmitt [13] and Kalogirou [16] who show in their dissertations the control of mass flow for two different kind of solar thermal system named Low-Flow and High-Flow without direct control of mass flow but only controlling the conditions for switch on and off the solar circulation pump. This control is based on the differential temperature between the collectors and the thermal storage. They also give some indication on the impact of the electrical consumption of the pump in relation with the heat available at the outlet of the solar installation. Streicher in [14] analyzes different schemes of solar thermal systems with internal and external heat exchange and the effect of these characteristics on the behavior of the whole system.

Also in [21], the simple electronic temperature difference regulation is reported as the main control strategy adopted for control the primary solar circuit (collectors, pump, heat storage or external exchanger). Here, two temperature sensors are required, one measures the temperature at the hottest part of the solar circuit (normally the outlet collectors temperature) and the other measures the temperature of the store (normally at the height of the heat exchanger). The pump is switched on when a temperature difference is reached (standard value are from 5 to 8 K [21] but could vary in relation to the length of the pipes installed between the collectors and the thermal storage). An hysteresis is normally adopted for such a control to avoid rapid on/off cycles (the value usually adopted for switch off the pump is 3 K [21]). Normally also an overheating protection is installed (in according with EN 12976 [28]) with a temperature sensor in the part of the thermal store where the highest temperature is reached. When this temperature is reached, the circulating pump is stopped and the collector fluid could start to boil in the collectors. A suitable expansion vessel allow the increase of volume due to the partial evaporation of the liquid (as reported in [21]).

Another techniques adopted for controlling the solar thermal systems is using a radiation sensor that is installed on the collector fields. The strategy adopted in this case is to switch on the pump only when enough radiation is present but in relation with the thermal level of the storage. This avoids having the primary pump of the solar collectors when the radiation is too low for charging the store. This set point on the radiation not fixed, avoid long running operating times of the pump without yields [21].

Going more in detail with papers related to the solar circuit optimal mass flow, Badescu [29] studied the optimal control of the flow in a solar system for DHW with a closed loop flat plate collector system adopting two levels of constant mass flow in the systems. For an open loop, the same author [30] find the optimal flow in order to maximize the exergy extraction from a solar thermal system for DHW. Different strategy for operation of flat-plate collectors are reported in [31]. Here, the best strategy to control the systems, for optimize the collectors efficiency, is to control a constant inlet temperature (in order to allow simple connection with other system) when flow-rate control is not possible (best at  $7.8 \text{ l/hm}^2$ ). For application where a set point temperature is required as a output of collectors, the control of mass flow-rate (with a max of  $7.8 \text{ l/hm}^2$ ) give the best performance in terms of useful energy and collectors efficiency.

As reported in [30] different control study as carried out in the past with optimization of the different objective functions. Kovalik and Lesse [32] and Bejan and Schultz [33] study the optimization of the mass-flow rate for the control of a solar system and storage respectively, as well as Hollands and Brunger [34] that studying the optimization of the flow for a closed loop system. Additional comments could be found in De Winter [35]. In a recent study, Park [36] analyze briefly the behavior of the numerical model of a solar thermal installation in Korea modifying the mass flow related to the collectors area.

A deep analysis on the mass flow's changing effect on the collectors performance of a small and large SDHW system is reported in Furbo [37]. In this paper small SDHW systems ( $4\text{m}^2$  ; 200l) are studied, claiming greatest performance at a flow rate from 12 to  $18 \text{ l/hm}^2$  for combi-tank systems and 18 to  $24 \text{ l/hm}^2$  for preheating systems. Moreover the system performance analysis are reported when the mass flow control is based on a linear correlation with the temperature difference (DT between the output of the collectors and the bottom of the storage  $m'=1.5*DT \text{ [l/hm}^2\text{]}$ ) or on the global radiation on the collectors ( $G \text{ [W/m}^2\text{]}$ , resulting  $m'=0.6*G^{0.5} \text{ [l/hm}^2\text{]}$ ). These two approaches show an increasing of the system thermal performance by 0.9% and 0.8% respectively. For large scale systems ( $20\text{-}50\text{m}^2$ ; 1000-2400l) two configurations are analyzed a low flow system with a mantel tank system and a spiral tank or storage equipped with external exchange system. Also for these configurations some analysis are made in order to understand the effect of the different control strategies. In the last part of this thesis, the application of the advanced control to a simple solar thermal system is done. Regarding these analysis, the main conclusion of this paper [37] is that significant thermal increases cannot be achieved by means of advanced control strategies.

Two other studies have been carried out on the control of solar thermal system using a variable mass flow on the collectors, using an optimal function between the mass flow

and the difference of temperature (between collectors and storage)[38] or with not prefixed switch-on and switch-off temperature differences [39].

Regarding the control strategy of the more complex Solar Combi+ in [17] a structure in three parts is reported. The first one is related to the solar circuit control that can be controlled on the temperature difference between the collectors and the storage or a minimum level of radiation, as reported previously for the simple solar systems. The second part is related to the sorption machine operation control. When the solar energy is stored and the thermal level is sufficient for driving the sorption technology and cooling demand is present, the pumps on three sides of the machine (generator, evaporator and condenser) and the heat rejection system are switched on. If the cooling demand is present when not enough energy is stored or the minimum driving temperature is not reached, an auxiliary heat source is used or a cooling backup is adopted for satisfy the load. The third part is more related to the control strategy of the sorption machine connected to the usage of the thermal energy stored, in particular when no backup system is installed. Mainly two strategies are normally adopted. The first one is keeping the temperature at cooling level required reducing the mass flow and connected the cooling power. The second one is focused on the maximization of the chilling power, at variable chilled water temperatures.

Different papers study the control of sorption machine when reducing cooling capacity is requested [18][40][41][42]. In [18] the control working on the driving source of the sorption machine. Two approaches are possible. In the first one a reduction of the temperature is obtained using a three-way valve maintaining a constant mass flow. In the second one the level of the temperature is maintained constant while the mass flow is reduced using a two-way valve or a variable mass flow pump. In order to control a reduction of the cooling load, a control on the return temperature (from the load) is implemented decreasing the driving heat power with one of the two approaches presented (reducing temperature or mass flow). Another option, presented also in [43], is to reduce the cooling capacity of the sorption machine working on the heat rejection system fan speed. This allow to increase the heat rejection temperature decreasing from one side the chilling capacity of the sorption machine, from the other the electrical consumption of the heat rejection system. In [44] different strategy to control the heat rejection system is studied with the aim to reduce the electrical consumption that is crucial for this kind of applications.

Looking the structure of the controller, as reported in [18], a two level control is normally adopted. A first level “supervisory control” that specifies set points and the dependent modes of operation while a second level “local-loop control” which attempts to meet the set point using actuators (pumps, valves, fans). The aim of the control is to meet the loads (cooling, DHW, heating) ensuring internal comfort and at the same time minimizing the energy consumption (reaching high solar fractions) and avoiding malfunctioning. This could be done using a minimum monitoring equipment installed on the system. Finally, in [45] is underlined the importance of the overall system control. In this paper the hydraulic structure and the control has been divided in three functional groups related to the three sources that are connected to a normal sorption machine.

# Chapter 2. Numerical models for solar thermal systems

## 2.1 Introduction

As underlined in the executive summary, the complex solar thermal systems used for satisfy the DHW, heating and cooling loads consist of an elevate number of components. The control optimization of such a systems is performed simulating the transient behavior of the different components performing numerical dynamic simulations with the software Trnsys [48]. The Solar Combi+ system used as case study is presented in the fourth chapter (Solar Combi+ systems for residential application [46],[47]) while here, in the second chapter, an overview of the numerical models adopted for the numerical simulation is given. Before to analyze these numerical models, the analysis of the boundary conditions are presented. For such systems the boundary conditions are related to the climatic data considered (temperature, radiation and humidity profiles during the year) and the loads that the system has to be able to satisfy (heating, cooling and DHW demand). The chapter starts with an analysis of the climatic data considered for two climatic locations considered, following by the sensitivity analysis of the residential building characteristics (in terms of yearly energy requests for heating and cooling). Finally, an overview and a brief explanation of the numerical models adopted for the various components is given.

## 2.2 Climatic data considered

In building simulations, the weather data used for reproducing the climatic conditions affect the behavior of the numerical model computed. In order to better understand the level of this influence, two “typical year” profiles have been considered. The two profiles considered are:

- **“Standard”** weather data (STD) is an hourly profile created using default models for the calculation of the radiation [49][50] while for the temperatures, the model used produces hourly extremes temperatures which correspond to the mean of the extreme values.
- **“Extreme”** weather data (EXTR) is an hourly profile generated considering hourly extreme temperatures equal to the extreme values of the 10 years. Extreme monthly

conditions are additionally considered, both for the calculation of the monthly data of radiation and temperature using monthly maxima data and monthly minima data, respectively during summer and winter in the 10 years. With this approach, a cold winter together with a hot summer have been considered in order to have a climatic profile that allow the evaluation of the worst possible case scenario.

The climatic data, are generated with Meteonorm software. For the “STD” profile the Trnsys default data is used, and it was generated with Meteonorm 5 but any information is given from the exact database considered. While the “EXTR” profile has been created with Meteonorm7 software [51] and based on a stochastic analysis of 10 years of data for temperatures (from 2000 to 2009) and on 20 years of data for radiations (from 1986 to 2005). In the following graphs the frequency of the dry bulb temperature (DBT) and global horizontal radiation (GHR) are reported for the two locations analyzed for the whole year showing columns related to frequency and curves that represents the cumulative frequency of the single series of data considered.

Analysing the DBT distribution of Bolzano (Fig.2.1) the EXTR data is clearly distributed in the low temperatures (extreme winter conditions) and in the high temperatures (extreme summer conditions). In winter, the amount of hours where the temperature is below 0°C move from the 18% (790 h) to 32% (1300 h) of the winter hours (defined with the average on the external temperature less than 12°C). During summer, analysing the temperature above 24°C, the hours move from 17% (770 h) to 34% (1600 h) of the total summer hours (computed as the difference between the total hours of one year and the winter hours). The cumulative curve reflects this behaviour (higher at low temperature and lower at high temperature).

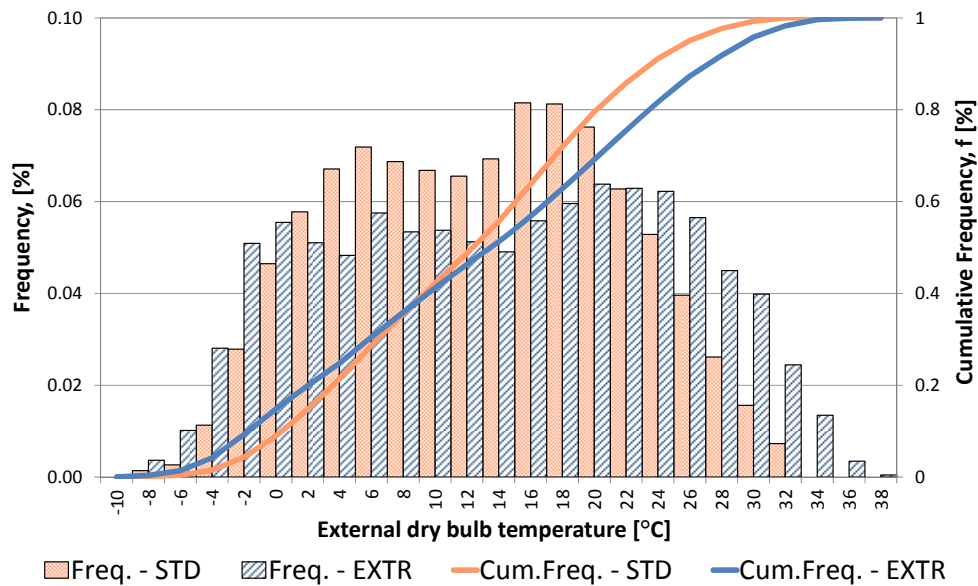


Fig.2.1 - External Dry Bulb Temperature - Bolzano.

Also the GHR for the EXTR data displays a percentage of the radiation bigger for the higher level of GHR (Fig.2.2). It is interesting to note these differences also in the Tab.2.1, where the comparison between the two climatic data is reported in terms of max and min temperatures, HDD and GHR computed for the whole year.

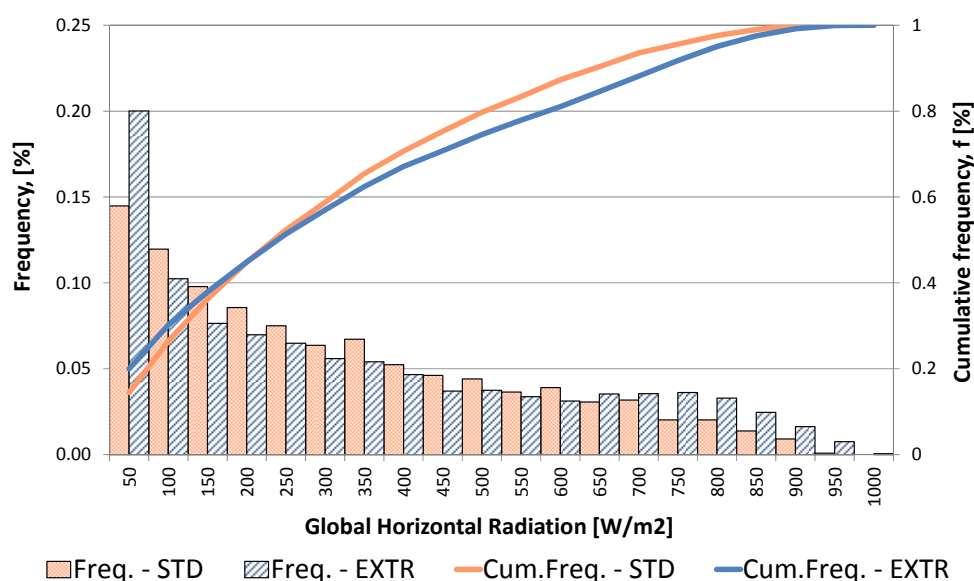


Fig.2.2 - Global Horizontal Radiation - Bolzano.

Tab.2.1 - Temperature, total energy on the horizontal surface and HDD - Bolzano.

Bolzano		STD	EXTR
Tmin	[°C]	-8.75	-9.90
Tmax	[°C]	31.75	37.16
GHR	[kWh/(m <sup>2</sup> *year)]	1251	1438
HDD 12/20		2711	2770

In the analysis of the Rome climatic data, the same differences found in Bolzano analysis are visible (Fig.2.3 and Fig.2.4). Also in Rome, the extreme profile of the external dry bulb temperature (Fig.2.3) has a distribution more diffused at the low and high values. During winter the amount of hours where the temperature is below 5°C is the 16% (485 h) in STD profile while in the EXTR is the 28% (906 h) of the total winter hours (defined with the average of the external temperature on the 24h less than 12°C). For the summer analysis the temperature is greater than 24°C for 19% (1124 h) in the STD profile while in the EXTR profile this value growing to 29% (1596 h) of the total summer hours (computed as the difference between the total hours of one year and the winter hours). Also for this case this differences in the temperature is reflected in the global horizontal radiation profile reported in Fig.2.4 and in the yearly values reported in Tab.2.2.

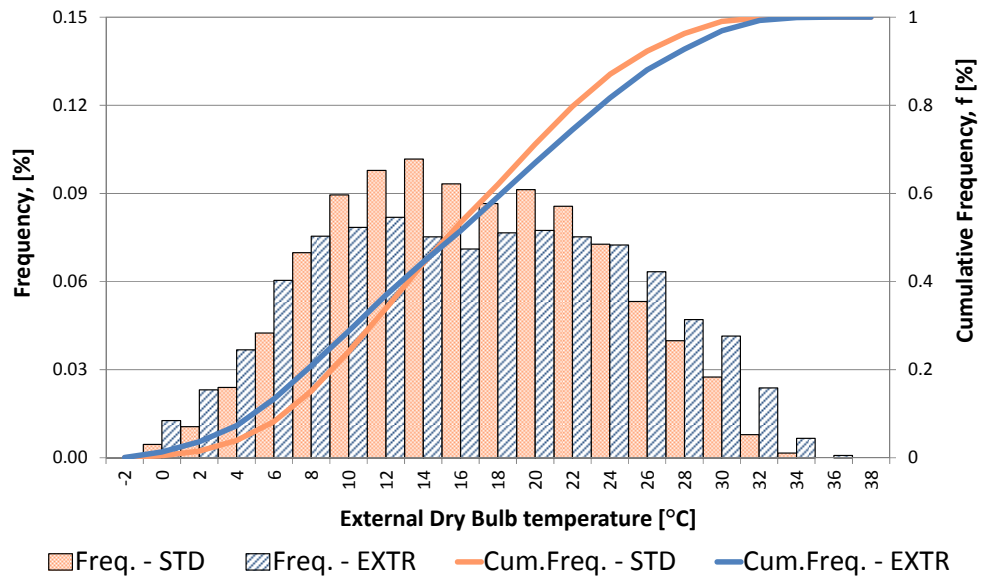


Fig.2.3 - External Dry Bulb Temperature - Rome.

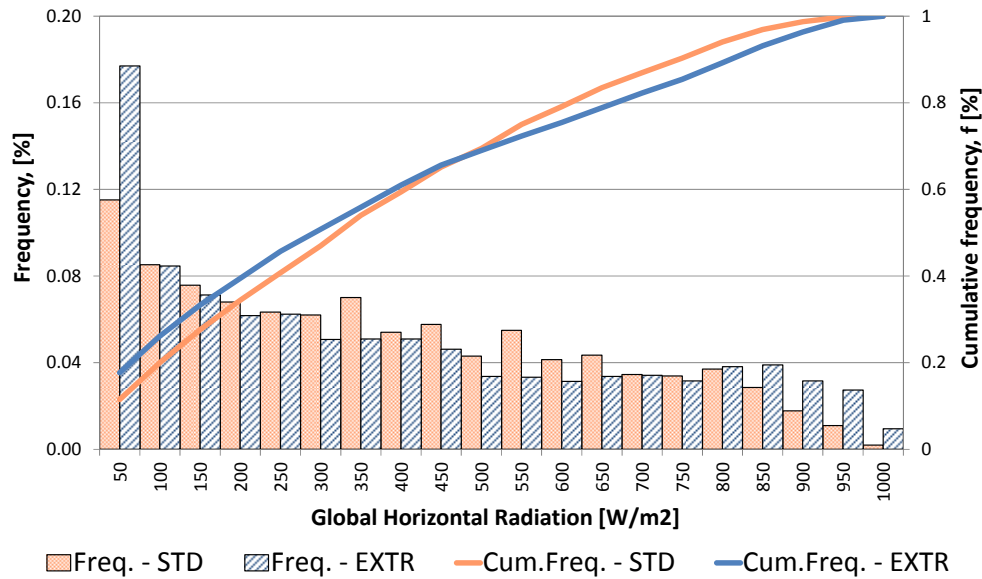


Fig.2.4 - Global Horizontal Radiation - Rome.

Tab.2.2 - Temperature, total energy on the horizontal surface and HDD - Rome.

Rome		STD	EXTR
Tmin	[°C]	-2.3	-2.4
Tmax	[°C]	33.1	34.5
GHR	[kWh/(m²*year)]	1561	1668
HDD 12/20		1371	1690



### 2.3 Buildings description

The building analysis has been started from the knowledge of the norms that limit the opaque and transparent surfaces transmittance. The norm that has been used is: "Decreto Ministeriale 26/01/2010" [55] and successive changes. The Italian norm specifies the climatic zones of Italy and the limit on transmittance for external walls, floors and windows. These values are showed on Tab.2.3.

Tab.2.3 - Limits of Italian law for the transmittance of walls, floors and roofs [55]

Zona climatica	Strutture opache verticali	Strutture opache orizzontali o inclinate		Finestre comprensive di infissi
		Coperture	Pavimenti*	
A	0,54	0,32	0,60	3,7
B	0,41	0,32	0,46	2,4
C	0,34	0,32	0,40	2,1
D	0,29	0,26	0,34	2,0
E	0,27	0,24	0,30	1,8
F	0,26	0,23	0,28	1,6

In the analysis performed, buildings sited in Bolzano (Climatic zone E) and in Rome (Climatic zone D) have been considered.

The building that has been analyzed is a residential house (Fig.2.5), with an area of 180 m<sup>2</sup> divided equally on two floors. The net volume of the building is around 600 m<sup>3</sup>, then the ratio between external surface and gross volume (S/V) is around 0.7 m<sup>-1</sup>. The roof's area is equal to 123 m<sup>2</sup> and external surfaces dimensions, percentages of glasses for each orientation are reported in Tab.2.4.

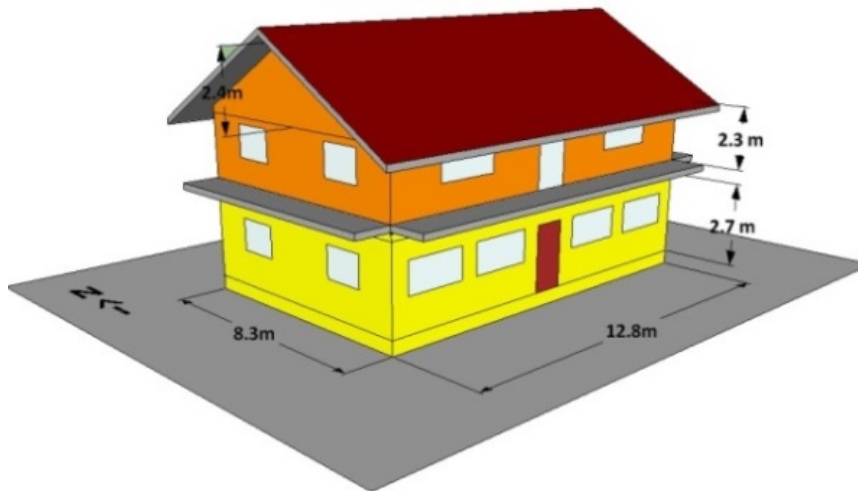


Fig.2.5 - Buildings analysed

Tab.2.4 - External surface and fenestration ratio for two floors building

Floor \ Surfaces	Orientation	External	Windows	
	-	m <sup>2</sup>	m <sup>2</sup>	%
Ground floor	North	34.7	2.1	6%
	East	22.4	2.2	10%
	West	22.4	2.2	10%
	South	34.7	6.9	20%
First floor	North	29.6	1.8	6%
	East	29.0	2.9	10%
	West	29.0	2.9	10%
	South	29.6	5.9	20%

For the two climatic locations selected (Bolzano and Rome), the envelope characteristics have to be chosen in order to respect the limits of the standard mentioned above (Tab.2.3). Using typical stratigraphy of exterior walls, roof and floors the level of insulation has been varied to respond to this request. In the following Tab.2.5 and Tab.2.6, the thermal characteristics and thicknesses are reported for the two climatic locations analyzed.

### 2.3.1 Stratigraphy for Bolzano base model

The envelope characteristics are here reported in the following tables for the two climatic location considered.

Tab.2.5 - Thermal characteristics and thickness of the envelope stratigraphy for Bolzano

External Walls	s	λ	ρ	c
	[m]	[W/m*K]	[kg/m <sup>3</sup> ]	[kJ/kg*K]
Internal plaster	0.02	0.90	1600	0.90
Brick	0.25	0.25	1380	0.84
Insulation (Eps)	0.10	0.04	17	1.20
External plaster	0.02	0.70	1800	0.90
Roof	s	λ	ρ	c
	[m]	[W/m*K]	[kg/m <sup>3</sup> ]	[kJ/kg*K]
Internal plaster	0.02	0.90	1600	0.90
Brick	0.16	0.50	1100	0.84
Concrete	0.05	1.20	2000	0.78
Insulation (Eps)	0.14	0.04	17	1.20
External tile	0.03	0.90	530	0.90

U	U <sub>lim</sub>
[W/m <sup>2</sup> *K]	[W/m <sup>2</sup> *K]
<b>0.27</b>	<b>≤0.27</b>

U	U <sub>lim</sub>
[W/m <sup>2</sup> *K]	[W/m <sup>2</sup> *K]
<b>0.24</b>	<b>≤0.24</b>

Internal walls	s	$\lambda$	$\rho$	c
	[m]	[W/m*K]	[kg/m <sup>3</sup> ]	[kJ/kg*K]
Internal plaster	0.02	0.90	1600	0.90
Brick	0.08	0.25	1380	0.84
External plaster	0.02	0.90	1600	0.90
Active floor (ground floor)	s	$\lambda$	$\rho$	c
	[m]	[W/m*K]	[kg/m <sup>3</sup> ]	[kJ/kg*K]
Ceramic	0.015	1.20	2000	0.88
Screed	0.045	1.20	1600	1.00
Active layer				
Screed	0.03	1.20	1600	1.00
Insulation (VELTA_XPS)	0.05	0.030	35	1.20
Concrete lightweight	0.05	0.12	1200	0.84
Reinforced concrete	0.25	0.33	1500	0.84
Insulation (VELTA_XPS)	0.01	0.030	35	1.20
Active floor (first floor)	s	$\lambda$	$\rho$	c
	[m]	[W/m*K]	[kg/m <sup>3</sup> ]	[kJ/kg*K]
Wood	0.014	0.15	600	1.30
Screed	0.045	1.20	1600	1.00
Active layer				
Screed	0.03	1.20	1600	1.00
Insulation (VELTA_XPS)	0.05	0.030	35	1.21
Concrete lightweight	0.05	0.12	1200	0.84
Reinforced concrete	0.25	0.33	1500	0.84
Internal plaster	0.03	0.90	1600	0.90

U
[W/m <sup>2</sup> *K]
<b>1.872</b>

U	U <sub>lim</sub>
[W/m <sup>2</sup> *K]	[W/m <sup>2</sup> *K]
<b>0.29</b>	<b>≤0.30</b>

U
[W/m <sup>2</sup> *K]
<b>0.31</b>

### 2.3.2 Stratigraphy for Rome base model

Starting from Bolzano's stratigraphy we have reduced the thickness of insulation in order to reach the limits of the norm (Tab.2.3) for the climatic zone D. The results for different kind of opaque structures are listed on the table below.

Tab.2.6 - Thermal characteristics and thickness of the envelope stratigraphy for Rome

External Walls	s	$\lambda$	$\rho$	c	U	U <sub>lim</sub>
	[m]	[W/m*K]	[kg/m <sup>3</sup> ]	[kJ/kg*K]		
Internal plaster	0.02	0.90	1600	0.90	[W/m <sup>2</sup> *K]	[W/m <sup>2</sup> *K]
Brick	0.25	0.25	1380	0.84	<b>0.29</b>	<b>≤0.29</b>
Insulation (Eps)	0.09	0.04	17	1.20		
External plaster	0.02	0.70	1800	0.90		
Roof	s	$\lambda$	$\rho$	c	U	U <sub>lim</sub>
	[m]	[W/m*K]	[kg/m <sup>3</sup> ]	[kJ/kg*K]		
Internal plaster	0.02	0.90	1600	0.90	[W/m <sup>2</sup> *K]	[W/m <sup>2</sup> *K]
Brick	0.16	0.50	1100	0.84	<b>0.26</b>	<b>≤0.26</b>
Concrete	0.05	1.20	2000	0.78		
Insulation (Eps)	0.13	0.04	17	1.20		
External tile	0.03	0.90	530	0.90		
Internal walls	s	$\lambda$	$\rho$	c	U	U <sub>lim</sub>
	[m]	[W/m*K]	[kg/m <sup>3</sup> ]	[kJ/kg*K]		
Internal plaster	0.02	0.90	1600	0.90	[W/m <sup>2</sup> *K]	
Brick	0.08	0.25	1380	0.84	<b>1.872</b>	
External plaster	0.02	0.90	1600	0.90		
Active floor (ground floor)	s	$\lambda$	$\rho$	c	U	U <sub>lim</sub>
	[m]	[W/m*K]	[kg/m <sup>3</sup> ]	[kJ/kg*K]		
Ceramic	0.015	1.20	2000	0.88	[W/m <sup>2</sup> *K]	[W/m <sup>2</sup> *K]
Screed	0.045	1.20	1600	1.00	<b>0.32</b>	<b>≤0.34</b>
Active layer						
Screed	0.03	1.20	1600	1.00		
Insulation (VELTA_XPS)	0.05	0.030	35	1.20		
Concrete lightweight	0.05	0.12	1200	0.84		
Reinforced concrete	0.25	0.33	1500	0.84		
Insulation (VELTA_XPS)	0	0.030	35	1.20		

Active floor (first floor)	s	$\lambda$	$\rho$	c		
	[m]	[W/m*K]	[kg/m <sup>3</sup> ]	[kJ/kg*K]		
Wood	0.014	0.15	600	1.30		
Screed	0.045	1.20	1600	1.00		
Active layer						
Screed	0.03	1.20	1600	1.00		
Insulation (VELTA_XPS)	0.05	0.030	35	1.21		
Concrete lightweight	0.05	0.12	1200	0.84		
Reinforced concrete	0.25	0.33	1500	0.84		
Internal plaster	0.03	0.90	1600	0.90		

<b>U</b>
[W/m <sup>2</sup> *K]
<b>0.31</b>

The floors stratigraphy for both locations has been chosen related to the Velta product (commercial product "Velta Calore"). The top layer selected has been ceramic and wood respectively for the ground and for the first floor.

In the analysis conducted, another class of buildings have been considered "BLD" (Buildings with Low energy Demand) instead of "BHD" (Buildings with High energy Demand) that, as described previously, respect the value of transmittance imposed by the norm [55]. This second class of buildings BLD are created starting from the BHD characteristics increasing the level of insulation (-11% of the average transmittance on the opaque and transparent elements) for the two climatic conditions analyzed in order to better understand the effect of different level of loads on the solar combi+ system analyzed in the Chapter 4. In the following Tab.2.7, the two buildings analyzed (with different insulation level) for the two different climatic locations considered (Bolzano and Rome) are reported with the opaque and transparent surfaces characteristics.

Tab.2.7 - Building envelope characteristics for two climatic zones and two level of insulations

Elements			Bolzano		Rome	
			BHD	BLD	BHD	BLD
External Walls	U	[W/(m <sup>2</sup> *K)]	0.27	0.24	0.29	0.26
Roof	U	[W/(m <sup>2</sup> *K)]	0.24	0.21	0.26	0.23
Ground Floor	U	[W/(m <sup>2</sup> *K)]	0.3	0.27	0.3	0.3
Windows	U	[W/(m <sup>2</sup> *K)]	1.8	1.6	2	1.8
	g	[-]	0.6	0.6	0.6	0.6

### 2.3.3 Shading systems

In the building numerical models analyzed (one floor and two floors), fixed shadings have been considered due to balconies and roof overhangs, as showed in the Fig.2.5. This shading systems mainly modify the solar energy that arrive on the surfaces on South, West and East orientations. In the Fig.2.6, a particular of the geometrical characteristics of the shadings (on the south/west corner) are reported.

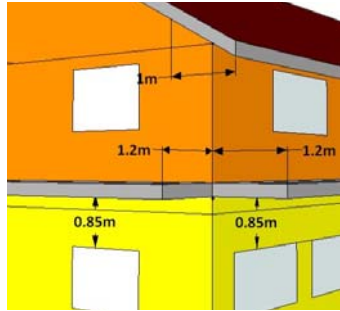


Fig.2.6 - Detail of fixed shading geometry for the 2 floors building

### 2.3.4 Internal gains

For both building models internal gains have been considered, referring to the schedule of presence indicated in the Italian norm UNI/TS 11300 [54] (UNI EN ISO 13790 [53]) and reported in the following Tab.2.8. These values are referred to a detailed approach for residential buildings considering a typical usage profile of the building. This approach has been followed because no national gains values are available (as prescribed by the norm [53]).

Tab.2.8 - Internal gains considered [53]

Days	Hours	Living room [W/m <sup>2</sup> ]	Other areas [W/m <sup>2</sup> ]	Internal gains used [W/m <sup>2</sup> ]
From Monday to Friday	From 07 to 17	8	1	3.8
	From 17 to 23	20	1	8.6
	From 23 to 07	2	6	4.4
Average	24h	9	2.67	5.2
Saturday and Sunday	From 07 to 17	8	2	4.4
	From 17 to 23	20	4	10.4
	From 23 to 07	2	6	4.4
Average	24h	9	3.83	5.9
<b>Weekly average</b>		<b>9</b>	<b>3</b>	<b>5.4</b>

For all the buildings considered the internal gains have been shared on the total area of the building, considering 40% of area with living room gains and 60% for other area gains. This approach allow to reach an internal gains average value of 5.4 W/m<sup>2</sup>.

### 2.3.5 Infiltrations

For all the buildings examined an infiltration ratio has been considered independently from the geographical location of the buildings. For BLD buildings a leakage of 0.35 ACH has been implemented, with a value comes from [53] with tailored analysis. For the other kind of buildings a leakage of 0.45 ACH has been used for simulate the different occupants behavior from the standardized one.

### 2.3.6 Natural night ventilation

During summer, in addition, natural ventilation effect has been considered, during night time, simulating the behavior of the occupants through the windows opening. The approach adopted was developed from IEA SHC for Task 32 [56] where free driven tilted ventilation was described by equations based on simple CFD analysis [57].

The effect of the night ventilation is computed only when some conditions are met:

- Night time: between 21.00 and 08.00;
- Average of external temperature on 24 hours is greater than 12°C;
- Room temperature is above 23°C;
- Difference of temperature between internal and external is at least 2°C.

When these conditions are reached an air exchange rate through windows is calculated in function of difference between internal and external temperature, geometry of window and opening tilt angle. We simulated night ventilation by the usage of windows on face East (or West) with one window each floor (Dimensions: 1.0 m x 1.0 m).

The equations used are:

$$\dot{V}(\alpha) = C_k(\alpha) \cdot C_d \cdot H \cdot W \cdot \frac{1}{3} \sqrt{\frac{\Delta T}{T}} \cdot g \cdot H \quad (\text{eq.2. 1})$$

$$C_d = 0.0147 \cdot \alpha - 0.0928 \frac{H}{W} + 0.4116 \quad (\text{eq.2. 2})$$

$$C_k(\alpha) = 2.6E-7 \cdot \alpha^3 - 1.19E-4 \cdot \alpha^2 + 1.86E-2 \cdot \alpha \quad (\text{eq.2. 3})$$

Where:

$\dot{V}(\alpha)$	[m <sup>3</sup> /s]	: volume flow at opening tilt angle $\alpha$ ;
$\alpha$	[°]	: opening tilt angle;
$C_d$	[-]	: discharge coefficient;
$H$	[m]	: window height;
$W$	[m]	: window width;
$\Delta T$	[K]	: temperature difference between room and ambient;

- $T$  [K] : average temperature between room and ambient;  
 $g$  [m/s<sup>2</sup>] : earth's gravity acceleration;  
 $C_k(\alpha)$  [-] : relative volume flow rate at opening tilt angle  $\alpha$ .

### 2.3.7 Domestic hot water demand

The request profile for domestic hot water has been computed using the software *DHWcalc* [58][59] developed from the University of Kassel ([www.solar.uni-kassel.de](http://www.solar.uni-kassel.de)) for IEA-SHC Task 26 [2] on solar combisystems. As reported in the first chapter, in this task different solar combisystems from different part of Europe were compared and this software was used to generate realistic profiles of domestic hot water consumption. A profile of DHW consumption has been generated for a single family house with four draw-off categories (bath, shower and two washbasins). The water flow rate for each category has been chosen in according with UNI 9182 [60] and the probability distribution used is a Gaussian with constant curves during all weeks and during the year without reduction for holiday. The mean value for water consumption for each day has been set to 200 l/day. The inlet temperature of water considered has been based on the formula adopted on IEA SHC Task 32 [56]:

$$T_{CW} = T_{CW,Av} + dT_{CW,Amp} \cdot \sin \left( \frac{\left( 360 \cdot \frac{\text{time}}{24} - dt_{CW,Shift} \right)}{365} \right) \quad (\text{eq.2. 4})$$

Where:

- $\text{time}$  [h] : year time;  
 $T_{CW}$  [°C] : cold water supply temperature;  
 $T_{CW,Av}$  [°C] : yearly average of cold water supply temperature;  
 $dT_{CW,Amp}$  [°C] : amplitude of sine-curve describing the time dependency of cold water temperature over the year;  
 $dt_{CW,Shift}$  [day] : shift of day with minimum cold water temperature with respect to January first.

Tab.2.9 - Parameters considered for the simulation of DHW demand

$T_{CW,Av}$	10	°C
$dT_{CW,Amp}$	2	°C
$dt_{CW,Shift}$	137	day



### 2.3.8 Distribution control for active layer in the two floors building

In the two floors building model, a more precise distribution control has been considered. A winter curve has been implemented, related to the winter operation. In this heating curve, the supply temperature of the radiative system is regulated in function of the external ambient temperature. A specific mass flow of  $7 \text{ kg}/(\text{m}^2 \cdot \text{hr})$  has been considered in this analysis. The heating curve used in winter in the Bolzano installation is reported in the Fig.2.7. Here, two more curves are reported, because for decreasing the on/off cycles of the compression heat pump (when a simple reversible heat pump without inverter is used as in the case study here studied and presented in the Chapter 4), an hysteresis on the curve has been adopted. The maximum temperature considered for the supply is of  $34.5^\circ\text{C}$  at the minimum temperature of the climatic location considered (e.g. in the case reported in Fig.2.7 the minimum temperature is  $-8.25^\circ\text{C}$ ). During summer time a fixed point has been used considering the minimum operative temperature ( $14^\circ\text{C}$ ) to avoid condensation phenomena (reaching the wet bulb temperature of the air). Also in this case an hysteresis has been implemented with the same purpose of the winter range.

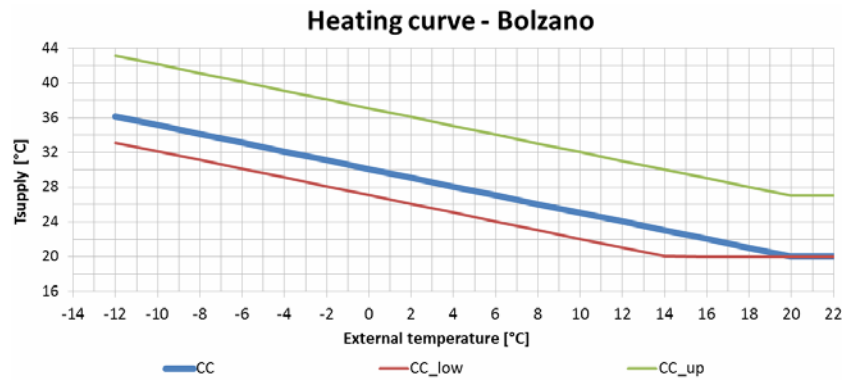


Fig.2.7 - Winter climatic curve considered

### 2.3.9 Sensitivity analysis with Morris method

In order to understand the parameters effect on the building loads simulation, a sensitivity analysis has been conducted in order to investigate two main aspects that characterize the numerical model of the building: 1) building inhabitant behavior and 2) envelope construction. The building models used for this analysis have transmittance of the opaque and transparent surfaces equal to the value imposed by the norm (as the buildings introduced in the previous subchapter "BHD"), located in Rome and Bolzano. The weather considered during this analysis is the STD reported previously. In the first issue the parameters considered are related to the typical building profile usage (schedule of internal gain, infiltration rate, night ventilation) while in the second aspect is related to the difference between the building really constructed and the design model (shading device, internal walls, transmittance of the opaque surfaces).

The sensitivity analysis is based on the Morris Method. This methodology permits to increase the awareness about the single parameter effect on the simulation results. It is used to prioritize the parameters, giving information related on their effects on the outputs [65]. Before to go more in detail with the parameters investigated, a brief introduction on Morris method is given.

The Morris Method (MM) belongs to the screening methods [66] where all parameters are varied “one at time” (OAT). The main objective is to isolate those inputs that can affect the response of the model, by classifying their influence as (1) negligible, (2) linear or additive and finally (3) nonlinear or involved with some other factors.

The elementary effect of the MM is defined for the  $i$  parameters, on the  $k$  input analyzed:

$$EE_i = \frac{[y(x_1, \dots, x_{i-1}, x_i + \Delta, x_{i+1}, \dots, x_k) - y(\bar{x})]}{\Delta} \quad (\text{eq.2. 5})$$

Varying the  $x_i$  within a realistic range  $\Delta$ , using  $r_i$  different number of steps for each  $i$  parameter, the Elementary Effects  $EE_i$  are evaluated. With the Elementary Effects of each input, the single elementary effect  $EE_i$  average  $\mu_i$  and the standard deviation  $\sigma_i$  are then computed.

$$\mu_i = \frac{1}{r_i} \sum_{t=1}^{r_i} EE_{i,t} \quad (\text{eq.2. 6})$$

$$\sigma_i = \sqrt{\frac{1}{r_i - 1} \sum_{t=1}^{r_i} (EE_{i,t} - \mu_i)^2} \quad (\text{eq.2. 7})$$

The  $\mu_i$  (eq.2.6) is the mean parameter influence on the output, while the standard deviation  $\sigma_i$  (eq.2.7) gives an idea on the nonlinear behavior or interaction with other factors of the input.

The use of the absolute elementary effect  $\mu_i^*$  average (eq.2.8) is suggested [67], rather than  $\mu_i$ , to prevent the possible error during the sum of the  $EE_i$  with negative sign, that present a decreasing effect. Plotting the value of  $\sigma_i$  related to the absolute value of the mean  $\mu_i^*$ , the inputs closest to the origin indicates less influence on the output.

$$\mu_i^* = \frac{1}{r_i} \sum_{t=1}^{r_i} |EE_{i,t}| \quad (\text{eq.2. 8})$$

The sensitivity analysis has been conducted through a campaign of simulations in Trnsys . The inputs of the model analyzed, the range and step considered are summarized in the Tab.2.10. The transmittances of opaque surfaces are the average of external walls, roof and floor weighted with the correspondent area of exchange for the two climatic zones studied. The overhang length is 1 m, chosen for simulate the balconies and roof

overhangs shading effect. The internal gains are the average on the single day for detailed approach, as reported previously and in according with [53]. The night ventilation input is related to the operable window area ranging from 0 to 4 m<sup>2</sup>. The orientation input is considered using the angle between the South orientation and the South façade of the reference. The fenestration ratio is the sum of all the windows on different orientations.

Tab.2.10 - Parameters investigated and range of variation for Bolzano and Rome.

n	Parameters	Dimensions	Ref.	Min	Max	Step
1	Overhang	[m]	1	0.6	1.4	0.2
2	Internal Gains	[W/m <sup>2</sup> ]	5.2	2.6	7.8	1.3
3	Infiltration rate	[ACH]	0.45	0.25	0.65	0.1
4	Night ventilation	[m <sup>2</sup> ]	4	0	4	1
5	Orientation	[°]	0	0	360	45
6	Transmittance (Bolzano)	[W/m <sup>2</sup> K]	0.269	0.161	0.377	0.054
	Transmittance (Rome)	[W/m <sup>2</sup> K]	0.284	0.170	0.398	0.057
7	Fenestration ratio	[m <sup>2</sup> ]	27	21.6	32.4	2.7
8	Thermal inertia	[kJ/K]	2.2·10 <sup>5</sup>	2·10 <sup>5</sup>	2.5·10 <sup>5</sup>	1·10 <sup>4</sup>

The output used for sensitivity analysis of the system analyzed is the end energy demand for heating and cooling of the building with the set point of internal temperature of 20°C for winter and 24.5°C for summer. The distribution system considered is a radiative low temperature floor with the inlet temperature imposed using a climatic curve function of the external temperature (as reported in Fig.2.7).

The graphical representation of the MM is a scatter graph, where each point plotted is related to the elaboration on elementary effects of each parameter analyzed. The graph reports on the x-axis the absolute mean and the standard deviation on the y-axes. Values closer to the origin represent parameters with less influence and linear effect on the output. A dotted line is also reported, representing the threshold between linear or non-linear influence on the output.

Two different outputs are evaluated in order to understand the parameters effect: seasonal cumulated heating and cooling demands.

Starting from the analysis on the heating demand, for both climatic locations (Fig.2.8 and Fig.2.9), a linear effect with high mean value is visible in the graphs with regards to the envelope parameters (transmittance and infiltration) and inhabitants behavior (internal gains). Secondly the building orientation has an effect close to nonlinear behavior or correlated with other parameters. Small linear effect is noticeable with regards to the two envelope parameters (variation of shading device and fenestration ratio); the night ventilation effect is null because the conditions for simulating this effect are not reached during winter.

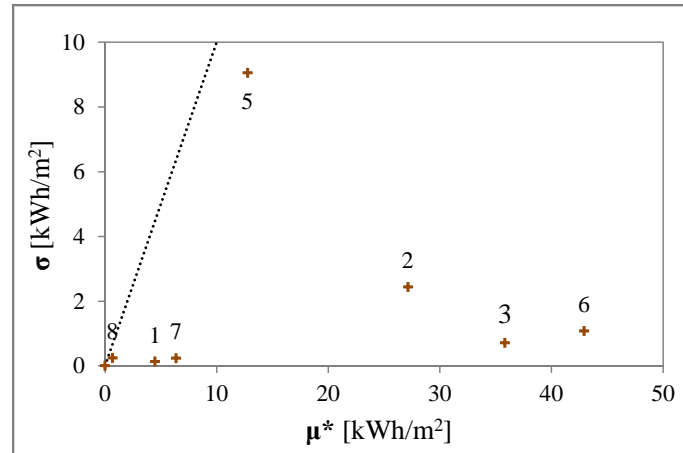


Fig.2.8 - Estimated mean ( $\mu^*$ ) and standard deviation ( $\sigma$ ) for each input factor on heating energy demand - Bolzano.

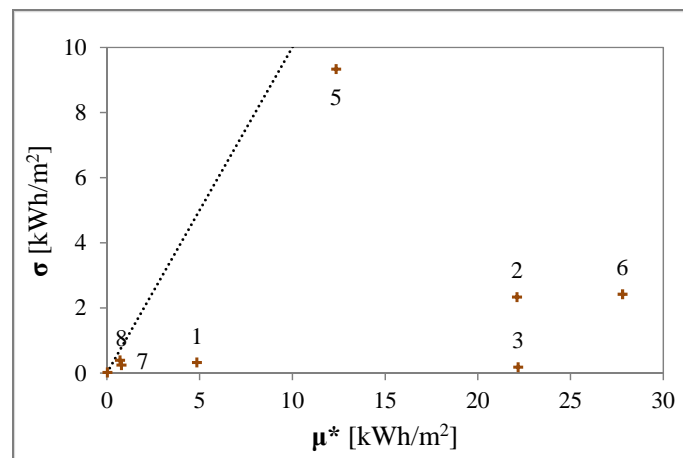


Fig.2.9 - Estimated mean ( $\mu^*$ ) and standard deviation ( $\sigma$ ) for each input factor on heating energy demand - Rome

For the cooling analysis, the internal gains have the highest impact on the energy demand for both buildings located in Bolzano and in Rome (Fig.2.10 and Fig.2.11). The fenestration ratio variation, differently from what is showed in the heating analysis, has a strong linear influence on the cooling energy because this parameter is directly connected to the solar gains. The orientation has a significant linear influence. The parameters that show a minor influence, compared with the analysis on the heating demand are the transmittance and the infiltration. Their minor effect is mainly due to the lower difference between internal and external temperature in summer season. For the same reason, also the variation of the operable window area, simulating the night ventilation, has a small impact on the cooling demand.

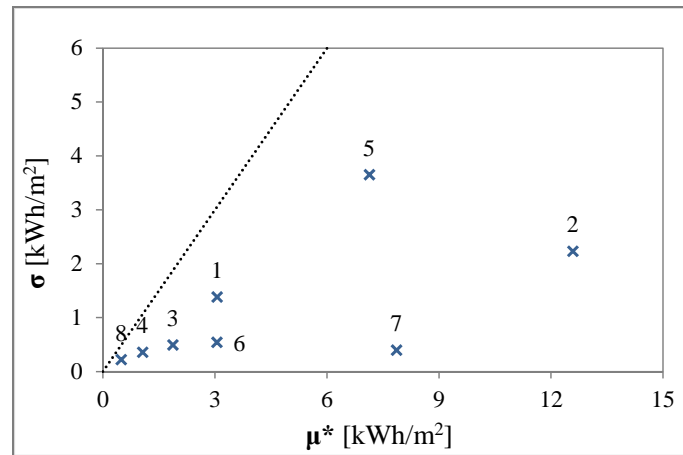


Fig.2.10 - Estimated mean ( $\mu^*$ ) and standard deviation ( $\sigma$ ) for each input factor on cooling energy demand - Bolzano.

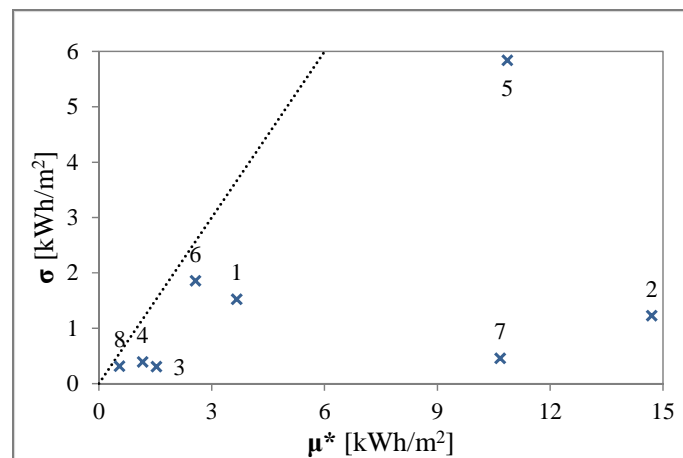


Fig.2.11 - Estimated mean ( $\mu^*$ ) and standard deviation ( $\sigma$ ) for each input factor on cooling energy demand - Rome.

A ranking of the design parameters influencing the sensitivity of the energy used for heating and cooling is reported in the Tab.2.11. Here, the predominant parameters are clearly reported for both output and climatic location considered. As mentioned before, the envelope characteristics and behavioral aspects have strong influence, on the one hand, on the heating loads with transmittance of opaque walls, infiltrations and internal gains. On the other, the cooling demand is mainly affected from internal gains and fenestration ratio. The orientation of the building is an important parameter for both analysis of the heating and cooling needs.

Tab.2.11 - Ranking parameters

Parameters	Dimension	Rank Heating		Rank Cooling	
		Bolzano	Rome	Bolzano	Rome
Overhang	[m]	6	5	4	4
Internal Gains	[W/m <sup>2</sup> ]	3	3	1	1
Infiltration rate	[ACH]	2	2	6	6
Night ventilation	[m <sup>2</sup> ]	8	8	7	7
Orientation	[°]	4	4	3	2
Transmittance	[W/m <sup>2</sup> K]	1	1	5	5
Fenestration ratio	[m <sup>2</sup> ]	5	6	2	3
Thermal inertia	[kJ/K]	7	7	8	8

The Morris Method shows a strong influence of the envelope and construction aspects (transmittances, infiltration, orientation, fenestration ratio and shading devices) and behavioural aspects (internal gains) on the heating and cooling demand.

In order to reach a certain energy performance target or to modify the building numerical simulations, this awareness allows prioritizing the studied parameters and tuning the models starting from the most important parameters.

### 2.3.10 Building simulation results

Tab.2.12 - Heating and cooling demand for two floor buildings - STD weather data

		Heating	Cooling	DHW
		[kWh/(m <sup>2</sup> *year)]		
Bolzano	BLD	40	13	14
	BHD	53	12	14
Roma	BLD	17	18	14
	BHD	26	18	14

Tab.2.13 - Heating and cooling demand for two floor buildings - EXTR weather data

		Heating	Cooling	DHW
		[kWh/(m <sup>2</sup> *year)]		
Bolzano	BLD	45	24	14
	BHD	59	24	14
Roma	BLD	25	25	14
	BHD	35	25	14

The analysis of different climatic data, and the definition of a climatic database is important in order to assess simulations allowing a comparison between different solutions or systems in a structured and verified manner. Considering the complex solar thermal systems, their performance are strongly affected by the boundary condition (climatic conditions and loads) due to different interaction through the multiple components that compose such systems. The two class of buildings analyzed (BLD, BHD) simulated using the two different climatic data (STD, EXTR) show a different energy demand for heating and cooling. In particular, for Bolzano, the heating demand increase of 10% to 14% moving from STD climatic data to EXTR respectively for BHD and BLD. An huge difference is visible in the cooling demand that is almost the double passing from STD to EXTR for the BHD building. For Rome an increase around 40-50% is visible as the cooling as the heating demand for the two levels of buildings considered.

## 2.4 Other components used

In this last chapter an overview of the numerical models (types) normally used in Trnsys for simulate solar Combi+ systems are listed and briefly explained. In particular, the Trnsys numerical system explained and analyzed in the following Chapter 4, has been simulated using types reported in the following Tab.2.14.

Tab.2.14 - List of components used into the numerical model

Component	Number	References
Dry cooler	Type 880	Eurac development [61]
Adsorption machine	Type290	Acs08 -2010 [62]
Heat exchanger	Type 5b	[46]
Compression heat pump	Type 847	Eurac development
Collectors	Type 1c	[46]
Thermal storages	Type 340	[63]
Circulation pump	Type 110	[46]
Valves	Type 11	[46]

### 2.4.1 Dry cooler

The dry cooler adopted in the simulations is a model developed by Besana [61] (Type 880). This type is a numerical model where the user can set up the dry cooler parameters accordingly to the system simulated. The calculation is based on the  $\epsilon/NTU$  method. Capacitance effects are also included by time averaging the thermal response (outlet fluid temperature and mass flow rate) on a user-defined time. The model has embedded a sort of PID controller, because in the mode of function used in these simulations (Mode 2), the fans rotational speed is adjusted for reach a certain level of outlet water temperature

function of the inlet air temperature. Some modifications (volumetric flow, electrical consumption and inertia) have been made on the model developed by Besana for better simulate the real behavior. These modifications are reported in the validation chapter (Chapter 3).

#### **2.4.2 Adsorption machine**

The model used for the dynamic simulations of the adsorption machine is a numerical model, developed directly by Sortech [62]. This model works on fixed maps, based on rated manufacturer data including a delay in the starting phase for simulate the machine heating up. The manufacturer provide the DLL of the model so no code modification is possible on this type. During the process of validation, as reported in the Chapter 3, a sort of filter has been developed on the output thermal fluxes, as explained later.

#### **2.4.3 Flat plate heat exchanger**

The heat exchanger used is a normal Type5 of the basic library of Trnsys [46]. This is used in the modality “b”, because in this way a counter flow heat exchanger is simulated. In this model all the inlet parameters are given (temperatures and mass flows) on the two side (hot and cold) including the overall heat transfer coefficient of the exchanger. The subroutine following the  $\epsilon$ -NTU method, calculate with these data the outlet parameters (temperatures) of the heat exchanger. Also for this component, in the Chapter 3, the validation has been computed in order to find the validated overall heat transfer coefficient given a certain inlet temperatures and mass flows levels.

#### **2.4.4 Compression heat pump**

The compression heat pump mode used in the simulation is a model developed starting from the standard Trnsys model Type 668 [46]. This subroutine models a single-stage reversible heat pump. Two operation modes are possible. In the first (cooling mode) the model reject energy to a liquid stream while in the second (heating mode) the model absorb energy from a liquid stream. The model works on two maps given by the user that are normally based on manufacturer data of thermal power exchanged and electrical power absorbed by the unit for a certain pair of load and source temperatures with a nominal fixed mass flow. The user can adopt this model as an on/off heat pump. When the control signal is one the heat pump give all the thermal power possible absorbing the related electrical power. When inlet temperatures of source and load are given and the values are not the exact value that has reported in the map, the subroutine calculate a linear interpolation between the two closest data.

A modification has been performed on this subroutine allowing to work at different mass flows, in order to optimize the heat pump operation logic using different values of the mass flow compared to the nominal one. In this way the matrix of data given to the subroutine is not function only to the inlet temperatures (2 variables) but function of



temperatures and mass flows (4 variables). The new maps used are developed using data from stationary test made in the Eurac laboratory.

#### **2.4.5 Collectors**

The subroutine used for simulate the flat plate collectors is the standard Type1 of Trnsys [46]. This subroutine models a quadratic efficiency collector following the Hottel-Whillier equation [15] (eq.1.6). In particular, the model used is the “c” where also the single-axis incidence angle modifier has to be implemented. In this model, using manufacturer data, a map of points function of the incidence angle is given following the eq.1.7. The type receive the total radiation and the incidence angle on the surface of the collectors with, the total and diffuse radiation on the horizontal and the external dry bulb temperature. Furthermore it receives the fluid inlet temperature and the mass flow. From standard test on the collectors in the subroutine the 3 coefficients of the efficiency curve ( $c_0$ ,  $c_1$ ,  $c_2$  of the eq.1.6) has to be indicated. A correction factor is given in order to compute the number of series, and also his number has to be indicate in the subroutine. The type return the outlet temperature and the mass flow for a computed condition given by external temperature, radiation and inlet temperature, following the theory given in the Chapter 1.

#### **2.4.6 Thermal storages**

The thermal storages are simulated using the Type 340 [63]. This subroutine allow to reproduce the behavior of a stratifies fluid storage tank with double ports to simulate the direct connection for thermal charging and discharging and internal heat exchangers. All the characteristics have to be set, from the geometrical point of view (dimensions, volume, connections position, heat exchangers parameters, etc.) and from the energy point of view (physical property of fluid, thermal losses, overall heat exchanger coefficient, etc.). Parameters related to the stratification effect simulation were validated [64] with monitoring data. These coefficients are computed in the model and correlate the internal heat exchanger heat transfer coefficient to the mass flow and to the difference of temperature in the different nodes that compose the numerical model of the storage [63].

#### **2.4.7 Circulation pumps**

For the hydraulic pumps, the Trnsys model of variable speed pump are used (Type110) [46]. This type is able to maintain the mass flow on the outlet between zero and a fixed rated value. The mass flow varies linearly with the control signal given to the pump. Also the electrical consumption of the pump is computed in function of the control signal using some parameters that represent the coefficients of the electrical consumption quadratic curve (as reported in the Chapter 3). Other coefficients have to be set in order

to understand the fraction of the electrical energy converted by the pump in thermal energy and given to the fluid increasing its temperature.

#### **2.4.8 Valves**

Different kind of valves are employed in the model. All these components are including in the subroutine of Trnsys (Type11) [46]. Different configurations of this type simulated different kind of valves (flow diverter or mixer with or without control, tempering valve, mixing T-piece) and for each of this configuration the inlet (one or two) temperatures and mass flows and eventually the control function are given with the results of the computation of the outputs (one or two) temperature and mass flows. When tempering valve is considered also the set point temperature and the hot reference temperature as to be indicated for the correct function of the subroutine.

# Chapter

## 3.

### Numerical model validation

#### 3.1 Introduction

In the field of complex thermal system simulation, the numerical model validation process is crucial, because after this process, the validated model allows to predict long term performance of the systems and at the same time build credibility in the numerical models. This process allows to quantify the models approximation and enables to extrapolate reliable simulation results (prediction) under different conditions (loads, weather conditions) for which the computational model has not been validated. After the validation procedures, the numerical model resulting can be used to improve the efficiency of the real system through the control optimization. Moreover, the validated model can be used in the fault detection, where the comparison between the real system behavior and the numerical model results is done. This difference is the variable considered for the fault identification. In this manner, imposing a threshold of acceptance, the irregular system operation can be easily detected.

In literature, there are different approaches to the validation issue. In some works ([68], [69]) the validation is divided in two steps with a first called “calibration” and a second called “validation”. In these two phases a different monitoring database have been used for a first tuning and afterward verify the model in order to leads similar good agreement between numerical and monitored outputs. Usually, the calibration procedures are connected to the numerical models tuning process (more often the measure devices) with laboratory controlled conditions while in some literature the terms calibration and validation are used with the same meaning [70].

Some works have been found in literature on the topic of numerical model Validation and Verification (V&V) ([71], [72]). In particular, these papers are related to the procedures definition. In this V&V procedure reported in Fig.3.1, the right branch illustrates the process of developing and exercising the model and the left branch illustrates the process of obtaining experimental data via physical test.

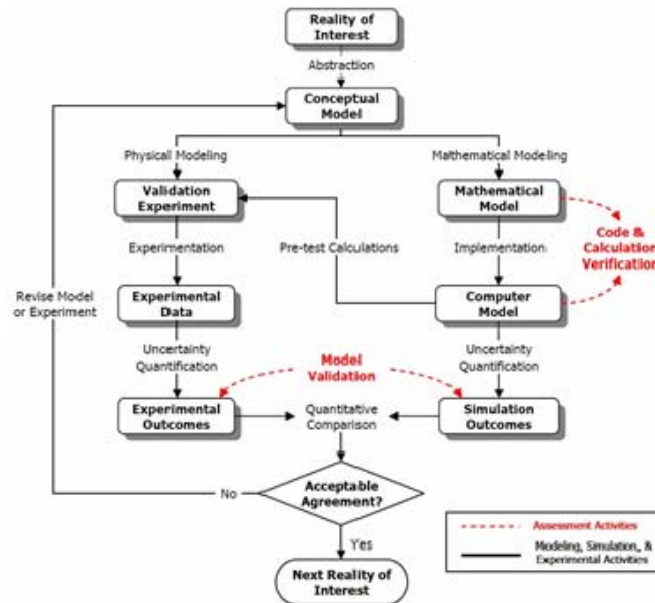


Fig.3.1 - Validation and verification procedure [71]

Observing this scheme, is important to underline some issues still open in the numerical validation field. The validation procedure has the core on the “**Quantitative Comparison**”, based on the comparison of the two outputs using some indicators and checking if they are in the field of acceptable agreement. On this comparison there is no accordance on the variables analyzed and on the usage of instantaneous or integral values. Normally, for comparison between the numerical models and the monitored data in the field of energy systems, thermal powers or temperatures and mass flows are used while there are no commonly accepted indicators (cost functions like residual error: RE, root mean square error: RMSE and coefficient of variance: CV) and thresholds of confidence. In some works for the validation of chillers the objective function used was the CV less than 8% or RE less than 5% [69] while in the work [68], related to solar cooling plant, the indicator is the daily energy (for the single component) deviation between simulated and monitored system within an acceptable range of 5-10% [68] or deviation of the yearly energy less than 8% [73]. Another important question for the characterization of the model, not yet well defined, is the acquisition time used for the experimental data and the of length monitoring campaign. Also for this issue, different approach is found in the literature with 5 days [70], four months [74] or an entire season [69].

The method developed (Fig.3.2) can be applied for the model validation of a generic energy system when monitoring data and simulation outputs are available. It is an extension of usual V&V methods [75] obtained by integrating new techniques for a more effective and consistent validation result.

As first step, it is essential to gather all the necessary information of the monitoring system set-up (e.g. temperature sensors and flow-meter position, acquisition time step).

This phase, defined as “**Numerical Model Definition**” (see Fig.3.2), is essential for defining the outputs and the requirements that the numerical model has to fulfill.

When a large amount of raw monitoring data are collected, it is important to manage them properly from statistical/mathematical point of view. Bin Method Analysis (BMA) [76] is here used as the main technique for data reduction. This technique consists in time-averaging instantaneous monitoring data, with the aim of reducing the influence of unsteady conditions and deriving a clear understanding of the system component behavior. The so-arranged data can be further averaged in bins and typical component performance curves (e.g. efficiency curve, heat transfer coefficient, ...) can be derived. This analysis can be carried out on raw or post-processed monitoring data, accordingly to the case or the needs. In general, it can be stated that the larger the number of data, the more consistent the output from the BMA.

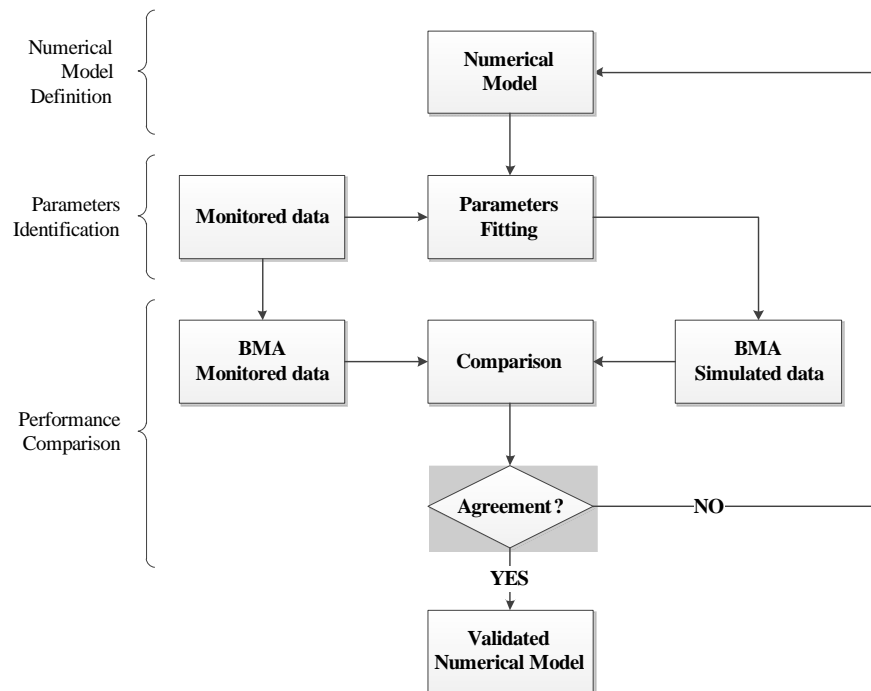


Fig.3.2 - Iterative validation procedure [64]

In order to test the adherence of the simulations to the reality, a phase of “**Parameter Identification**” (PI) (see Fig.3.2) follows, where monitoring data (temperatures and mass flow rate) are used as boundary conditions to the simulation models, while simulated and monitored outlets quantities are compared. During the PI, minor component parameters have been varied within realistic bounds, in order to minimize the objective function. The historical data period on which carrying out the PI should represent typical working conditions of the system component [77].

As example, a specific objective function OBJ has been developed for a work related to the validation of an immersed heat exchanger using two parameters [64]. It is a

combination of two correlation coefficients based on the simulated (x) and monitored (y) heat transfer power: the first is known as Pearson product-moment Correlation Coefficient PCC [77] and the second is known as Theil Inequality Coefficient TIC [75], [78], [79]. The objective function OBJ is defined in a way that the optimum value has to tend to 0, when PCC and TIC tend to 1 and 0 respectively [64].

When the PI converges towards the minimum, the maximum agreement has been found. This however, does not say anything on the accuracy of the model. Therefore, a comparison of the numerical results with the monitoring data has to be performed on the basis of quantitative performance figures. To this purpose, a further BMA is made on the simulation outputs. A quantitative comparison among the monitoring and simulated BMA curves is then performed (**“Performance Comparison”**, see Fig.3.2). If the Root Mean Square Error (RMSE) value of the curves is within the acceptance criterion defined by the user, then the validation is accomplished, otherwise the numerical model has to be revised or upgraded. This process is repeated until an adequate level of agreement is found.

$$RMSE = \sqrt{\frac{\sum_{i=1}^n (x-y)^2}{n}} \quad (\text{eq.3.1})$$

### 3.2 Validation of the Dry Cooler numerical model

The dry cooler validation has been made using monitoring data comes from a pilot plant. Using these data and following the procedure previously explained, different modes of function have been validated using a simple Trnsys model (Fig.3.3). Here, the numerical model of Trnsys has been posed in the same conditions of the real system using monitoring data. The outputs monitored and simulated have been compared. In particular the two parameters compared are the thermal power exchanged and the fan electrical power consumption.

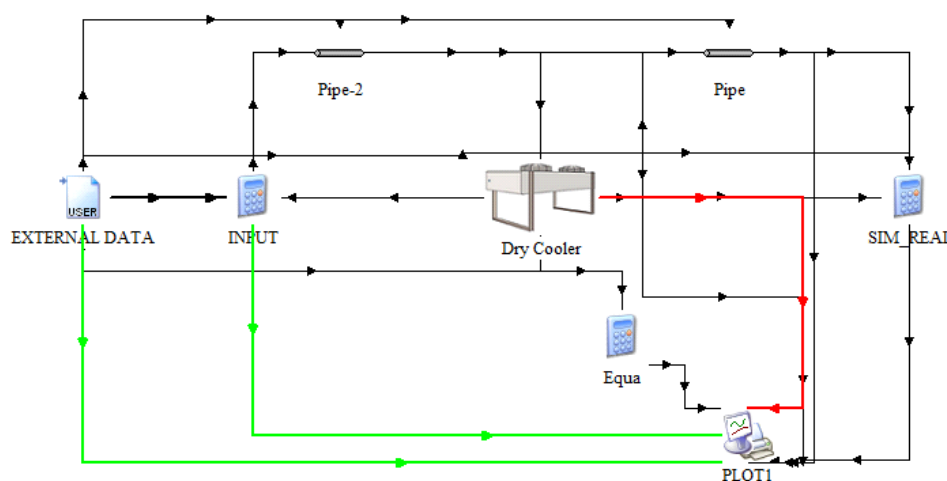


Fig.3.3 - Trnsys model used for the validation procedure

The dry cooler installed the solar Combi+ system analyzed in the following chapter (Chapter 4), has been employed as the heat rejection system in common between two different machines, the adsorption and the compression heat pump. For this reason almost three different range of work can be identified and validated. The first mode validated has been related with the function of the dry cooler with the compression machine in cooling mode (as heat rejection) while the second with the same compression machine but that function in heat pump mode (as heat sorption). The third mode has been related to the connection with the adsorption machine as function of heat rejection. The controller, implemented in the Trnsys subroutine (as reported in Chapter 2) adjust the fan speed in order to reach a certain temperature of the outlet fluid temperature. During this phase the dry cooler is equipped with sprinkles that increase the cooling effect of the heat rejection using the evaporative phenomena of the water on the fin surface of the heat exchanger. In this phase the heat rejection is a hybrid cooler (Fig.3.4) as introduced in the Chapter 1.



Fig.3.4 - Dry cooler scheme

Before to start with the validation procedure, a relation between the signal of the fan and the electrical consumption has been elaborated. In the original model developed by Besana [61], the electrical consumption of the fans was computed as the rated electrical power of the fan multiplied by the cubic power of the control fan's signal. During the validation process, the ideal cubic curve of consumption has been modified with four parameters as follows:

$$W_{el} = W_{rated} \cdot (f_4 + f_3 \cdot Y + f_2 \cdot Y^2 + f_1 \cdot Y^3) \quad \left[ \frac{kJ}{h} \right] \quad (eq.3.2)$$

The four parameters have been selected for fit the monitoring curve, as reported in Fig.3.5. The resulting parameters are reported in Tab.3.1.

Tab.3.1 - Parameters used for validation of the fan electrical consumption

$W_{rated\_1FAN} \left[ \frac{kJ}{h} \right]$	$f_1$	$f_2$	$f_3$	$f_4$
2520	0.5238	0.8175	-0.0833	0

Also for the volumetric air flow rate elaborated by the fan, this difference between ideal behavior has been computed, using the same approach of the electrical consumption. In the case of volumetric flow, only some points of function were available coming from the manufacturer data. The equation implemented is the follow and the parameters used are reported in Tab.3.2.

$$\dot{V} = \dot{V}_{MAX} \cdot (fv_4 + fv_3 \cdot Y + fv_2 \cdot Y^2 + fv_1 \cdot Y^3) \quad \left[ \frac{m^3}{h} \right] \quad (eq.3.3)$$

Tab.3.2 - Parameters used for validation of the volumetric flow of the fan

$\dot{V}_{MAX} \left[ \frac{m^3}{h} \right]$	$fv_1$	$fv_2$	$fv_3$	$fv_4$
2520	0.5238	0.8175	-0.0833	0

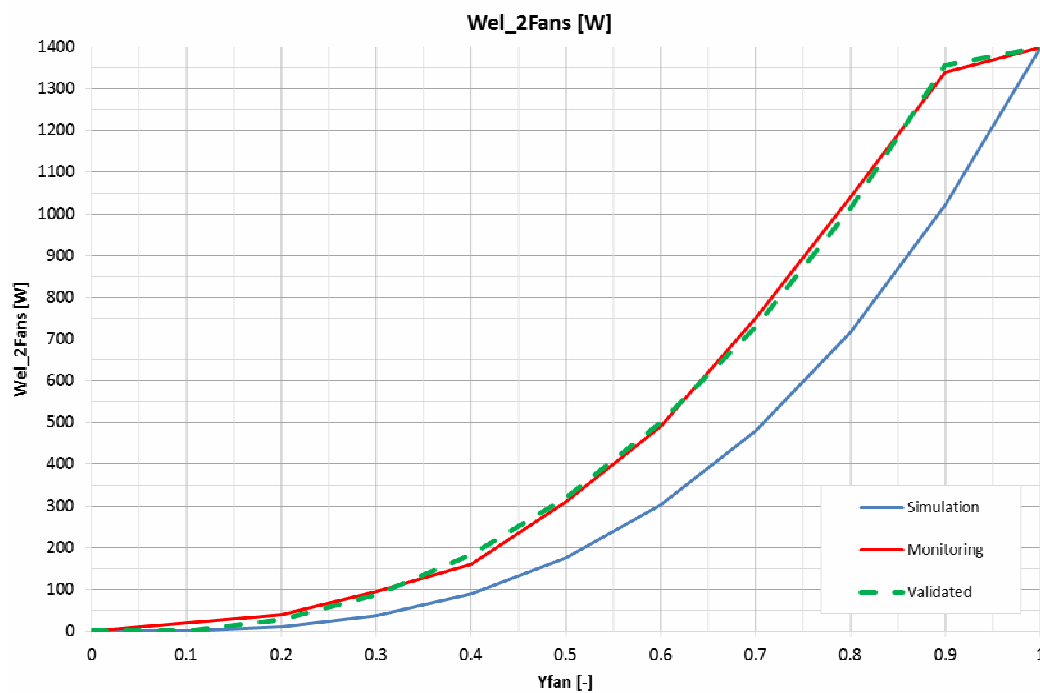


Fig.3.5 - Comparison between electrical consumption of fans  
(ideal: cubic function, monitored and validated)

Defined the equation for compute the fans electrical consumption and the volumetric air flow elaborated by the dry cooler, the three different mode of work have been validated. Starting from the first, as presented in the introduction, the idea was to modify the model to reach good agreement between the model results and the effective behavior of the component, tuning parameters of the numerical model. In the first model a comparison between the simulated and monitored thermal and electrical power absorbed by the dry



cooler have been compared. As reported in Fig.3.6 and Fig.3.7, clouds of data monitored and simulated with a time step of one minute for all the summer season (from June to September 2012) show a good agreement respectively for thermal and electrical powers. Using the process of data reduction BMA explained in the introduction, data have been reduced and two curves of behavior have been computed using respectively 5 and 9 BINS with an integrative time of 1 minute. The Fig.3.8 and Fig.3.9 show these analysis with an implementation of a delay in the response of the numerical model of 2 minutes in order to simulate the inertia due to the water flow in the air/water heat exchanger of the dry cooler. Good agreement is notable in the electrical power of the fan and in the thermal power exchanged. Here the huge difference between the two curves is visible for high temperature with a RMSE of 5% and with a difference in terms of thermal energy exchanged and electrical energy consumed during the whole summer season around 10%. This difference is mainly due to the fact that in the real plant, the rejection of the heat pump is controlled maintaining constant the pressure of condensation, instead of the numerical model used (that is not a physical model of the machine but only a subroutine that works on fixed maps) where is controlled the return temperature of the dry cooler function of the external temperature.

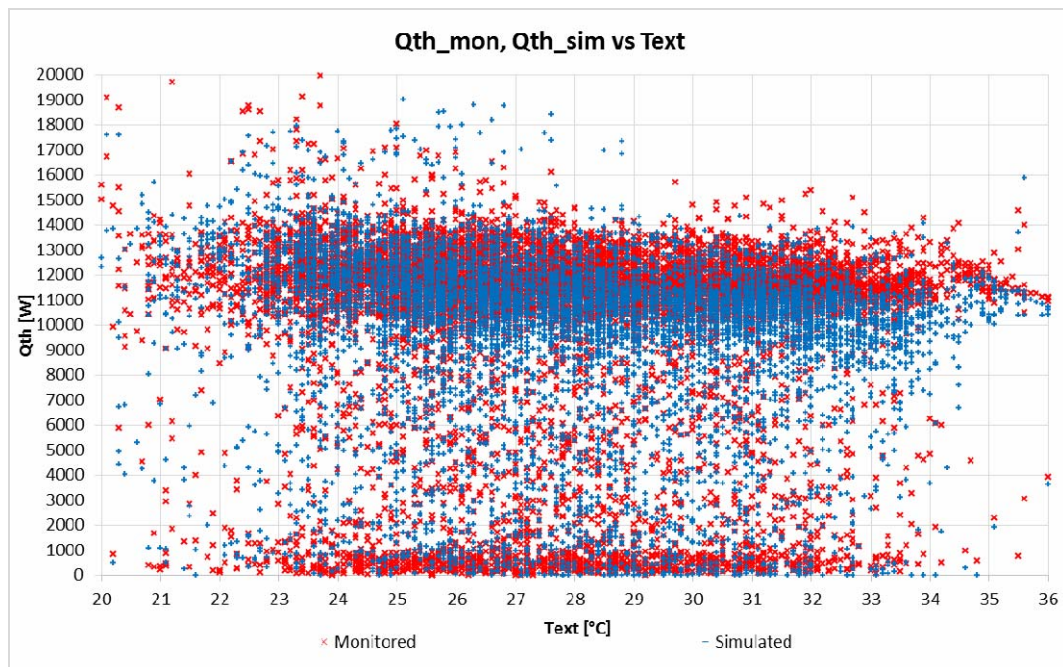


Fig.3.6 - Comparison between thermal power exchanged  
(Cooling season - Compression machine. Months: 06-07-08-09/2012)

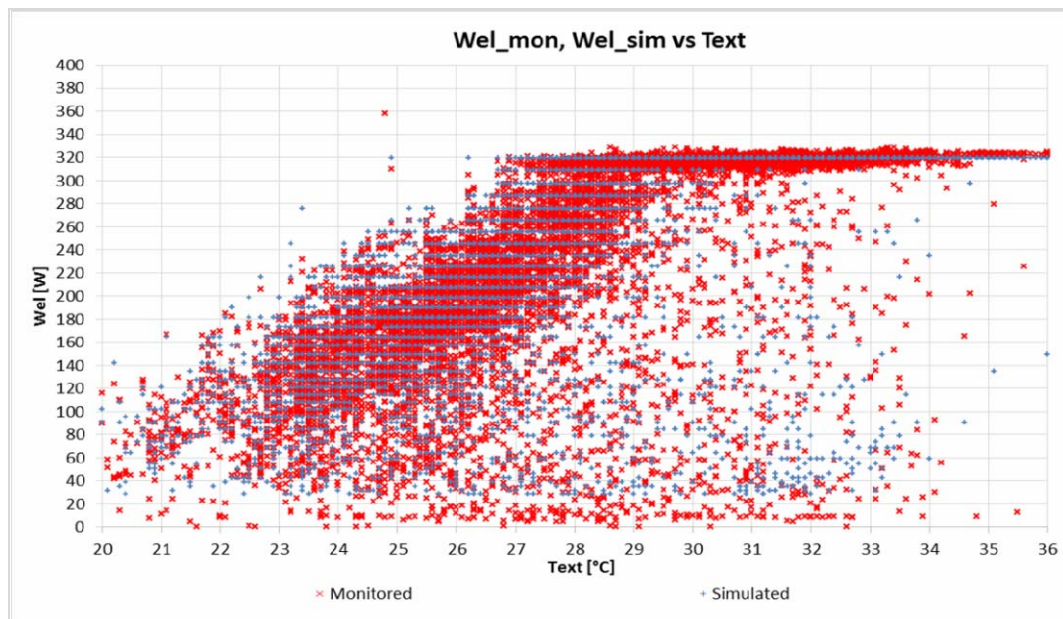


Fig.3.7 - Comparison between electrical power exchanged  
(Cooling season - Compression machine. Months: 06-07-08-09/2012)

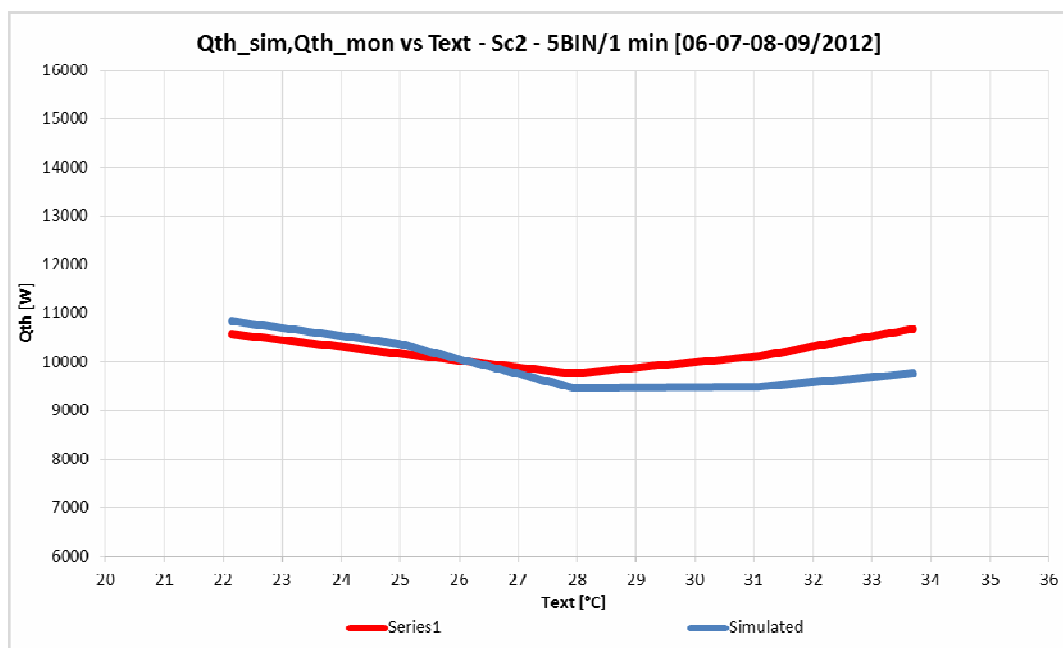


Fig.3.8 - BMA between thermal power exchanged  
(Cooling season - Compression machine. Months: 06-07-08-09/2012)

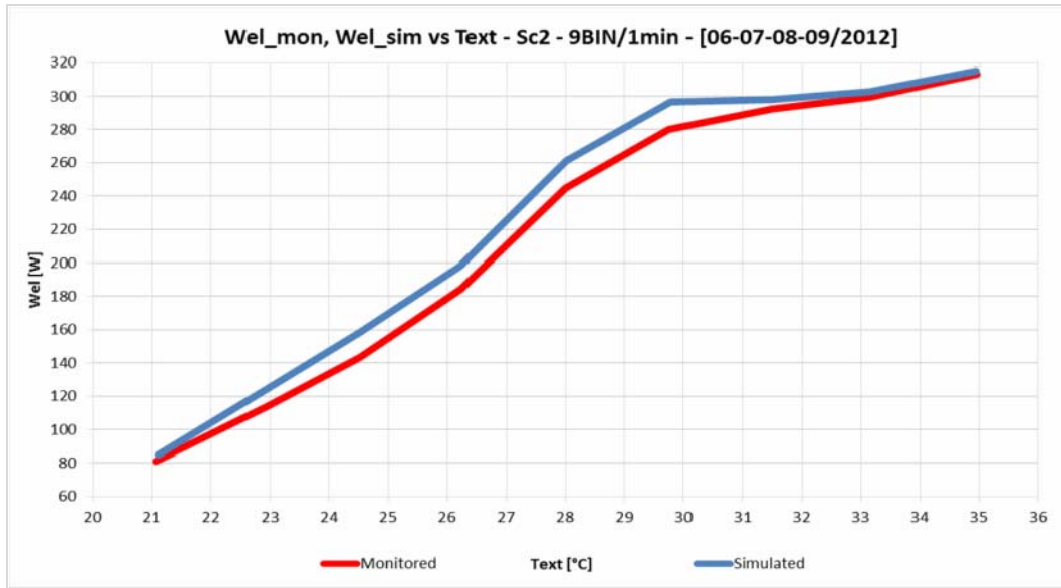


Fig.3.9 - BMA between electrical power exchanged  
(Cooling season - Compression machine. Months: 06-07-08-09/2012)

After this analysis, the behavior of the dry cooler during winter season (connected with the evaporative side of the reversible compression heat pump) has been validated, using the same approach. From the first data analyzed an incongruence between the numerical model and the monitored data was visible. The difference was due to the fact that the numerical model of the dry cooler not consider an increasing of thermal power caused by the condensation of the humidity that is present in the air. For compute this part of energy easily without have a model that represent perfectly this effect, an amount of thermal energy has been summed to the heat exchanged. The way choose for compute this fraction of energy is try to correlate the amount of this thermal energy to the external temperature and humidity. A simple way to relate the condensing power to external temperature has been followed, using these equations:

$$\dot{Q}_{lat} = \frac{\dot{Q}_{cond}}{a} \cdot T_{amb} + \dot{Q}_{cond} \quad T_{amb} < 0 \quad \left[ \frac{kJ}{h} \right] \quad (eq.3.4)$$

$$\dot{Q}_{lat} = \dot{Q}_{cond} \quad T_{amb} \geq 0 \quad \left[ \frac{kJ}{h} \right] \quad (eq.3.5)$$

Using a value of  $\dot{Q}_{cond} = 950W$  and parameter  $a=15$  for the installation studied (in Bolzano) and the range of temperature where our system works ( $T_{amb} > -6^{\circ}C$ ). Using this approximation, for the monitoring data of February 2012 the thermal heat exchanged is reported in Fig.3.10 while the electrical power of the fan is reported in Fig.3.11. The BMA analysis on these two energies are reported respectively in Fig.3.12 and in Fig.3.13 with 5 BINS and an integrative time of 1 minute.

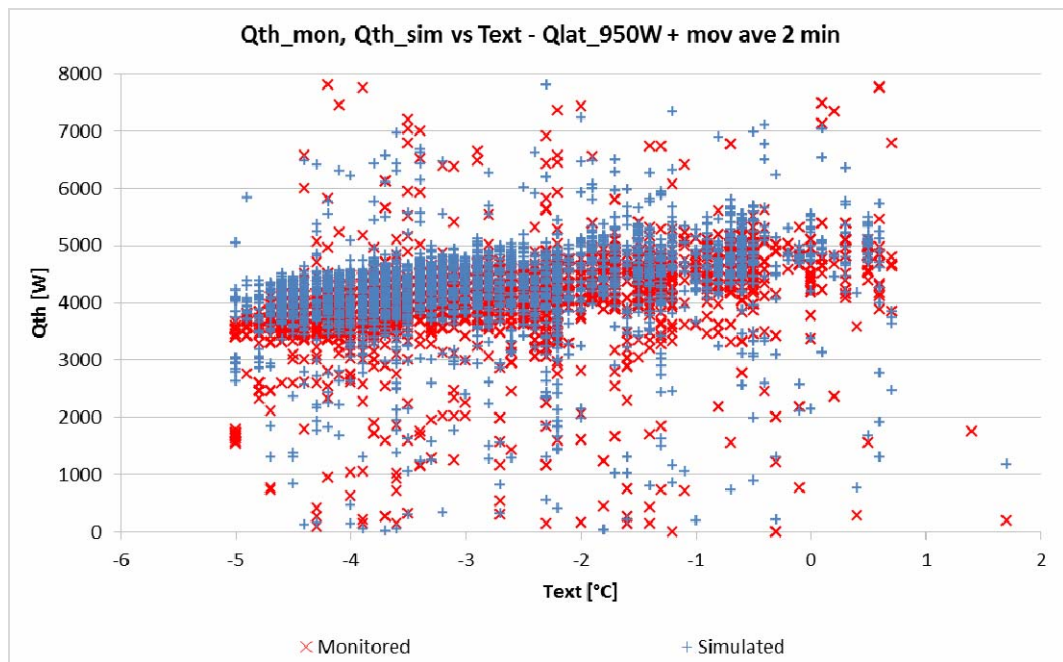


Fig.3.10 - Comparison between thermal power exchanged  
(Heating season - Compression machine. Month: 02/2012)

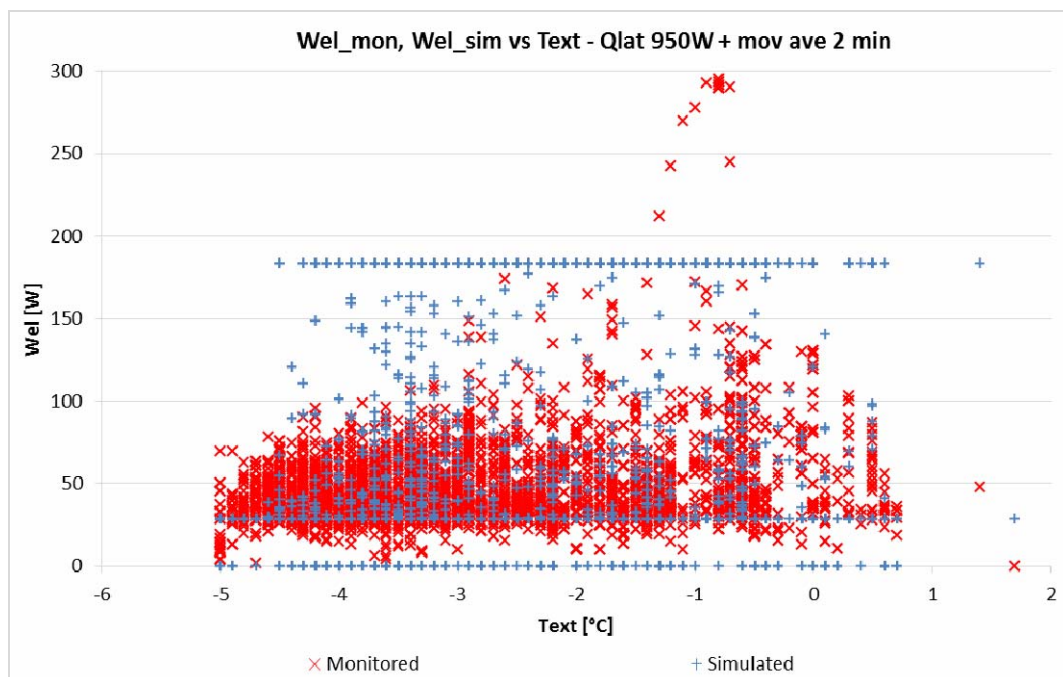


Fig.3.11 - Comparison between electrical power exchanged  
(Heating season - Compression machine. Month: 02/2012)

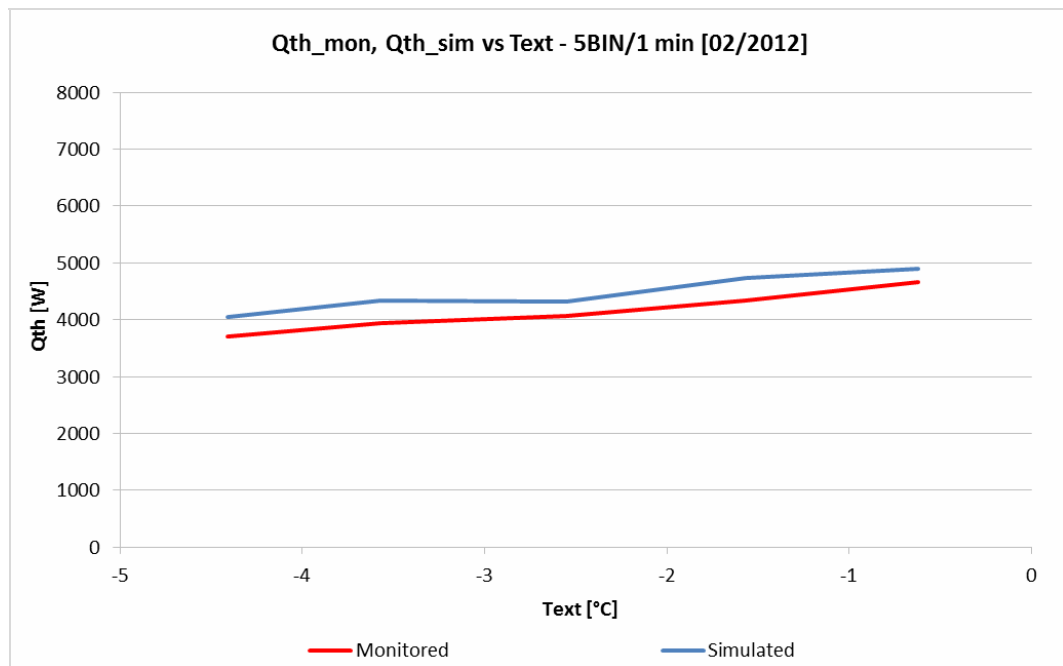


Fig.3.12 - BMA between thermal power exchanged  
(Heating season - Compression machine. Month: 02/2012)

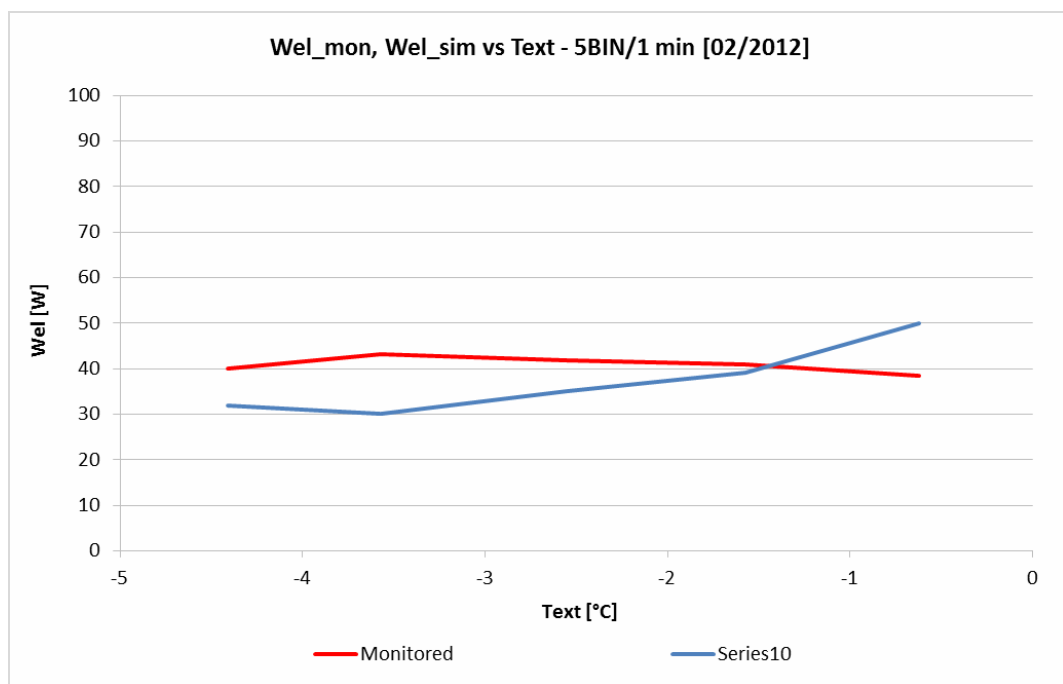


Fig.3.13 - BMA between electrical power exchanged  
(Heating season - Compression machine. Month: 02/2012)



The validation process on these component has been made in order to fulfill the thermal and electrical power exchanged and consumed by the dry cooler and the amount of energy consumed by this component during the month analyzed. The RMS error, using the approximation on thermal energy for condensation for the electrical power is around 20% and 8% on thermal energy. In terms of thermal energy exchanged during the month used for validate the model is around 15% and electrical energy around 3%. This difference is mainly due to the absence of a correct model to simulate the thermal energy exchanged in the condensation and icing phases that affect also the electrical consumption of the fan caused by the increased heat transfer during these phenomena. The third working mode, related to the heat rejection of the adsorption machine, include also the effect of the sprinkles that increase the heating rejection capacity of the dry cooler. For this reason only the monitored data of August (08/2012) could be useful for characterize the behavior of the dry cooler in heat rejection mode. In the Fig.3.14 and Fig.3.15 the thermal and electrical power exchanged are reported while in the Fig.3.16 and Fig.3.17 the BMA analysis reported. The data time integration, also in this case, has been 1 minute with 5 BINS. The results show a good agreement between thermal energy simulated and monitored but the electrical consumption analysis shows a difference between monitored and simulated, mainly due to the pressure losses effect due to the water between the fins of the heat exchanger and the evaporative effect of the water in this model not considered. Further development on the model will be done in the future to solve this problem, describing better this phenomena and the behavior of the Dry cooler in this conditions. In terms of energy the electrical consumption is simulated 5% less than the monitored while the thermal energy is increased of 2% using the monitoring data of the month analyzed.

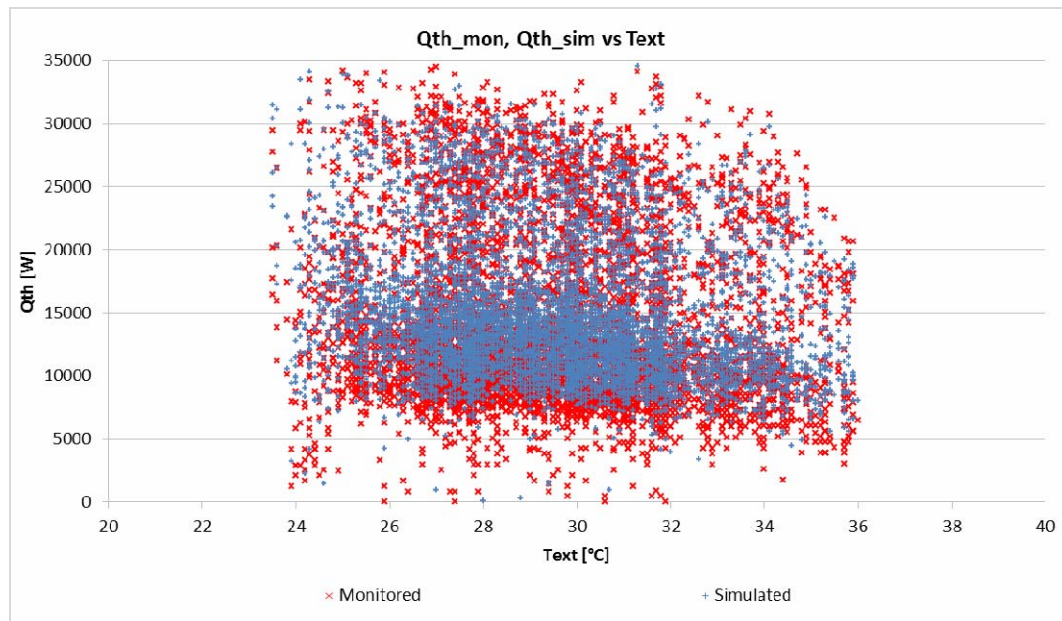


Fig.3.14 - Comparison between thermal power exchanged

(Cooling season - Adsorption machine. Month: 08/2012)

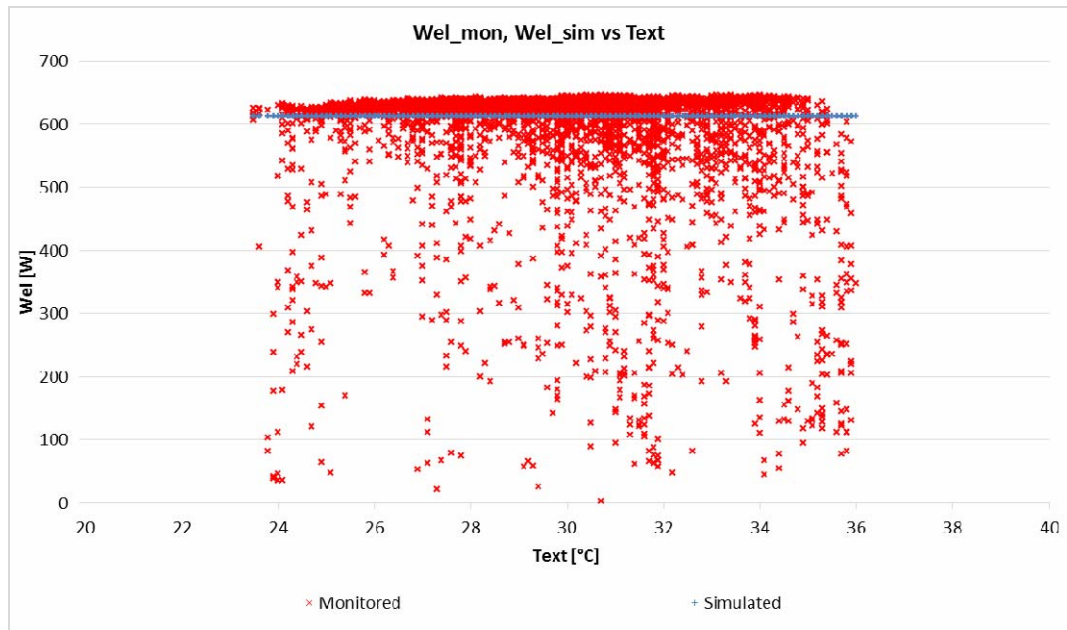


Fig.3.15 - Comparison between electrical power exchanged  
(Cooling season - Adsorption machine. Month: 08/2012)

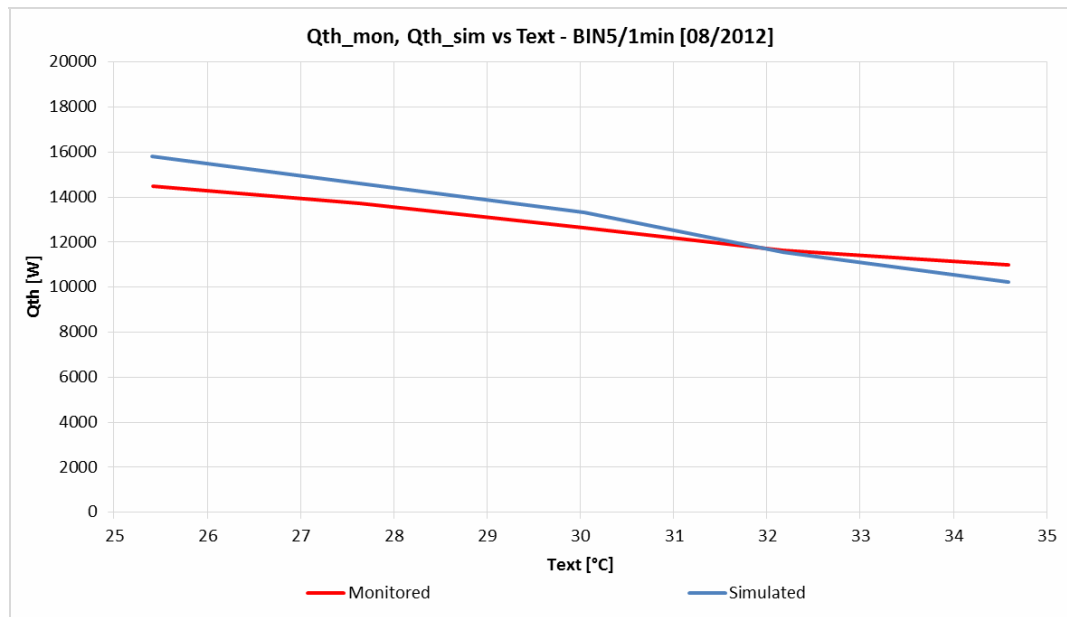


Fig.3.16 - BMA between thermal power exchanged  
(Cooling season - Adsorption machine. Month: 08/2012)

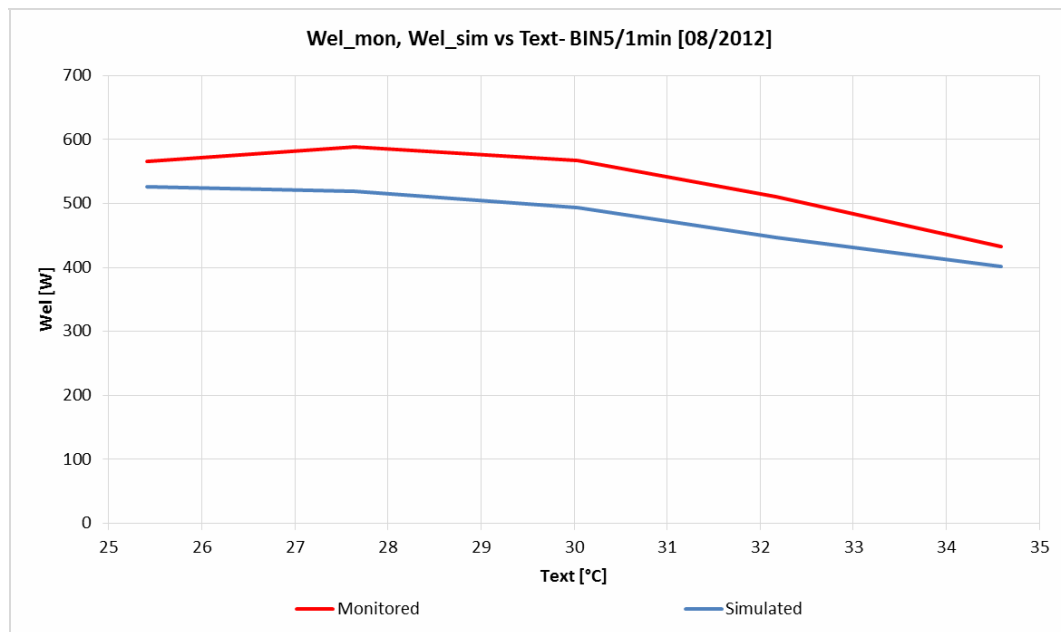


Fig.3.17 - BMA between electrical power exchanged  
(Cooling season - Adsorption machine. Month: 08/2012)

### 3.3 Validation of the adsorption machine numerical model

The validation of the adsorption machine has been made using in data from stationary and dynamic test in the laboratory of Eurac. Firstly a comparison between manufacturer data and stationary lab test has been implemented in order to find the difference between the manufacturer and the test data. After that, the numerical model has been modified in order to fit better the data from stationary test. During a second phase, the comparison between curves and points of dynamic test has been made in order to check the computed stationary curve with dynamic operative points.

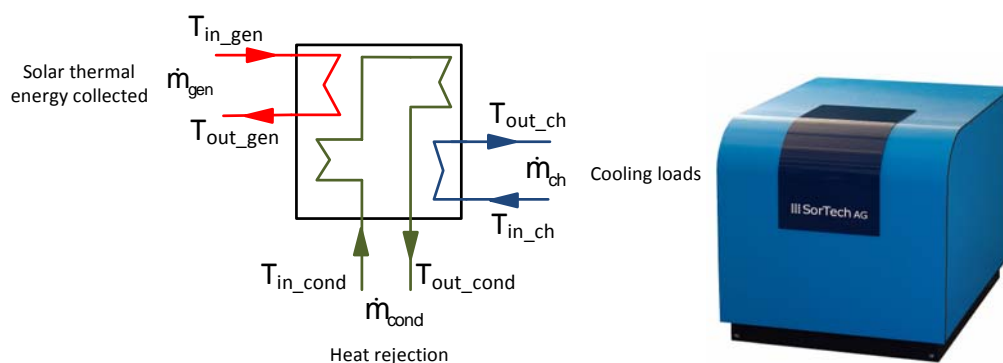


Fig.3.18 - Adsorption machine scheme with connections



The numerical model used for simulate the adsorption machine is a fixed model produced by the manufacturer of the adsorption machine (as introduced in the Chapter 2) that working on fixed maps. In order to modify the behavior of the model a sort of “filter” has been built in order to modify the outputs of the model with a correction factor opportunely computed. The following equations show the idea followed during the validation phase.

The adsorption machine receive three inputs (temperatures) with fixed mass flow rate equal to the nominal (as reported in Fig.3.18). The high temperature level related to the driving thermal power of the generator (“\_gen”), a middle level of temperature related to the heat rejection (“\_cond”) and the chiller part, with the low level used for satisfy the cooling loads of the users (“\_ch”).

The filter works mainly on the thermal power of the generator and chilling sides. The validated values of powers exchanged are equal to the model computed value summed by a contribution, as reported in the following equations:

$$\dot{Q}_{ch\_val} = \dot{Q}_{ch} + D\dot{Q}_{ch} \left[ \frac{kJ}{h} \right] \quad (eq.3.6)$$

$$\dot{Q}_{gen\_val} = \dot{Q}_{gen} + D\dot{Q}_{gen} \left[ \frac{kJ}{h} \right] \quad (eq.3.7)$$

The two other parameters are normally used for characterize the behavior of the sorption machines are the thermal power of condensation and the energy efficiency ratio ( $EER_{th}$ ) of the machine. As mentioned in the Chapter 1 (eq.1.8), the  $EER_{th}$  is computed as the ratio between the thermal power used for cooling and the thermal power adsorbed by the machine. Here, during the validation, this ratio has been calculated using the two validated values of the thermal power explained before. Following this approach the two new parameters are:

$$\dot{Q}_{cond\_val} = \dot{Q}_{ch\_val} + \dot{Q}_{gen\_val} \left[ \frac{kJ}{h} \right] \quad (eq.3.8)$$

$$EER_{th} = \frac{\dot{Q}_{ch\_val}}{\dot{Q}_{gen\_val}} \quad [-] \quad (eq.3.9)$$

For compute the validated thermal powers in the evaporator and generator sides, two terms have been summed to the power computed by the numerical model. These terms have been defined function of the inlet chilling temperature (as reported in Fig.3.18). The equations considered are quadratic function of this temperature and defined respectively as:

$$D\dot{Q}_{ch} = a \cdot T_{ch\_in}^2 + b \cdot T_{ch\_in} + c \left[ \frac{kJ}{h} \right] \quad (eq.3.10)$$

$$D\dot{Q}_{gen} = d \cdot T_{ch\_in}^2 + f \cdot T_{ch\_in} + g \left[ \frac{kJ}{h} \right] \quad (eq.3.11)$$

The manufacturer data for this sorption machine is given for only one level of  $T_{ch\_in}$  (18°C) while the stationary test has been performed with three different levels of this temperature (18°C / 20°C / 22°C). The minimum temperature was assessed to 18°C caused by the application of such a machine with low temperature radiative system, where the minimum supply temperature is 15°C to avoid condensation problems.

The data of the thermal power in the evaporator and generator side are given in function of the three thermal levels of the machine. In other word, for a given inlet chilling temperature, the curves of thermal cooling and generator power are given for different inlet generator temperature varying the condensing inlet temperature (as reported in the following figures). As example of the approach, for  $T_{ch\_in}=18^\circ\text{C}$ , the evaporative and driving thermal power curves are reported (Fig.3.19, Fig.3.20). In these figures can be appreciate the conservative approach, during the validation of the thermal power exchanged by the adsorption machine with profiles of the thermal evaporative power lower than the stationary data and bigger for the driving thermal power curves. This choice has been made in order to better fit all the conditions verified with different driving temperatures and different evaporative temperatures, for stationary and dynamic tests.

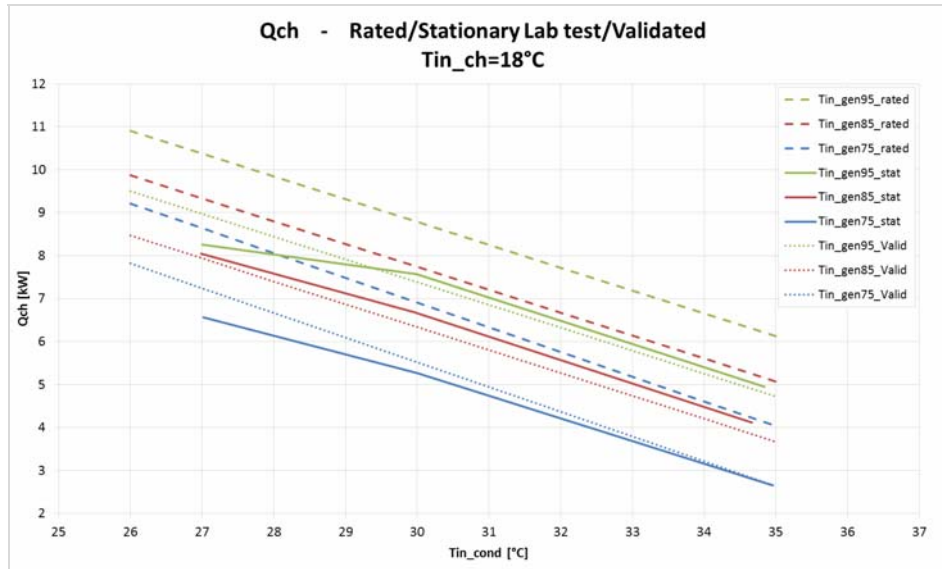


Fig.3.19 - Thermal chilling power for different driving temperatures at fixed chilling temperature (rated curve (\_rated), stationary test (\_stat) and filtered curve (\_Valid))

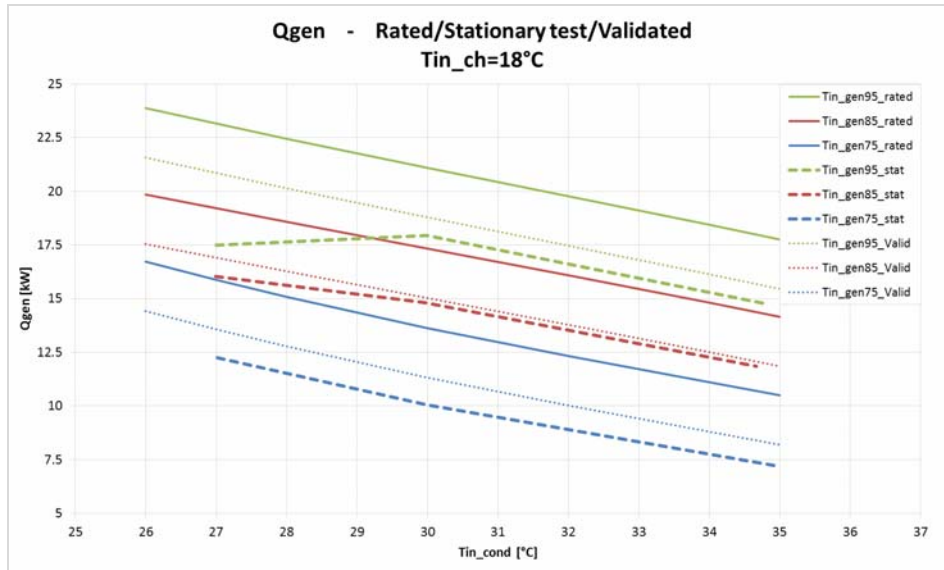


Fig.3.20 - Thermal driving power for different driving temperatures at fixed chilling temperature (rated curve (\_rated), stationary test (\_stat) and filtered curve (\_Valid))

In a second step, the comparison has been made with data coming from dynamic tests, averaged on the swap cycle that is characteristic of this kind of machines. As example of the results, the two following figures (Fig.3.21 and Fig.3.22), show a comparison between filtered curve (\_Valid) and data from dynamic test of chilling and driving thermal power for a given driving temperature and different inlet chilling temperatures.

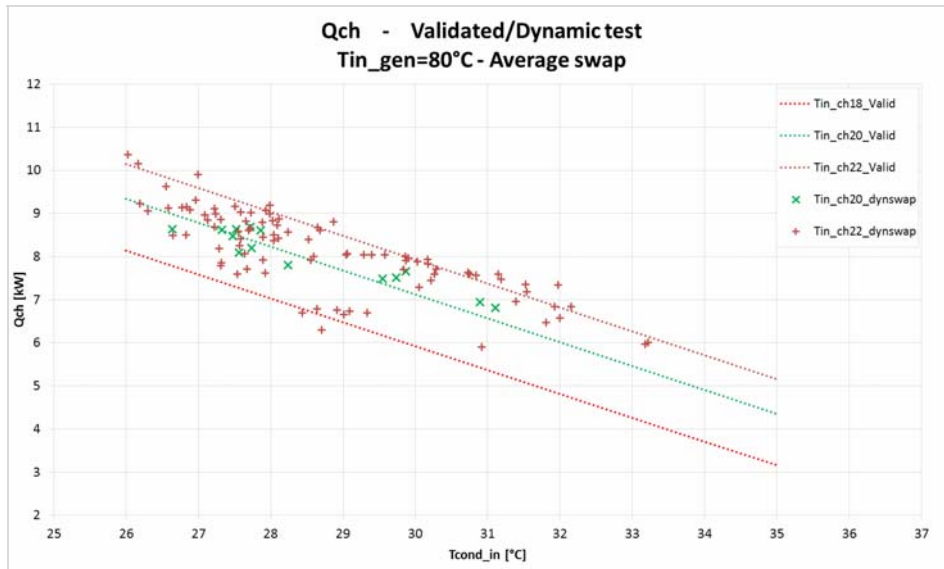


Fig.3.21 - Thermal chilling power for different chilling temperatures at fixed driving temperature (filtered curve (\_Valid) and dynamic test data (\_dynswap))

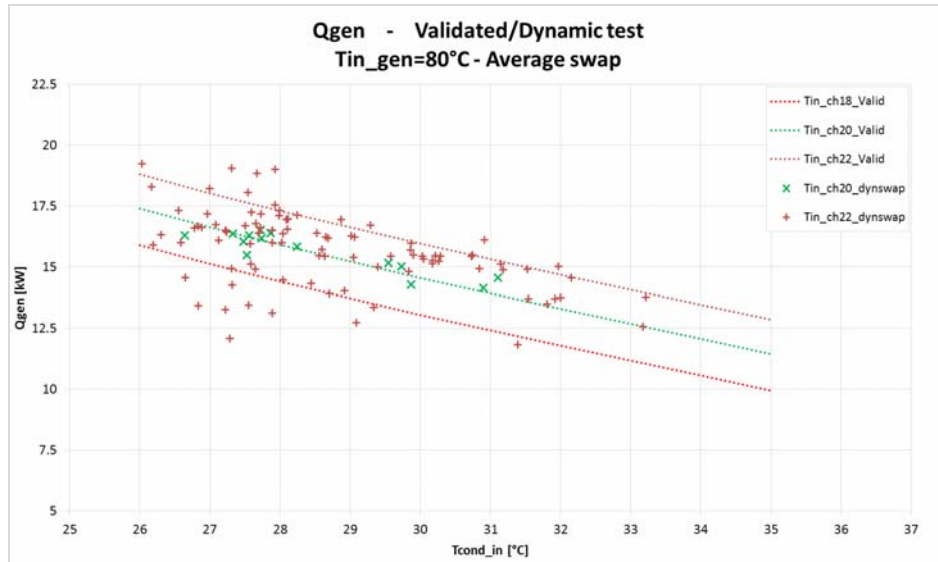


Fig.3.22 - Thermal driving power for different chilling temperatures at fixed driving temperature (filtered curve (\_Valid) and dynamic test data (\_dynswap))

### 3.4 Validation of the heat exchanger numerical model

The process of validation made on the heat exchanger start from the analysis of the Trnsys type used, as introduced into the Chapter 2. In the configuration studied, the heat exchanger has been simulated as an ideal counter flow with unmixed sides where the inputs (mass flows, temperatures, specific heats and the overall heat transfer coefficient) have been given to the system and internally the calculation of the outputs (temperatures, thermal power computed) has been made, based on simple calculation briefly reported in the following.

In the installation of Solar Combi+ studied, a flat plate heat exchanger has been installed between the thermal storages and the machines of the system. This disconnection has been realized between the storages and the evaporator side of the compression heat pump and the generator side of the adsorption machine using the heat exchanger. This because in the circuit between the machine and the heat exchanger a water and glycol mixture is flowing instead of simple water stored in the thermal storages. In Fig.3.23 is reported a schematic representation of the two heat exchanger connections.

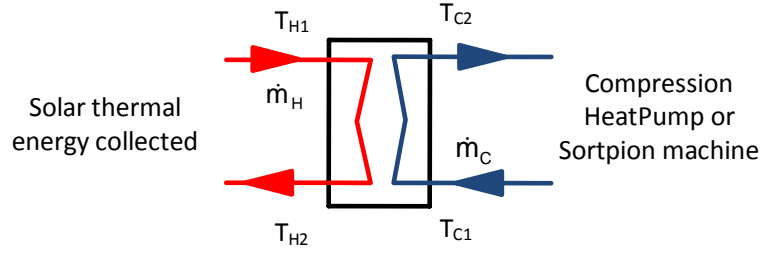


Fig.3.23 - Heat exchanger connections

In this system the equations computed are the followings. Minimum and maximum capacity rates are calculated as follows using the specific mass flow and the specific heat for the two sides of the heat exchanger (named hot "H" and cold "C"):

$$C_{\min} = \min(cp_H \cdot \dot{m}_H, cp_C \cdot \dot{m}_C) \quad \left[ \frac{\text{kJ}}{\text{h} \cdot \text{K}} \right] = \left[ \frac{\text{kJ}}{\text{kg} \cdot \text{K}} \right] \cdot \left[ \frac{\text{kg}}{\text{h}} \right] \quad (\text{eq.3.12})$$

$$C_{\max} = \max(cp_H \cdot \dot{m}_H, cp_C \cdot \dot{m}_C) \quad \left[ \frac{\text{kJ}}{\text{h} \cdot \text{K}} \right] = \left[ \frac{\text{kJ}}{\text{kg} \cdot \text{K}} \right] \cdot \left[ \frac{\text{kg}}{\text{h}} \right] \quad (\text{eq.3.13})$$

The code of the subroutine is based on the  $\varepsilon/\text{NTU}$  approach. Here the counter flow unmixed heat exchanger efficiency, is computed function of the value of the heat capacity ratio. Three cases are possible:

$$C_r = 1 \quad \varepsilon = \frac{\text{NTU}}{\text{NTU} + 1} \quad (\text{eq.3.14})$$

$$C_r = 0 \quad \varepsilon = 1 - \exp(-\text{NTU}) \quad (\text{eq.3.15})$$

$$C_r < 1 \quad \varepsilon = \frac{1 - \exp(-\text{NTU}(1 - C_r))}{1 - C_r \cdot \exp(-\text{NTU}(1 - C_r))} \quad (\text{eq.3.16})$$

Where :

$$C_r = \frac{C_{\min}}{C_{\max}} : \text{the heat capacity ratio;} \quad (\text{eq.3.17})$$

$$\text{NTU} = \frac{UA}{C_{\min}} : \text{the Number of Thermal Unit.} \quad (\text{eq.3.18})$$

The heat exchanger thermal power and the outlet temperatures are computed using the following equations, function of the inlet temperatures:

$$Q_{th} = \varepsilon \cdot C_{min} \cdot (DT) \quad [kW] \quad (eq.3.19)$$

$$T_{H2} = T_{H1} - \frac{\varepsilon \cdot C_{min} \cdot (DT)}{cp_H \cdot \dot{m}_H} \quad [K] \quad (eq.3.20)$$

$$T_{C2} = T_{C1} + \frac{\varepsilon \cdot C_{min} \cdot (DT)}{cp_C \cdot \dot{m}_C} \quad [K] \quad (eq.3.21)$$

Where :

$$DT = T_{H1} - T_{C1} \quad [K] \quad (eq.3.22)$$

is the maximum difference of inlet temperature of the heat exchanger. In the numerical model adopted in the simulation, the value of UA has been given and it has been calculated using manufacturer data for a flat plate heat exchanger. The system analyzed is characterized by two function modes. The first one was related to the function of the adsorption machine and the second one related to the connection of the thermal energy stored with the evaporator side of the reversible compression heat pump, in heating mode. The first one has been characterized with high temperature ( $65^\circ C < T_{H1} < 90^\circ$ ) instead of the second where low temperature ( $T_{H1} < 40^\circ C$ ) has been present caused by the priority in the control strategy given to the domestic hot water preparation (as explained more accurately in Chapter 4).

For represent these two function modes, the coefficients of the eq.3.23 (UA function of  $C_r$  and DT) have been extrapolated from the manufacturer data. The equations used are the following, where the U-value is a logarithmic function of the heat capacity ratio weighted with the coefficients a, b. These parameters (a, b) have been computed as linear function of DT, in order to correlate the heat transfer coefficient with mass flow and the level of temperature. The equations considered are:

$$U = a \cdot \ln(C_r) + b \quad \left[ \frac{W}{m^2 \cdot K} \right] \quad (eq.3.23)$$

$$a = a_1 \cdot DT + a_2 \quad (eq.3.24)$$

$$b = b_1 \cdot DT + b_2 \quad (eq.3.25)$$

The idea to correlate the heat transfer coefficient with a logarithm function of  $C_r$  and linear function to the difference of temperature is related to the definition of efficiency that are an exponential function of  $C_r$  and the thermal power exchanged is a linear equation to the difference of temperature DT.

For the cooling mode with higher temperatures level, the relation only on the DT did not fit well the manufacturer data of the heat exchanger. Further relations have been used in order to better fit the data using relations with the inlet temperature of the heat side. These relations are:

$$a_1 = a_{11} \cdot T_{H1} + a_{12} \quad (eq.3.26)$$

$$a_2 = a_{21} \cdot T_{H1} + a_{22} \quad (eq.3.27)$$

$$b_1 = b_{11} \cdot T_{H1} + b_{12} \quad (eq.3.28)$$

$$b_2 = b_{21} \cdot T_{H1} + b_{22} \quad (eq.3.29)$$

For the two modes of function the parameters from the data interpolation process are reported in the following Tab.3.3.

Tab.3.3 - Parameters used in the heat transfer coefficient calculation

	$a_1$		$a_2$		$b_1$		$b_2$	
Heating ( $T_{H1} < 40^\circ\text{C}$ )	3.1		601.9		11.4		2175	
	$a_{11}$	$a_{12}$	$a_{21}$	$a_{22}$	$b_{11}$	$b_{12}$	$b_{21}$	$b_{22}$
Cooling mode ( $65^\circ\text{C} < T_{H1} < 90^\circ\text{C}$ )	0.07	-12.4	6.8	756.1	0.08	-15	17.2	2299

The process followed in the parameters identification adopted for UA calculation, started with the use of the manufacturer data for different working conditions (range of temperature, mass flow). Using these data, for each group a relation between U-value and  $C_r$  has been computed, as reported in Fig.3.24. Here two parameters for each series of data have been detected (parameters “a”, “b”) with the relation reported in (eq.3.22). Afterwards, using all parameters “a” and “b” detected, a correlation between these parameters and DT have been calculated but, as we introduced before for the cooling mode, the data showed a clear correlation also with the  $T_{H1}$  (as reported in Fig.3.25). Finally following the same approach, a relation between parameter  $a_1$ ,  $a_2$ ,  $b_1$ ,  $b_2$  and the  $T_{H1}$  has been computed as reported in Fig.3.26. The final data computed are reported in Tab.3.3 and used for the calculation of the U value function of  $C_r$ , DT and  $T_{H1}$ .

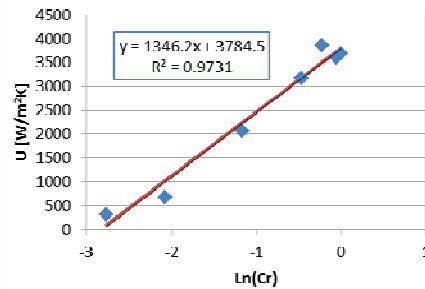


Fig.3.24 - Relation between heat transfer coefficient U and heat capacity ratio  $C_r$  (Cooling mode  $65^\circ\text{C} < T_{H1} < 90^\circ\text{C}$ )

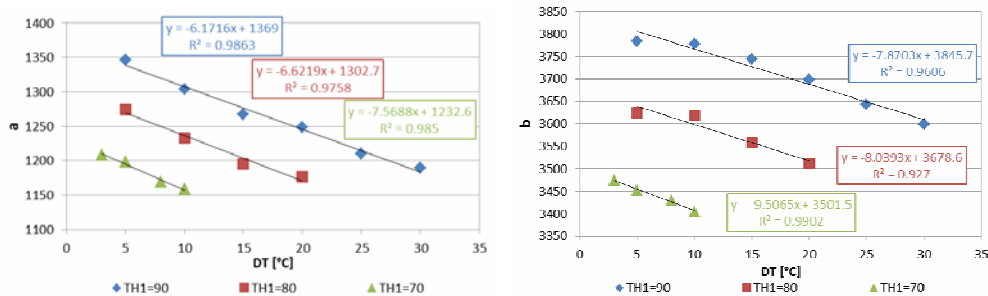


Fig.3.25 - Relation between parameters a, b and DT for different inlet temperature (Cooling mode  $65^\circ\text{C} < T_{H1} < 90^\circ\text{C}$ )

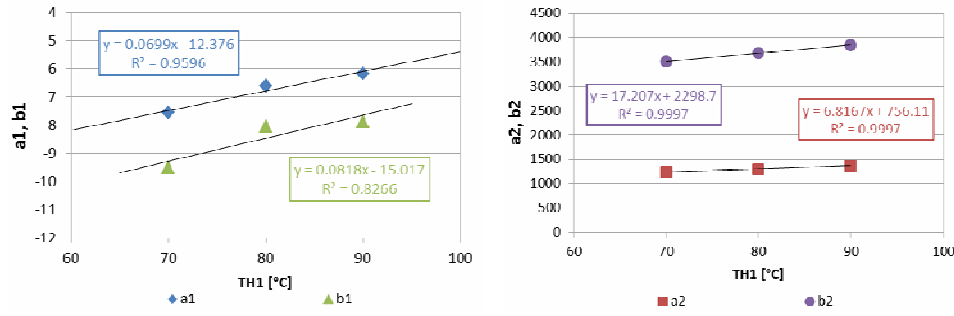


Fig.3.26 - Relation between parameters  $a1$ ,  $a2$ ,  $b1$ ,  $b2$  and  $T_{H1}$   
(Cooling mode  $65^\circ\text{C} < T_{H1} < 90^\circ\text{C}$ )

After this process, using manufacturer data for different operative conditions (changing different operative conditions:  $T_{H1}$ ,  $m'_H$ ,  $T_{C1}$ ,  $m'_C$ , in the operative range where the heat exchanger will be work during the two function modes considered), the model has been verified showing a good agreement between rated data and simulated ones. In the following figure the behavior of the cooling mode is showed for some working points given by the manufacturer and the value computed with the equation previously presented. In fact, the Fig.3.27 shows a comparison between the heat transfer coefficient for low temperature behavior. It is notable a maximum deviation of 10% between the manufacturer and computed data for low values of  $C_r$  (0.1-0.2), related to high difference of temperatures in the heat exchanger and low mass flow in the cold side. In this range, the approach followed to find the UA parameters has been conservative. In fact, the equation used, underestimate the heat exchanged with a maximum difference of 10% in the worst case.

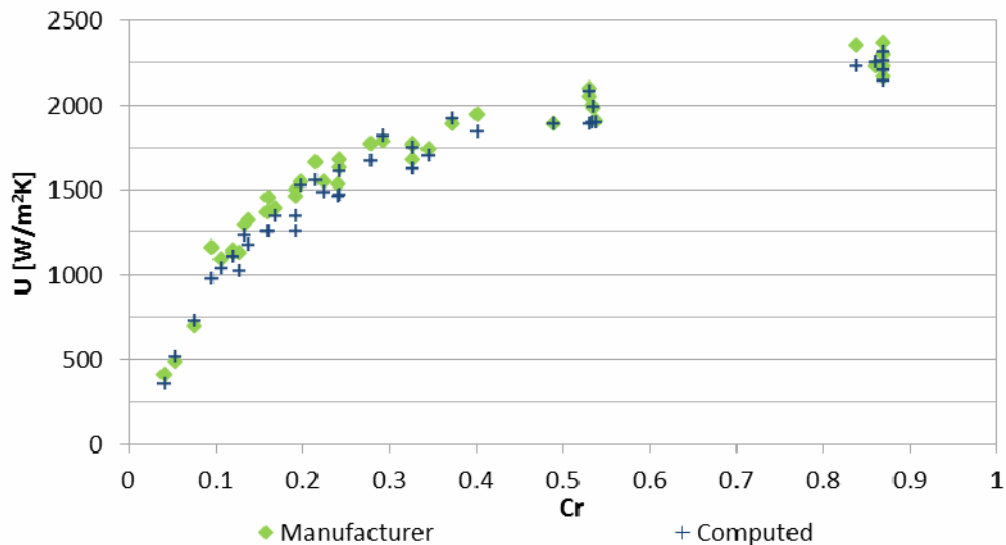


Fig.3.27 - Comparison between manufacturer and computed data of heat transfer coefficient (Cooling mode  $65^\circ\text{C} < T_{H1} < 90^\circ\text{C}$ )



After the validation of the model, an additional thermal losses has been computed. The 10% of the thermal power exchanged has been subtracted to the final calculation, in order to consider the heat losses (convective and radiative thermal losses) with the external ambient.

### 3.5 Validation of the variable circulation pump model

For this component a simple variation on the electrical consumption curve has been performed, using monitoring data of the solar circulation pump. In the normal centrifugal pump used in the Trnsys (Type110) the electrical consumption of the pump is computed using the following equation:

$$W_{el} = W_{rated} \cdot (a_0 + a_1 \cdot Y + a_2 \cdot Y^2) \left[ \frac{kJ}{h} \right] \quad (eq.3.30)$$

Where the electrical consumption is a quadratic function of the pump control signal “Y”, using parameters  $a_0$ ,  $a_1$ ,  $a_2$ .

Before the validation a quadratic curve has been set in the range where the pump operates. For the circulation pump of the solar circuit the coefficients used are reported in the following Tab.3.4.

Tab.3.4 - Coefficient used before validation process

$W_{rated} \left[ \frac{kJ}{h} \right]$	$a_0$	$a_1$	$a_2$
45	1	0	2.26

These parameters have been computed using the manufacturer consumption curve of a circulation pump (Wilo- Stratos Para 25/1-7 [80]) Fig.3.28, assuming that the pump worked in the worst conditions in terms of consumption. After this preliminary phase, during the validation process, coefficients of the curve are adjusted in order to reproduce the monitored curve of the electrical consumption and the new parameters used are reported in Tab.3.5 moving from the blue curve to the red one (reported in Fig.3.29).

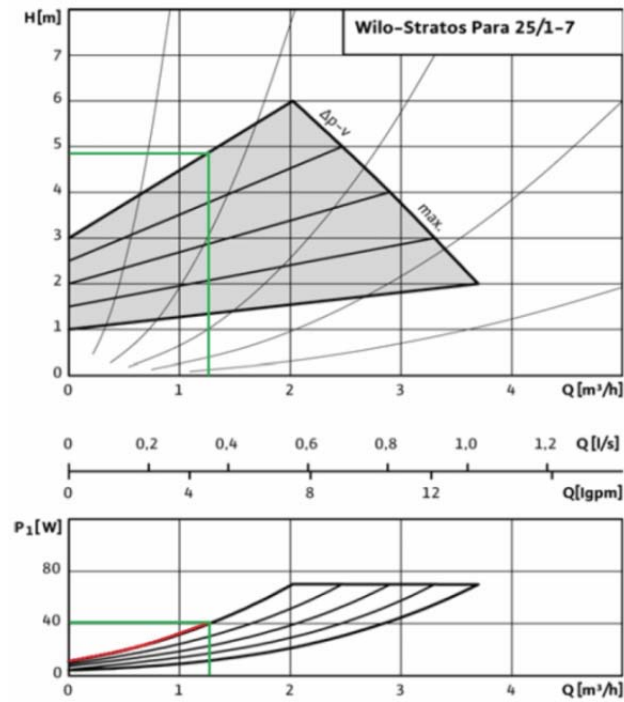


Fig.3.28 - Curve of head and electrical consumption of the pump (Wilo- Stratos Para 25/1-7 [80])

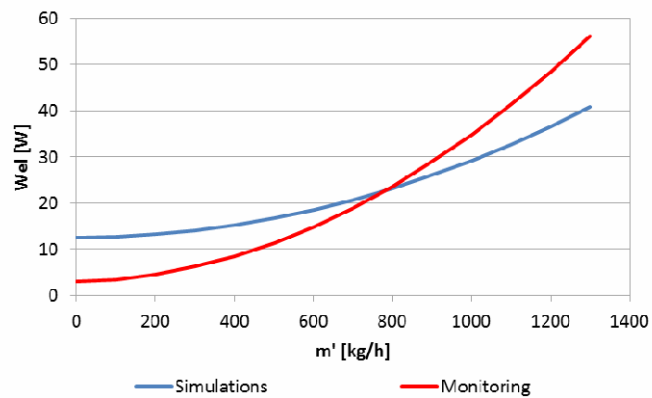


Fig.3.29 - Comparison between simulated and monitored electrical consumption curves

Tab.3.5 - Coefficient used after validation process

$W_{rated} \left[ \frac{kJ}{h} \right]$	$a_0$	$a_1$	$a_2$
10.39	1	0.86	17.57

After the calculation of the electrical consumption coefficients also the thermal energy transfer to the fluid by the pump has been computed, setting the parameters related to

the total efficiency of the pump and the motor efficiency respectively equal to 0.52 and 0.95. In this manner, given 100% the electrical consumed by the pump, the 5% is lost for the electrical efficiency of the engine, the 52% is used effectively for increasing the pressure in the hydraulic system, the 33% is given to the fluid and the 10% is lost with the ambient around the pump. The numerical model used in Trnsys compute this effect increasing the fluid outlet temperature. As the electrical power consumed by the pump is relative low (in the order of 0-50W), the increasing in temperature is limited.

### **3.6 Other components numerical model validation**

The validation process has been also made on the other components such as collectors, thermal storages and compression machine, following the same approach used for the component analyzed in this chapter. For the flat plate collectors the parameters of the efficiency curve have been defined, while for the compression machine the maps used by the numerical model has been modified comparing the manufacturer data with data from stationary laboratory. The thermal storages have been validated using the monitoring data from the pilot plant. All the components validated have been included in a validated numerical Trnsys model in order to execute on it the optimization control phases. As reported in the following chapter, the detection of the most important parameters that influence the model has been detected using a sensitivity analysis. On these parameters an optimization process on the control strategy has been performed. This with the aim to maximize the performance or increasing the renewable energy used by the Solar Combi+ system.

# Chapter

## 4.

# Traditional control strategies

### 4.1 Introduction

In this chapter is reported an overview of traditional control strategies applied to Solar Combi+ systems. This analysis is conducted on a residential application and starts with the introduction of the different operative schemes. After that, the control structure is presented and finally is showed the control logic of the single components that compose the Solar Combi+ system analyzed. In particular, a deep analysis has been performed on the heat pump sources control logic. In the final part of the chapter a sensitivity and parametrical analysis are reported with the performance of the Solar Combi+ system considered before and after the validation and with the optimized control.

### 4.2 Working schemes

As introduced in the Chapter 1, a Solar Combi+ is a class of systems that use solar thermal energy for satisfying the thermal load of heating, domestic hot water and cooling through a sorption machine, that is a particular kind of thermally driven machine.

As reported in Fig.4.2, the system studied is a particular application of Solar Combi+ system related to residential application (industrial project developed with Velta Italia).

The components present in the installation studied are flat plate collectors, two thermal storages (solar storage 500 l and DHW storage 1000 l), adsorption machine (Sortech [62] with 8 kW of cooling thermal power and nominal  $EER_{th}=0.6$ ), a reversible compression heat pump (Clivet [81] with 9.4 kW and 10.7 kW of heating and cooling thermal power respectively) and an heat rejection system in common among the two machines. The hydraulic connection between the various components is reported in Fig.4.1. The first step done for design the control is the definition of the operative schemes. The different schemes are related to the system operation when different conditions on the variables controlled are met. Going more in detail, ten different working schemes are defined and their descriptions are reported in Tab.4.1.

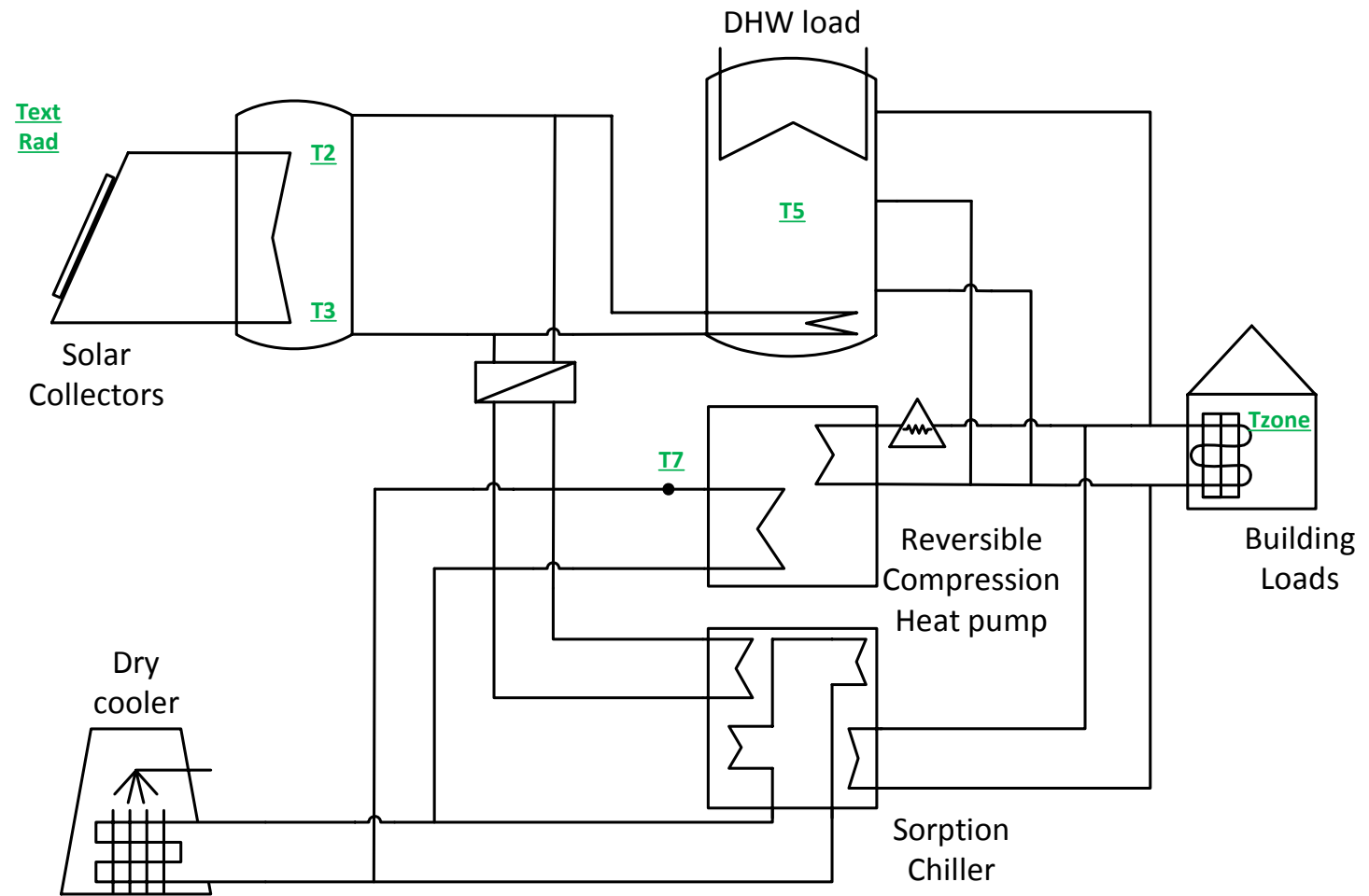


Fig.4.1 - Scheme of connection for a Solar Combi+ application

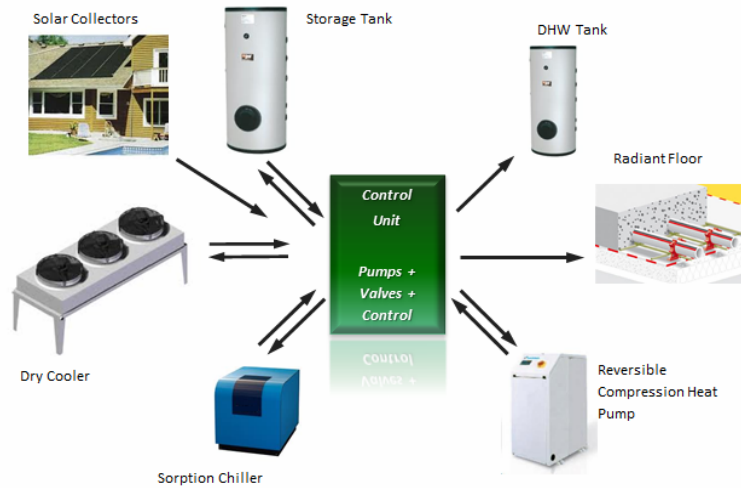
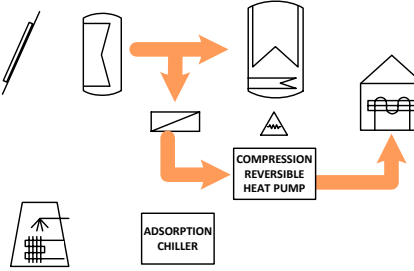
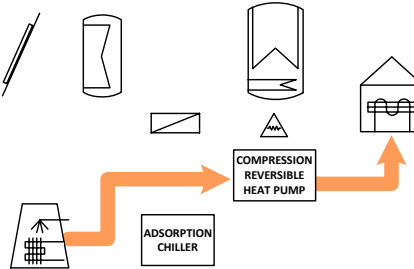
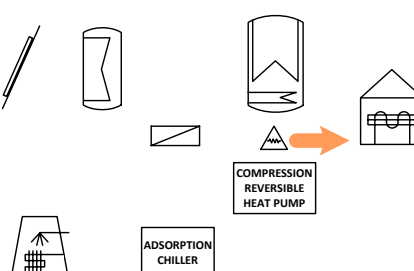


Fig.4.2 - Solar Combi+ system components

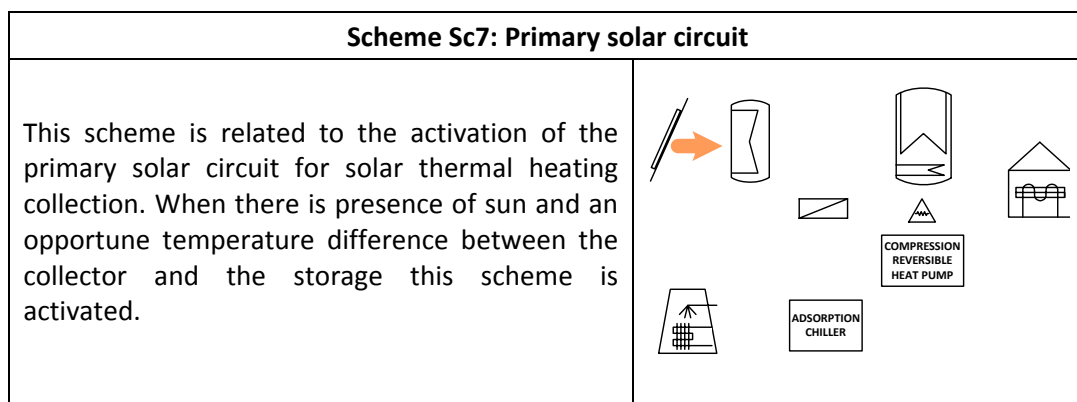
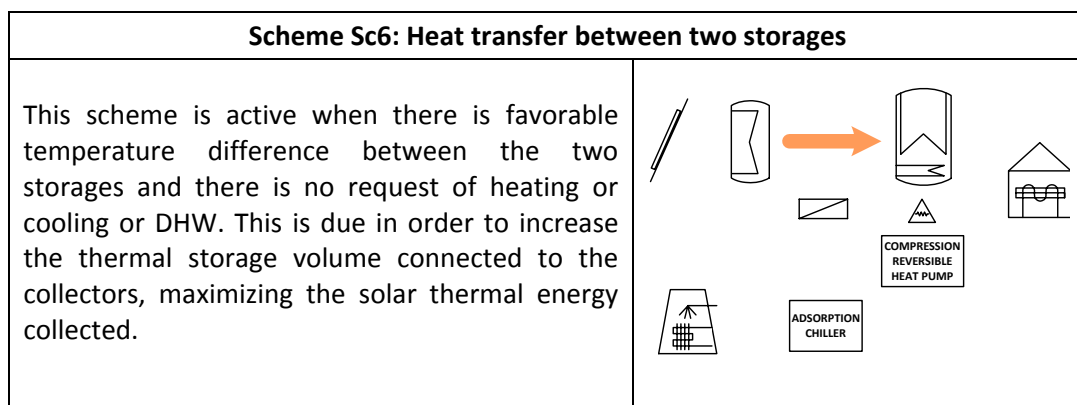
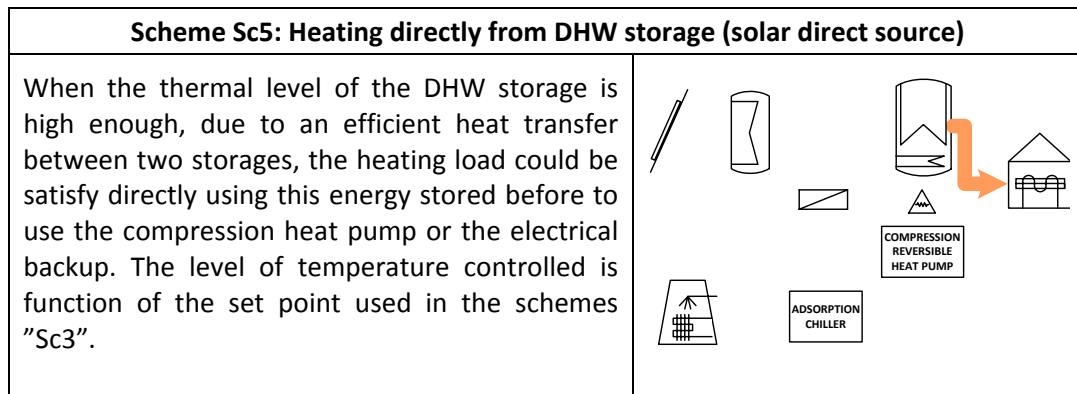
Tab.4.1 - Operative schemes description

Scheme Sc1: Cooling with adsorption chiller	
<p>In this scheme, during the summer season, the cooling request of the building is satisfied by the usage of the adsorption chiller. This machine could be activated when enough solar thermal energy is saved in the storage (controlling the storage temperature) and in this scheme also the energy transfer between two storages is allowed.</p>	
Scheme Sc2: Cooling with compression reversible heat pump	
<p>This scheme is activated, equal to the previous one, during the summer season. In this period if the building cooling request cannot be satisfied by the adsorption machine, the compression machine is switched on in order to satisfy this load. The two schemes Sc1 and Sc2 are exclusive. It means that when the compression chiller is running the adsorption machine has to be switched off. In order to manage possible adsorption machine fault, this scheme is activated also when there is presence of thermal energy stored but the capacity of the adsorption machine is not enough to satisfy the building cooling load.</p>	

<p><b>Scheme Sc3b: DHW with compression reversible heat pump (solar indirect source)</b></p> <p>In this scheme the reversible compression machine is used with the aim to maintain a certain temperature level in the DHW storage in order to cover the DHW requests. In this first mode of the reversible heat pump for DHW function, the evaporator is connected with the solar thermal energy stored. The inlet temperature of the evaporator side is controlled with a fixed set point and the specific mass flow on the primary side of the heat exchanger is controlled in function of this set point temperature.</p>	
<p><b>Scheme Sc3c: DHW with compression reversible heat pump (air source)</b></p> <p>In this scheme, as in the Sc3b, the reversible heat pump is used to maintain a certain level of temperature in the DHW storage. Here, differently from the previous scheme, the source used is air then the evaporator side of the heat pump is connected with the dry cooler. In this case no set point evaporator inlet temperature is fixed.</p>	
<p><b>Scheme Sc3d: DHW with electrical backup</b></p> <p>The last mode of function for this class of scheme ("3") related to DHW is represented by the usage of electrical backup that works only when there is no presence of solar thermal energy stored and the external temperature is too low for the correct operation of the reversible compression heat pump. In these conditions the electrical backup is switched on for maintain the required level of temperature in the DHW storage.</p>	

<p><b>Scheme Sc4b: Heating with compression reversible heat pump (solar indirect source)</b></p> <p>In this scheme the compression machine is used to satisfy the building heating demand during the winter season. In particular also here, as in the case of DHW, the reversible compression machine could be connected to two different sources. In this case the evaporator utilize the thermal solar energy stored and, as in Sc3b, the inlet evaporator temperature is controlled with a fixed set point temperature.</p>	
<p><b>Scheme Sc4c: Heating with compression reversible heat pump (air source)</b></p> <p>The second source used from the reversible compression heat pump is the external air. In this scheme, as in the Sc4b, the reversible heat pump is used to satisfy the heating demand of the building and, as in Sc3c, the evaporator is connected with the dry cooler without temperature control.</p>	
<p><b>Scheme Sc4d: Heating with electrical backup</b></p> <p>Also in the class of schemes “4”, as in the schemes “3” related to DHW requests, when no solar thermal energy is available and the external temperature is too low for the correct operation of the heat pump, the heating load is satisfied using the electrical backup. The control logic for the usage of the two sources and the electrical backup is explained later in the chapter.</p>	





The schemes reported in the Tab.4.1 are all exclusive, so when one is activated the other are disconnected, in order to avoid superposition of signals to the component due to the simultaneous schemes presence. The unique scheme that could be activated simultaneously to other scheme is the Sc7, related to the solar primary circuit. In this case this scheme could be controlled separately from other control scheme because is the only

scheme that activate or deactivate the primary solar circuit pump when conditions on temperature and radiation are met.

During the design phase of a control system, a flow diagram is usually defined. For the application studied this is reported in Fig.4.3 and it is an helpful tool used for prioritize the schemes and identify the essential control variables (referred to Fig.4.1). From this figure it is possible firstly to underline the priority given to the DHW demand that has to be always ensured using the heat pump or the electrical backup system. Furthermore, during winter time when the heating demand is present, the control logic has structured as firstly try to use the direct solar energy stored in the DHW thermal storage and after to adopt the heat pump or the electrical backup. Also during the summer season, when cooling demand appears the priority is given to the adsorption chiller that use the thermal energy stored while subsequently only if is not possible to satisfy the cooling load through adsorption machine, the compression machine is activated. The energy transfer scheme is the less important and is activated only when no demand for DHW, heating or cooling are present. In this flow diagram is not reported the scheme for the solar primary circuit control. This because, as we explained before, this scheme of function (Sc7) is superposed to other schemes and works independently.

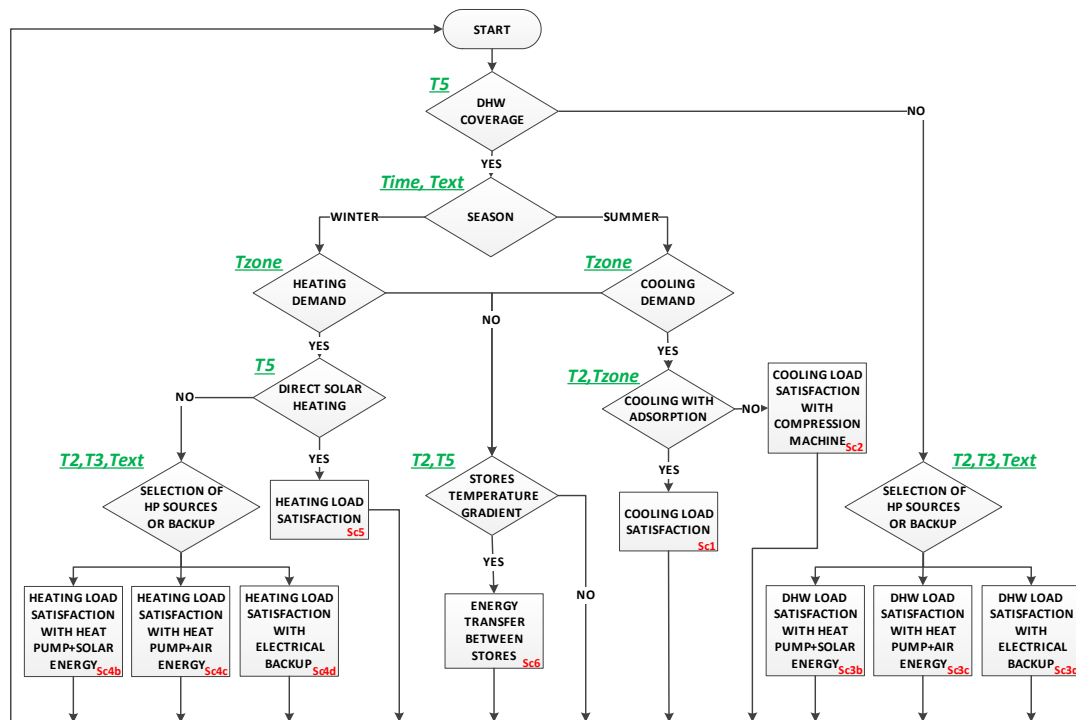


Fig.4.3 - Flow diagram of different mode of function for Solar Combi+ system

Once defined the different schemes of function and their priority, the combination of the different control signals on control variables has to be composed in order to allow the correct operation of the controller without schemes overlapping. Normally the control signals used in the definition of the schemes is based on an hysteresis control system on

the control variables. This approach is preferred to the simplest on/off control for increasing the stability of the controller that could be instable when a fast effect on the control variable is caused by the scheme activation as in the simulation model as in the real installation. A traditional control structure followed is reported in Fig.4.4. In this scheme the variable signals (black line), the boolean signals (green line) and the continuous signal between 0 and 1 (blue line) are highlighted.

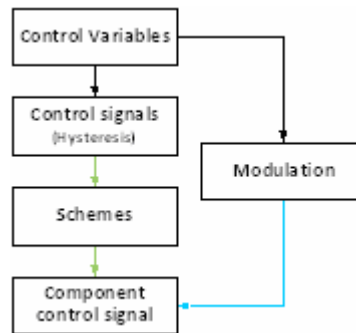


Fig.4.4 - Traditional control structure

A list of the control signals is reported in order to describe which variables are controlled and the logic adopted. The combination of these control signals for the schemes definition is reported in Tab.4.2. These combinations are designed following the diagram previously presented (Fig.4.3).

The control signals (or control hysteresis), referred to the control variables in Fig.4.1, are defined as:

- **Signal A:** signal related to the season (winter/summer), could be defined as fixed hour of the year or function of the external temperature averaged on 24h;
- **Signal B:** controller on the high temperature of the solar storage T2 and used for the correct operation of the adsorption machine;
- **Signal C:** controller on the building internal ambient temperature for cooling demand;
- **Signal D:** controller on the building internal ambient temperature for heating demand;
- **Signal E:** control of the solar storage lower temperature T3, used for control the primary solar circuit and for control the proper function of the heat pump in the schemes type "b" when solar energy is used;
- **Signal F:** temperature control of the DHW thermal storage T5 used as fixed set point temperature to maintain into the DHW storage;
- **Signal G:** control on the radiation on the collectors plane for solar primary circuit control;
- **Signal H:** temperature difference control between the output of the collectors and the lower part of the solar thermal storage;
- **Signal I:** control on the solar storage higher temperature T2 to avoid stagnation problem;
- **Signal L:** control of the DHW storage temperature T5 used for control the direct heating from this storage;

- **Signal M**: temperature difference control between the two storages;
- **Signal N**: control on the external temperature for the correct operation of the heat pump in the scheme type “c” when air is used as source for evaporation;
- **Signal O**: additional control on internal ambient temperature for verify the correct operation of the adsorption chiller;
- **Signal P**: temperature level control in the solar storage for the heating transfer between the two storages;
- **Signal Q**: temperature control on the hydraulic junction between the solar thermal system and the building distribution;
- **Signal S**: additional control on the solar storage temperature T2 for manage the sources of the heat pump (air/solar) when heating or DHW are needed;
- **Signal T**: additional control on external temperature for manage the sources of the heat pump (air/solar) when heating or DHW are needed.

Tab.4.2 - Relation between schemes and control signals

Schemes	Control signals combination
Sc1	$A*B*\text{not}(O)*C*Q$
Sc2	$A*(\text{not}(B)+B*O)*C*F*Q$
Sc3b	$\text{not}(F)*E*\text{not}(T)*(\text{not}(N)+N*S)$
Sc3c	$\text{not}(F)*N*(T+\text{not}(T)*(E*\text{not}(S)+\text{not}(E)))$
Sc3d	$\text{not}(F)*\text{not}(E)*\text{not}(N)*\text{not}(T)$
Sc4b	$\text{not}(A)*\text{not}(D)*F*\text{not}(Q)*\text{not}(L)*E*\text{not}(T)*(\text{not}(N)+N*S)$
Sc4c	$\text{not}(A)*\text{not}(D)*F*\text{not}(Q)*\text{not}(L)*N*(T+\text{not}(T)*(E*\text{not}(S)+\text{not}(E)))$
Sc4d	$\text{not}(A)*\text{not}(D)*F*\text{not}(Q)*\text{not}(L)*\text{not}(E)*\text{not}(N)*\text{not}(T)$
Sc5	$\text{not}(A)*\text{not}(D)*F*L$
Sc6	$M*P*\text{not}(C)*D*F$
Sc7	$G*H*\text{not}(I)$

### 4.3 Components activation logic and signals

Starting from the components that are activated in the scheme of cooling with adsorption chiller (adsorption machine, generator, evaporator, heat rejection pumps and dry cooler), all these components are activated when the scheme Sc1 is active and the system conditions (temperature level in the storage and cooling requests) are met. Also the secondary solar circuit pump has to be activated allowing the thermal energy to flux from the storage to the heat exchanger. Here a modulation is implemented for increase or decrease the mass flow to the heat exchanger modifying the thermal energy transferred between the two thermal storages. This modulation is computed function of the two

thermal level of the storages ( $Mod5=f(T2,T5)$ ). The logic followed to control the adsorption machine is a simple on/off control in which the adsorption machine provides all the cooling power with fixed mass flow on the generator, evaporator and condenser sides.

When the cooling is not satisfy by the adsorption machine, the scheme Sc2 is activated and the compression machine (in cooling mode) is switched on. Furthermore the dry cooler and the heat rejection circuit pump between the heat pump and the dry cooler are activated. Also the circulating pump on the load side of the compression machine, between the heat pump and the load (typically the hydraulic junction between the primary circuit and the building distribution system) is started.

Going more in detail in the definition of the components activated in the schemes for DHW and heating demands (Schemes Sc3b/Sc3c/Sc3d, Sc4b/Sc4c/Sc4d), the combination of the two sources employed (solar, air) by the reversible compression heat pump and the electrical backup is designed as follows.

Tab.4.3 - Relation between schemes and control signals for priority of the sources

Schemes	Control signals combination
<b>Sc3b</b>	$\text{not}(F)*E$
<b>Sc3c</b>	$\text{not}(F)*\text{not}(E)*N$
<b>Sc3d</b>	$\text{not}(F)*\text{not}(E)*\text{not}(N)$
<b>Sc4b</b>	$\text{not}(A)*\text{not}(D)*F*\text{not}(Q)*\text{not}(L)*E$
<b>Sc4c</b>	$\text{not}(A)*\text{not}(D)*F*\text{not}(Q)*\text{not}(L)*\text{not}(E)*N$
<b>Sc4d</b>	$\text{not}(A)*\text{not}(D)*F*\text{not}(Q)*\text{not}(L)*\text{not}(E)*\text{not}(N)$
<b>Sc5</b>	$\text{not}(A)*\text{not}(D)*F*L$

A first approach to the problem was to implement a cascade controller in the form reported in the Tab.4.3, where priority was given to solar energy, after air and in the end electrical backup when there is no presence of solar energy or the external temperature is too low for the compression machine operation. As reported in Tab.4.3, the signal “E” is the hysteresis that allow to use solar source excluding the air source and electrical backup. This signal, as introduced previously, controls the thermal level of the solar storage avoiding the freezing problem and set a minimum temperature of the store for the function of the solar schemes. The control signal “N” allowed use air instead of solar source or electric backup controlling the minimum external temperature at which the heat pump can be function correctly. Finally, when both of these operation are neglected, the electrical backup is used. For the heating schemes (Schemes “4”), moreover, a signal “L” was used for given priority to direct use of solar energy for heating, through the scheme Sc5 before to use indirectly the solar energy, the air energy or the electrical backup.

Adopting this logic a first problem is detected in the usage of solar thermal energy instead of air also when the air is more efficient from the heat pump performance point of view (i.e. when the external air temperature is greater than the set point used at the inlet evaporator temperature in the solar schemes). Subsequently, from the analysis of the whole system performance, a wide and clear effect on the total performance has to be ascribed to the usage of the electrical backup that decreases heavily the seasonal performance of the whole system (in particular in the coldest climatic installation e.g. Bolzano).

In order to overcome these limitations (related to the control logic reported in Tab.4.3), another logic has been developed with the aim to reduce the electrical backup function increasing the usage of renewable energy through a better managing of the air and solar sources. For this reason two more signals ("S" and "T") have been implemented for, from one side save solar thermal energy in the store using air also when solar energy is present (signal "S"), from the other use the air source when its employment is more efficient compared with solar energy with a fixed set point temperature (signal "T"). Following this logic could be defined a sort of "areas of function" in the (T2, T3) vs. external temperature (Text) plane, as reported in the Fig.4.5, where the three function modes (using solar energy, energy from air and the electrical backup) are reported with the four signals employed in the controller (signals "E", "N", "S", "T"). The combination of these signals to create the scheme of function are reported in Tab.4.2.

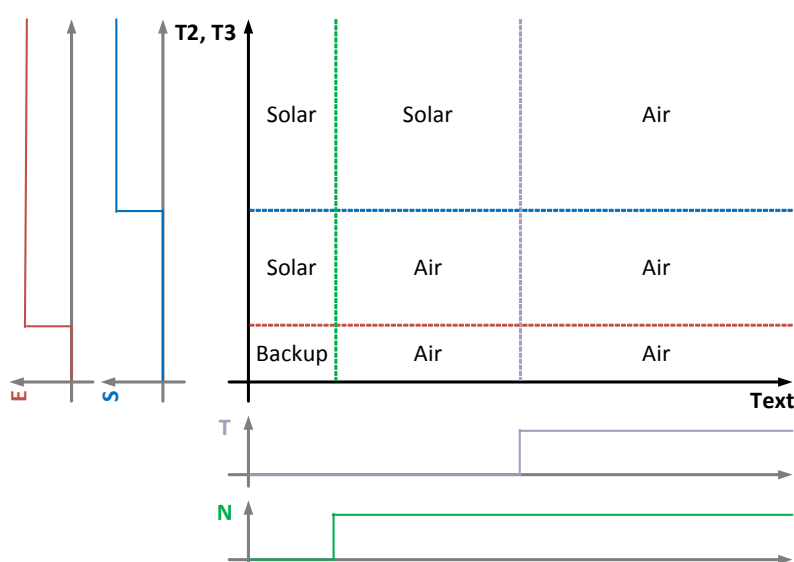


Fig.4.5 - Area of function of different sources/strategies for reversible compression heat pump and electrical backup control

Here (Fig.4.5 related to the control logic reported in Tab.4.2 ) could be appreciate that the solar energy (Schemes "b") can be used when the storage is not too cold (freezing protection controlled by the signal "E" on the T3) and when the external air is less than the set point of the inlet source temperature of the heat pump in solar schemes (signal

“T” on the Text). When these two conditions are met, the two other signals are considered, allowing the system to use solar energy when or the external temperature is below the minimum of heat pump operation (signal “N” on the Text) or the external temperature is between this two limits (signal “N” and signal “T” on the Text) but the thermal level of the solar energy stored is higher (signal “S” on the T2). During these schemes (“b”) the load and the source pumps of the heat pump are switched on with a constant mass flow and also the pump on secondary solar circuit (between the two storages) is switched on and controlled with a modulation function of the storages thermal levels and the set point of the inlet source temperature of the heat pump (temperature set point T7).

The other areas, related to the function with the air source (Schemes “c”) are activated when the external temperature is greater than the minimum of heat pump function (signal “N” on the Text) and or the external temperature is greater than the set point of the inlet source temperature of the heat pump in solar schemes (signal “T” on the Text) or when the external temperature is between these two levels (signal “N” and signal “T” on the Text) and the thermal level of the solar energy stored is not high (signal “S” on the T2) or, for consider all cases, when the temperature of the storage is too low (freezing protection, signal “E” on the T3). During these schemes (“c”) the load pump, the source pump of the heat pump and the dry cooler are switched on. For increasing the functioning time of the heat pump in heating or DHW mode with the air source, a modulation of the mass flow on the external pump is implemented in order to increase the mass flow when the external temperature is less than zero ( $\text{Mod7} = f(\text{Text})$ ). This allow to decrease the temperature difference between inlet and the outlet of the heat pump heat exchanger on the source side and, at the same time, to reduce the temperatures difference between the dry cooler, increasing the working hours of the heat pump in this condition.

Finally the electrical backup (Schemes “d”) starts only when no solar thermal energy is stored (signal “E” on the T3) and when the external temperature is too low for the correct function of the heat pump (signal “N” on the Text). In these class of schemes only the load pump is switched on with constant mass flow.

For the heating mode also in this new logic of control the priority is given to the solar direct heating when enough thermal energy is present in the DHW storage (signal “L” on the T5); when this happen the load pump is switched on with constant mass flow rate.

The modulation is also used for control the primary solar circulation pump, activated in the scheme Sc7. In this case the scheme is activated when there is presence of solar radiation (radiation controlled by the signal “G”), when the difference of temperature (collectors-thermal storage) is favorable (signal “H”) and when no stagnation problem is observed (signal I). In this condition the Sc7 is multiply by a linear modulation function of the radiation present and this signal is given to the circulation pump of the solar primary circuit ( $\text{Mod2} = f(\text{Rad})$ ). A deep analysis on this control is reported in the end of the Chapter 5 where the control of a simple solar thermal system for DHW is analyzed. Other modulations are computed in order to control, in function of the storage temperature, the mixing valve present between the two storages. Regarding the secondary solar circuit

pump it is switched on when the solar energy stored is used by the machines (adsorption during summer or heat pump during winter) using an opportune modulation to control the mass flow or with fixed mass flow when energy is transferred between the two thermal storages.

#### 4.4 Sensitivity analysis and optimization of the control

Following the methodology used in the Chapter 2.3.9, also for the whole solar Combi+ system a sensitivity analysis has been made using the Morris Method. The numerical model adopted has been a solar combi+ system located in Bolzano ("STD" climatic data) and building with low energy demand "BLD". In the case of the whole solar Combi+ system, the objective of this step has been to find the control parameters that mostly affect the performance of the systems, in terms of total SPF. The SPF is defined as the ratio between the yearly thermal energy satisfied divided by the yearly electrical energy used (see eq.4.8). Differently from the previous analysis in this case the parameters have been not varied one at time starting from a reference configuration but trajectories have been developed studying the combination of the parameters considered. During this analysis 15 parameters have been selected, as reported in Tab.4.4 (for the definition of the signals referring to the previous chapter).

Tab.4.4 - Parameters investigated and range of variation.

n	Parameters	Ref.	Min	Max	Step
1	Delta Signal E [°C]	4	2	8	2
2	Min Signal F [°C]	35	35	50	5
3	Delta Signal F [°C]	7	4	10	2
4	Min Signal H [°C]	5	5	8	1
5	Max Signal H [°C]	2	2	5	1
6	Min Signal P [°C]	30	20	50	10
7	Delta Signal P [°C]	10	0	15	5
8	Min Signal S [°C]	30	10	40	10
9	Delta Signal S [°C]	5	4	10	2
10	Min Signal T [°C]	10	4	10	2
11	Mass flow solar circuit pump [kg/h]	900	400	1000	200
12	Set point HP heating (T7_heat) [°C]	5	4	10	2
13	Set point HP DHW (T7_DHW) [°C]	10	3	15	4
14	Max value of radiation for solar circuit pump control curve [W/m <sup>2</sup> ]	600	400	1000	200
15	Mass flow source pump heat pump in the solar schemes (Sc3b and Sc4b) [kg/h]	1000	1000	1300	100



The choice of the trajectories used for the Morris Method has been made with an algorithm that starts creating randomly an huge number of trajectories (as combination of the 15 parameters in the range defined). Between these trajectories the relation is the modification of one parameter at time, as reported in the Morris Method definition [65]. From these huge amount of combinations, a few trajectories have been selected (160 trajectories that means less simulation effort compared to all combinations created) following the idea to explore in an efficient manner the n-dimensional space of the parameters combination values with a low number of simulations. Following this idea the trajectories selected were the most distant each other, using the definition of distance based on the geometrical position of the trajectories points [81].

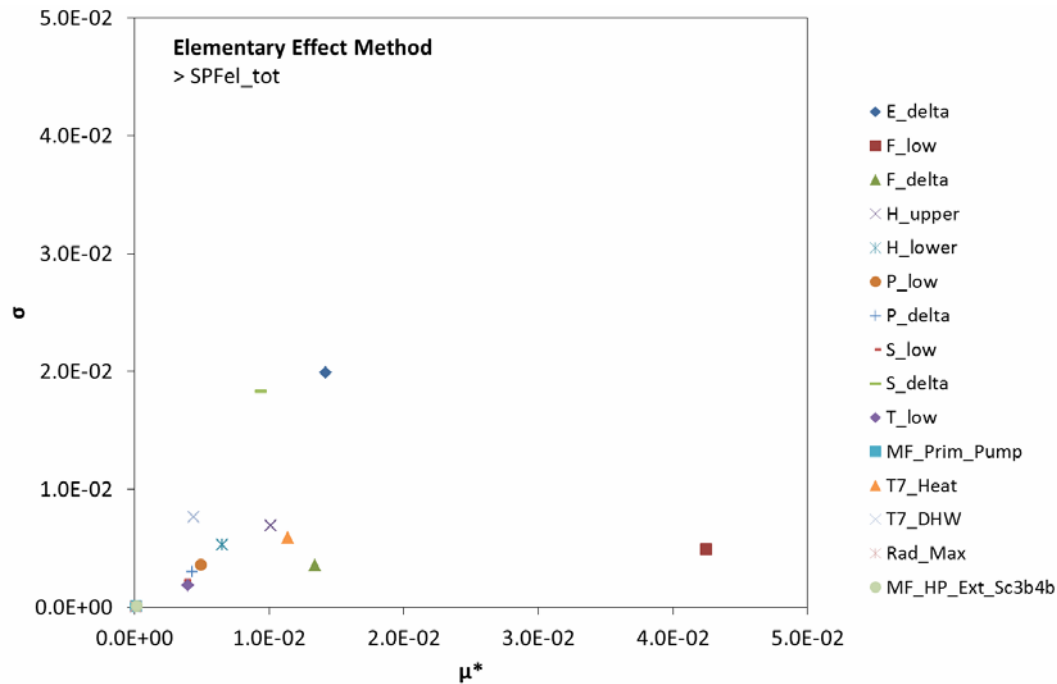


Fig.4.6 - Morris Method conducted on the 15 parameters of Solar Combi+ system

Checking the results of the sensitivity analysis on 15 parameters, 6 of that have been used for the parametrical analysis with the aim to optimize the control strategy. The parameters selected for the optimization are related to the DHW storage temperature (Signal F: “F\_low” and “F\_delta”), the two set point temperature on the source side of the heat pump for the solar schemes (Sc3b, Sc4b) as explained before (“T7\_Heat”, “T7\_DHW”) and the parameter “E\_delta” related to the set point temperature of the solar storage used for control the use of heat pump between solar and air schemes (Sc3b, Sc3c and Sc4b, Sc4c). Moreover two other parameters the “T\_low” and the “S\_delta” have been considered, related to the control logic of the two heat pump sources (solar/air) and electrical backup in heating or DHW operation modes. As results from the Morris analysis, the parameter “F\_Low” is the most important (higher  $\mu^*$ ). However, this

parameter cannot be modified because it allows to cover the DHW loads at the set point temperature imposed (40°C). On the other parameters selected, as the most important, a parametrical analysis have been conducted in order to find the combination that allow the best results in terms of total seasonal performance factor.

#### 4.5 Results of Solar Combi+ system considered

The simulation results on the solar Combi+ system is presented in table that reports the performance of the systems using yearly performance figures such as:

- Solar fraction “SF”: for each of the loads satisfied by the solar Combi+ system, the SF indicates the coverage degree of such load with solar energy (DHW, heating, cooling). The loads are computed as the integral on the year.

$$SF_{DHW} = \frac{\int_{year} \dot{Q}_{solarDHW} dt}{\int_{year} \dot{Q}_{loadDHW} dt} [-] \quad (eq.4.1)$$

$$SF_{HEAT} = \frac{\int_{year} \dot{Q}_{solarHEAT} dt}{\int_{year} \dot{Q}_{loadHEAT} dt} [-] \quad (eq.4.2)$$

$$SF_{COOL} = \frac{\int_{year} \dot{Q}_{solar,COOL} dt}{\int_{year} \dot{Q}_{load,COOL} dt} [-] \quad (eq.4.3)$$

- Air Fraction “AF”: for each of the loads satisfied by the solar Combi+ system, the AF indicates the coverage degree of such a load using energy extracted from the external air through compression heat pump (DHW, heating). The loads are computed as integral on the year.

$$AF_{DHW} = \frac{\int_{year} \dot{Q}_{air,DHW} dt}{\int_{year} \dot{Q}_{loadDHW} dt} [-] \quad (eq.4.4)$$

$$AF_{HEAT} = \frac{\int_{year} \dot{Q}_{air,HEAT} dt}{\int_{year} \dot{Q}_{loadHEAT} dt} [-] \quad (eq.4.5)$$

- Collectors efficiency: is the ratio between the yearly energy collected by the solar system and the energy that arrive on the collector.

$$\eta_{coll} = \frac{\int_{year} \dot{Q}_{coll} dt}{\int_{year} I_G \cdot A_{coll} dt} [-] \quad (eq.4.6)$$

- Gross solar Yield “GSY”: estimates the energy captured from solar field referred to the collectors area. Like the collectors efficiency, this parameter represents how efficiently works the collectors.

$$GSY = \frac{\int_{year} \dot{Q}_{coll} dt}{A_{coll}} \left[ \frac{kWh}{m^2} \right] \quad (eq.4.7)$$

- Total seasonal performance factor “SPF”: is the ratio between the thermal loads (for heating, cooling and domestic hot water) and the electric energy needed to cover these loads (comprehensive of chiller, solar circuits pumps, heat rejection system fans, etc.). In the results presented in this chapter, also the seasonal performance factor for heating cooling and DHW are reported showing the ratio between thermal energy and electrical energy used for satisfy the single load.

$$SPF_{el\_TOT} = \frac{\int_{year} \dot{Q}_{loadHEAT} dt + \int_{year} \dot{Q}_{loadDHW} dt + \int_{year} \dot{Q}_{loadCOOL} dt}{\int_{year} W_{el\_TOT} dt} [-] \quad (eq.4.8)$$

- Primary energy savings: is an environmental figure comparing the total yearly primary energy needs for cover the loads with a reference system operated with traditional technologies (gas boiler + air/water compression chiller + solar domestic hot water system) and the innovative solar Combi+ solution. Also for this index, the three single specific primary energy for cooling, heating and DHW are reported.

$$\Delta PE = PE_{traditional} - PE_{innovative} \left[ \frac{kWh}{m^2} \right] \quad (eq.4.9)$$

(For the calculation of the primary energy, the coefficients used for the conversion between final energy and primary energy are 0.48 for electrical energy and 0.95 for thermal energy).

- CO<sub>2</sub> emissions savings: this parameter, related to the previous one, counts the CO<sub>2</sub> produced during the systems operation (traditional or solar Combi+). Also this parameter is expressed as the difference between the traditional installation and the innovative.

$$\Delta CO_2 = CO_{2,traditional} - CO_{2,innovative} [tonn] \quad (eq.4.10)$$

(For the calculation of the CO<sub>2</sub> emissions savings, the coefficients used for the emission for the traditional technology are 0.45 kgCO<sub>2</sub>/kWh for electrical energy and 0.23 kgCO<sub>2</sub>/kWh for thermal energy).

A specific case has been firstly simulated: solar Combi+ system located in Bolzano with 32m<sup>2</sup> of collectors, installed oriented to south with 30° of slope on the horizontal plane and applied to satisfy the energy demands of the building “BLD” (defined in Chapter 2.3). The Tab.4.5 reports the performance related to the three steps followed from the “Base case” that is the system not validated with a control not optimized. The second one “Validated” is the system with all the components validated as reported in the Chapter 3 and the third one, “Optimized”, where the control is modified and the set point optimized (using the sensitivity and parametric analysis explained before). The climatic data considered is the standard “STD” profile (defined in the Chapter 2.2).

Starting from the comparison between the two first steps (Tab.4.5), the validated model shows a decrease of the solar fraction for cooling and heating mainly due to the collectors performance that are decreased between the two cases and the validation of the thermal storages. From the other side, between the two air fractions a small increasing is visible followed by a small increase of the electrical backup usage for cover the heating demand. The electrical backup is computed as the difference between the total load and the load cover by the solar source and air source.

Tab.4.5 - Performance of solar Combi+ system installed in Bolzano - 1/2

BLD Bolzano 32m <sup>2</sup>	SF <sub>cool</sub>	SF <sub>heat</sub>	SF <sub>DHW</sub>	SF <sub>heat+DHW</sub>	AF <sub>heat</sub>	AF <sub>DHW</sub>	$\eta_{coll}$	GSY
	[-]	[-]	[-]	[-]	[-]	[-]	[-]	$\left[\frac{\text{kWh}}{\text{m}^2}\right]$
Base	57%	52%	95%	66%	30%	3%	23.6%	346
Validated	54%	49%	95%	64%	32%	4%	24.1%	353
Optimized	52%	27%	93%	49%	72%	7%	22.5%	330

Considering the optimized solution, on the solar fraction no huge difference is visible for the cooling but for the heating and the DHW coverage, the new control strategy change the percentage of use of the renewable sources exploited by the heat pump (SF<sub>heat</sub> from 49% to 27% and AF<sub>heat</sub> from 32% to 72%), as explained previously (Chapter 4.3). The performance of the collectors does not change heavily between the two first steps and this is due mainly to the validation of the internal heat exchange of the solar thermal storage and the collectors. On the other hand, the optimized solution shows a reduction of the efficiency of the collectors, mainly due to the increasing of the storages thermal

levels during winter with the new control strategy. This behaviour could be appreciated also analysing the GSY that is decreased between the validated and the optimized solution (-7%).

Looking the performance figures related to the seasonal performance factors (reported in Tab.4.6), an increasing of the performance on the SPF for cooling is visible, between the base and the validated cases, mainly due to the validation of the dry cooler and the adsorption machine and compression heat pump, while for heating and DHW the SPF is decreased and this affect also the total SPF of the system. This is explained from the fact that the building BLD heating demand, as reported in Tab.2.12, is greater than cooling and DHW demands and, for this reason, the heating performance has bigger impact on the total performance of the system. The decreasing of the performance is reflected also in the reduction of the primary energy saving (for heating, DHW and total) and the CO<sub>2</sub> emission savings. For the primary energy savings the reference system evaluated is formed by a compression chiller with EER of 3.5 and a gas boiler with seasonal efficiency of 0.85 have been considered. Moreover, a solar system for DHW has been also considered in the traditional solution (4 m<sup>2</sup> of collectors and 300 l of storage) that cover the 50% of the yearly DHW energy demand (for Bolzano and for Rome).

Tab.4.6 - Performance of solar Combi+ system installed in Bolzano - 2/2

BLD Bolzano 32m <sup>2</sup>	SPF <sub>cool</sub>	SPF <sub>heat</sub>	SPF <sub>DHW</sub>	SPF <sub>el_tot</sub>	ΔPE <sub>tot</sub>	ΔCO <sub>2</sub>	Heat <sub>demand</sub>	Cool <sub>demand</sub>	DHW <sub>demand</sub>
	[-]	[-]	[-]	[-]	$\left[\frac{\text{kWh}}{\text{m}^2}\right]$	[tonn]	$\left[\frac{\text{kWh}}{\text{m}^2}\right]$		
Base	5.08	2.74	18.26	3.98	23	0.94	40	13	14
Validated	6.01	2.37	14.86	3.56	19	0.76			
Optimized	5.76	3.95	21.56	5.49	34	1.34			

The performance are heavily improved, in terms of total SPF by the optimization of the control (third step), mainly for the improvement of the heating SPF. In particular, the increasing of the performance is due to the improved control on the coverage of the heating demand satisfaction, reducing the electrical backup usage as reported in the control chapter (Chapter 4.3). The two strategies followed, changing in the priority of the heat pump sources and the increasing of the mass flow on the source side of the heat pump (that allow to decrease the difference of temperatures function of the external temperature) have an huge impact on the whole system performance because they from one hand reduce the electrical backup usage, from the other increase the direct use of the solar energy. In particular, the SPF<sub>el\_tot</sub> increases of the 54% moving from 3.56 to 5.49. In other words, comparing this solution with a traditional system a total seasonal performance factor of 5.49 allows to save more than half (55%) of the primary energy

needed for heating cooling and DHW equal to 34 kWh/m<sup>2</sup>. This is also reflected in the increasing of the CO<sub>2</sub> saved due to the increased performance.

Going more in detail with the heat pump sources priority control in heating and DHW mode, the Tab.4.7 and Tab.4.8 report the system performance using the two control strategies explained in the previous Chapter 4.3. The logic named “old control logic” is referred to the cascade logic: solar, air, electrical backup instead of the name “Optimized” referred to the system with the more complex sources management. In these tables, the first row is related to the system with the optimized control, as analyzed previously. The other row is related to the same case with the cascade control strategy to manage the sources (solar, air and electrical backup) with the priority given to solar energy, energy from the air and finally electrical backup. Looking the performance results in the Tab.4.7, the huge effect of the new control strategy is the values variation of solar and air fraction for heating ( $SF_{\text{heat}}$  from 46% to 27% and  $AF_{\text{heat}}$  from 50% to 72%). As previously noticed, this new control strategy allows to store more energy in the solar storage with the aim to use it when unfavorable conditions are present (external temperature too low for the heat pump correct operation). Typically during a winter day, the controller allows to use the heat pump during the day with air source, collecting solar energy and saving it for using during the night when the temperature drops below the minimum operative temperature of the heat pump. In this condition, with the old logic of control, only the electrical backup could cover the heating demand. With the new logic, the energy stored during the day is useful for cover more efficiently the heating load in this condition, compared with the electrical backup. From the other side, a decreasing of the collectors efficiency is visible between the new and the old control management of the sources, due to the higher store temperature in the new logic that affect the performance of the collectors as the GSY (-7%).

Tab.4.7 - Performance of solar Combi+ system installed in Bolzano, different control logic of the renewable sources of the heat pump - 1/2

BLD Bolzano 32m <sup>2</sup>	$SF_{\text{cool}}$	$SF_{\text{heat}}$	$SF_{\text{DHW}}$	$SF_{\text{heat+DHW}}$	$AF_{\text{heat}}$	$AF_{\text{DHW}}$	$\eta_{\text{coll}}$	GSY
	[-]	[-]	[-]	[-]	[-]	[-]	[-]	$\left[\frac{\text{kWh}}{\text{m}^2}\right]$
Optimized	52%	27%	93%	49%	72%	7%	22.5%	330
Old control logic	52%	46%	93%	62%	50%	6%	24.3%	356

From the seasonal performance point of view (Tab.4.8), the SPF for heating and DHW are increased ( $SPF_{\text{heat}}$  from 3.57 to 3.95 and  $SPF_{\text{DHW}}$  from 14.96 to 21.56) mainly for the decreased usage of the electrical backup and in the case of heating, the increasing of the solar energy direct usage in the operative scheme Sc5 (from around 6.3 kWh/m<sup>2</sup> to

around 7.8 kWh/m<sup>2</sup> that is respectively the 16% and the 20% of the total building heating demand) allowing better performance of the whole system. The higher storages temperatures allows to increase the energy exchanged between the two stores, increasing the possibility to use that energy directly to cover the heating demand. All these effects are reflected in an increasing of the total SPF of the system about 10% moving from total SPF of the system from 4.92 to 5.49.

Tab.4.8 - Performance of solar Combi+ system installed in Bolzano, different control logic of the renewable sources of the heat pump - 2/2

BLD Bolzano 32m <sup>2</sup>	SPF <sub>cool</sub>	SPF <sub>heat</sub>	SPF <sub>DHW</sub>	SPF <sub>el_tot</sub>	$\Delta PE_{tot}$	$\Delta CO_2$	Heat <sub>demand</sub>	Cool <sub>demand</sub>	DHW <sub>demand</sub>
	[-]	[-]	[-]	[-]	$\left[ \frac{kWh}{m^2} \right]$	[tonn]	$\left[ \frac{kWh}{m^2} \right]$		
Optimized	5.76	3.95	21.56	5.49	34	1.34	40	13	14
Old control logic	5.71	3.57	14.96	4.92	31	1.22			

Doing the same analysis on the new control logic on a system installed in Rome (with the same characteristics of the case analyzed in Bolzano, then building “BLD” with 32m<sup>2</sup> installed with south orientation and 30° of slope on the horizontal) the results are reported in Tab.4.9 and Tab.4.10. Looking the first table (Tab.4.9), also for Rome an huge variation on the solar and air fractions for heating are visible between the two control strategies adopted (SF<sub>heat</sub> from 82% to 58% and AF<sub>heat</sub> from 18% to 42%) and similarly to what happen in Bolzano, also here the efficiency of the collectors and the GSY decreases (-4%).

Tab.4.9 - Performance of solar Combi+ system installed in Rome, different control logic of the renewable sources of the heat pump - 1/2

BLD Rome 32m <sup>2</sup>	SF <sub>cool</sub>	SF <sub>heat</sub>	SF <sub>DHW</sub>	SF <sub>heat+DHW</sub>	AF <sub>heat</sub>	AF <sub>DHW</sub>	$\eta_{coll}$	GSY
	[-]	[-]	[-]	[-]	[-]	[-]	[-]	$\left[ \frac{kWh}{m^2} \right]$
Optimized	58%	58%	98%	80%	42%	2%	22.6%	408
Old control logic	59%	82%	99%	91%	18%	1%	23.5%	425

Looking to the seasonal performance (Tab.4.10), it is evident an increasing of the total performance of the system, mainly due to the increasing of the SPF for heating and DHW. In this climatic condition there is no use of electrical backup ( $SF_{\text{heat}} + AF_{\text{heat}} = 100\%$ ) then the improvement of the performance is due to the better management of the solar energy between the two storages that allow to cover the heating and the DHW loads using directly the solar energy reducing the usage of the compression machine. Also in the system simulated in the Rome climatic condition, between the old and the optimized control strategy the direct heating is different, moving from  $8.6 \text{ kWh/m}^2$  to  $9.6 \text{ kWh/m}^2$  that represent respectively the 50% and the 56% of the building heating demand. Finally, also for this climatic condition the control strategy of the sources allowing an increase of the total seasonal performance factor of 5% moving from 9.3 to 9.78.

Tab.4.10 - Performance of solar Combi+ system installed in Rome, different control logic of the renewable sources of the heat pump - 2/2

BLD Rome 32m <sup>2</sup>	SPF <sub>cool</sub>	SPF <sub>heat</sub>	SPF <sub>DHW</sub>	SPF <sub>el_tot</sub>	$\Delta PE_{\text{tot}}$	$\Delta CO_2$	Heat <sub>demand</sub>	Cool <sub>demand</sub>	DHW <sub>demand</sub>
	[-]	[-]	[-]	[-]	$\left[\frac{\text{kWh}}{\text{m}^2}\right]$	[tonn]	$\left[\frac{\text{kWh}}{\text{m}^2}\right]$		
Optimized	5.93	7.64	57.72	9.78	25	0.98	17	19	14
Old control logic	5.95	7.05	43.67	9.30	24	0.95	17	19	14

During the optimization of the control also the number of starts on and stops of the components have been improved, in order to decrease the components damage risk increasing the expected life. In the Tab.4.11 the yearly number of starts and stops for the systems critical components of two simulated numerical models (before and after optimization of the control), located in Bolzano with 32m<sup>2</sup> of collectors and building BLD are reported. Between the two cases presented in the table, a better control strategy of the distribution system is implemented using the winter and the summer curves implemented in the control signal “Q” (as reported in Chapter 0). This allows to decrease the number of heat pump starts and stops in heating and cooling mode. From the table is visible a decreasing of the total start and stop numbers for the heat pump around the 45%, mainly due to the reduction in heating mode where this hysteresis (signal “Q”) has less limitations. This is also reflected in the number of dry cooler start and stop that is shared between the reversible compression heat pump and the adsorption machine. Looking the pump of the primary solar circuit “Prim\_Pump” and the secondary solar circuit “Sec\_Pump”, the optimization of the set point used and the different strategy related to the priority given to the two different renewable heat pump sources, return also a better control of the component in terms of starts/stops, decreasing the number of switch on and off of the two components.



Tab.4.11 - Number of starts and stops of the critical component of the solar Combi+ system installed in Bolzano.

BLD Bolzano 32m <sup>2</sup>	HP <sub>Heat &amp; DHW</sub>	HP <sub>Cool</sub>	HP <sub>tot</sub>	Prim_Pump	Sec_Pump	Dry Cooler
Validated	1659	1582	3241	1289	1345	2326
Optimized	674	818	1492	964	527	1435

A summary is given in the Tab.4.12 with the performance figure for a system located in two conditions (Rome and Bolzano) applied to two different levels of buildings (BLD and BHD) with 32 m<sup>2</sup> of collectors installed at 30° and with south orientation and considering the standard climatic profile (STD). For both locations, the performance of the system in terms of solar fractions and air fractions are similar, but the total seasonal performance of the systems are decreased passing from the low load (BLD) to the high load buildings (BHD) mainly due to the seasonal performance of the system for heating. For Rome the seasonal performance for DHW (SPF<sub>DHW</sub>) is increased passing from BLD to BHD because in this system we are able to use more solar thermal energy directly (without heat pump) to meet the DHW demand instead of heat pump with air source.

Tab.4.12 - Performance of solar Combi+ system installed in Bolzano (BZ) and Rome (RM) with two different building loads (low demand BLD, high demand BHD) - 32m<sup>2</sup> - STD

Location	Buildings	SF <sub>cool</sub>	SF <sub>heat</sub>	SF <sub>DHW</sub>	AF <sub>heat</sub>	AF <sub>DHW</sub>	SPF <sub>cool</sub>	SPF <sub>heat</sub>	SPF <sub>DHW</sub>	SPF <sub>el_tot</sub>	ΔPE <sub>tot</sub>	Heat <sub>demand</sub>	Cool <sub>demand</sub>
		[-]	[-]	[-]	[-]	[-]	[-]	[-]	[-]	[-]	[ $\frac{\text{kWh}}{\text{m}^2}$ ]		
BZ	BLD	52%	27%	93%	72%	7%	5.76	3.95	21.56	5.49	34	40	13
	BHD	53%	27%	92%	72%	8%	5.73	3.87	19.92	5.04	43	53	12
RM	BLD	58%	58%	98%	42%	2%	5.93	7.64	57.72	9.78	25	17	18
	BHD	62%	53%	99%	47%	1%	6.09	6.83	67.05	9.14	33	26	18

Looking the system performance related to the primary energy saving, the relative saving for both class of buildings is almost the same (around 50% for Bolzano and around 65% for Rome) but looking in absolute terms, for the system installed in building with high demand (BHD) the total primary energy savings is increased (from 34 to 43 kWh/m<sup>2</sup> for Bolzano and from 25 to 33 kWh/m<sup>2</sup> for Rome). From the economical point of view the solution installed in buildings with high demand is more interesting, because also with worst total performance (in terms of SPF<sub>el\_tot</sub>), allow greater primary energy savings. This

is underlined in order to explain that this kind of system became more interesting, compared with traditional solutions, when enough primary energy saving is realized. This because, the primary energy saved, is the economic index for evaluate the return time of the investment of this solution compared with the traditional one. The cost of the adsorption machine and the collectors play, from this point of view, an important role in particular when the comparison is made with solution that adopt renewable energy (e.g. compression heat pump with photovoltaic system).

As a conclusion of this chapter, the performance of the application studied is affected mostly on the different sources usage politic. Firstly, a correct control of the electrical backup, in particular for the coldest location, could affect heavily the performance. Related to this concept, the thermal level of the storages could increase or decrease the performance of the system helping in the reduction of the usage of non-renewable sources (such as the electrical backup). Other parameters to control carefully are the temperatures at which the solar energy stored is used (heat pump inlet source set point temperature) that can affect in one hand the performance of the heat pump (thermal level of evaporation in heat pump mode) but from the other could increase the time of the heat pump function with solar thermal energy, allowing to better overcome of the electrical backup areas of function.

In the Annex1 the validation process results are reported, showing the effect of the validation of each component on the whole system performance (considering the case analyzed in this chapter: building BLD, located in Bolzano with 32m<sup>2</sup> of collectors). Moreover for the two different locations analyzed (Rome and Bolzano), for the climatic profiles considered (standard and extreme) and for the two class of buildings analyzed (BLD, BHD) the performance are reported. From these data could be appreciate the different loads, boundary conditions and performance of the system simulated with the two different climatic data considered. This analysis have been performed in order to underline that the simulated performance of such a complex systems that have an high interaction with the climatic conditions (exploiting renewable energies mainly come from air and sun) are heavily conditioned by the boundary conditions adopted. In particular, when different solutions that use renewable energy are studied, an analysis of the dynamic, the frequency distribution, the profile of temperature and radiation (climatic data) and the loads (class of building used) is fundamental for correctly compare the performance of the different solutions. From the other side, the simulation of such systems with different boundary conditions can increase the awareness on the behavior (and possible operation limit points) when conditions different from the standard (design conditions) occur.

# Chapter

## 5.

# Innovative control system

### 5.1 Introduction

As mentioned in the executive summary, the process of modelling, validating and optimizing the control of solar thermal systems is a time consuming procedure. In order to overcome this limitation two promising methodologies, that seems interesting applying to the control of solar thermal systems, have been presented in the chapter. Firstly a brief introduction on the fuzzy logic is given with particular focus on the application of this theory to the control. After that, an introduction on the reinforcement learning theory is given, with a focus on the Q-learning method. This second step is fundamental in order to allow to the controller (based on fuzzy logic) to self-understand with a “try and evaluate” process, what is the best controlling action to do on the system. The chapter follows describing the application of this two methodologies in the design of the controller for a thermal systems and, in the final part of the chapter, an application to a simple solar thermal system for DHW is presented focusing on the results and on the future developments.

### 5.2 Fuzzy Logic

Fuzzy logic (FL) is a method of rule-based decision making used for expert system and process control. FL is an infinite valued logic developed from the theory of fuzzy sets, a theory which relates to classes of objects with unsharp boundaries in which membership is a matter of degree. The main difference between traditional Boolean Logic (BL) and fuzzy is that FL allows for partial membership in a set (not only the values 0 or 1 but all the values in the range between 0 and 1 are considered). It is usual to refer to this property as the degree of membership. Thinking to this property from the geometrical point of view, as reported in Fig.5.1, the classical BL is able to describe the corner of a cube of unitary dimension while FL is able to describe every point of the same volume. BL is based on two state 0 and 1 that could be seen, in FL, as the representation of the absolute membership (1) or no membership (0).

This logic was developed by Lofti Zadeh in the early 1960s as a way to model the uncertainty of natural language [89][90] and successfully applied to several areas of science and technology, in particular to system control [92]. One important advantage of

the FL is its ability to handle “imprecise” or “noisy” data in order to find solution of a particular problem, using a sort of mapping between given system inputs and its output using an inference decision process, based on the behavior of the system.

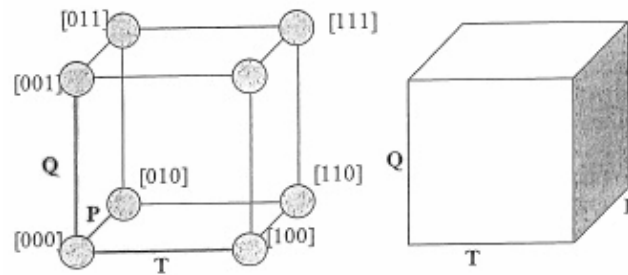


Fig.5.1 - Difference between Boolean and Fuzzy degree of truth [83]

Before to explain the application of FL in control systems it is useful to define some terminology use to describe the fuzzy systems. The first concept is the one of **linguistic variable**, which are variables representing inputs or outputs of a system with a related range of expected values. In the application of FL to the control of a single-input single-output (SISO) systems, one input linguistic variable and one output linguistic variable are requested. Instead, in the case of multiple-input multiple-output (MIMO) systems where two or more inputs and outputs linguistic variables are required. The number of **linguistic terms** (or linguistic values or categories) of the input or output needed to represent the universe analyzed, is chosen on the basis of the physical quantity represented and the application. Normally the linguistic variables have an odd number of linguistic terms, with a middle category and symmetric linguistic terms at each extreme.

The linguistic terms (or categories or values), assumed by the linguistic variables considered, are defined mathematically by numerical functions called **membership functions** (MF). A membership function represent the degree of membership of linguistic variable within their linguistic terms. The degree of membership is a real number between 0 and 1 where 0 is equal to 0% membership and 1 is equal to 100% membership. There are some different normalized standard membership functions of different shapes:

- TRIANGULAR;
- TRAPEZOIDAL;
- BELL (Gaussian type);
- VERTICAL LINE (singleton type).

In the following Tab.5.1 some of the common shapes used in the membership functions are reported with the mathematical definition.

Regarding the definition of the membership functions, as reported in [95], the effect of the overlapping of membership function on the input, strongly affect the response of the fuzzy system. Instead of this effect, the overlapping degree of membership functions on the output (consequent part) has no significant influence on the result on the output

signal of the fuzzy system. Normally is used to overlap the different membership functions at 50% of the definition [95].

Regarding the membership functions of the outputs, as reported in [95], the result of the fuzzy system does not depend strongly on how much the MFs are overlapped as long as they cover the universe of discourse. Sparse MFs can instead affect the response of the fuzzy system.

Tab.5.1 - Common membership functions [96]

Functions		Graphical representation
TRIANGULAR	$\mu(x) = \begin{cases} 0, & x < a; x > c \\ \frac{x-a}{b-a}, & a \leq x \leq b \\ \frac{c-x}{c-b}, & b \leq x \leq c \end{cases}$	
TRAPEZOIDAL	$\mu(x) = \begin{cases} 0, & x < a; x > d \\ \frac{x-a}{b-a}, & a \leq x \leq b \\ 1, & b < x < c \\ \frac{d-x}{d-c}, & c \leq x \leq d \end{cases}$	
GAUSSIAN	$\mu(x) = e^{\frac{-(x-c)^2}{2\sigma^2}}$	
BELL	$\mu(x) = \frac{1}{1 + \left[ \left( \frac{x-c}{a} \right)^2 \right]^b}$	

The last central concept of the FL are the **rules** that are used to describe the relationships between input and output linguistic variables based on their linguistic terms. “Rule-base” is normally referred to a set of rules for fuzzy system. Rules are composed by an “Antecedent”, or “If portion”, where one or more inputs are combined and “Consequent” or “Then portion” with the outputs. Normally rules appear in this form:

**If (“Antecedent”) Then (“Consequent”)**

for this reason sometimes is used the name “If-Then” logic referring to FL.

In the “Antecedent” an input linguistic variable is combined with a corresponding linguistic term while the “Consequent” an output linguistic variable is associated with the corresponding linguistic term. The results of the rule represent the action desired that fuzzy control done if the linguistic terms of the inputs linguistic variables in the rule are met. As an example:

**If A is A<sub>1</sub> AND B is B<sub>1</sub> OR C is C<sub>1</sub> Then U is U<sub>1</sub>** (eq.5.1)

Where A, B, C and U are fuzzy variables while A<sub>1</sub>, B<sub>1</sub>, C<sub>1</sub> and U<sub>1</sub> are linguistic terms described by their membership functions. AND, OR are connectives that will be explained later; this rule is formed by three antecedent and one consequent. From the operative point of view, the rules are developed for compute the inference process of the fuzzy system that allow to know what is the output when certain combination of the inputs is given.

The total of possible rules for a fuzzy system is defined in function of the number of input linguistic variable (m) and the number of linguistic terms used for each input (p).

The total number of rules possible (N) are defined:

$$N = p^m \quad (\text{eq.5.2})$$

The rule base is normally reported in a table, in this manner the inconsistency or the rule missing could be easily detected. In case of a large amount of inputs a cascading fuzzy system is used in order to avoid a large number of rule bases. In this solution, the first fuzzy system serve as the inputs of the second fuzzy system until the last controller [86].

For a controller with multiple input (e.g. MIMO) the two (or more) input linguistic variables and terms are normally combined using connectives. In order to calculate the value of the aggregated rule different connectives are used:

$$\text{AND (Minimum)} \quad \mu_{AB} = \min(\mu_A, \mu_B) \quad (\text{eq.5.3})$$

$$\text{AND (Product)} \quad \mu_{AB} = \mu_A \cdot \mu_B \quad (\text{eq.5.4})$$

$$\text{OR (Maximum)} \quad \mu_{A+B} = \max(\mu_A, \mu_B) \quad (\text{eq.5.5})$$

$$\text{OR (Probabilistic)} \quad \mu_{A+B} = (\mu_A + \mu_B) - (\mu_A \cdot \mu_B) \quad (\text{eq.5.6})$$

The AND minimum specify to use the smallest degree of membership of the antecedents as the truth value of the aggregated rule antecedent, while the AND product specifies to use the product of the degrees of membership of the antecedent. Instead the OR

(Maximum) compute the maximum between the two degree of membership of the two antecedents, while the probabilistic OR specifies the use of the sum of the degree of membership of the two antecedents.

In this way the inputs are combined using connectives in order to determine the truth value for the aggregated rule. In the consequent of the rule, one (for SISO systems) or more (for MIMO) outputs are defined.

### 5.2.1 Fuzzy Logic Controllers

A Fuzzy Logic Controller FLC is commonly defined as a control system that emulates an human expert using predefined FL rules, starting from the current value of input variables and calculating one or more output signals. FLCs consist of three components, as reported in Fig.5.2:

1. Fuzzifier
2. Inference mechanism/engine
3. Defuzzifier

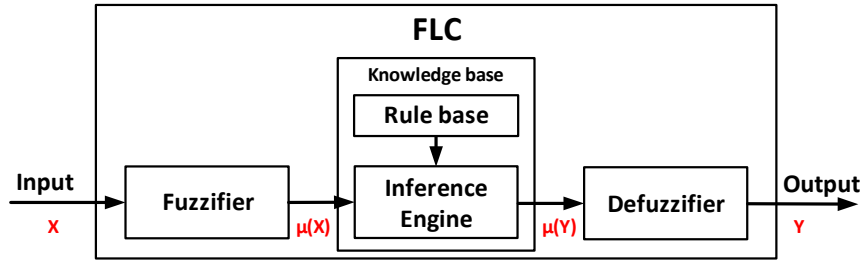


Fig.5.2 - Fuzzy controller process

These components carry out a process which starts with a transformation from the real word domain using real numbers to a fuzzy domain where fuzzy numbers are used. On these numbers, a set of fuzzy inferences are used for decision-making process while in the final stage an inverse transformation from fuzzy to real word is realized. The result is a static nonlinear mapping between inputs and outputs (Fig.5.3).

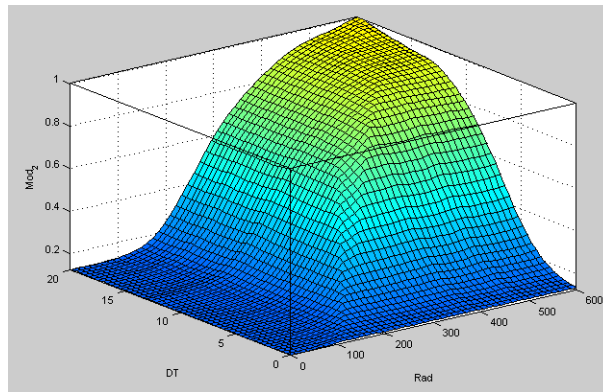


Fig.5.3 - Fuzzy static map between two inputs and one output

Before explaining the three parts that compose the FLC, a typical structure of fuzzy logic controller in a real installation is reported in Fig.5.4. Here, the inputs of the controller come from the sensors, pass through a couple of transformation (analog to digital and crisp to fuzzy) reach the Inference engine and pass, in reverse order, another couple of transformations (fuzzy to crisp and digital to analog) before to reach the plant as a control signal.

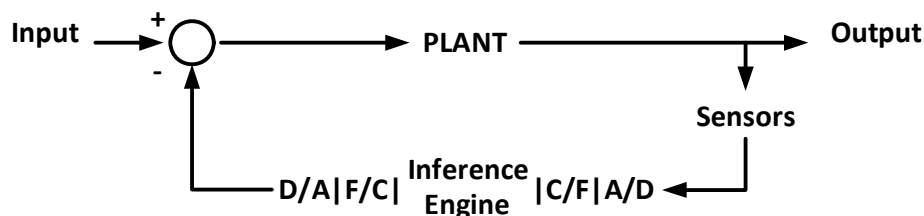


Fig.5.4 - Fuzzy controller [85].

### 5.2.2 Fuzzification process

“Fuzzification” is the process of associating to a crisp or numerical input value the linguistic terms of the corresponding input linguistic variable. The crisp value of input comes from a sensors or physically quantities is scaled in a mapped linguistic universe of discourse. E.g. a fuzzy controller might associate the temperature reading from a thermometer with the linguistic terms “low”, “moderate” or “high” for the current temperature linguistic variable. Depending on the membership functions defined, a certain value of temperature, or the input processed, might correspond to one or more of the linguistic terms with a different degree of membership. After this phase the crisp input value is converted into fuzzy values in the interval  $[0,1]$  using the membership functions that carry linguistic labels, as described before.

### 5.2.3 Inference mechanism/engine

The inference mechanism represents the knowledge base and reasoning structure of the FLC. Its function is twofold: on one hand it determines the extent to which each rule is relevant for the current situation as characterized by the value of the inputs involved and, on the other hand, it draws conclusions using the current inputs and the information captured in the rule-base.

The rule-base, as reported before, is the set of rules a fuzzy system uses to determine the resulting linguistic terms of the output linguistic variables. The idea at the base of these mechanism is to convert the linguistic statements of human operators into an effective control rule. The method has some shortcomings due to the facts that in the real plant is not always possible to describe the control of the process using fuzzy logic, even by someone with experiences on the process and, moreover, there is no theoretical method to determine the minimum or even an adequate number of control rules. Another limitation using FL to control complex systems, are the practical difficulties in correlating



the verbal reports of operators with the actual rules they applied during an actual control task. Starting from an experienced operator is not a trivial task to design the rules of a FLC.

As mentioned before, once defined a system of rules that are combined obtaining a rule-base these are used by the Fuzzy Inference System (FIS). Traditionally in literature two FIS are commonly used: Takagi and Sugeno (TS) and Mamdani. The difference of the two FIS is in the THEN clause, where TS method uses algebraic linear combination of fuzzy variables, the Mamdani method makes use of linguistic variables. Mamdani fuzzy inference system is preferable in FLC instead of TS because of two reasons. First, since the IF-THEN rules of the Mamdani method are given in natural-language form, it is more intuitive to build the fuzzy rules so that the parameters can be determined later in the optimization or learning phase. Secondly, this methodology is well established because in the scientific papers found in literature is the more widely used (compared to TS).

#### 5.2.4 Defuzzification process

In the Defuzzification stage, the value of the linguistic output variable inferred by the fuzzy rules is translated into a crisp value usable for a concrete real word control action. The objective is to derive a single crisp numeric value that best represents the inferred fuzzy values of the linguistic output variable. Defuzzification, opposite to fuzzification, is an inverse transformation which retranslates the output from the fuzzy domain into the crisp domain. Several methods are defined in literature for the defuzzification process. The most important processes are three:

- Center of Area (CoA);
- Center of Maximum (CoM);
- Mean of Maximum (MoM).

The CoA method is the most common used and is also referred to as Center of Gravity (CoG) method because it computes the “centroid” of a composite area representing the output fuzzy term. In this method is calculated first the area under the scaled membership functions and within the range of the output variable. It calculates the best compromise between multiple output linguistic terms and is computed as follow:

$$\text{CoA} = \frac{\int_{x_{\min}}^{x_{\max}} f(x) \cdot x dx}{\int_{x_{\min}}^{x_{\max}} f(x) dx} \quad (\text{eq.5.7})$$

Where  $x$  is the value of the linguistic variable and  $x_{\min}$  and  $x_{\max}$  represent the range of the linguistic variable.

The CoM method consider only the peak of the membership functions represented in the output variable universe of discourse, the areas for the membership functions being ignored. Here, the FLC evaluates the mean of the numerical values corresponding to the

degree of membership at which the membership function was scaled, for each scaled membership function. The FLC computes the CoM using the following equation:

$$\text{CoM} = \frac{(x_1 \cdot \mu_1 + x_2 \cdot \mu_2 + \dots + x_n \cdot \mu_n)}{(\mu_1 + \mu_2 + \dots + \mu_n)} \quad (\text{eq.5.8})$$

Where  $x_1, x_2, \dots, x_n$  are typical value for the scaled membership function 1, 2, ..., n, and  $\mu_1, \mu_2, \dots, \mu_n$  are the degree of membership at which membership function n was scaled.

The MoM method is developed because the CoM method does not work whenever the maxima of the membership functions are not unique. The implementation is similar to the CoM method a part that it calculates the most plausible result. Rather than averaging, this methodology selects the typical value of the most valid output linguistic term.

For closed-loop control application of FL the methods CoA and CoM are normally applied [95]. These methods usually result in continuous output signals because a small change in input values does not change the best compromise value for the output. Considering a fuzzy system with a complete rule base and overlapping membership functions, the defuzzification method that more seems adequate and most used in literature is CoA. For these reasons in the work here presented this methodology was preferred to the others.

Going back to a more general analysis of the FLC features, since it doesn't have the characteristics of Learning or adaptation phase [84], the FLC is normally coupled with a learning or adaptations mechanism, as reported in Fig.5.5 [85]. Here the fuzzy inference is connect to a knowledge base, in a supervisory or adaptive mode. In the system reported in the Fig.5.5, in particular, a crisp controller is used and a Fuzzy adaptation algorithm is built in order to optimize the parameters of the controller (e.g. PID), in order to cope with the system's unmolded dynamics, disturbances or plant parameters changes like an adaptive control system.

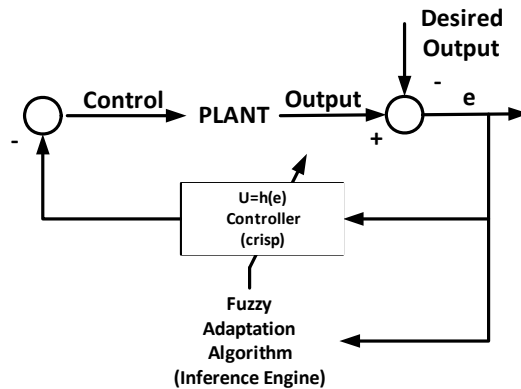


Fig.5.5 - Adaptive or Supervisory Fuzzy Algorithm [85].

### 5.3 Reinforcement learning

When we think about the learning process, we could easily refer to the interaction that humans have with the nature. If we speak, for example, about an infant that approach the real space around him, he trying to explore it without having a a-priori knowledge or a teacher that give him information about the universe that he is discovering. He has only a direct sensorial contact with this environment. During this phase of exploration, the child trying to learn information using a simple cause-effect process, where the consequence of his actions bring him to reach a determinate goal in the most simple and pleasant way. During all our lives, these interactions with the surroundings are undoubtedly ones of the major source of knowledge about our environment and ourselves [101].

Focusing on these interactions, the theory of Reinforcement Learning RL was developed in the 1979 [101]. Here, similarly to the interaction process between human and the ambient around him, an active system usually called “Agent”, interacts with the connected “Environment”. As reported in the Fig.5.6, the agent makes an action on the environment, receives from it an information related to the characteristics modification of the environment (State) and some evaluative feedback signal usually called reinforcement that could be a reward or a punishment. This leads to clarify better the meaning of learning process that is based on trial and error interaction between agent and environment with the result of discovering which actions yields the most reward by trying them.

The objective of the whole learning process is to map situations (States) to actions in order to find the best policy to use for maximize the positive effect giving by the environment in form of rewards. In other words, in RL the agent learns how to act when it is in a certain state, given an observation of the environment. All the actions have an impact on the environment, and the environment “guides” the learning process of the Agent giving him a feedback in form of rewards.

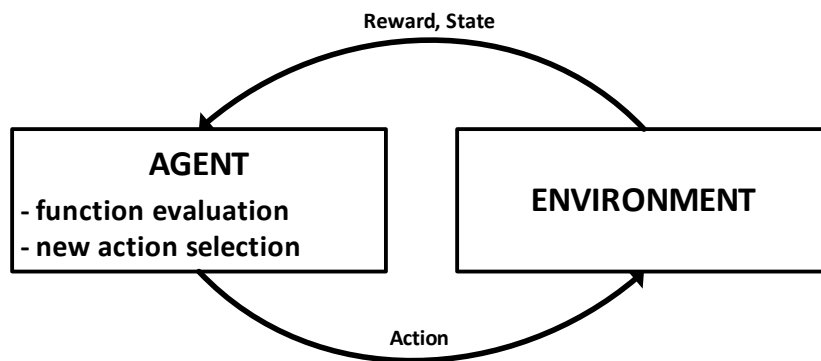


Fig.5.6 - Reinforcement learning scheme [101]

In RL, the state-space is generally defined as the set of all the possible states that the agent can occupy at different stages of the learning process. At any time step the agent will be at any one of the state from the entire state space instead the action space is

related to the set of possible action that the agent can be take on the environment. Both of these space (states and actions) have to be define in the beginning phase of the process. This means that a general knowledge of the limits or the range of the environment state and the action applicable has to be known previously.

The main problem of these kind of processes is when a large number of states occur to describe correctly the environment or when, operatively, the discretization of the single state require high number of divisions of the state space. In this condition the amount of data required to develop the methodology are huge and the number of combinations state/action require a long process of training which makes this method not applicable in practice and computationally expensive. This problem is known as “curse of dimensionality”[103] and for this particular class of problems, instead of large number of state space pairs a sort of function approximation is needed.

Normally there are many parameterized classes of functions that can be used to prefer such approximation, but the most applied are the Neural Networks, due to the ability to represent and learn non-linear functions as Multi Layer Perceptrons and Radial Basis Functions network [104] [105].

In general the learning process could be divided in two families. When the agent learns from the input-output pairs, normally referred to as supervised learning and when no data are previously available for the training of the agent, normally referred to as unsupervised learning or model free learning [106].

Another classification could be made, dividing the learning approaches in direct learning and indirect learning. Also here, the indirect learning using some collected data for training the agent off line in order to, ultimate the learning phase, apply the agent to the system. Differently, in the direct learning, the optimal policy is learned without first learning an explicit model or an off-line model training on collected data.

The methodology presented here, where an agent learns an optimal policy maximizing an objective function, is based on the information about the system current state  $s_t$  and the subsequent state  $s_{t+1}$ , without using the prior history. This approach is justified if the reward, that is used for the learning evolution, depends only on the current state and current actions. Normally this kind of methods belong to Markov Decision processes (MDP) that are stochastic processes where the probability of transition from one state to the next one depends only on the characteristics of the system in the actual state. A RL task satisfies the Markov property of convergence [102].

The methodology that we are going to present more in detail in this chapter, has applied to the control of a solar thermal system, belongs to this family and to the direct learning approach [102]. We refer to this class of methods (unsupervised learning) because they are the most used in practice mainly due to the absence of environment model.

### **5.3.1 Q-learning**

Going more in detail with the analysis of the model-free RL, the agent does not have a prior knowledge of all the system characteristics in the new reachable state. Essentially, the agent does not know what are the effects of all the possible actions on the

environment in the next state but only has information on the actions experimented in the next state at antecedent steps. Therefore it could not choose the optimal action in the new state but only scan the effect of the actions tried in the new state and choose the optimal of that.

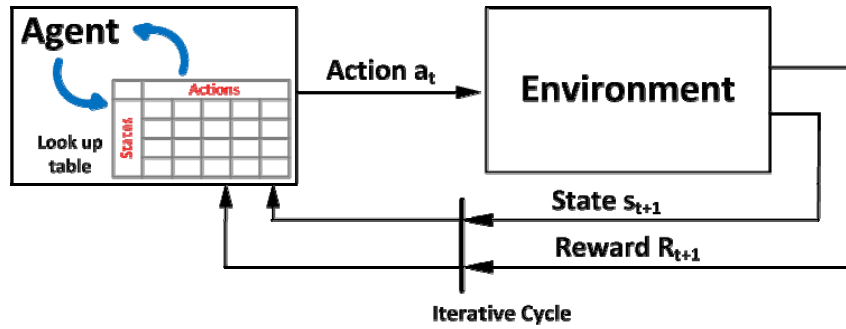


Fig.5.7 - Q-learning process.

In the Q-learning method [103], which is one of the basic RL algorithm, an evaluation function is defined  $Q(s_t, a_t)$  related to the effect of an action  $a_t$  carried out in the state  $s_t$ . The value of this function indicate how good is to perform action  $a_t$  in a certain state  $s_t$ . The objective of the Q-learning is to find a policy  $\pi^*$  that the agent has to follow in order to obtain the optimal action at each stage. This is a sort of mapping from the perceived states of the environment to the actions to be taken (when in those states) in order to optimize a certain objective function strictly connected with the reward. A characteristic of all unsupervised learning methods, and the Q-learning algorithm in particular, is that the agent learns on the field both the optimal policy and the objective function. In the Q-learning the Q values of a state action pair  $Q(s_t, a_t)$  are stored in a lookup table [Q] (as reported in Fig.5.7), used for define after the learning phase the optimal policy with the following equation:

$$\pi^*(s) = \underset{a}{\operatorname{argmax}} Q(s, a) \quad (\text{eq.5.9})$$

The approach used in this methodology is a value iteration (as reported in Fig.5.8). In this way every step (that could be the same evolutionary time of the system or a cycle where the state and the reward are integrated) of the learning process the agent dialogues with a table [Q] where all the Q values are stored and elaborated during the learning process. Looking the structure of the lookup table [Q] (as reported in Fig.5.7), on the rows are reported the states while on the columns are reported the actions. Before starting the table [Q] for all states and all actions are initialized to zeros. The value of each iteration is computed in the following form:

$$Q_{t+1}(s_t, a_t) = Q_t(s_t, a_t) + \alpha \cdot [R_t + \gamma \max_a Q_t(s_{t+1}, a) - Q_t(s_t, a_t)] \quad (\text{eq.5.10})$$

Where  $\alpha$  is the learning rate and  $\gamma$  is called discount factor and both takes values in the  $[0,1]$  interval. These two factors weight, respectively, the increment to the present Q-value (learning speed), and the contribution from the future states (decay). The value multiplied by factor  $\alpha$  is also known as Temporal Difference error [101]. The  $R_t$  is the return value measured on the environment and is the main mechanism of this procedure. Going more in detail on the return value, this is the actual reward received by the agent while following a certain policy and may refer to the total reward received or that one received after a given amount of time or steps. The return is used mainly to update the value function, in this case Q value (eq.5.4), because in fact is the result of the agent's interaction with the environment. There are different manners to define the return as a total reward, the average of the rewards or the most used in literature, the total discounted reward. The latter being defined as:

$$R_t = r_t + \gamma \cdot r_{t+1} + \dots + \gamma^k \cdot r_{t+k} + \dots = \sum_{i=0}^{\infty} \gamma^i \cdot r_{t+i} \quad (\text{eq.5.11})$$

using the discount factor for assign greater weight to immediate reward and define the present value of the future rewards. This methodology was developed mainly for robot motion [107] where a target as to be reach following a multistep procedure. The return is calculated through the sum of rewards of the different steps. Differently, in the application of the RL to continual problem as the process control, the methodology used never terminate in a target but, on the contrary, continue indefinitely. In this class of problems the value function is updated following for example one step-backup methods, where the value function, Q value in our case, is updated using the value observed in the next state, to update the current state of the lookup table [Q]. This approach was defined by Watkins as one step Q-learning [103]. In this case the return value is equal to the reward of the step analyzed. This approximation on the reward is reported also in [118] where this analysis is reported with the comparison between RL and dynamic programming.

The reward used in RL defines the goal of the problem. Usually, in robot applications or movement applications, it is a function that is connected with the desirability level of the state reached. More generally, the reward defines what are the good or the bad events for the agent.

In general, the iterative process of the Q-learning could be summarized as the scheme reported in Fig.5.8. In the scheme proposed for the iterative process, any indication is reported on the methodology followed for the new action's selection. Going in detail with this issue, the main RL challenges is the trade-off between Exploration and Exploitation [101]. In order to obtain the optimal action on the environment the agent must prefer actions that it has tried in the past. But for this reason the agent has to discover the effect of all the possible actions starting from a state, in order to know what is the best one to do in every situation. Practically, the agent has to exploit an action that it already knows in order to optimize reward but at the same time it has to explore in order to optimize the future actions on the system.

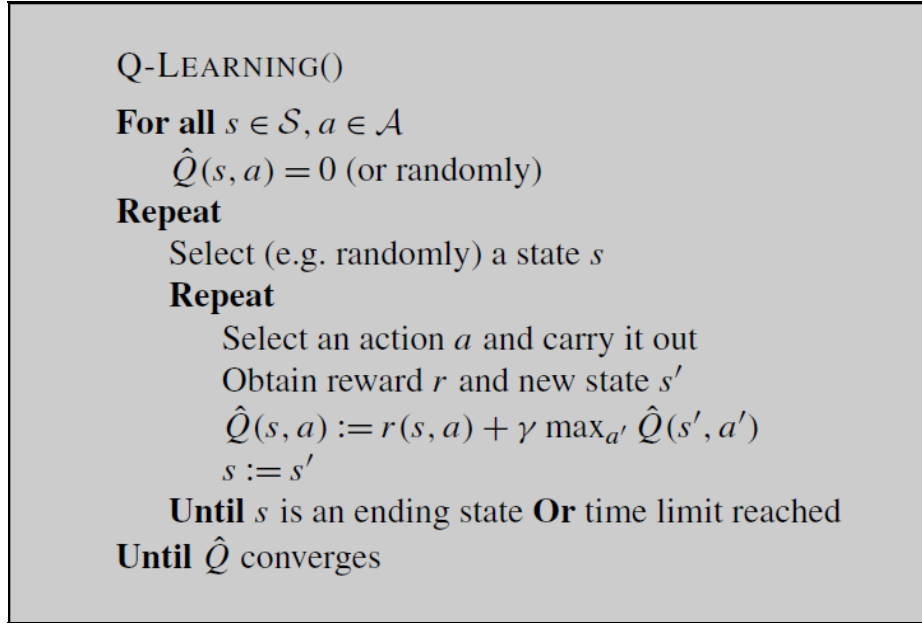


Fig.5.8 - Q-learning iterative process [102]

For the action selection, as usually referred as “Exploration problem”, could be followed a random selection. This method has the problem of slow convergence in order to explore all possible actions or policies. Other two simple local methodology are mainly followed: the  $\epsilon$ -greedy method and the Softmax method.

In the  $\epsilon$ -greedy method, the new action  $a_n$  is selected between value stored in the table [Q] or through random selection. With probability  $\epsilon$ , that is parameter previously set constant or decreasing during the learning process, the action selected is that one which maximize the value in the table [Q] at state  $s_n$ . In this way the agent exploit current knowledge in order to maximize the immediate reward.

$$a_n = \underset{a'}{\operatorname{argmax}} Q(s_n, a') \quad (\text{eq.5.12})$$

Otherwise, the action is selected with probability  $1-\epsilon$  through an uniform random selection. Differently from this one, in the Softmax method the action is selected according to Gibbs or Boltzmann distribution. The probability to choose the new action is:

$$p(a) = \frac{e^{\frac{Q_t(a)}{\tau}}}{\sum_{b=1}^n e^{\frac{Q_t(b)}{\tau}}} \quad (\text{eq.5.13})$$

In the optimizer  $\tau$  is a positive parameter called temperature. With high value of temperature all the actions could be all equiprobable (as in the  $\epsilon$ -greedy method) instead with  $\tau \rightarrow 0$  the action selection become the same as greedy selection.

### 5.3.2 Application of RL and Q-learning

Before to analyze the applications of RL, an interesting review of the history of RL is reported in the book of Sutton and Barto [101] where all the development steps are reported with an exhaustive bibliography.

In the past years many applications of RL are reported in literature, starting from the application of combinatorial search and optimization process like board games (TD gammon) [108] or industrial process control, manufacturing, robotics and power system. An application of RL to the automatic generation control of a power system is reported in [109], [110] where a RL algorithm performance is compared with a properly designed linear controller underlining the potential related to the flexibility in specifying the control objective before the learning phase. In this field some applications are reported in the thesis of Jasmin [111] focused on the application of RL to power system scheduling.

In the robotic field, it is the main characteristic of being model free method which makes it suitable for control of Robots where several experiments on robot control are made using Q-learning methodology (see, for example, [112]). Other interesting applications of Q-learning is related to elevator control task [113] for reducing the average squared wait time for passengers, the application of RL to autonomous helicopter flight [114] or an industrial optimization process application for optimize the functioning sequence of ten different workstations [115].

An application of Q-learning applied to fuzzy combined with PI controller are reported in [116] and previously the same authors [117] worked on the definition of two RL algorithms with fuzzy logic, defining Fuzzy Q-learning and Dynamical Fuzzy Q-learning with the target to improve the rule base of a fuzzy controller.

Going in detail with the application of RL to thermal system, Anderson [118] presents in his work a comparison between different strategy to control an heating coil in a simulated case. Here, the RL is combined with a PI controller in order to reduce the error of the control variable over the time. The results of the application of this combination shows, after an opportune training phase, a reduction of the RMS error compared with the simple PI controller.

A couple of papers of Dalamagkidis and Kolokotsa [119][120] present an implementation of RL using a TD error method for optimizing the control of the thermal comfort for commercial building without requiring a model of the environment. In this works the authors coupled the RL with a recursive least square methods in order to increase the convergence speed of the method. In the [120], in particular, the author showed the use of a reward composed by different parameters, properly weighted, in order to minimize the energy consumption and maximizing, at the same time, the comfort and the air quality. The state of the system is related to the internal and external temperature and the actions are related to the control of the function of the heat pump, of the compression chilling system or the control of the automatic opening system of the windows. One of the issue underlined from the authors is the lacking of paper in literature related to the application of this methodology to control of internal comfort therefore the choice of the parameter of the reinforcement learning was made on the



experience and test effectuated on the system. The authors, moreover stress the importance of the reward mechanism in the learning process and future development will be addressed on this topic. In addition also the inertia of the environment as to be deeply analyzed in order to understand the response time of the environment to the action and correctly compute the effect in the learning analysis.

A work based on two papers developed by Liu and Henze [121], [122] present the application of RL to the optimal control of building passive and active systems. In particular a thermal passive system is controlled in order to minimize the energy consumption of the HVAC system installed in a commercial test structure. In this work an interesting hybrid approach is presented based on two different phases: simulated learning phase and implemented learning phase. This idea originated from the observation that the RL method for control give near optimal results compared with optimal control strategy based on predictive control but takes an unacceptably long time during the learning phase. Starting from these premises the hybrid approach is developed for attempt to combine the positive features of both, the model based and the RL approach. In this way, in the first phase of learning the agent is trained using a model of the system following by a refined learning phase (or tuning phase) when the agent finalize the learning phase in direct connection with the real system.

Moreover in a previously work, Henze [122], [123] showed for the same class of problem, related to the charging and discharging phases control of a cool thermal storage systems, an increasing of the peak saving and a reduction of the cost using a model free RL to optimize the control. Henze points out that the developed RL control does not reach the best performance of a model based predictive optimal control but shows a favorably comparison with conventional cool thermal control strategies. Furthermore, the RL approach allows, using past experience and actual exploration to account for the non-stationary features of the physical environment related to seasonal changes and the system degradation in the choice of the future actions.

An interesting work of Yu and Dexter [124] presents the application of RL on the tuning of a supervisory Fuzzy controller for low-energy building system. In this work the authors show an application of online learning scheme based on pre-generated fuzzy rule-based. Here, the learning process is accelerated with the use of  $Q(\lambda)$  algorithm with a fuzzy discretization of the state variable and eligibility trace back and the successful application of RL to the supervisory control of buildings is strongly dependent on reducing the state space and action space of the controller. As reported in the other papers, also here is underlined the importance of off-line learning, here included in the knowledge used for assess the rules of the fuzzy controller. The approach based solely in on-line learning take an unacceptably long training time.

#### **5.4 Application of RL and Fuzzy logic**

In the work presented here, the Q-learning methodology is applied in conjunction with Fuzzy logic controller. In Tab.5.2 a literature research on the coupled application of Fuzzy and Reinforcement learning shows only few applications.

Tab.5.2 - Conjunction approaches based on fuzzy and reinforcement learning cross with algorithms.

Applications Algorithms	Wireless Network	Internal comfort/Energy consumption	Manufacturing Systems	Financial	Autonomous Car driving	Underactuated unicycle system	Robot Movement	PI PD controller
Q-Learning and FLC	[126]	[124]					[128] [129]	[116] [125]
Actor critic learning and Neural Network Fuzzy			[130]					
RL and ANFIS				[131]				
FLC and on-line learning					[127]			
FLC and iterative learning						[132]		

### 5.5 Application of FLC and RL to thermal system

As mentioned in the introduction, in this subchapter is described the reinforcement Q-learning and fuzzy logic controller application to a solar thermal systems. Starting from the Q-learning, this is a unsupervised reinforcement learning process. As mentioned in the Q-learning presentation (Chapter 5.3.1) and more generally for the Reinforcement Learning methods, these methods allow to find an optimal policy (essentially the optimal action to do for each state) when all the possible actions in each single state can be evaluated. It means that every possible pair of state/action has to be tested before understanding what is the best action to do for a given state. The evaluation process, normally called "exploration phase" is based usually on the  $\epsilon$ -greedy method [101], where the new action to explore is selected randomly setting a parameter  $\epsilon$  related to the probability to a new action selection. This is also reported in the iterative process presented in the Fig.5.8.

Differently from other applications, in the thermal systems the acquisition frequency is typically in the order of few Hertz, with observation periods in the order of 5-10 minutes. This is a consequence of the relatively high thermal inertia and long transport delays of such systems, where it is always required to wait some time before the effect of an action on the system can be measured by its sensors. Of course, long observation periods reduce the volume of collectable data, making the Q-learning algorithm slower to understand how the environment behaves and at the same time making more valuable the exploring action performed at each observation period.

Being the number of actions used for exploration relatively few, a problem arise applying  $\epsilon$ -greedy algorithms for the exploration phase, which are usually based on the generation

of pseudo-random numbers. In fact, when the number of trials is small enough there is no guarantee that the various actions in each state are explored enough to obtain the best performances. It certainly would be the case with a large number of trials but that in our application that could mean waiting months (if not years) and these figures are totally unacceptable.

In order to overcome this limitation, a sort of guided exploration has been implemented. The basic idea was to develop an exploration phase where, given a certain state (row index of the [Q] table), the agent starts to explore the action whose outcome that is the less known. In order to define a “level of knowledge” of each action for a given state, a second matrix [Q\_count] has been implemented that counts the number of events experimented each pair state/action. This second lookup table [Q\_count] has the same dimensions of the matrix [Q] (referring to the Fig.5.7) and contains the number of the events experimented for each the state/action pair. Given a certain state, the new action is selected evaluating the minimum of the [Q\_count] matrix, in other word evaluating the minimum of the row corresponding to this state. In this way from one side the exploration of each possible action is ensured and, from the other the counts of the events tested for each state/action pair is saved in the [Q\_count] matrix.

Using this approach, also a convergence criteria has been established for changing the operative conditions of the reinforcement learning from exploration to exploitation (as reported in the eq.5.3). This is a local criteria because is evaluated for each single state. Going more in detail, a minimum value of events (actions) to be explored in each state has to be set (Nev) in order to guarantee a minimum number of attempts for each action. To evaluate the degree of convergence of the learning method, the following equations have been implemented based on the convergence of the elements in the whole matrix. In particular for each state i, using the matrix [Q\_count], a parameter “count<sub>i</sub>” is evaluated in order to check which states have reached convergence.

$$\begin{cases} \sum_j^L Q\_count_{i,j} \geq Nev_{tot} \longrightarrow count_i = 1 \\ \sum_j^L Q\_count_{i,j} < Nev_{tot} \longrightarrow count_i = 0 \end{cases} \quad (eq.5.14)$$

$$Nev_{tot} = Nev \cdot L \quad (eq.5.15)$$

Where:

- L is the number of actions;
- K is the number of states used;
- Nev is the minimum number of attempts for each action;

- Matrix [Q] and matrix [Q\_count] have dimension:  $[Q], [Q\_count] \in \mathbb{R}^{K \times L}$ .

Using all the parameters “count<sub>i</sub>”, the convergence of the whole matrix have been easily computed. Normally three cases can be found:

I. Starting exploration phase:  $\sum_i^K \text{count}_i = 0$  (eq.5.16)

II. During exploration phase:  $0 < \sum_i^K \text{count}_i < K$  (eq.5.17)

III. All the matrix is explored :  $\sum_i^K \text{count}_i = K$  (eq.5.18)

A parameter “conv” that indicates the percentage of the matrix explored, and consequently the progress of the learning process has been computed as:

$$\text{conv} = \frac{\sum_i^K \text{count}_i}{K} \quad (\text{eq.5.19})$$

This parameter can be represented versus time in order to show the time trend of the learning process, looking the speed of learning and the percentage of the matrix explored (as reported in the following Fig.5.19).

The matrix [Q\_count] can also be useful when, after the exploration-exploitation process, the system (or more generally the environment) changes its behavior due to ageing or to the changing boundary conditions. In these circumstances, the agent should to be able to recognize the new distribution of the optimal actions to do.

Making an analogy with the human learning process, this difficulty is similar to the one everybody faces when trying to correct a bad habit (or “wrong learning”). If an output pattern or a sequence of events has been tried a lot of time, it brings with itself an experience (the data stored in the matrix [Q]) that is difficult to discard when the optimal policy changes.

For solving this problem the Q-learning method could be reset periodically, forcing a restart of the exploratory phase from the beginning. The implementation of the Q-learning algorithm of this work provides this feature, which is useful to verify the learning process quality by comparison of learning phases relative to different time frame. To clarify this point, an example of the worst case is given. When the learning phase is totally wrong, the matrices [Q] and [Q\_count] have to be reset to zero, restarting the learning process and forgetting all the information that the system have gained in the first period. Discarding totally the knowledge acquired from the past observations is however not

adequate for tracking slow changes of the system parameters such as fouling. In this case a “partial reset” of the information could be more useful. In this case the new matrices in the learning process will be  $[Q^*]$  and  $[Q\_count^*]$  computed as:

$$[Q^*] = \beta [Q] \quad (\text{eq.5.20})$$

$$Q\_count_{t,j}^* = \beta \cdot Nev \quad (\text{eq.5.21})$$

Where the parameter  $\beta$  that can be between 0 and 1 is useful for define a sort of “exploration degree” when a certain time a new exploration is planned. At this time the agent stops using the old  $[Q]$  and  $[Q\_count]$  matrices and begins using the matrices  $[Q^*]$  and  $[Q\_count^*]$ , allowing a new exploration phase more or less long and deep in function of the parameter  $\beta$  selected. Also in this step, the graph of convergence versus time presented previously, can be used for show the speed of the new learning phase.

The application of the Q-learning with fuzzy logic controller is based mainly on two aspects. The first one is related to the easiness with which the complex control curves could be designed and modified with fuzzy logic, allowing to manage them with just few parameters. This is useful also when the learning phase of the FLC is developed with Q-learning process. As we described previously, in thermal applications no many events can be allocated for the learning process, so a limited number of actions can be set. Moreover it is often impossible to leave the agent total freedom in selecting the action to prefer on a commissioned plant. A balance between what is the best to explore and what is the best for protect the investment needs to be found.

Considering the limited number of possible actions, the FLC and RL has been designed as described by the scheme reported in the Fig.5.9. The actions made by the Q-learning agent are performed directly on the Fuzzifier part of the FLC, modifying the input membership functions (referring to Chapter 5.2 for the characteristics of Fuzzy logic and fuzzy logic controller).

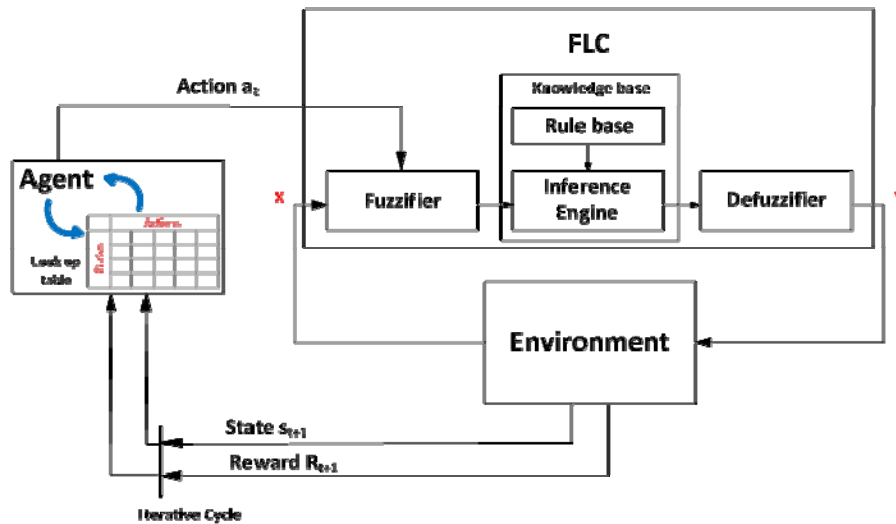


Fig.5.9 - Combination of Q-learning and Fuzzy logic controller

As an example, the Fig.5.10 reports the shape of the membership functions for a case with three triangular membership functions on the input. In the first case the membership function of the “high” value is varied, while in the second case different membership functions for the “medium” value are tested on a system with single input/single output. The resulting characteristics of the FLC, for these two cases are reported in the Fig.5.11 where 7 different values of the higher (the graph on the left) and the medium (the graph on the right) membership functions are plotted, respectively.

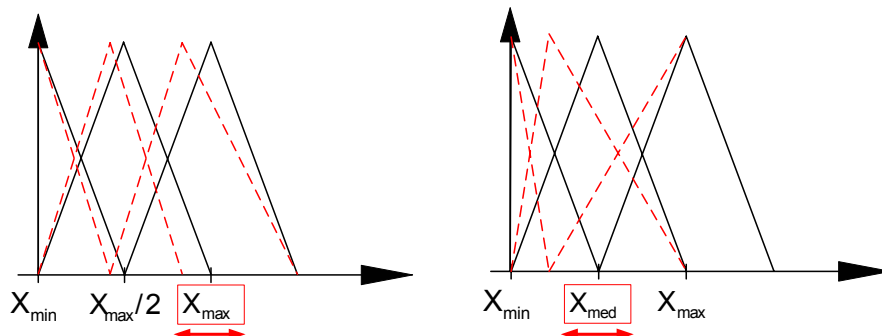


Fig.5.10 - Modification of the input membership functions definition.

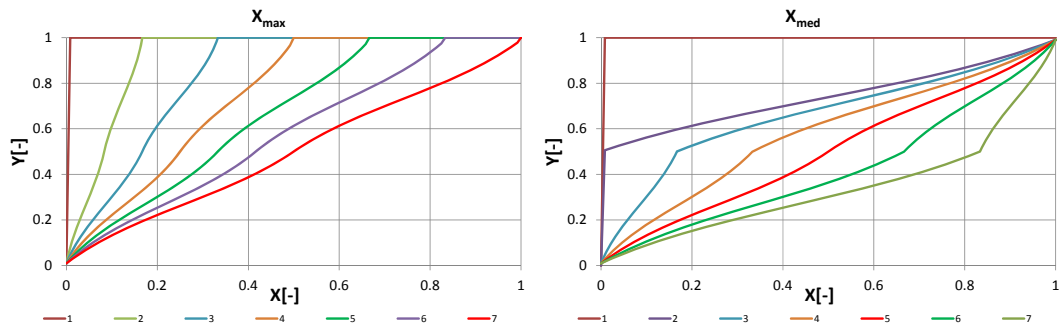


Fig.5.11 - Output signal of FLC with two different MF variation policies.

The second aspect that push us to apply the RL with FLC is more related to the element controlled correct operation. If we applied directly the reinforcement learning to find the best control curve without using the FLC, the agent try to use all the range of control function between 0 and 1 introducing of high frequency changes in the beginning of the learning phase. This behavior of the control should reduce the component expected life then extra measures have been taken to ensure a smooth operation of it. On the contrary, the FLC could test the different curves reducing this negative effect but at the same time, exploring a finite number of curves in a reduced area of control.

The tool used for the design of the fuzzy controller and the Q-learning algorithm is LabVIEW. This software has a fuzzy toolbox with some features that allow an easy implementation of the fuzzy controller and along with its hardware platform, it is widely used for the monitoring and the control of energy system. This characteristic makes this software useful for the development of a control software that can be used at the same time in a simulation and in the real installation, saving development time. Furthermore, this software can be integrated, albeit not seamlessly because of unfortunate naming conventions of the two programs, with the simulation software Trnsys [46], normally adopted for the energy system simulations.

The Annex 2 reports the schemes and the explanation of the algorithm that has been designed in LabVIEW while in the Annex 3 the code of the mask used in Trnsys for reading the DLL created in LabVIEW is showed. The idea behind in the design of such a system is to develop the controller in LabVIEW and to plug it in with Trnsys as a dynamic linking library (DLL) in order to perform the simulation of the energy fluxes. After the design of the controller in LabVIEW and compiled into the DLL, Trnsys reads it through an opportune mask as reported schematically in Fig.5.12.

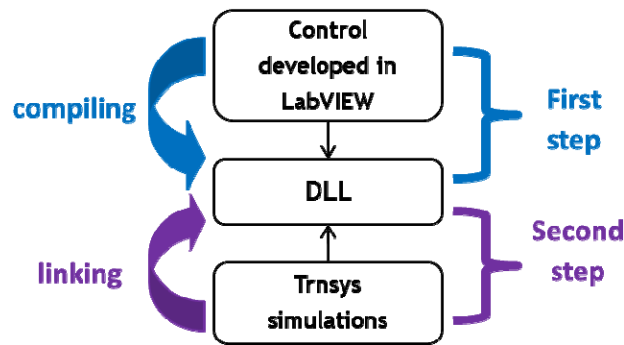


Fig.5.12 - Interaction Trnsys/Labview

## 5.6 Example of FLC and RL application to a SDHW

As application example of the methodology explained previously, a simple traditional solar thermal system for domestic hot water (SDHW) is considered and hereafter analyzed. A Trnsys [46] model of the system has been developed in order to understand the effect of the different control strategies studied on the solar system. The design of the components dimensions and characteristics have been made starting from the thermal storage because the numerical model of this component was validated using monitoring data from the SolarCombi+ installation reported in the Chapter 4 [64].

The thermal storage consists of a container storing 1000 l of water with two internal heat exchangers, one for solar primary loop and one for domestic water loop as reported in Fig.5.13. A stratification device has been installed inside the storage in order to promote stratification of the internal temperature increasing the heat exchange process between the stored water and the heat exchanger for DHW. On the primary loop a mixture of water and propylene glycol (30% in volume) has been used in order to avoid freezing during winter seasons. A collectors area of 12 m<sup>2</sup> has been selected using standard design rules of thumbs of solar thermal systems for DHW [14]. The DHW request profile has been computed using DHWcalc [58][59], considering a multifamily house with a daily consumption of 50 l/gg for person and three families composed of 4 persons each one. An electrical backup systems has been considered in order to fulfill the energy demand reaching the DHW set temperature of 40°C when not enough solar energy is harvested and stored in the tank. The configuration with two heat exchangers has been used for avoid the problem of legionella, as underline in the Chapter 1.3.1.



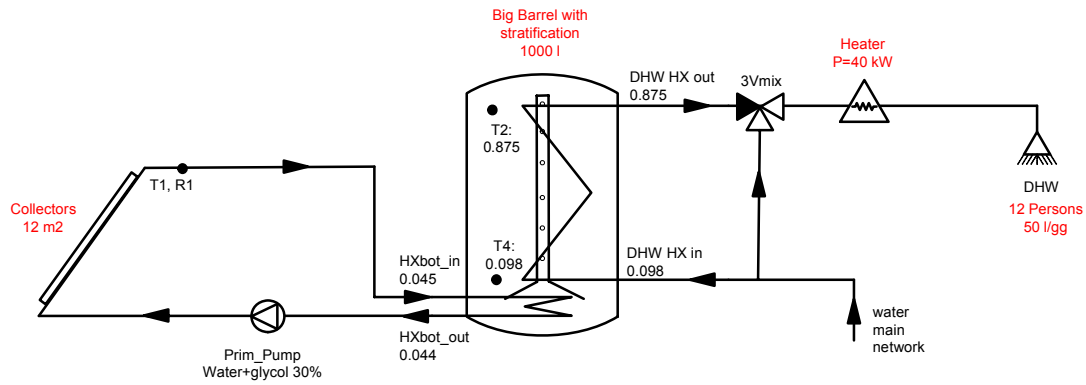


Fig.5.13 - Layout of SDHW

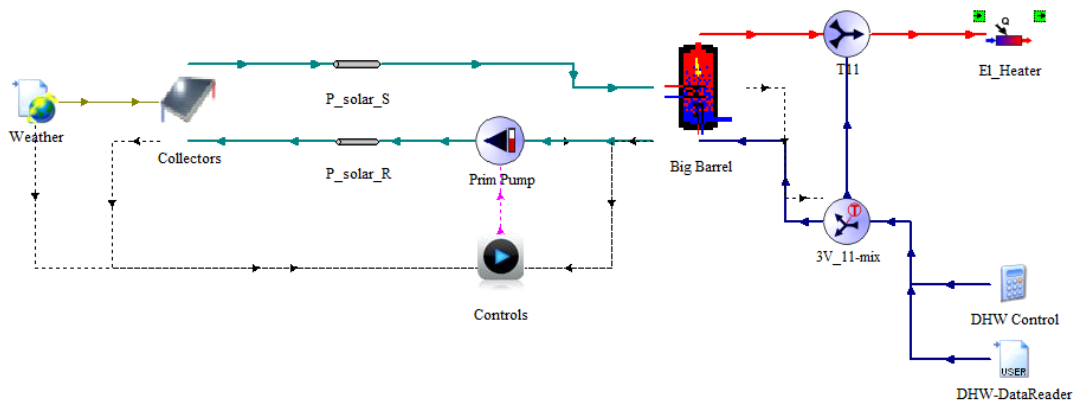


Fig.5.14 - Trnsys model of the SDHW considered

As introduced in the Chapter 1.8, the logic traditionally adopted for control the SDHW systems is based on the difference between the collectors outlet temperature and the storage temperature. More evolved systems are based on the minimum radiation control at which the system is switched on and, as reported in [37], the control signal of the pump can be function of the radiation.

Following what was found in literature, four control strategies for this system have been tested in order to set a solid base of reference cases:

- Control of the temperature between the collectors and the thermal storage using an hysteresis with fixed values (2-7°C);
- Control of the minimum radiation for starting the system, using an hysteresis with fixed values (100-150 W/m<sup>2</sup>);
- Control with combination of A) and B) with at the same time minimum radiation of starting and difference of temperatures between the collectors and the thermal storage;
- Control with combination of C) control and modulation of the mass flow in function of the radiation (linear modulation with maximum at 600 W/m<sup>2</sup>).

For all these four cases, a further control on the maximum temperature allowed in the storage has been implemented in order to avoid stagnation problems in the solar circuit and overheating.

The comparison of different control strategies has been made using the performance figures introduced in the Chapter 4. Moreover, a seasonal performance factor of the primary solar circuit has been evaluated as the ratio between the thermal energy captured and the electrical energy used by the circulation pump evaluated monthly or yearly.

$$SPF_{coll} = \frac{\int_{month, year} \dot{Q}_{coll} dt}{\int_{month, year} W_{el, pump} dt} \quad [-] \quad (eq.5.22)$$

Furthermore, the electrical energy consumed by the pump and by electrical backup have been computed (respectively  $W_{el\_pump}$  and  $W_{el\_Backup}$ ) with the global radiation on the collectors plane ( $GR_{30^\circ}$  collectors with slope of  $30^\circ$  on horizontal and faced to south) and the thermal energy lost when the difference of temperature between the collectors and the storage is negative ( $Q_{loss}$ ). This can happen normally during the starting phases of the system when the difference of temperature between inlet and outlet temperatures of the internal heat exchanger of the solar circuit is negative.

Starting from the analysis of the four control strategies explained before, in the Tab.5.3 the comparison between the yearly data are reported while in the Fig.5.15 and Fig.5.16 monthly data are showed. From this table can be appreciated the increase of the seasonal performance factor of the solar circuit  $SPF_{coll}$  (between case B, and cases A, C and D) mainly due to the control of the system using two parameters (radiation and temperature) that allows a reduction of the thermal losses and the electrical consumption of the pump. The best performance of  $SPF_{coll}$  is related to the case "D" (that is also the strategy adopted for controlling the solar circuit in the solar Combi+ system analyzed in the Chapter 4) where the control of temperature, radiation and also the modulation of the pump in function of the radiation is adopted. From the system performance point of view the best performance  $SPF_{DHW}$  are reached when the losses are decreased (control on DT) with higher levels of temperature in the storage and less usage of electrical backup (case "C"). In this case, however, the number of start and stop of the pump is higher, according with the monthly profile reported in Fig.5.16.

An increasing on the difference of temperature used for the case A, C, D for the temperature hysteresis (from  $2-7^\circ C$  to  $2-14^\circ C$ ) allow to decrease the number of on/off cycles reducing, at the same time, the performance. The number of times the pump is switched on and off, however, remain elevated (as reported in Tab.5.4 with the cases namely A\*, C\*, D\* that are the same cases A, C, D in with the hysteresis values modified).

Tab.5.3 - Comparison between the four different control strategies - yearly data

Case	$\eta_{\text{coll}}$	$\text{SPF}_{\text{coll}}$	on/off pump	GSY	GR <sub>30°</sub>	$W_{\text{el\_pump}}$	DHW <sub>demand</sub>	$\text{SPF}_{\text{DHW}}$	$W_{\text{el\_Backup}}$	$Q_{\text{loss}}$
	[-]	[-]	[-]		$\left[\frac{\text{kWh}}{\text{m}^2}\right]$	$[\text{kWh}]$		[-]	$[\text{kWh}]$	
A	0.410	<b>301</b>	47426	602	1467	24.3	7660	<b>5.394</b>	1396	95
B	0.398	<b>159</b>	371	583		44.6		<b>4.962</b>	1499	215
C	0.398	<b>267</b>	11046	635		28.9		<b>5.531</b>	1356	56
D	0.413	<b>319</b>	7606	606		23.1		<b>5.288</b>	1425	52

Tab.5.4 - Comparison between different control strategies with hysteresis on the difference of temperature (2-14°C) - yearly data

Case	$\eta_{\text{coll}}$	$\text{SPF}_{\text{coll}}$	on/off pump	GSY	GR <sub>30°</sub>	$W_{\text{el\_pump}}$	DHW <sub>demand</sub>	$\text{SPF}_{\text{DHW}}$	$W_{\text{el\_Backup}}$	$Q_{\text{loss}}$
	[-]	[-]	[-]		$\left[\frac{\text{kWh}}{\text{m}^2}\right]$	$[\text{kWh}]$		[-]	$[\text{kWh}]$	
A*	0.448	<b>285</b>	7342	658	1467	28.1	7660	<b>5.535</b>	1356	53
C*	0.446	<b>287</b>	7169	655		27.8		<b>5.484</b>	1369	53
D*	0.418	<b>327</b>	5212	613		22.8		<b>5.235</b>	1440	49

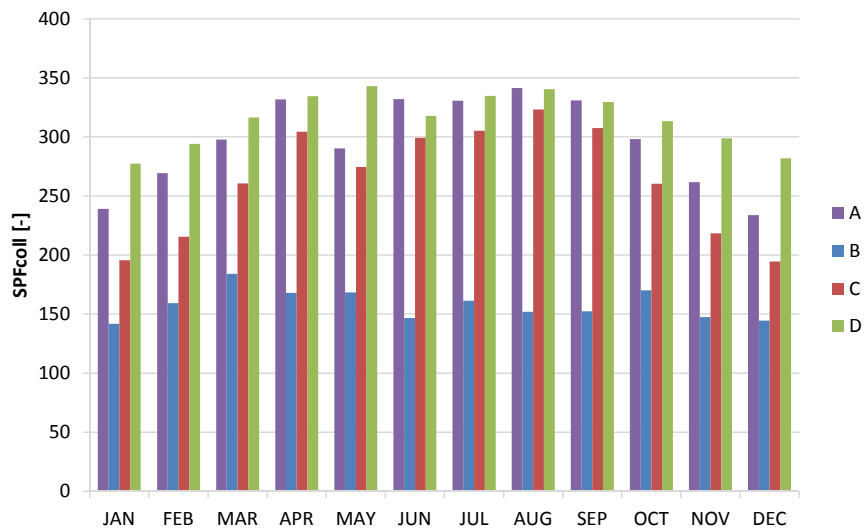


Fig.5.15 - Monthly profile of the  $\text{SPF}_{\text{coll}}$  between the four different control strategies

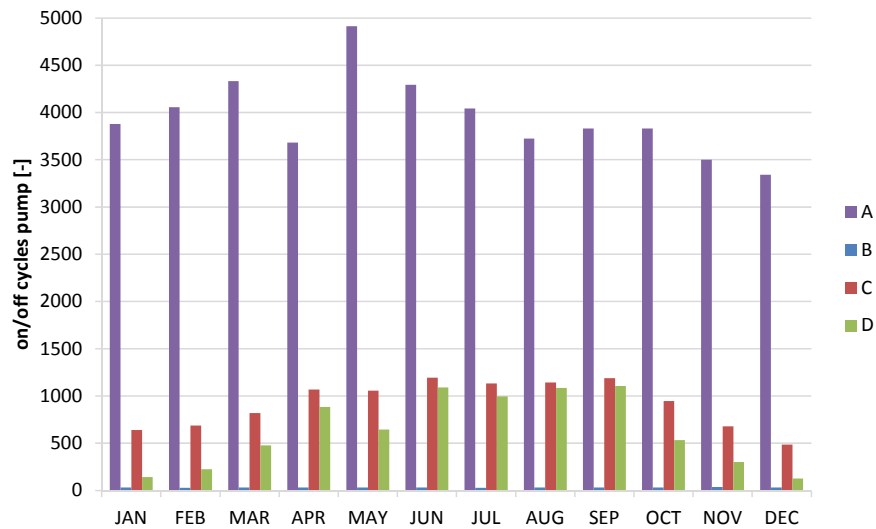


Fig.5.16 - Monthly profile of the solar pump on/off cycles between the four different control strategies

Following the idea to increase the control performance of the system, as from the on/off cycles of the pump and as from the performance point of view, a further analysis on the control strategy “B” (only on the radiation) has been made designing a fuzzy logic controller with single input and single output. The radiation has been selected as input, while the pump command as output. Three triangular membership functions have been implemented, as reported in Fig.5.10, where the membership function center relative to the linguistic term “low” has been set to 0 W/m<sup>2</sup>, the “medium” to 600 W/m<sup>2</sup> and the “high” to 1200 W/m<sup>2</sup>. The membership functions overlap at 0.5, as reported in the introduction on fuzzy logic. The output membership functions have been defined in the same way, with three triangular membership functions, equally distributed on the universe of controlling parameter (between 0 and 1). The method used for the defuzzification phase is the center of area (referring to Chapter 5.2) and three rules are defined, that relate the three membership functions on the input with three membership functions on the output (low radiation with low speed, medium radiation with medium speed and high radiation with high speed).

Two different kind of FL controllers have been implemented, as introduced in Fig.5.10. In the first one the membership functions are parameterized by the “high” radiation while in the second one the parameterization is done by the “medium” membership functions also shown in Fig.5.10 with dotted line. In both cases a family of FL controller is obtained by varying the parameter. The families are those described in Fig.5.11, where the 7 members used in the analysis are plotted.

In the following tables, the yearly results of the Fuzzy Logic Controllers are reported and compared (in Tab.5.5 those obtained by varying the “high” radiation while in Tab.5.6 those obtained by varying the “medium” radiation). These analysis have been conducted in order to understand the effect of the different fixed curves of Fuzzy controller (given by

the definition of the level of radiation) and to have an idea of what to expect from the Q-learning controller. The Q-learning algorithm has to learn, trying different actions (related to the different curves) what is the best one in order to reach the highest performance in every state. The analysis has been conducted using as actions the 7 levels of radiation used to evaluate the performance.

Tab.5.5 - Comparison of performance using different high radiation level - yearly data

High Radiation level		$\eta_{coll}$	$SPF_{coll}$	on/off pump	GSY	$GR_{30^\circ}$	$W_{el\_pump}$	DHW <sub>demand</sub>	$SPF_{DHW}$	$W_{el\_Backup}$	$Q_{loss}$
$\left[\frac{W}{m^2}\right]$		[-]	[-]	[-]		$\left[\frac{kWh}{m^2}\right]$	$[kWh]$		[-]	$[kWh]$	
a1	0	0.391	114	367	574	1467	61.1	7660	4.901	1502	547
a2	200	0.396	150	399	581		46.9		5.052	1470	458
a3	400	0.398	188	414	584		37.8		5.139	1453	387
a4	600	0.399	231	406	585		30.8		5.136	1461	326
a5	800	0.398	287	420	584		24.7		5.105	1476	271
a6	1000	0.397	352	428	583		20.1		5.005	1510	243
a7	1200	0.396	415	413	580		17.0		4.915	1542	212

Tab.5.6 - Comparison of performance using different medium radiation level - yearly data

Medium Radiation level		$\eta_{coll}$	$SPF_{coll}$	on/off pump	GSY	$GR_{30^\circ}$	$W_{el\_pump}$	DHW <sub>demand</sub>	$SPF_{DHW}$	$W_{el\_Backup}$	$Q_{loss}$
$\left[\frac{W}{m^2}\right]$		[-]	[-]	[-]		$\left[\frac{kWh}{m^2}\right]$	$[kWh]$		[-]	$[kWh]$	
a1	0	0.395	215	377	580	1467	32.7	7660	5.051	1484	493
a2	200	0.397	264	414	583		26.8		5.128	1467	366
a3	400	0.398	336	423	584		21.1		5.068	1491	258
a4	600	0.395	422	419	580		16.7		4.894	1549	194
a5	800	0.391	529	436	573		13.2		4.654	1633	150
a6	1000	0.385	633	423	565		10.8		4.395	1732	122
a7	1200	0.380	691	415	558		9.8		4.211	1809	104

Looking the Tab.5.6 an higher level of  $SPF_{coll}$  can be reached with this set-up but this occurs at the expenses of the captured solar energy (GSY) and decreasing the electrical consumption of the pump. Monthly data of  $SPF_{coll}$  are also reported in the Fig.5.17 with lines for the seven different actions introduced (7 different levels of definition of the high

radiation membership function) starting from 0 to 1200 W/m<sup>2</sup> compared with the previous four control strategies and showed in the Fig.5.15. Looking this graph, the big difference notable is between the case D and the FLC with the action a7 (high radiation MF imposed to 1200 W/m<sup>2</sup>) that allow, to reach the best performance in terms of SPF<sub>coll</sub>.

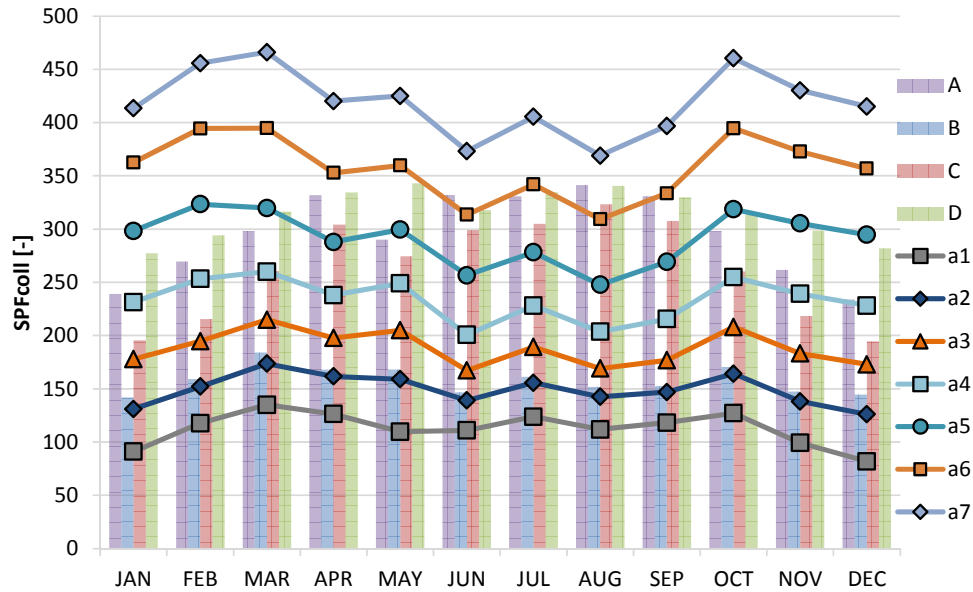


Fig.5.17 - Monthly profile of the SPF<sub>coll</sub> using different level of the maximum radiation in the definition of the input membership function compared with the four basic control strategies.

To both cases of control introduced above (FLC on high membership function and on medium membership function) the Q-learning methodology introduced in the previous chapter is applied. The application of the Q-learning method to the FLC (Fig.5.9) has been started from the definition of the states/actions matrices [Q] and [Q<sub>count</sub>].

The states of the analyzed system has been structured on the two parameters that better describe the system dynamics (radiation on the collectors plane and thermal level of the storage). No reference was found in literature related to the definition of the states then the following discretization have been used:

- Average of storage temperature: starting from 10 to 90°C with 9 steps;
- Radiation on the collectors plane from 0 to 1000 W/m<sup>2</sup> with 11 steps.

Regarding the actions adopted, these are the same experimented and analyzed previously (the 7 fixed curves of the FLC), in order to verify the correctness of the method. Finally, the parameters selected for the Q-learning method are summarized in the following Tab.5.7.

Tab.5.7 - Parameters used for the Q-learning process

N_states	99	[-]
N_actions	7	[-]
Nev	10	[-]
$\alpha$	0.5	[-]
$\gamma$	0.5	[-]
Iterative cycle $\Delta t$	5	[min]
$w_1$	1	[-]
$w_2$	370	[-]

The reward function used in the learning process is the following:

$$r = \frac{w_1 \cdot \int_{\Delta t} \dot{Q}_{coll} dt - w_2 \cdot \int_{\Delta t} W_{el,pump} dt}{\int_{\Delta t} GR_{30^\circ} \cdot A_{coll} dt} \quad [-] \quad (eq.5.23)$$

This function is related to the objective function to be maximized,  $SPF_{coll}$ . This additive form of the reward has been proved to give better results than using directly the fractional form of the  $SPF_{coll}$ .

As reported in the Fig.5.7 and in the Fig.5.9 the length of the iterative cycle used for the evaluation of the rewards is defined by  $\Delta t$ . A previous analysis has been conducted using directly the  $SPF_{coll}$  as reward but this analysis showed that the learning does not work well and the maximum of the  $SPF_{coll}$  is not reachable. For this reason a different reward has been implemented (eq.5.17).

The results of two simulations with Q-learning of 5 years are reported in the following Tab.5.8 for the two cases analyzed (the Q-learning in the first 5 rows works on the membership function high radiation and the second five rows on the membership function medium radiation). From the tables could be appreciate that for both systems analyzed, after the second year, a value of the  $SPF_{coll}$  close to the maximum reachable by the simpler controllers is visible (referring to the Tab.5.5 and Tab.5.6). In the Fig.5.18, analyzing the case of the Q-learning that works on the high radiation membership function, the monthly profile for the five years of learning (reported also in the first five rows of the Tab.5.8) shows a gap between the first and the second year while the other years values are close each other's. In particular, for the first year, the learning phase happens during the first seven months between January and August.

Tab.5.8 - Q-learning applied to the FLC on the high radiation and medium radiation levels

Case	year	$\eta_{coll}$	$SPF_{coll}$	on/off pump	GSY	$GR_{30^\circ}$	$W_{el\_pump}$	DHW <sub>demand</sub>	$SPF_{DHW}$	$W_{el\_Backup}$	$Q_{loss}$
		[-]	[-]	[-]	$\frac{kWh}{m^2}$		[kW <sub>h</sub> ]		[-]	[kW <sub>h</sub> ]	
MF - High Radiation	1st	0.397	370	446	582	1467	19.1	7660	4.969	1523	225
	2nd	0.396	409	425	581		17.3		4.936	1535	217
	3rd	0.396	408	422	581		17.3		4.930	1537	216
	4th	0.396	410	420	581		17.2		4.928	1537	216
	5th	0.396	411	422	581		17.2		4.924	1539	215
MF - Medium Radiation	1st	0.385	611	437	565	1467	11.2	7660	4.377	1739	114
	2nd	0.382	680	414	561		10.0		4.285	1778	104
	3rd	0.382	685	409	560		9.9		4.266	1786	102
	4th	0.382	682	415	560		10.0		4.263	1787	104
	5th	0.382	687	416	560		9.9		4.278	1781	102

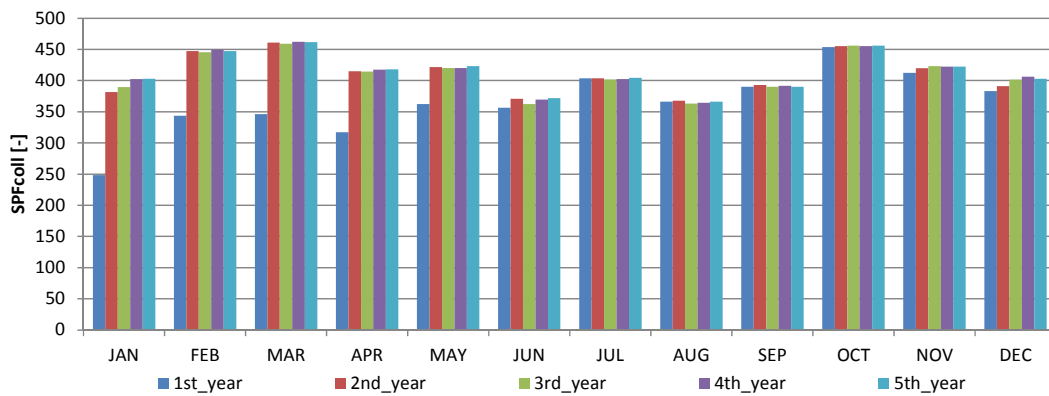


Fig.5.18 - Monthly profile of the  $SPF_{coll}$  with Q-learning on the membership function of the high radiation, comparing the monthly performance of the different year during the learning.

The convergence of the matrix is reported in the Fig.5.19. Comparing this figure with the graph in Fig.5.18, after the first year the maximum of the monthly  $SPF_{coll}$  is reached. In particular, the 70% of the matrix exploration is reached after five months. Minor increasing is due in the following 7 months, related to the states that are not often visited during the normal operation of the system. The learning does not reach the 100% of matrix convergence because some states (for example low temperature of the storage



<10°C with high level of radiation >1000W/m<sup>2</sup>) are never reached and then never explored.

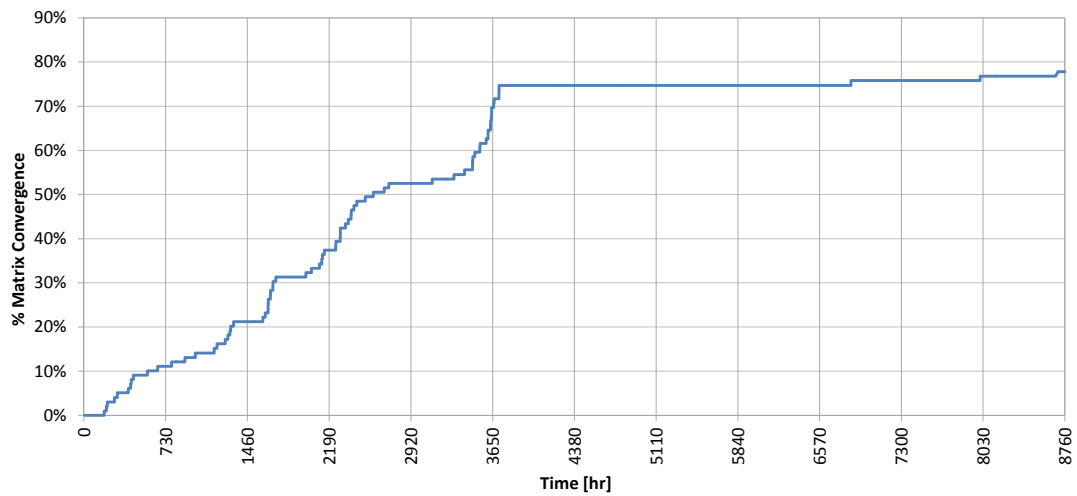


Fig.5.19 - Matrix convergence

Different analyses have been conducted increasing the Q-learning cycle time  $\Delta t$  or the minimum number of event  $N_{ev}$ . Both of these parameters have been showed an increasing of the convergence time, maintain unvaried the results of the learning process, but increasing the time at which the Q-learning method converge. Similarly, the increasing of the number of states (regarding for example, the temperature) doesn't return a better performance of the learning process, extending the learning time due to the increased dimension of the matrix [Q].

For the case where the Q-learning was acting on the maximum radiation, different analysis have been conducted by varying the Q-learning related parameters. The following figures report monthly performance and the convergence of the learning method changing the parameters alpha (Fig.5.20 and Fig.5.21) and gamma (Fig.5.22 and Fig.5.23). These graphs show that these parameters affect only modestly the convergence figure and the  $SPF_{coll}$  on a monthly and yearly profile and also the convergence of the matrix.

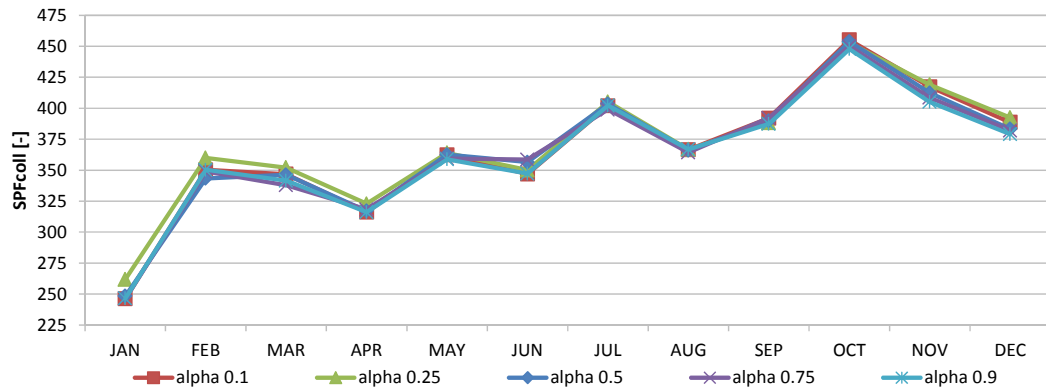


Fig.5.20 - Monthly profile of the SPFColl with Q-learning and different parameters alpha.

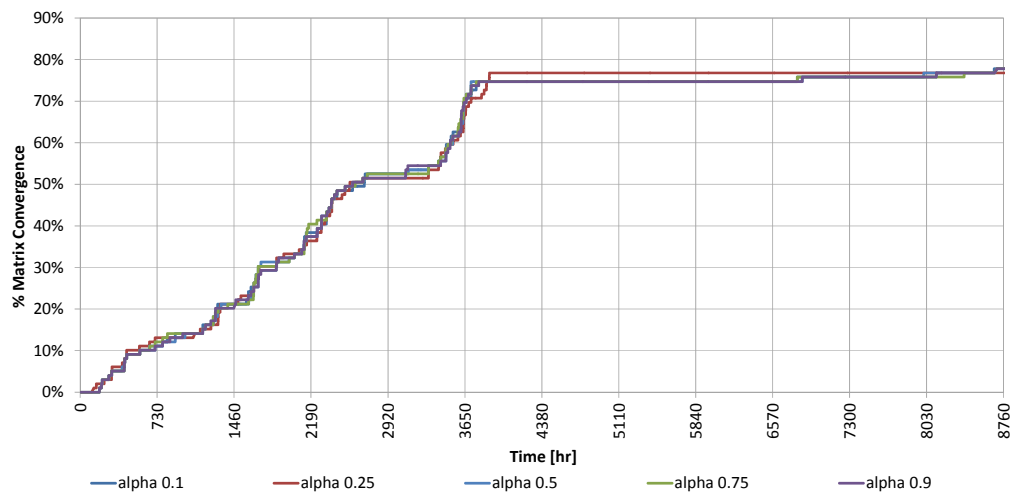


Fig.5.21 - Convergence of learning method with different parameters alpha.

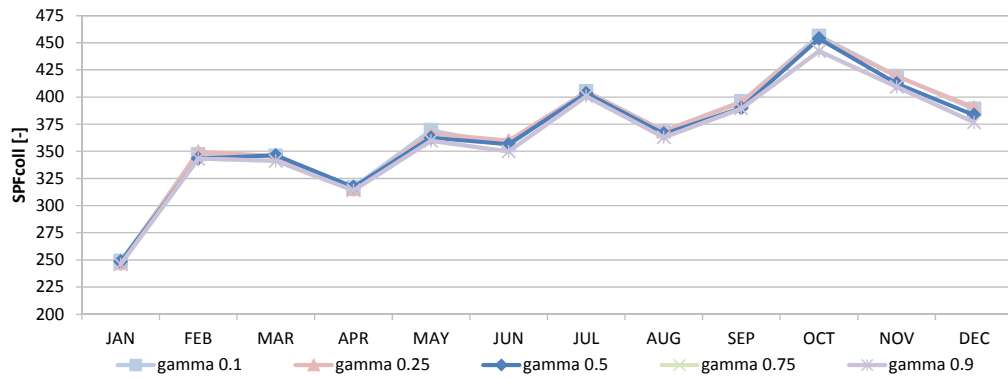


Fig.5.22 - Monthly profile of the SPFColl with Q-learning and different parameters gamma.

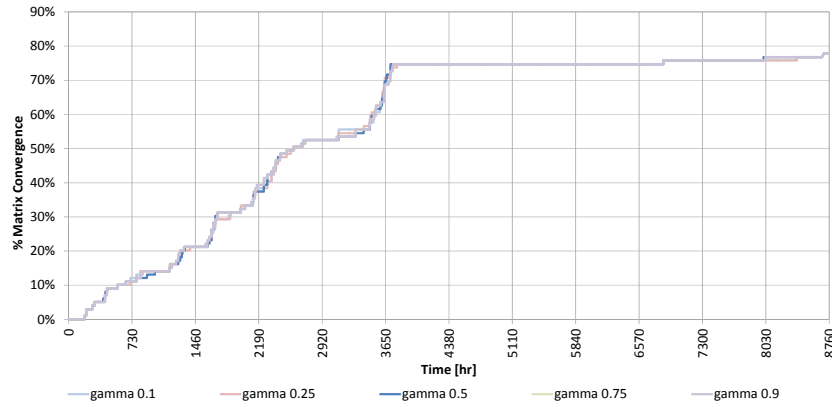


Fig.5.23 - Convergence of learning method with different parameters gamma.

Coming to the point regarding how the Q-Learning algorithm behaves in the case the system or the boundary conditions change with time, the following extreme case is presented. The Q-Learning controller is let to explore and exploit the system for 5 years. After this period a sudden and radical change of the system is simulated by introducing a change in the meaning of the actions performed by the agent. If the action a1 usually meant using the minimum value of the parameter, now it means using the maximum. If the action a7 meant using the maximum value of the parameter, now it means using the minimum.

This rather academic example of course has no physical meaning but is extremely useful to test the behavior of the system because what has to be expected is a-priori known and the outcome are clearly visible on the values stored in the matrix [Q]. Test have been done by varying physical parameters of the solar system, i.e. the collectors efficiency and the pump electrical consumption, resulting in changes too small to change the optimal control policy.

Another interesting result regards the “partial reset” feature of the Q-learning algorithm implemented in this study. As introduced in the previous chapter, the process restarts the exploration phase after a change in the matrices reported in the equations (eq.5.14 and eq.5.15). Three different values of  $\beta$  are used in this example: 0.2, 0.5, 0.8. The results are shown in the graph (Fig.5.24) then the  $SPF_{coll}$  relative error (with respect to the convergence values after five years) for four different values of  $\beta$  is plotted. The same comparison in terms of convergence figure is shown in Fig.5.25.

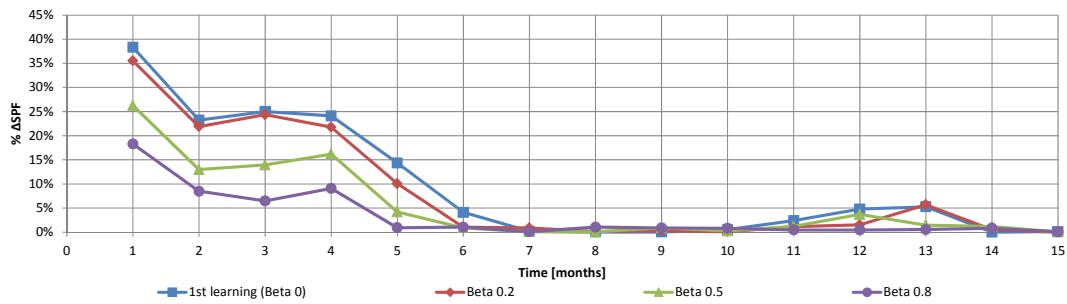


Fig.5.24 - Monthly SPFcoll relative error (convergence values after five years) comparing the first learning and the second learning phase with different  $\beta$  (0.2, 0.5, 0.8)

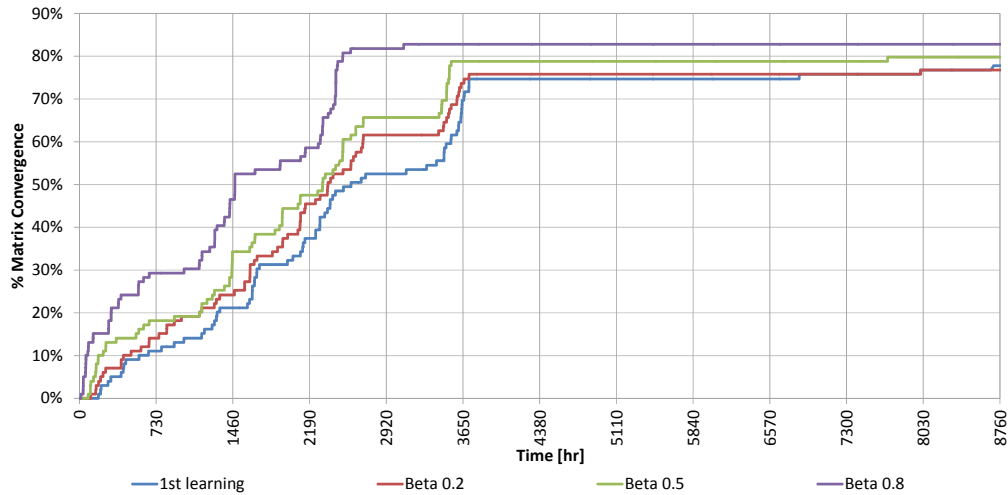


Fig.5.25 - Convergence of learning method comparing the first learning and re-learning with different  $\beta$  (0.2, 0.5, 0.8)

## 5.7 Future development

The application of the new control paradigms to a simple SDHW system has shown clearly that the self-learning paradigm can be successfully applied to solar systems and it has highlighted that there are opportunities to improve the concept in many aspects. Regarding the Q-learning algorithm, other methods for improving the convergence speed can be attempted, moving from the exploration based on the minimum number of pair state/action to other exploration methodologies (e.g. Softmax exploration [101]). The definition of the control objective function and an appropriate reward are two important aspects for the RL implementation. In this terms, the exergy concept can be applied as objective function, in order to optimize from one side the heating captured by the solar thermal system taking in account the thermal level of the energy stored from the other reducing the electrical consumption. Looking at the state definition, the adoption of a state space including also the time (in order to create seasonal matrices) and/or the load

due to DHW consumption could be helpful for increasing the performance of the learning process. In general it could be interesting to investigate the relation between the  $\gamma$  parameter, the Q-learning cycle time  $\Delta t$  and the characteristic time constant of the system.

Regarding the FLC, it would be interesting to test a MIMO controller based on two variables, moving from a single control on radiation to another based on radiation and the temperature of the store or difference of the temperature between collectors and the thermal storage.

Regarding the combination of Q-learning and FLC, the focus could be moved from the membership function definition (as made in this work) to the rule-base definition which seems more in line with the standard FLC practice but with an increase of the action to be tested.

Finally the application of this methodology to different part of the solar Combi+ system could reveal to be a powerful tool for the optimization of the complex thermal systems. This process will start from the parameters that the sensitivity analysis indicates to be the more important in the control of such a system.

# Annex 1

In the following Tab.5 the performance of the system during the process of validation are reported. The first and the last row are related to the beginning model (before validation - “BASE”) and the final model (“Validated”) where all the components are validated. The intermediate case are related to the base starting model where only one component is validate, in order to understand the effect of the validation of the single component on the whole system performance. Two huge effects on the seasonal performance factor can be detected on the step related to the validation of the heat pump ( $SPF_{el\_tot}$  from 3.98 to 3.61) and the heat exchanger ( $SPF_{el\_tot}$  from 3.98 to 3.77) mainly due to the decreased performance for heating ( $SPF_{heat}$  from 2.74 to 2.43 for the heat pump and from 2.74 to 2.66 for the heat exchanger). Moreover the heat exchanger validation affects also the performance for cooling satisfaction with a decrease of the  $SPF_{cool}$  (from 5.08 to 4.91). Looking the total effect, related to the whole validation process, a decreasing of the solar fraction for cooling and heating ( $SF_{cool}$  from 57% to 54% and  $SF_{heat}$  from 52% to 49%) is notable with an increasing of the air fractions ( $AF_{heat}$  from 30% to 32% and  $AF_{DHW}$  from 3% to 4%). Finally a decrease of 10% is visible on the total performance  $SPF_{el\_tot}$  (moving from 3.98 to 3.56).

Tab.5 - Performance of solar Combi+ system installed in Bolzano applied to “BLD” building with “STD” weather data for each single step of validation (single component validated and finally model with all the component validated)

BLD Bolzano 32m <sup>2</sup>	$SF_{cool}$	$SF_{heat}$	$SF_{DHW}$	$SF_{heat+DHW}$	$AF_{heat}$	$AF_{DHW}$	$SPF_{cool}$	$SPF_{heat}$	$SPF_{DHW}$	$SPF_{el\_tot}$	$\Delta PE_{tot}$	$\Delta CO_2$	$\eta_{coil}$	$GSY$	$Heat_{dem}$	$Cool_{dem}$	$DHW_{dem}$	ON/OFF Pumps	ON/OFF Hp
	[-]				[-]		[-]			$SPF_{el\_tot}$	$\frac{[kWh]}{m^2}$	[tonn]	[-]	$\frac{[kWh]}{m^2}$		$\frac{[kWh]}{m^2}$		[-]	
BASE	57%	52%	95%	66%	30%	3%	5.08	2.74	18.26	3.98	23	0.94	23.6%	346	40	12	14	17185	3061
Collectors	56%	53%	95%	67%	29%	3%	4.99	2.76	18.76	4.00	23	0.94	24.8%	364	40	12	14	13048	2938
DHW Storage	56%	52%	95%	66%	30%	3%	5.06	2.75	16.64	3.97	23	0.93	23.6%	347	40	12	14	16937	3037
Dry Cooler	56%	52%	95%	66%	30%	3%	6.11	2.75	17.58	4.07	24	0.97	23.6%	346	40	12	14	17129	3073
Solar Storage	54%	51%	95%	65%	31%	3%	5.04	2.74	16.71	3.95	23	0.93	23.1%	340	40	12	14	12754	3175
Adsorption	58%	52%	95%	66%	30%	3%	5.35	2.78	18.26	4.05	24	0.97	23.6%	345	40	12	14	14572	3050
Heat Pump	56%	55%	95%	68%	27%	3%	5.37	2.43	16.48	3.61	20	0.79	23.5%	345	40	12	14	17304	3119
Heat Exchanger	52%	45%	95%	60%	37%	4%	4.91	2.66	17.05	3.77	24	0.96	23.9%	350	43	13	14	14597	2342
Validated	54%	49%	95%	64%	32%	4%	6.01	2.37	14.86	3.56	19	0.76	24.1%	353	39	12	14	9542	3241

Looking the Tab.6, the performance of the system located in Bolzano is reported. The fourth rows are related to the Solar Combi+ system simulated using the two levels of loads (building with low demand “BLD” and building with high demand “BHD”) and using the two climatic profiles (standard “STD” and extreme “EXTR”). Regarding the cooling loads, the solar fraction  $SF_{cool}$  and the seasonal performance factor  $SPF_{cool}$  remain almost constant instead huge difference is visible between the simulation results using STD and the EXTR climatic data profile for the heating and DHW indexes with a decreasing of the solar fraction ( $SF_{heat}$  and  $SF_{DHW}$ ) and an increasing of the usage of the electrical backup. This is reflected in a decreasing of the SPF for heating and DHW and consequently in the  $SPF_{el\ tot}$ . In particular this performance figure for both level of building loads decreases about 18-19% moving from 5.49 to 4.46 for BLD and form 5.04 to 4.14 for BHD. This behavior is also reflected in the primary energy saved that maintain almost the same absolute value for the two levels of building load (38 kWh/m<sup>2</sup> for BLD and 45-47 kWh/m<sup>2</sup> for BHD) but in percentage it decreases from 57-58% of the total primary energy needed for both building with STD climatic profile to the 46-47% with the EXTR data file. Looking the performance of the collectors an increase of the performance for both building loads analyzed is visible moving from the STD data profile to the EXTR profile. The number of switch On and Off are increased using the two different building loads but huge difference is visible between the simulations that use different climatic data, mainly due to the number of On/Off cycles of the heat pump in cooling mode.

Tab.6 - Performance of solar Combi+ system installed in Bolzano with optimized control strategy, varying the climatic data (“STD”, “EXTR”) and the building loads (“BLD”, “BHD”)

Bolzano 32m <sup>2</sup>	$SF_{cool}$	$SF_{heat}$	$SF_{DHW}$	$SF_{heat+DHW}$	$AF_{heat}$	$AF_{DHW}$	$SPF_{cool}$	$SPF_{heat}$	$SPF_{DHW}$	$SPF_{el\ tot}$	$\Delta PE_{tot}$	$\Delta CO_2$	$\eta_{coll}$	$GSY$	$Heat_{dem}$	$Cool_{dema}$	$DHW_{dema}$	ON/OFF Pumps	ON/OFF HP
	[-]				[-]		[-]			$\left[\frac{kWh}{m^2}\right]$	[tonn]	[-]	$\left[\frac{kWh}{m^2}\right]$	$\left[\frac{kWh}{m^2}\right]$	[-]				
BLD_STD	52%	27%	93%	49%	72%	7%	5.76	3.95	21.56						40	13	14	4762	1492
BLD_EXTR	56%	23%	89%	43%	70%	10%	5.78	3.12	15.07	4.46	33	1.32	24.8%	413	45	24	14	6926	2609
BHD_STD	53%	27%	92%	44%	72%	8%	5.73	3.87	19.92	5.04	43	1.70	23.1%	339	53	12	14	5468	1814
BHD_EXTR	54%	21%	89%	37%	72%	10%	5.66	3.09	13.96	4.14	40	1.61	24.6%	411	59	24	14	7280	2778

In the following Tab.7 the simulation results for the system located in Rome are reported. Also here, as in the previous table, two levels of building load (low demand BLD and high demand BHD) and two different climatic data (standard STD and extreme EXTR) are analyzed. Here the cooling behavior is different because using EXTR profile instead of STD results an increasing of the solar fraction of 10% for both building loads considered. This is reflected on an increasing of the  $SPF_{cool}$  of 4% (moving from 5.93 to 6.19 in BLD) and 2% (moving from 6.09 to 6.20 in BHD) related to the increasing usage of the sorption machine instead of compression chiller. Also in this case huge difference is visible in the  $SF_{heat}$  and  $AF_{heat}$  with a decrease of the  $SF_{heat}$  from 58% to 31% (for building BLD) and from 53% to 27% (for building BHD) and a decreasing of the  $SPF_{heat}$  of 36% (from 7.64 to 4.86) and of 30% (from 6.83 to 4.72). This is due to the direct usage of the solar energy that decrease between the two climatic profiles adopted moving from around the 50% of the load (with STD profile for both buildings considered) to 25% of the load (with EXTR profile). This behavior is also reflected in a decreasing of the total seasonal performance factor (-27%) moving from 9.78 to 7.10 for the BLD and from 9.14 to 6.61 for the BHD. Also here an increasing of the performance of the collectors is visible between the two climatic profile considered and between the two building loads analyzed. The number of switch On and Off also here shows an increasing when the simulation is performed using the EXTR profile, mainly due to the increasing of the On/Off cycle of the heat pump.

Tab.7 - Performance of solar Combi+ system installed in Rome with optimized control strategy, varying the climatic data ("STD", "EXTR") and the building loads ("BLD", "BHD")

Rome 32m <sup>2</sup>	SF <sub>cool</sub>	SF <sub>heat</sub>	SF <sub>DHW</sub>	SF <sub>heat+DHW</sub>	AF <sub>heat</sub>	AF <sub>DHW</sub>	SPF <sub>cool</sub>	SPF <sub>heat</sub>	SPF <sub>DHW</sub>	SPF <sub>el_tot</sub>	$\Delta PE_{tot}$	$\Delta CO_2$	$\eta_{coll}$	GSY	Heat <sub>dem</sub>	Cool <sub>dem</sub>	DHW <sub>dem</sub>	ON/OFF Pumps	ON/OFF HP
	[-]				[-]		[-]				[kWh m <sup>2</sup> ]	[tonn]	[-]	[kWh m <sup>2</sup> ]	[kWh m <sup>2</sup> ]		[-]		
BLD_STD	58%	58%	98%	80%	42%	2%	5.93	7.64	57.72	9.78	25	0.98	22.6%	408	17	18	14	4714	1363
BLD_EXTR	66%	31%	95%	59%	69%	5%	6.19	4.86	33.25	7.10	30	1.20	24.8%	464	25	25	14	6549	2333
BHD_STD	62%	53%	99%	73%	47%	1%	6.09	6.83	67.05	9.14	33	1.29	23.9%	433	26	18	14	5425	1677
BHD_EXTR	67%	27%	95%	52%	73%	5%	6.20	4.72	33.39	6.61	38	1.50	25.4%	476	35	25	14	7389	2721



# Annex 2

## Development of the Q-learning and Fuzzy Logic controller algorithm in LabVIEW

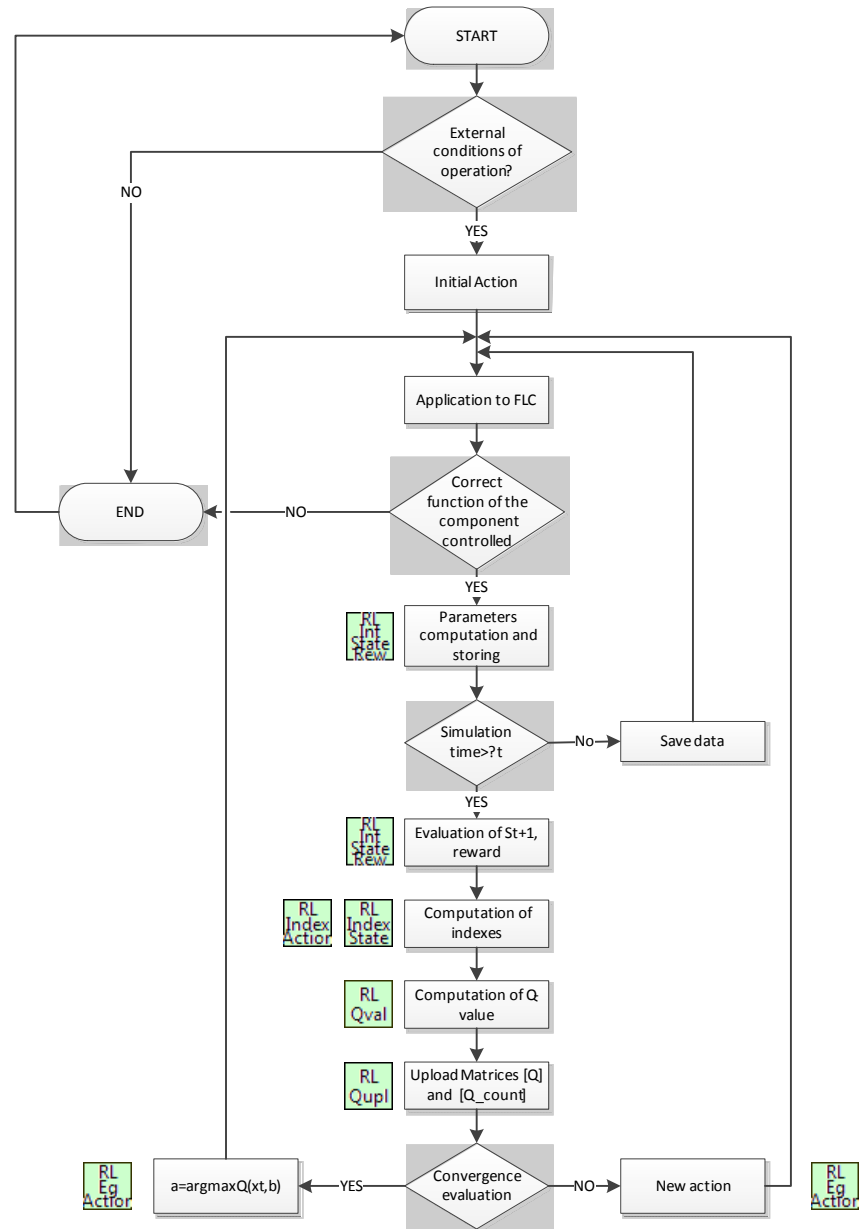


Fig.10 - Flux diagram of the Q-learning and Fuzzy Logic controller algorithm developed in LabVIEW (reference on the vi used in LabVIEW)



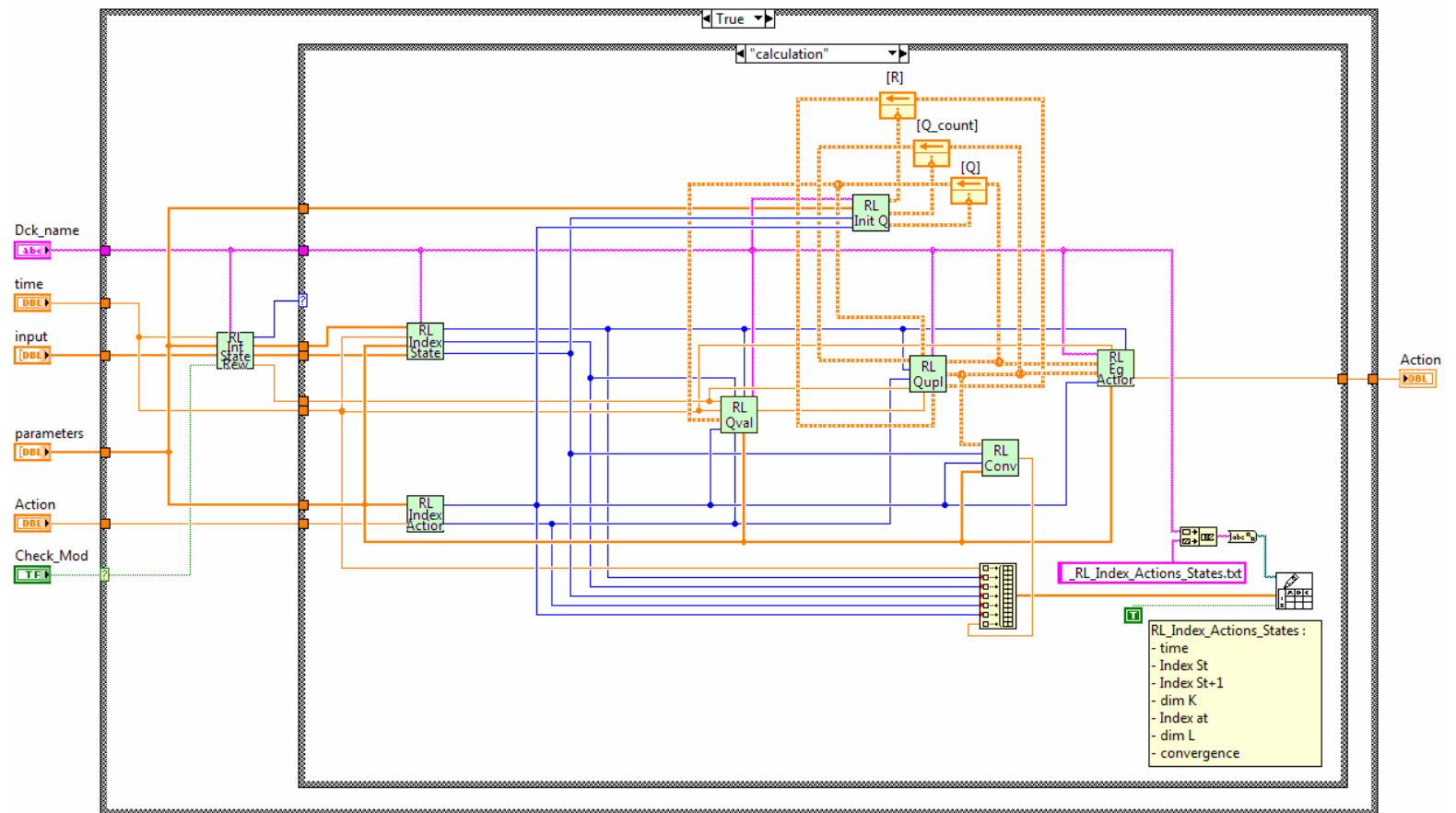


Fig.12 - Q-learning algorithm developed in LabVIEW

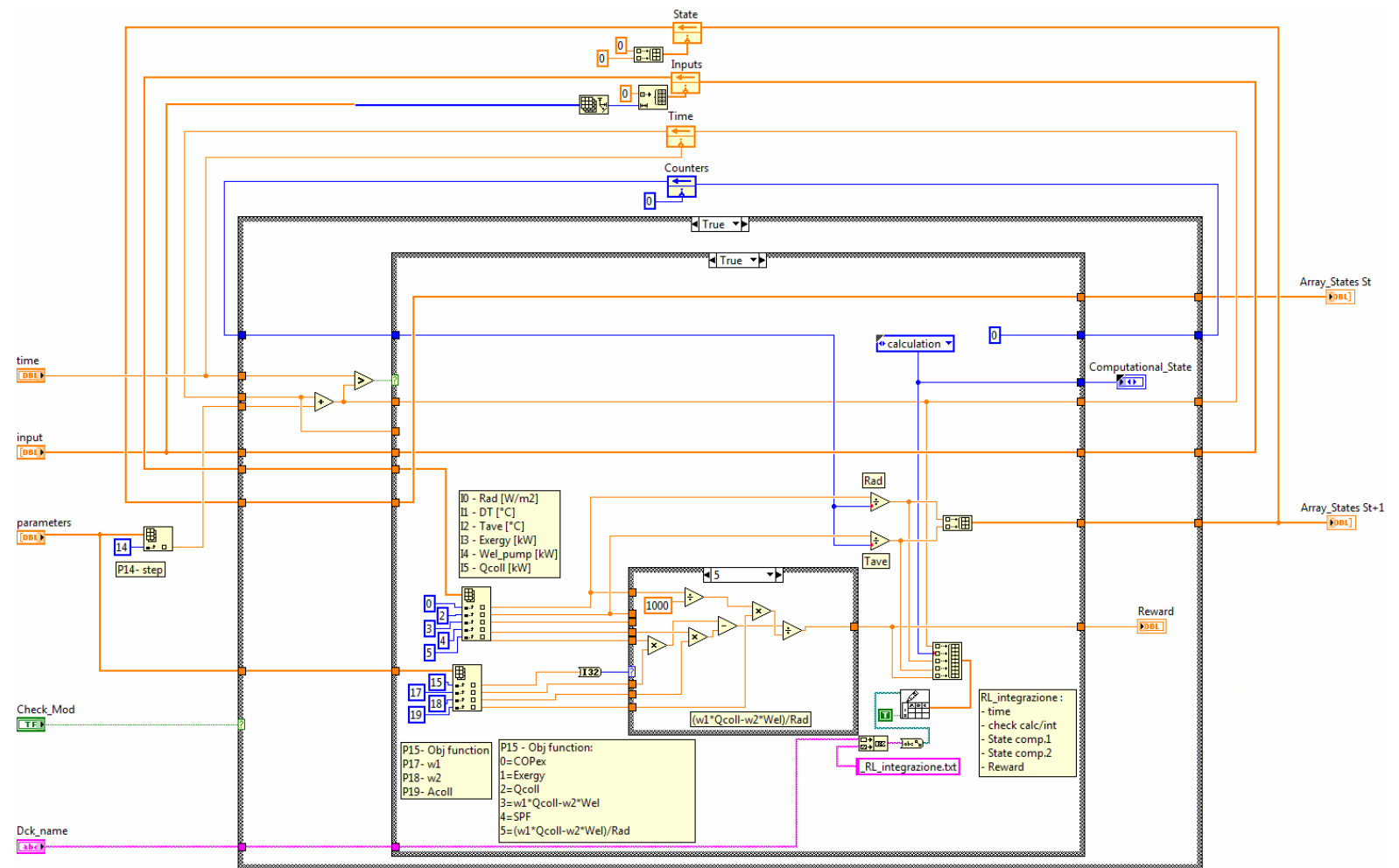


Fig.13 - LabVIEW vi for the evaluation of the reward and states

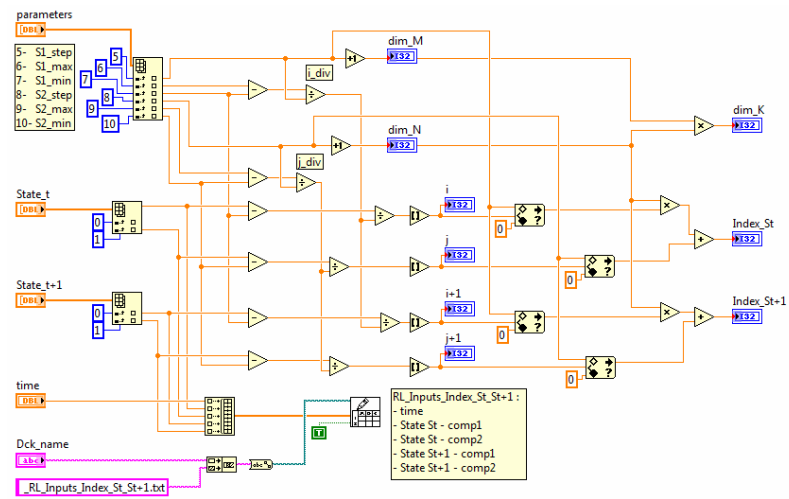


Fig.14 - LabVIEW vi for the state index evaluation

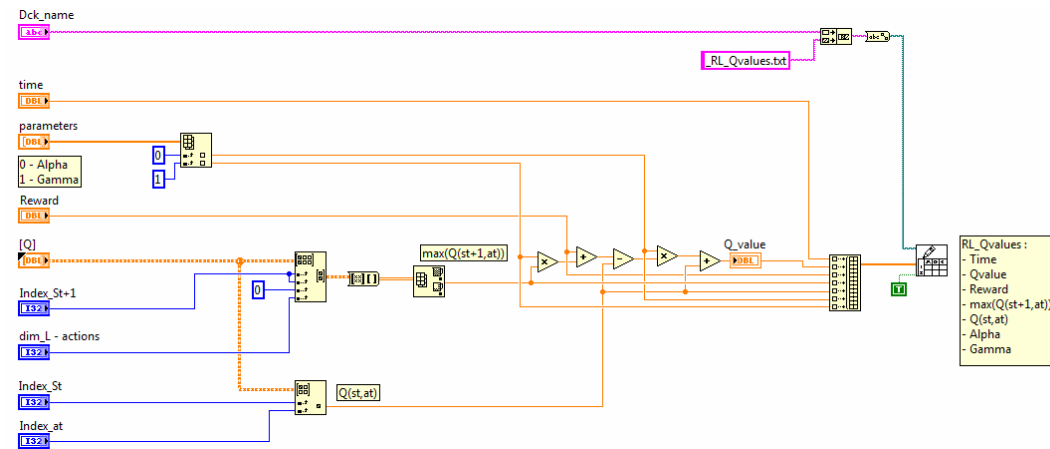


Fig.15 - LabVIEW vi for the computation of the Q-value

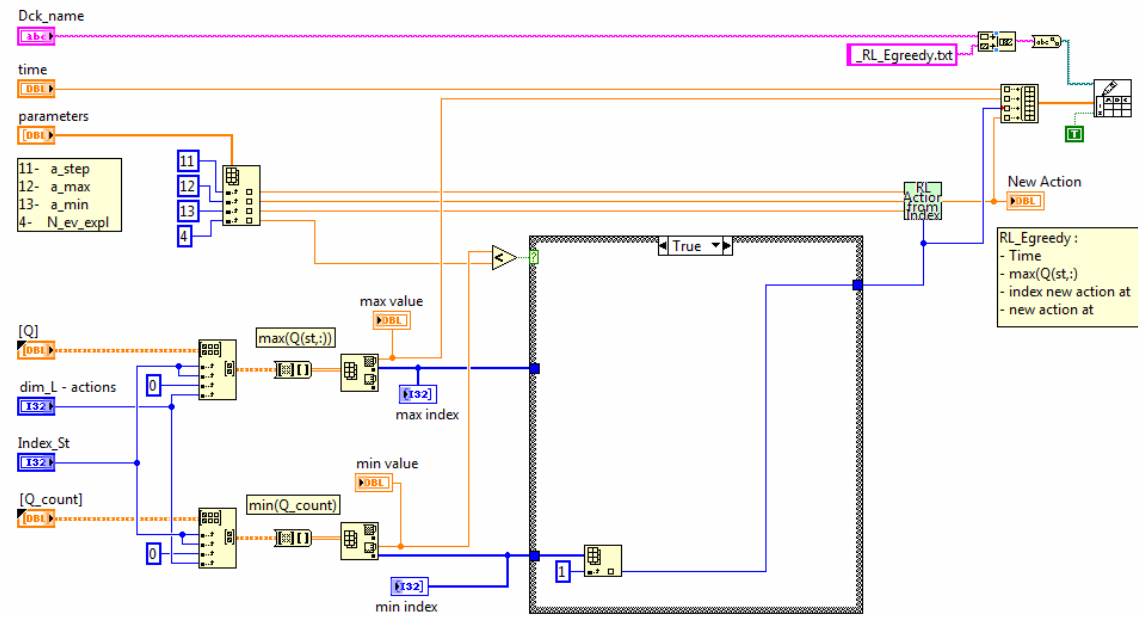


Fig. 16 - LabVIEW vi for the computation of the new action

# Annex 3

Fortran code of the mask used for reading the DLL compiled in LabVIEW.

```
SUBROUTINE TYPE883 (TIME,XIN,OUT,T,DTDT,PAR,INFO,ICNTRL,*)
C*****
C SUBROUTINE FOR CHARGING EXTERNAL DLL CREATED IN LABVIEW WITH
FUZZY LOGIC CONTROLLER AND REINFORCEMENT LEARNING
C WRITTEN BY: Eurac - Bolzano - DBettoni, ASoppelsa - 04/2013
C*****
! Copyright © 2013 Eurac Research. All rights reserved.
C-----
!Export this subroutine for its use in external DLLs.
  !DEC$ATTRIBUTES DLLEXPORT :: TYPE883
!Import the library created in Labview during the DLL development
  !DEC$ATTRIBUTES DLLIMPORT :: TRN_LV_INTERFACE
C-----
C   TRNSYS access functions (allow to access TIME etc.)
  USE TrnsysFunctions
  USE TrnsysConstants
C-----
C   TRNSYS DECLARATIONS
  IMPLICIT NONE !force explicit declaration of local variables
  DOUBLE PRECISION XIN,OUT,TIME,PAR,T,DTDT,TIME0,TFINAL,DELT
  INTEGER*4 INFO(15),NP,NI,NOUT,ND,IUNIT,ITYPE,ICNTRL
  CHARACTER*3 OCHECK,YCHECK
C   Return the name of the input (Deck) file name
  CHARACTER(LEN=maxPathLength)DeckName !INPUT FILE NAME
C-----
C   SET THE NUMBER OF PARAMETERS(NP),INPUTS(NI),OUTPUTS(NOUT),AND
DERIVATIVES(ND)
C   THAT MAY BE SUPPLIED FOR THIS TYPE
  PARAMETER (NP=20,NI=8,NOUT=3,ND=0)
C-----
C   REQUIRED TRNSYS DIMENSIONS
  DIMENSION XIN(NI),OUT(NOUT),PAR(NP),YCHECK(NI),OCHECK(NOUT)
C-----
C   DECLARATIONS AND DEFINITIONS FOR THE USER-VARIABLES HERE
  DOUBLE PRECISION Y_IN,Y_OUT,Y_PAR
  DIMENSION Y_IN(NI),Y_OUT(NOUT),Y_PAR(NP)
C-----
C   TRNSYS FUNCTIONS
  TIME0=getSimulationStartTime()
  TFINAL=getSimulationStopTime()
  DELT=getSimulationTimeStep()
  DeckName=getDeckFileName()
C-----
```

```

C      CALL MESSAGES(-1,'START','NOTICE',INFO(1),INFO(2))
C-----
C      SET THE VERSION INFORMATION FOR TRNSYS
      IF(INFO(7).EQ.-2) THEN
        INFO(12)=16
C      CALL MESSAGES(-1,'CTRL INFO(7)=-
2','NOTICE',INFO(1),INFO(2))
        RETURN 1
      ENDIF
C-----
C      PERFORM END OF SIMULATION MANIPULATIONS
      IF (INFO(8).EQ.-1) THEN
C      CALL MESSAGES(-1,'CTRL INFO(8)=-
1','NOTICE',INFO(1),INFO(2))
        RETURN 1
      ENDIF
C-----
C      PERFORM POST CONVERGENCE MANIPULATIONS AT THE END OF EACH
TIMESTEP
      IF (INFO(13).GT.0) THEN
C      CALL MESSAGES(-1,'CTRL
INFO(13)>0','NOTICE',INFO(1),INFO(2))
        RETURN 1
      ENDIF
C-----
C      DO ALL THE VERY FIRST CALL OF THE SIMULATION MANIPULATIONS
HERE
      IF (INFO(7).EQ.-1) THEN
C      CALL MESSAGES(-1,'CTRL INFO(7)=-
1','NOTICE',INFO(1),INFO(2))
C      RETRIEVE THE UNIT NUMBER AND TYPE NUMBER FOR THIS COMPONENT
FROM THE INFO ARRAY
        IUNIT=INFO(1)
        ITYPE=INFO(2)

C      SET SOME INFO ARRAY VARIABLES TO TELL THE TRNSYS ENGINE HOW
THIS TYPE IS TO WORK
        INFO(6)=NOUT
        INFO(9) = 1 !set the way in which this
component is to be called
        INFO(10) = 0 !set required number of spots
in the single precision storage structure

C      CALL THE TYPE CHECK SUBROUTINE TO COMPARE WHAT THIS
COMPONENT REQUIRES TO WHAT IS SUPPLIED
        CALL TYPECK(1,INFO,NI,NP,ND)

C      call the input-output check subroutine to set the correct
input and output units.

```



```

      DATA YCHECK
/'DM1','DM1','DM1','DM1','DM1','DM1','DM1','DM1'/
      DATA OCHECK /'DM1','DM1','DM1'/

C      CALL THE INPUT-OUTPUT CHECK SUBROUTINE TO SET THE CORRECT
INPUT AND OUTPUT UNITS
      CALL RCHECK(INFO,YCHECK,OCHECK)
      !return to the calling program
      RETURN 1
    ENDIF

C-----
C      PERFORM INITIAL TIMESTEP MANIPULATIONS
      IF (TIME.LT.(TIME0+DELT/2.)) THEN
C      SET THE UNIT NUMBER FOR FUTURE CALLS
C      CALL MESSAGES(-1,'INITIAL
TIMESTEP','NOTICE',INFO(1),INFO(2))
C      CALL TRN_LV_INTERFACE(TIME,Y_IN,NI,Y_PAR,NP,Y_OUT,NOUT)
      IUNIT=INFO(1)
      ITYPE=INFO(2)
      Y_PAR(1)=PAR(1)
      Y_PAR(2)=PAR(2)
      Y_PAR(3)=PAR(3)
      Y_PAR(4)=PAR(4)
      Y_PAR(5)=PAR(5)
      Y_PAR(6)=PAR(6)
      Y_PAR(7)=PAR(7)
      Y_PAR(8)=PAR(8)
      Y_PAR(9)=PAR(9)
      Y_PAR(10)=PAR(10)
      Y_PAR(11)=PAR(11)
      Y_PAR(12)=PAR(12)
      Y_PAR(13)=PAR(13)
      Y_PAR(14)=PAR(14)
      Y_PAR(15)=PAR(15)
      Y_PAR(16)=PAR(16)
      Y_PAR(17)=PAR(17)
      Y_PAR(18)=PAR(18)
      Y_PAR(19)=PAR(19)
      Y_PAR(20)=PAR(20)
C      PERFORM ANY REQUIRED CALCULATIONS TO SET THE INITIAL VALUES
OF THE OUTPUTS HERE
      OUT(1) = 0.
      OUT(2) = 0.
      OUT(3) = 0.
C      RETURN TO THE CALLING PROGRAM
      RETURN 1      !the first timestep is for initialization -
exit.
    ENDIF

C-----
C      THIS IS AN ITERATIVE CALL TO THIS COMPONENT ***
C-----

```

```

C      RE-READ THE PARAMETERS IF ANOTHER UNIT OF THIS TYPE HAS BEEN
CALLED SINCE THE LAST
C      TIME THEY WERE READ IN
      IF(INFO(1).NE.IUNIT) THEN
C      RESET THE UNIT NUMBER
      IUNIT = INFO(1)
      ITYPE = INFO(2)
C      PARAMETERS
      Y_PAR(1)=PAR(1)
      Y_PAR(2)=PAR(2)
      Y_PAR(3)=PAR(3)
      Y_PAR(4)=PAR(4)
      Y_PAR(5)=PAR(5)
      Y_PAR(6)=PAR(6)
      Y_PAR(7)=PAR(7)
      Y_PAR(8)=PAR(8)
      Y_PAR(9)=PAR(9)
      Y_PAR(10)=PAR(10)
      Y_PAR(11)=PAR(11)
      Y_PAR(12)=PAR(12)
      Y_PAR(13)=PAR(13)
      Y_PAR(14)=PAR(14)
      Y_PAR(15)=PAR(15)
      Y_PAR(16)=PAR(16)
      Y_PAR(17)=PAR(17)
      Y_PAR(18)=PAR(18)
      Y_PAR(19)=PAR(19)
      Y_PAR(20)=PAR(20)
      ENDIF
C----- INPUTS -----
      Y_IN(1) = XIN(1)      ![-]
      Y_IN(2) = XIN(2)      ![-]
      Y_IN(3) = XIN(3)      ![-]
      Y_IN(4) = XIN(4)      ![-]
      Y_IN(5) = XIN(5)      ![-]
      Y_IN(6) = XIN(6)      ![-]
      Y_IN(7) = XIN(7)      ![-]
      Y_IN(8) = XIN(8)      ![-]
C-----
      CALL
TRN_LV_INTERFACE( TIME,Y_IN,NI,Y_PAR,NP,Y_OUT,NOUT,DeckName )
C-----
C      SET OUTPUTS
C-----
      OUT(1) = Y_OUT(1)
      OUT(2) = Y_OUT(2)
      OUT(3) = Y_OUT(3)
C-----
C      EVERYTHING IS DONE - RETURN FROM THIS SUBROUTINE AND MOVE ON
      RETURN 1
      END

```

# Bibliography

## Chapter1

- [1] SHC Task 14 Advance Active Solar energy systems. 1990-1994 <http://task14.iea-shc.org/>
- [2] SHC Task 26 Solar Combisystems. 1998-2002 <http://task26.iea-shc.org/>
- [3] SHC Task 25 Solar Assisted Air Conditioning of Buildings. 1999-2004 <http://task25.iea-shc.org/>
- [4] SHC Task 38 Solar Air Conditioning and refrigeration. 2006-2010 <http://task38.iea-shc.org/>
- [5] SHC Task 48 Q&A Support Measures for Solar Cooling. 2011-2015 <http://task48.iea-shc.org/>
- [6] SHC Task 45 Large Scale Solar Heating and Cooling Systems. 2011-2014 <http://task45.iea-shc.org/>
- [7] Balaras, C.A., Grossman, G., Henning, H.-M., Infante Ferreira, C.A., Podesser, E., Wang, L., Wiemken, E., 2007. Solar air conditioning in Europe: an overview. *Renewable and Sustainable Energy Reviews* 11, 299–314.
- [8] Villa, E., Wiemken, E., Lopez, J.R, Thur, A., Carvalho, M.J., Mugnier, D., Calderoni, M., Cavallera, Q., Medved, S., Christodoulaki, R., Ayadi, O., van Steenberghe, T., Proville, M., 2009, SOLAIR - Increasing the market implementation of solar air conditioning systems for small and medium applications in residential and commercial buildings CLIMAMED2009 Lisbon, Portugal.
- [9] SOLAR COMBI + project. 2007-2010 <http://www.solarcombiplus.eu>
- [10] HIGH COMBI project. 2007-2011 <http://www.highcombi.eu>
- [11] Solar thermal market in Europe - Trend and market statistics 2012 (June 2013) – ESTIF.
- [12] IEA-SHC Solar Heating and Cooling Programme. Solar heat worldwide: market and contribution to the energy supply 2011. 2013 Edition [Online]. [www.iea-shc.org](http://www.iea-shc.org).
- [13] M. Kaltschmitt, W. Streicher, A. Wiese. *Renewable Energy technology, economics and environment*, 2007 Springer-Verlag Berlin Heidelberg.
- [14] W. Streicher. *Solar Thermal Heating Systems*, Lecture book, 06/2012.
- [15] J. A. Duffie and W. A. Beckman, *Solar engineering of thermal processes*. 2<sup>nd</sup> ed. Wiley-Interscience Publication, NewYork.
- [16] S. Kalogirou. *Solar energy engineering: processes and systems*, 2009, Elsevier/Academic Press.
- [17] H.-M., Henning, 2004. *Solar-assisted Air-conditioning in Buildings - A Handbook for Planners*. Springer-Verlag, ISBN 3-211-00647-8.
- [18] H.-M. Henning, M. Motta. *Solar Cooling Handbook A Guide to Solar Assisted Cooling and Dehumidification Processes*, 3<sup>rd</sup>. Edition, Springer Wien New York, Vienna, ISBN 978-3-7091-0841-3.
- [19] UNI EN 12977-1:2012. Impianti solari termici e loro componenti - Impianti assemblati su specifica - Parte 1: Requisiti generali per collettori solari ad acqua e

sistemi combinati.

- [20] M. Conde Engineering, 2011. Thermophysical properties of brines - models
- [21] Deutsche Gesellschaft für Sonnenenergie, Planning and installing solar thermal systems: a guide for installers, architects and engineers. London, 2010.
- [22] Weiss, W. "Industry Workshop", Solar Combisystems IEA-SHC Task 26, Delft, The Netherlands, April 2001.
- [23] Weiss W. Solar heating systems for houses: a design handbook for solar combisystems. Germany: Crownwell press; 2003.
- [24] H. Z. Hassan and A. A. Mohamad, A review on solar cold production through absorption technology, Renewable and Sustainable Energy Reviews, vol. 16, no. 7, pp. 5331–5348, Sep. 2012.
- [25] L. W. Wang, R. Z. Wang, and R. G. Oliveira, A review on adsorption working pairs for refrigeration, Renewable and Sustainable Energy Reviews, vol. 13, no. 3, pp. 518–534, Apr. 2009.
- [26] A. A. Askalany, M. Salem, I. M. Ismael, A. H. H. Ali, M. G. Morsy, and B. B. Saha, An overview on adsorption pairs for cooling, Renewable and Sustainable Energy Reviews, vol. 19, pp. 565–572, Mar. 2013.
- [27] H.-M. Henning, Solar Cooling Position Paper: Task 38 Solar Air-Conditioning and Refrigeration - October 2011
- [28] EN-12976: Guide for reliability test procedures of factory made solar thermal systems
- [29] V. Badescu, Optimal control of flow in solar collector systems with fully mixed water storage tanks, Energy Conversion and Management 49 (2008) 169-184
- [30] V. Badescu, Optimal control of flow in solar collectors, for maximum exergy extraction, International Journal of Heat and Mass Transfer 50 (2007) 4311–4322
- [31] E. Zamfir, V. Badescu. Different strategies for operation of flat-plate solar collectros. Energy 19 (12) (1994) 1245-1254.
- [32] M. Kovarik, P.F. Lesse, Optimal control of flow in low temperature solar heat collectors, Solar Energy 18 (5) (1976) 431–435.
- [33] A. Bejan, W. Schultz, Optimum flow-rate history for cooldown and energy storage processes, Int. J. Heat Mass Transfer 25 (8) (1982) 1087–1092.
- [34] K.G.T. Hollands, A.P. Brunger, Optimum flow rates in solar water heating systems with a counterflow exchanger, Solar Energy 48 (1) (1992) 15.
- [35] F. De Winter, Comments on optimum flow rates in solar water heating systems with a counterflow exchanger, Solar Energy 49 (6) (1992) 557–558.
- [36] Y. C. Park, L. M. Nhut, Performance prediction of a solar hot water system with change of circulating pump efficiency in solar collectors, International Conference on Renewable Energies and Power Quality (ICRE PQ'13) Bilbao (Spain), 2013
- [37] S. Furbo, L. J. Shah, Optimum Solar Collector Fluid Flow Rates, Department of Buildings and Energy, Technical University of Denmark, Proceedings of Eurosun 1996
- [38] L. M. Nhut and Y. C. Park, A study on automatic optimal operation of a pump for solar domestic hot water system, Solar Energy, vol. 98, pp. 448–457, Dec. 2013.

- [39] R. Kicsiny and I. Farkas, Improved differential control for solar heating systems, *Solar Energy*, vol. 86, no. 11, pp. 3489–3498, Nov. 2012.
- [40] C. Weber, M. Berger, F. Mehling, A. Heinrich, and T. Núñez, Solar cooling with water–ammonia absorption chillers and concentrating solar collector – Operational experience, *International Journal of Refrigeration*, Sep. 2013.
- [41] J. Albers, New absorption chiller and control strategy for the solar assisted cooling system at the German federal environment agency, *International Journal of Refrigeration*, Aug. 2013.
- [42] L. A. Bujedo, J. Rodríguez, and P. J. Martínez, Experimental results of different control strategies in a solar air-conditioning system at part load, *Solar Energy*, vol. 85, no. 7, pp. 1302–1315, Jul. 2011.
- [43] P. Kohlenbach, 2006. Solar cooling with absorption chillers: control strategies and transient chiller performance. Dissertation, Technische Universität Berlin.
- [44] U. Eicker, D. Pietruschka, and R. Pesch, Heat rejection and primary energy efficiency of solar driven absorption cooling systems, *International Journal of Refrigeration*, vol. 35, no. 3, pp. 729–738, May 2012.
- [45] S. Saulich, U. Jakob, and M. J. Cook, Performance analysis of a novel control system for solar collectors coupled with sorption chillers, *International Journal of Refrigeration*, vol. 35, no. 3, pp. 719–728, May 2012.

## Chapter2

- [46] D’Antoni M., Bettoni D., Fedrizzi R., Sparber W. Parametric analysis of a novel Solar Combi+ configuration for commercialization. In *Proc.: 4th International Air-Conditioning*, Larnaka, Cyprus, 2011.
- [47] Fabricatore M., Lantschner E., Bettoni D., D’Antoni M., Fedrizzi R. Design and numerical analysis for standardized control box for small scale Solar Combi+ applications. In *Proc.: 48th International Conference AiCARR*, Baveno, Italy, 2011.
- [48] Klein S.A. et al. Trnsys 17. A transient simulation program. Solar Energy Laboratory, Univeristy of Wisconsin, Madison, 2006.
- [49] Remund, J. (2008): Quality of Meteonorm Version 6.0. *Proceedings of 10th World Renewable Energy Conference*, Glasgow
- [50] Perez, R., P. Ineichen, E. Maxwell, R. Seals and A. Zelenka (1991): Dynamic Models for hourly global-to-direct irradiance conversion. Edited in: *Solar World Congress 1991. Volume 1, Part II. Proceedings of the Biennial Congress of the International Solar Energy Society*, Denver, Colorado, USA, 19-23 August 1991.
- [51] Meteonorm, 2012, Global meteorological database for engineers, planners and education, Version 7.0, [www.meteonorm.com](http://www.meteonorm.com).
- [52] Bettoni D., D’Antoni M., Fedrizzi R. Influence of the boundary conditions on the definition of a reference residential building for the Italian context 1st IBPSA Italy Conference “Building Simulation Application 2013”, Bolzano - Italy
- [53] UNI EN ISO 13790: Energy performance of buildings: Calculation of energy use for space heating and cooling.
- [54] UNI TS 11300-1: Prestazioni energetiche degli edifici - Parte 1: Determinazione del

- fabbisogno di energia termica dell'edificio per la climatizzazione estiva ed invernale.
- [55] DM 26/01/2010. Aggiornamento del decreto 11 marzo 2008 in materia di riqualificazione energetica degli edifici.
  - [56] SHC Task 32 Advanced Storage Concepts for Solar and Low Energy Buildings. 2003-2007 <http://task32.iea-shc.org/>
  - [57] Weber A., 1997. Modell für natürliche Lüftung durch Kippfenster, TRNSYS Usertag Stuttgart, 21. November 1997, EMPA Dübendorf
  - [58] Jordan U., Vajen K., 2000. Influence of the DHW profile on the Fractional Energy Savings: A Case Study of a Solar Combi-System. Solar Energy Vol.69, pp. 197-208.
  - [59] Jordan U., Vajen K., 2001. Realistic Domestic Hot-Water Profiles in Different Time Scales. FB. Physik, FG. Solar, Universität Marburg, D-35032 Marburg. [On-line]. Available: <http://sel.me.wisc.edu/trnsys/trnlib/iea-shc-task26>
  - [60] UNI 9182:2010. Impianti di alimentazione e distribuzione d'acqua fredda e calda.
  - [61] Besana F., 2009. Heat rejection problematic in Solar Combi+ system. University of Bergamo, PhD thesis.
  - [62] SorTech AG. SorTech Adsorption Chiller - Design Manual ACS08/ACS15. 2009.
  - [63] Drück H. Trnsys Type 340. Multiport Store- Model, version 1.99F. ITW Stuttgart University, Germany, 2006.
  - [64] D'Antoni M., Ferruzzi G., Bettoni D., Fedrizzi R. Validation of the numerical model of a turnkey Solar Combi+ system Solar Heating and Cooling Conference 2012, San Francisco, CA
  - [65] Max D. Morris 1991. Factorial Sampling Plans for Preliminary Computational Experiments. Technometrics 33, 161-174.
  - [66] Andrea Saltelli, Marco Ratto, Stefano Tarantola, Francesca Campolongo. 2005. Sensitivity Analysis for Chemical Models. Chemical Reviews
  - [67] Francesca Campolongo, Jessica Cariboni, Andrea Saltelli. 2007. An effective screening design for sensitivity analysis of large models. Environmental Modelling & Software 22, 1509-1518

### Chapter3

- [68] Fontanella G. et al., Calibration and validation of a solar thermal system model in Modelica, Building Simulation (2012), 1-8
- [69] Monfet D., Zmeureanu R., Simulation of a large central cooling and heating plant using trnsys and calibration with monitored data, 11th International IBPSA Conference Glasgow, 2009
- [70] Udomsria S., Bales C., Martin A. R., Martin V., Decentralised cooling in district heating network: Monitoring results and calibration of simulation model, Energy and Building 43 (2011) 3311-3321
- [71] Ben H. Thacker et al., 2004, Concepts of Model Verification and Validation. Los Alamos National Laboratory, Report LA-14167-MS
- [72] Sargent, R. G. Verification and validation of simulation models, Proceedings of the 2010 Winter Simulation Conference

- [73] Palacin F., Monné C., Alonso S., Evaluation, diagnosis and improvement of a solar cooling plant by means of experimental analysis and dynamic simulation. EUROSUN 2010, Graz (Austria).
- [74] McDowell T.P., Thornton J.W., Simulation and model calibration of a large-scale solar seasonal storage system. 3rd National Conference of IBPSA-USA, Berkeley, 2008
- [75] Murray-Smith D.J. Methods for external validation of continuous system simulation models: a review. *Mathematical and Computer Modelling of Dynamical Systems* 1998;4:5-31.
- [76] IEC 61400-12-1:2005. Wind turbines – Part 12-1: Power performance measurements of electricity producing wind turbines
- [77] Kleijnen J.P.C. Theory and Methodology. Verification and validation of simulation models. *European Journal of Operational Research* 1995;82:145-162.
- [78] White A.S., Sinclair R. Quantitative validation techniques data base (I). Simple example. *Simulation Modeling Practice and Theory* 2004;12:451-473.
- [79] Theil H. Economic forecasting and policy. North Holland, Amsterdam, 1970.
- [80] Catalogue Wilo-Stratos PARA - High-Efficiency pumps for OEM-Industry. Heating, Air Condition, Cooling, Geothermal heat, Solar heat

#### **Chapter4**

- [81] Catalogue Clivet - Elfo Energy Ground WSHN-EE 17-121
- [82] A. Saltelli, M. Ratto, T. Andres, F. Campolongo, J. Cariboni, D. Gatelli et al. Global sensitivity analysis - the primer. John Wiley & Sons Ltd., Chichester (2008)

#### **Chapter5**

- [83] M. Veronesi, A.Visioli. Logica Fuzzy: Fondamenti teorici e applicazioni pratiche
- [84] S. A. Kalogirou and A. Sencan, Artificial Intelligence Techniques in Solar Energy Applications. Solar Collectors and Panels, Theory and Applications, Book edited by RI Manyala, 2010.
- [85] A. Zilouchian and M. Jamshidi, Intelligent control systems using soft computing methodologies. CRC Press, 2001.
- [86] S.K. Oh, W.D. Kim, and W. Pedrycz, Design of optimized cascade fuzzy controller based on differential evolution: Simulation studies and practical insights, *Engineering Applications of Artificial Intelligence*, vol. 25, no. 3, pp. 520–532, Apr. 2012.
- [87] P. P. Wang and C.Y. Tyan, Fuzzy dynamic system and fuzzy linguistic controller classification, *Automatica*, vol. 30, no. 11, pp. 1769–1774, 1994.
- [88] Trung-Kien Dao and Chih-Keng Chen. Tuning Fuzzy-Logic Controllers - MICA Center, HUST - CNRS/UMI 2954 - Grenoble INP, Hanoi, Dayeh University, Changhua,
- [89] L.A. Zadeh, Fuzzy sets. *Information and control* 8, 338-353 (1965)
- [90] L.A. Zadeh, Fuzzy algorithms. *Information and control* 12, 94-102 (1968)

- [91] A.J. Van der Wal, Application of fuzzy logic control in industry, *Fuzzy Sets and Systems*, vol. 74, no. 1, pp. 33–41, 1995.
- [92] R.E. Precup and H. Hellendoorn, A survey on industrial applications of fuzzy control, *Computers in Industry*, vol. 62, no. 3, pp. 213–226, Apr. 2011.
- [93] Y. Dote and S. J. Ovaska, Industrial applications of soft computing: a review, *Proceedings of the IEEE*, vol. 89, no. 9, pp. 1243–1265, 2001.
- [94] P. P. Cruz and F. D. Ramáirez-Figueroa, *Intelligent Control Systems with LabVIEW*. Springer, 2009.
- [95] PID and Fuzzy Logic Toolkit User Manual. National Instruments Corporation, 2009.
- [96] R. M. del Toro Matamoros, Métodos clásicos y de soft-computing en la optimización de procesos complejos. Aplicación a un proceso de fabricación., PhD Thesis, Escuela Politécnica Superior - Universidad Autonoma de Madrid, Madrid, 2011.
- [97] T. J. Ross, *Fuzzy logic with engineering applications*. Chichester, U.K.: John Wiley, 2010.
- [98] Fuzzy Logic Toolbox™ - User's Guide- Matlab
- [99] Camacho, E.F., Berenguel, M., Rubio, F.R., Martínez, D. *Control of Solar Energy Systems - Advances in Industrial Control*, Springer, 2012
- [100] Shaw, Ian S. *Fuzzy Control of Industrial Systems - Theory and Applications*. Series: The Springer International Series in Engineering and Computer Science, Vol. 457. 1998.
- [101] R. S. Sutton and A. G. Barto, *Reinforcement Learning: An introduction*. MIT Press, 1998.
- [102] W. Ertel, *Introduction to artificial intelligence*. Springer, 2011.
- [103] C. J. C. H. Watkins, *Learnig from delayed rewards*, PhD Thesis, University of Cambridge, England, 1989.
- [104] S. Haykin, *Neural Networks - A Comprehensive Foundation*. Prentice Hall India, 2002.
- [105] B. Van Roy, *Neuro-dynamic programming: Overview and recent trends*, in *Handbook of Markov Decision Processes*, Springer, 2002, pp. 431–459.
- [106] L. Jouffe, Actor-critic learning based on fuzzy inference system, in *Systems, Man, and Cybernetics*, 1996., IEEE International Conference on, 1996, vol. 1, pp. 339–344.
- [107] P. Pecherková, M. Flídr, and J. Duník, *Robotics, automation and control*. [S. l.]: In-Teh, 2008.
- [108] G. Tesauro, Programming backgammon using self-teaching neural nets, *Artificial Intelligence*, vol. 134, pp. 181–199, 2002.
- [109] T. P. Imthias Ahamed, P. S. Nagendra Rao, and P. S. Sastry, A reinforcement learning approach to automatic generation control, *Electric power systems research*, vol. 63, no. 1, pp. 9–26, 2002.
- [110] T. I. Ahamed, P. S. Sastry, and P. N. Rao, A new reinforcement learning based automatic generation controller for hydro-thermal power systems, in *TENCON*



2003. Conference on Convergent Technologies for Asia-Pacific Region, 2003, vol. 1, pp. 63–66.
- [111] E. A. Jasmin, Reinforcement learning approaches to power system scheduling, PhD Thesis, Cochin University of Science and Technology, KERALA, INDIA, 2008.
  - [112] Z. Qin and J. Gu, Neural Q-learning in Motion Planning for Mobile Robot, presented at the International Conference on Automation and Logistics, Shenyang, China, 2009.
  - [113] R. H. Crites and A. G. Barto, Elevator group control using multiple reinforcement learning agents, *Machine Learning*, vol. 33, no. 2–3, pp. 235–262, 1998.
  - [114] H. J. Kim, M. I. Jordan, S. Sastry, and A. Ng, Autonomous helicopter flight via reinforcement learning, in *Advances in neural information processing systems*, 2003, p. None.
  - [115] E. Kehris and D. Dranidis, Application of Reinforcement Learning for the Generation of an Assembly Plant Entry Control Policy, *Journal of Intelligent Computation*, vol. 9, no. 2, pp. 214 – 220, 2005.
  - [116] H. Boubertakh and P.-Y. Glorennec, Optimization of a fuzzy PI controller using reinforcement learning, in *Information and Communication Technologies*, 2006. ICTTA'06. 2nd, 2006, vol. 1, pp. 1657–1662.
  - [117] P. Y. Glorennec, Fuzzy Q-learning and dynamical fuzzy Q-learning, in *Fuzzy Systems*, 1994. IEEE World Congress on Computational Intelligence., Proceedings of the Third IEEE Conference on, 1994, pp. 474–479.
  - [118] C. W. Anderson, D. C. Hittle, A. D. Katz, and R. M. Kretchman, Reinforcement learning, neural networks and PI control applied to a heating coil, in *Proceedings of the International Conference on EANN*, 1996, vol. 96, pp. 135–42.
  - [119] K. Dalamagkidis, D. Kolokotsa, K. Kalaitzakis, and G. S. Stavrakakis, Reinforcement learning for energy conservation and comfort in buildings, *Building and Environment*, vol. 42, no. 7, pp. 2686–2698, Jul. 2007.
  - [120] C. Weber, Reinforcement learning: theory and applications. Vienna: I-TECH Education and Pub., 2008 – Cap15 - K. Dalamagkidis, D. Kolokotsa, Reinforcement Learning for Building Environmental Control.
  - [121] S. Liu and G. P. Henze, Experimental analysis of simulated reinforcement learning control for active and passive building thermal storage inventory, *Energy and Buildings*, vol. 38, no. 2, pp. 148–161, Feb. 2006.
  - [122] S. Liu and G. P. Henze, Experimental analysis of simulated reinforcement learning control for active and passive building thermal storage inventory, *Energy and Buildings*, vol. 38, no. 2, pp. 142–147, Feb. 2006.
  - [123] G. P. Henze and J. Schoemann, Evaluation of Reinforcement Learning control for thermal energy storage systems, *HVAC&R RESEARCH*, vol. 9, no. 3, pp. 259–276, Jul. 2003.
  - [124] Z. Yu and A. Dexter, Online tuning of a supervisory fuzzy controller for low-energy building system using reinforcement learning, *Control Engineering Practice*, vol. 18, no. 5, pp. 532–539, May 2010.

- [125] Boubertakh, H., Tadjine, M., Glorennec, P.-Y., Labiod, S., 2010. Tuning fuzzy PD and PI controllers using reinforcement learning. *ISA Transactions* 49, 543–551.
- [126] Muñoz, P., Barco, R., de la Bandera, I., 2013. Optimization of load balancing using fuzzy Q-Learning for next generation wireless networks. *Expert Systems with Applications* 40, 984–994.
- [127] Onieva, E., Godoy, J., Villagr , J., Milan s, V., P rez, J., 2013. On-line learning of a fuzzy controller for a precise vehicle cruise control system. *Expert Systems with Applications* 40, 1046–1053.
- [128] Boubertakh, H., Tadjine, M., Glorennec, P.-Y., 2010. A new mobile robot navigation method using fuzzy logic and a modified Q-learning algorithm. *Journal of Intelligent & Fuzzy Systems* 21, 113–119.
- [129] Sharma, R., Gopal, M., 2008. A Markov Game-Adaptive Fuzzy Controller for Robot Manipulators. *IEEE Transactions on Fuzzy Systems* 16, 171–186.
- [130] Shin, M., Ryu, K., Jung, M., 2012. Reinforcement learning approach to goal-regulation in a self-evolutionary manufacturing system. *Expert Systems with Applications* 39, 8736–8743.
- [131] Tan, Z., Quek, C., Cheng, P.Y.K., 2011. Stock trading with cycles: A financial application of ANFIS and reinforcement learning. *Expert Systems with Applications* 38, 4741–4755.
- [132] Xu, J.-X., Guo, Z.-Q., Lee, T.H., 2012. Synthesized design of a fuzzy logic controller for an under actuated unicycle. *Fuzzy Sets and Systems* 207, 77–93.